BioMed Research International

Particulate Matter and Nanoparticles Toxicology

Guest Editors: Ernesto Alfaro-Moreno, Tim S. Nawrot, Abderrahim Nemmar, Irma Rosas, and Per Schwarze

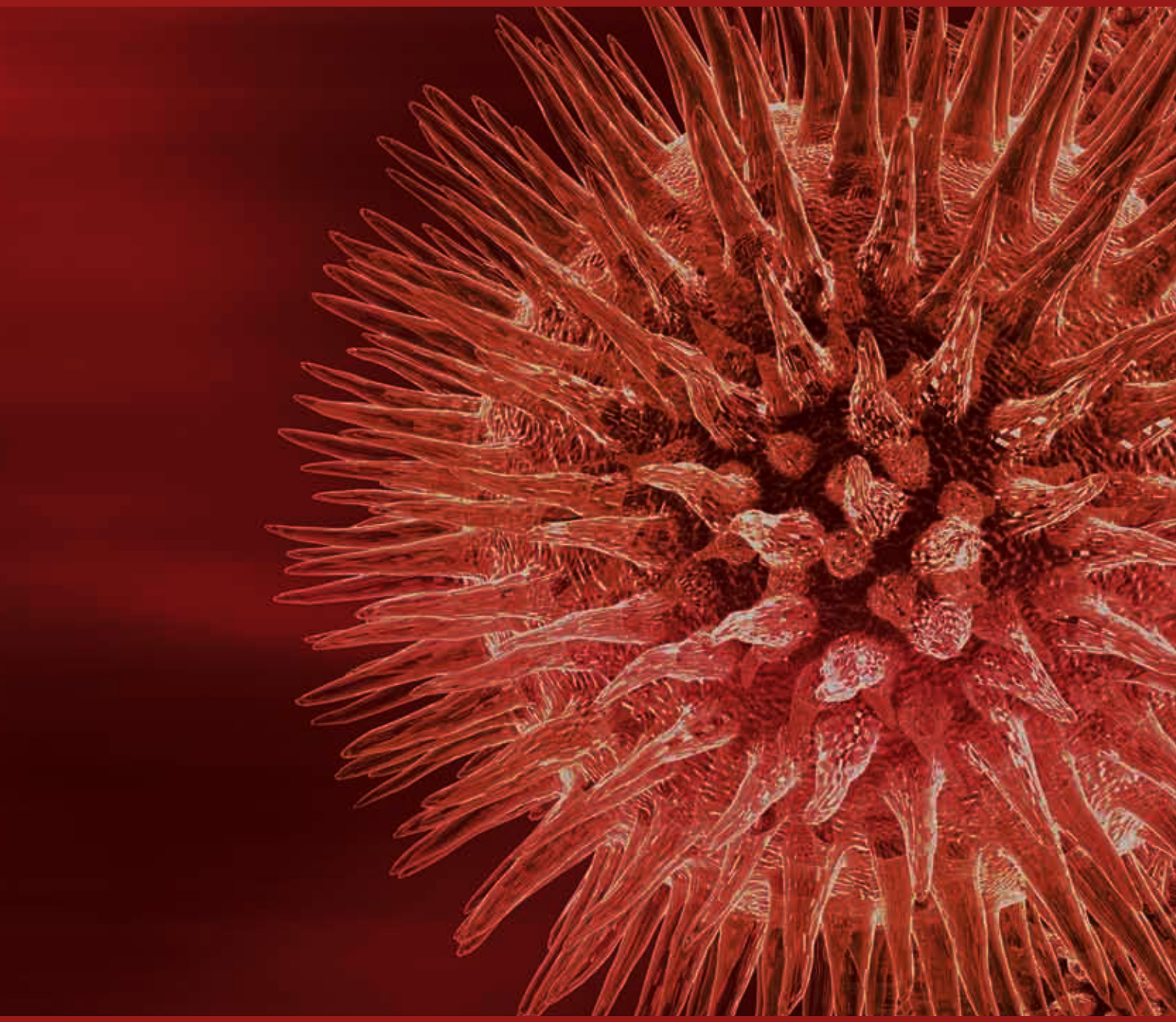

Particulate Matter and Nanoparticles Toxicology

BioMed Research International

Particulate Matter and Nanoparticles Toxicology

Guest Editors: Ernesto Alfaro-Moreno, Tim S. Nawrot, Abderrahim Nemmar, Irma Rosas, and Per Schwarze

Contents

Hindawi Publishing Corporation
BioMed Research International
Volume 2013, Article ID 642974, 2 pages
http://dx.doi.org/10.1155/2013/642974

Editorial

Particulate Matter and Nanoparticles Toxicology

Ernesto Alfaro-Moreno,[1] Tim S. Nawrot,[2,3] Abderrahim Nemmar,[4] Irma Rosas,[5] and Per Schwarze[6]

[1] *Environmental Toxicology Laboratory, Instituto Nacional de Cancerología, Avenida San Fernando 22, Tlalpan, 14080 México City, CP, DF, Mexico*
[2] *Centre for Environmental Sciences, Hasselt University, 3500 Hasselt, Belgium*
[3] *Department of Public Health, Leuven University (KU Leuven), 3000 Leuven, Belgium*
[4] *Department of Physiology, College of Medicine and Health Sciences, United Arab Emirates University, Al Ain 17666, UAE*
[5] *Aerobiology Laboratory, Atmospheric Sciences Center, Universidad Nacional Autónoma de México, 04510 México City, DF, Mexico*
[6] *Department of Air Pollution and Noise, Norwegian Institute of Public Health, 0403 Oslo, Norway*

Correspondence should be addressed to Ernesto Alfaro-Moreno; ealfaro.incan@gmail.com

Received 6 June 2013; Accepted 6 June 2013

Humans have been exposed for thousands of years to particulate matter (PM) from natural and anthropogenic sources. Since the first third of the twentieth century, health problems related to dust exposure in miners have been documented [1]. Early epidemiological data have shown evidence of the relation between inhalation of PM and several lung diseases, including lung fibrosis and lung cancer [2]. The Meuse valley fog of 1930 [3], the Donora smog incident of 1948 [4], and the London great smog event of 1952 [5] were the foundation to create a legislation regarding to air pollutants. In the US, the Clean Air Act was enacted in 1972. Before 1970, the main efforts in this field were aimed at measuring the PM suspended in the air and its relation to death increases associated to lung diseases. During the 1970s and 1980s, the measurements of environmental particles improved, and efforts to quantify particles with different aerodynamic sizes gave a view on how the particles could be related to different diseases. These methods helped to identify sources of different particles, leading to specific actions to control the emission of PM. During the 1990s and the first decade of this century, a great effort has been done to determine the cellular and molecular mechanisms related to the particle toxicity, and many studies have shown that particle size and composition play central roles in the biological effects. During the last 20 years, a great concern has grown regarding the use of nanoparticles (NPs) and its possible impact on workers and final users. To present, it is evident that inhaled particles may have local and systemic effects, and that the size, the composition, and the physicochemical characteristics of these airborne particles play a central role in their toxicity.

Despite all the clinical, epidemiological, and toxicological evidence, we are far from understanding the toxicology of particles, in part by the combined effects and interactions of various substances mixed within the particles. In addition, the lack of evidence of a threshold value makes it difficult to set safe limit values. Therefore, a constant growth in the total number of publications related to urban PM and NP is easy to observe when a simple search is done on PUBMED. When the words "particles" and "air pollution" are searched, 101 publications are found from 1900 to 1970. The number rises to 149 from 1971 to 1980. During the 1980s, the first efforts were done to evaluate the effects of particles with different aerodynamical sizes but the number of publications remained in 150. Later on, during the 1990s, the evaluation of particles with different aerodynamic sizes (PM_{10}, $PM_{2.5}$, and ultrafine particles) made the number of publications to grow up to more than 600. The continuous evaluation of urban particles and the arising use of nanomaterials led to almost 2000 publications during the first decade of this century. If the rate of publications on these fields keeps the same rhythm

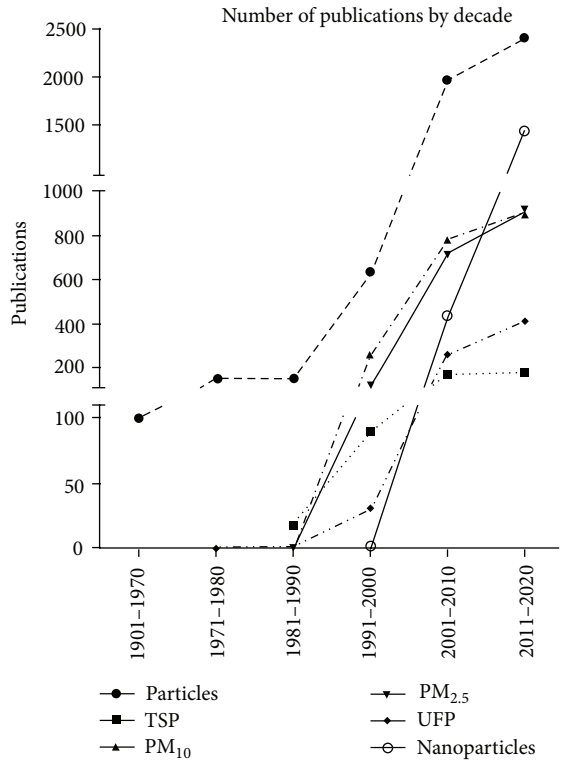

Figure 1

as the first two years of the present decade, we will find about 2400 publications for the 2011–2020 decade (Figure 1).

The previously-mentioned numbers gave a clear idea of why a special issue on particulate matter and nanoparticles toxicology is important for this field. In this special issue, we are publishing a selection of studies dealing with particle sampling and characterization, *in vitro* toxic effects characterization using traditional and novel models, *in vivo* effects of PM, and *in vivo* and *in vitro* effects of different types of NP.

We also include three reviews, discussing the cellular effects of diesel particles, another one discussing the evidence relating the exposure to particles and other inhaled pollutants to the increased risk of Alzheimer and Parkinson's diseases. Finally, a review of the state of the art in the *in vivo* and *in vitro* toxicological characterization of particles was prepared for this issue by the guest editors, where we discuss the latest evidence of local and systemic effects induced by inhaled particles.

Great efforts have been done during the last 50 years to understand the toxicology of particulate matter, and much information is available helping to understand the risks of exposure to different types of particles. Nevertheless, there is much to do in the field, and the efforts presented here will be of great value to push further the frontiers of our knowledge on the particulate matter toxicology field.

Abderrahim Nemmar
Ernesto Alfaro-Moreno
Irma Rosas
Per Schwarze
Tim S. Nawrot

References

[1] E. L. Collins, "Recent views on pneumoconiosis," *Proceedings of the Royal Society of Medicine*, vol. 24, no. 5, pp. 531–542, 1931.

[2] A. G. Heppleston, "Pulmonary toxicology of silica, coal and asbestos," *Environmental Health Perspectives*, vol. 55, pp. 111–127, 1984.

[3] B. Nemery, P. H. M. Hoet, and A. Nemmar, "The Meuse Valley fog of 1930: an air pollution disaster," *The Lancet*, vol. 357, no. 9257, pp. 704–708, 2001.

[4] J. G. Towsend, "Investigation of the smog incident in Donora, Pa., and vicinity," *American journal of public health*, vol. 40, no. 2, pp. 183–189, 1950.

[5] W. P. D. Logan, "Mortality in the London fog incident," *The Lancet*, vol. 261, no. 6755, pp. 336–338, 1953.

Hindawi Publishing Corporation
BioMed Research International
Volume 2013, Article ID 279371, 22 pages
http://dx.doi.org/10.1155/2013/279371

Review Article

Recent Advances in Particulate Matter and Nanoparticle Toxicology: A Review of the *In Vivo* and *In Vitro* Studies

Abderrahim Nemmar,[1] Jørn A. Holme,[2] Irma Rosas,[3] Per E. Schwarze,[2] and Ernesto Alfaro-Moreno[4]

[1] *Department of Physiology, College of Medicine and Health Sciences, United Arab Emirates University, Al Ain 17666, UAE*
[2] *Department of Air Pollution and Noise, Norwegian Institute of Public Health, N-0403 Oslo, Norway*
[3] *Aerobiology Laboratory, Atmospheric Sciences Center, Universidad Nacional Autónoma de México, 04510 Mexico City, DF, Mexico*
[4] *Environmental Toxicology Laboratory, Instituto Nacional de Cancerología, México. Avenido San Fernando 22, Tlalpan, 14080 Mexico City, DF, Mexico*

Correspondence should be addressed to Ernesto Alfaro-Moreno; ealfaro.incan@gmail.com

Received 7 March 2013; Revised 8 May 2013; Accepted 22 May 2013

Academic Editor: Tim Nawrot

Epidemiological and clinical studies have linked exposure to particulate matter (PM) to adverse health effects, which may be registered as increased mortality and morbidity from various cardiopulmonary diseases. Despite the evidence relating PM to health effects, the physiological, cellular, and molecular mechanisms causing such effects are still not fully characterized. Two main approaches are used to elucidate the mechanisms of toxicity. One is the use of *in vivo* experimental models, where various effects of PM on respiratory, cardiovascular, and nervous systems can be evaluated. To more closely examine the molecular and cellular mechanisms behind the different physiological effects, the use of various *in vitro* models has proven to be valuable. In the present review, we discuss the current advances on the toxicology of particulate matter and nanoparticles based on these techniques.

1. Introduction

Exposure to particulate matter (PM) is associated with increases in visits to emergency rooms and mortality [1]. The Meuse valley fog of 1930 [2], the Donora smog incident of 1948 [3], and the London great smog event of 1952 [4] triggered the studies of health effects related to the exposure to PM in large cities and later on the legislation regarding the level limits of PM. For instance, in the US, the Clean Air Act was enacted in 1972.

Inhaled particles penetrate into the respiratory tract where they target different anatomical sites, depending among other properties on the aerodynamic size. Particles are categorized according to aerodynamic size, PM_{10}, thoracic particles, ($\leq 10\,\mu$m) and $PM_{2.5}$ ($\leq 2.5\,\mu$m), or fine fraction. The particles with a range of aerodynamic sizes between 10 and $2.5\,\mu$m ($PM_{10\text{-}2.5}$) are know as coarse fraction. If the aerodynamic size is equal or less than $0.1\,\mu$m, the particles are called ultrafine particles (UFP), and one of the main sources of this type of primary particles is diesel exhaust (DEP). Engineered particles, measured by their geometric size and with at least one dimension smaller than $0.1\,\mu$m, are known as nanoparticles (NP) [5]. The primary anatomical target of particles with different sizes is summarized on Figure 1.

Air Quality Standards have been adopted by many countries around the world to protect public health and welfare against the adverse effects of air pollution. In fact, member countries of the World Health Organization (WHO) have adopted a constitution that sets guidelines on air pollutants. The WHO, which has representation from nearly 200 countries, recommends daily PM_{10} concentrations not to exceed $50\,\mu g/m^3$ [6]. Many countries, however, have chosen to set Air Quality Standards that are more relaxed or more stringent than the WHO Standard. Air Quality Standards

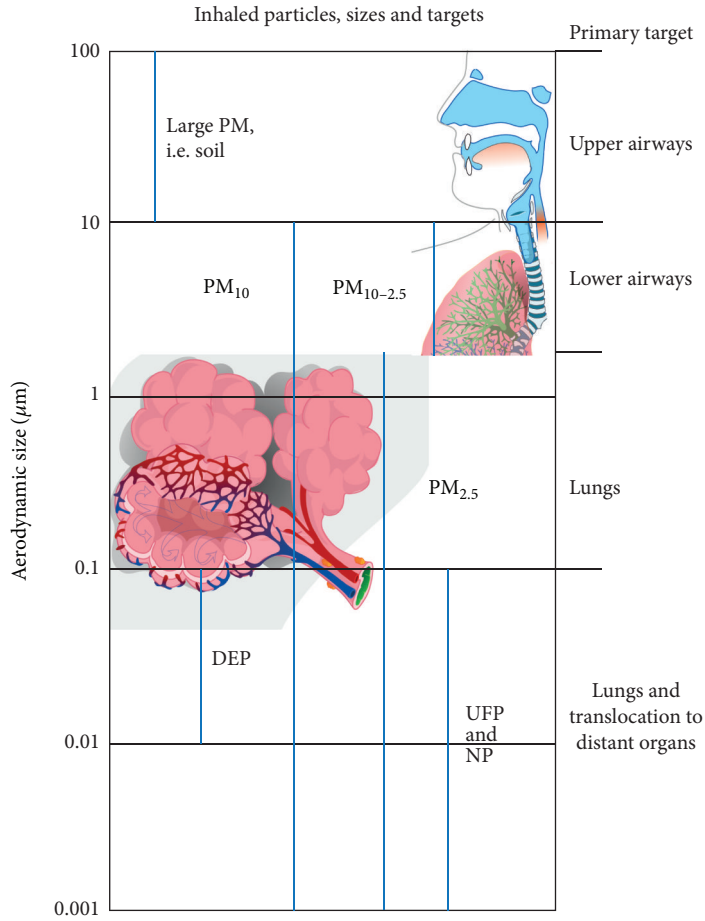

Figure 1: Schematization of the size and main target for particulate matter and nanoparticles.

are generally created or revised according to national policy and scientific information that demonstrates a plausible association between health-related illnesses and exposure to pollutants. The limits for PM_{10} and $PM_{2.5}$ that are used in different countries and regions are shown in Table 1 (Modified from [6]).

Despite all the efforts for measuring the health impact of inhaled particulate matter, we are still far from fully understanding all the effects and mechanisms related to those effects, and also, we still do not understand what is the role of the length (size), shape, and composition of particles in their biological effects. In the present paper, we reviewed the relevant information related to three main aspects of the problem: (1) the determination and role of the chemical and biological components of particles, (2) the evaluation of the *in vivo* effects, both at pulmonary and systemic targets, and (3) the evaluation of the mechanisms of the cellular effects of particles with different sizes, shapes, and composition. Among the large amount of articles that are published in these fields, we choose those that we consider are helping to understand the different problems and also those articles that are opening new questions, pushing the limits of our knowledge forward.

2. Characterization of Particles

Combustion particles from traditional fuels (biomass, coal, wood, crude oil, and diesel with high content in sulfur) are now found in much lower concentrations in air than 30–40 years ago due to improved and cleaner technology. The relative size distribution has changed, and other pollutants have gained prominence, such as ultrafine PM (UFP) [7]. These new and lighter airborne PM is found not only in big cities but also in large and small towns. Interestingly, they differ in composition with regard to various heavy metals and polycyclic aromatic hydrocarbons (PAHs) and are often found to have a higher oxidative and toxic potentials.

Depending on the source and composition of the PM different subsets of components may be found on different fractions. $PM_{2.5}$ comprises the soot fraction and particles grown from the gas phase with subsequent agglomeration. $PM_{2.5}$ includes inorganic ions such as sulfate, nitrate, and ammonia, as well as combustion-form carbon, organic aerosols, metals, and other combustion products. $PM_{10\text{-}2.5}$ is dominated by mechanically abraded or ground particles including finely divided minerals such as oxides of aluminum silicate, iron, calcium, and potassium [8].

Table 1: Comparison of the WHO guidelines and standards from different countries. Modified from WHO air quality guidelines, global update, 2005, a report on a Working Group meeting, Bonn, Germany, 18–20 October 2005 [5].

Source	Selected air quality guidelines and standards			
	PM_{10} ($\mu g/m^3$)		$PM_{2.5}$ ($\mu g/m^3$)	
	1 year	24 hours	1 year	24 hours
WHO [2]	20	50	10	25
European Union	40	50	25	
United States	50	150	12	35
California	20	50	15	65
Japan		100	12	65
Brazil	50	150		
Mexico	50	120	15	65
South Africa	60	180	15	65
India (sensitive populations/ residential/industrial)	50/60/120			
China (Classes I/II/III)	40/100/150	50/150/250		35

UFPs are composed of both primary and secondary particulate matters [9]. The primary fraction is the one that is emitted directly from the emission sources and often includes agglomerate/aggregates of smaller particles [9]. Their size is generally in the range between 30 and 100 nm [10, 11]. The primary fraction is generally associated with diesel engines and automobiles and biomass combustion which are thought to initially have been emitted at around the 30 nm diameter size (the so called nucleation mode) and later coagulate into the larger fraction of the ultrafine mode. The secondary fraction is composed of particulate matter formed in the atmosphere and includes sulfuric acid and sulfates and organic reaction products of low volatility [9]. Photoreactions of oxides of nitrogen (NOx) and sulfur dioxide (SO_2) are involved in this process; both of which are products of combustion. This fraction size is generally in the range between 100 and 200 nm, which is partially distinguishable from other directly anthropogenic sources.

The role of composition on toxic effects has been explored during the last decade by different authors. The dogma during the 1990's was that the size of the particle was the predominant factor of toxicity, the smaller particles being the more toxic [12]. Nevertheless, during the last 15 years, evidence has linked surface area, reactivity, and different components of the particles with their toxicity [13–15]. The first efforts were done by collecting samples from associated to different sources such as indoor and outdoor [16], different cities [17], or regions within a large city [18] and comparing their *in vitro* toxic effects. In some cases, partial chemical characterizations or determinations of the presence of some components were empirically related with differences in the intensity of toxic effects [19–21]. Later on, comprehensive characterizations were correlated using different statistical models [13–15]. Currently, the characterization of size, physicochemical, and chemical composition is necessary to understand the toxicology of particles. For instance, for nanoparticles (NP), the determination of particle size, the dynamics of agglomeration and aggregation, the area, and the charge are mandatory for any toxicological evaluation [22]. In the field of urban particles, considering that they are complex mixtures, there are no standard measurements of physicochemical and chemical components, but the determination of total carbon, black carbon, transitional metals, nitrates, sulfates, oxidative potential, and polycyclic aromatic hydrocarbons is among the most evaluated components [23, 24]. A recent report of a meta-analysis and multisite time series evaluating elemental carbon, organic carbon matter, sulfate, and nitrate on $PM_{2.5}$ and in its relation to hospital admissions demonstrates that changes in elemental carbon content are associated with cardiovascular hospital admissions [25]. The authors conclude that a stronger communication between risk assessors and epidemiologist would help to better understand the role of the components of air pollutants on population effects.

Among the many components that are present in PM, the biological components seem to play a central role in the biological effects. There is increasing evidence that when PM is inhaled the biological component is responsible for stimulating alveolar macrophages and respiratory epithelial tissue to release proinflammatory cytokines and chemokines. The biological components may also have synergetic effects with other components of the PM, such as diesel exhaust enhancing IgE production and thus facilitating allergic sensitization [26].

These biological components may be released by passive or active mechanisms from plants, soil, biofilms, solid, or liquid sources to become suspended in the air. The measurement of protein associated with PM is considered as a general indicator of how much of the PM comes from a biological source. It represents about 1–4% of the total mass of PM_{10} for urban and rural areas [27, 28].

Airborne biological particles or dust containing biological agents and/or substances of biological origin are important components of the coarse and fine PM. These components are represented by different types of primary or secondary (fragmented biological cells) biological aerosols [29]. The biological matter is predominantly comprised by plant pollen, spores, and microorganisms (mold and bacteria) or microbial metabolites [30, 31] and is related to allergic, toxic, and infectious responses in exposed individuals.

PM may be an efficient carrier of secondary allergens or proinflammatory compounds [32–34]. Recently, good correlation has been found for major allergens, mainly from pollen, and asthmatic patients. In fact, pollen from grasses, weeds and trees, among others were found onto different size of particles [35]. Most of the primary allergens (intact pollen, 10–100 μm) cannot reach the small airways; however, the secondary pollen allergens present in $PM_{2.5}$ can easily penetrate there [36].

Endotoxin lipopolysaccharides (LPSs) are other proinflammatory compounds from microbial origin present in PM. Endotoxin is a component of the cell wall of gram-negative bacteria, and its main source is debris deposited on urban or rural soil. When the LPS is resuspended and inhaled, it stimulates alveolar macrophages and respiratory epithelial

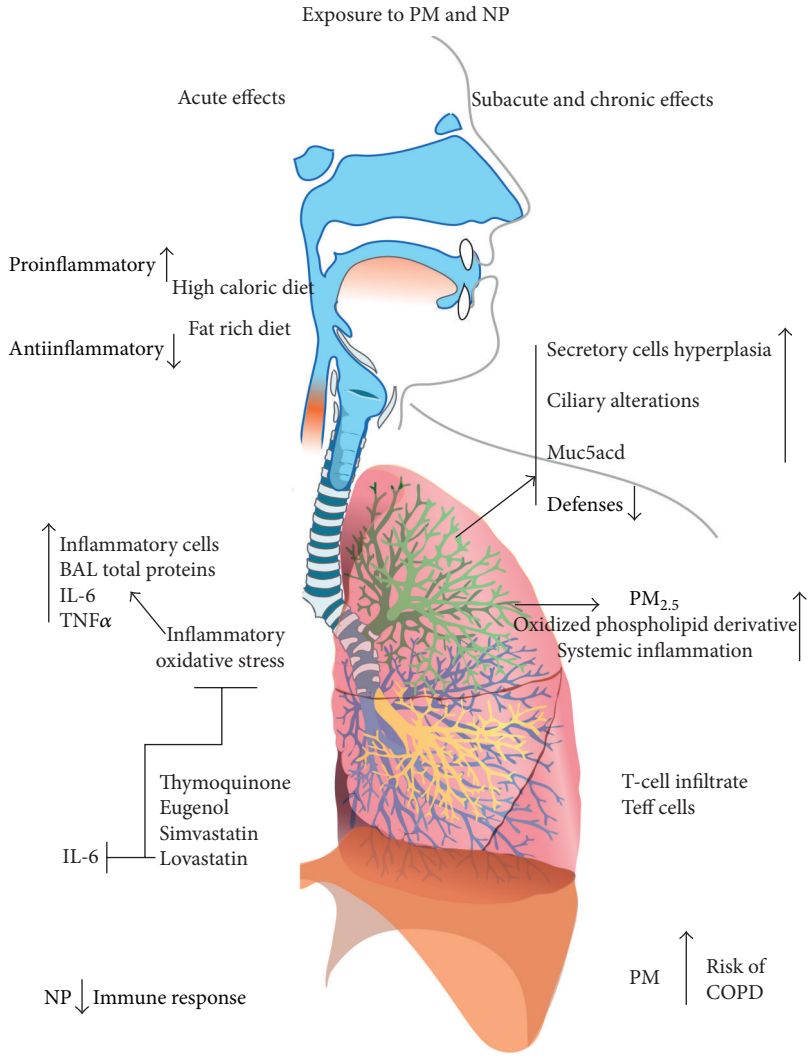

Figure 2: Schematization of the main acute, subacute, and chronic effects induced by inhaled particles and nanoparticles. In the acute side it is interesting to highlight that a high-caloric- and fat-rich diet provides a scenario facilitating proinflammatory effects of particles. Also, Tnymoquinone, eugenol, simstatin, and lovastin have a protective effect *in vivo*. In the subacute and chronic side, it is interesting to highlight the presence of tissue alterations, lung infiltration by T cells, and increases in the risk of COPD.

tissue to release cytokines/chemokines, initiating an inflammatory cascade [37, 38]. Another biological component with similar effects is the β-1,3-Glucan, a glucose polymer which is structural component of most fungal cell walls. β-1,3-Glucan has been used as an indicator of the presence of mold [39, 40].

3. *In Vivo* Studies

The main target for inhaled particles is the respiratory system, but there is strong evidence that systemic effects can be induced. We are presenting some of the most relevant studies regarding the local and systemic effects induced by inhaled particles. In Figure 2, we summarize some of the most relevant acute, subacute, and chronic effects induced *in vivo* by particles.

3.1. Respiratory Effect of Particles

3.1.1. Acute Effects. Several studies have investigated the respiratory effects of particulate air pollution and nanoparticles. While most of the studies have focused on the respiratory effects following inhalation, intratracheal or intranasal instillation, others have investigated the effects of intravenous, intraperitoneal, or oral administration.

It is well established that pulmonary exposure to particulate air pollution causes inflammation and oxidative stress [41–43]. It has been demonstrated that acute (within 24 h), single-dose intratracheal instillation of diesel exhaust particles (15–30 μg/mouse), a relevant type of $PM_{2.5}$, causes lung inflammation characterized by influx of inflammatory cells, increases total proteins, a marker of epithelial permeability, and oxidative stress [41, 42]. The release of interleukin-6 (IL-6) was found to increase in bronchoalveolar lavage (BAL)

fluid at 18 h but not at 4 or 24 h [42]. Similarly, at 18 h time point, airway resistance to methacholine measured invasively using forced oscillation technique increased significantly and dose-dependently following exposure to DEP [42]. Pretreatment with thymoquinone, a constituent of *Nigella sativa*, ameliorated DEP-induced pulmonary effects [42].

Acute exposure (24 h) of healthy mice by intranasal instillation to $PM_{2.5}$ (5 or 15 μg/mouse) collected from the urban area of Sao Paulo caused lung inflammation and oxidative stress and worsened lung impedance in dose-dependent pattern [44]. The same research group has more recently reported that pretreatment of mice with eugenol, a methoxyphenol component of clove oil with anti-inflammatory and antioxidant properties, prevented the changes in lung mechanics, pulmonary inflammation, and alveolar collapse elicited by acute exposure to DEP [45].

The statins are hydroxy-methyl-glutaryl-CoA reductase inhibitors, broadly used in the treatment of hyperlipidemia. They play a key role in the primary and secondary prevention of atherosclerotic heart disease and stroke. Moreover, they have been reported to have potential benefits for a variety of other cardiovascular and noncardiovascular diseases, including cancer, respiratory and neurological disorders [46, 47]. Interestingly, Ferraro and coworkers [48] reported that residual oil fly ash (ROFA) and Urban Air Particle (UAP) from Buenos Aires produced an acute pulmonary injury in mice, characterized by a neutrophilic inflammation, a rise in O_2^- generation, and production of the proinflammatory tumour necrosis alpha (TNFα) cytokine. Simvastatin pretreatment had no significant effect per se on any of these biomarkers but prevented the pulmonary cytotoxicity and inflammation induced by ROFA and UAP. More recently, Miyata and coworkers [49] found that pulmonary exposure to PM_{10} in rabbits accelerated the turnover of polymorphonuclear leukocytes (PMNs) by shortening their transit time through the marrow. Interestingly, they found that lovastatin dampens these systemic responses by decreasing the levels of PM_{10}-induced circulating mediators (IL-6), thereby suppressing the bone marrow stimulation. The effect of statins was predominant on PMNs in the postmitotic pool as evident by the use of 5′-bromo-2′-deoxyuridine (BrdU/G3). Interestingly, statins also reduced the retention of these newly released PMNs in the lung tissues. These results corroborate the previous finding from the same research group reporting that PM_{10} particles induced systemic inflammatory responses characterized by an increase in systemic proinflammatory mediators such as IL-6 [50].

The metabolism of L-arginine plays an important homeostatic role in the airways, through synthesis of the bronchodilating molecule, nitric oxide (NO), from L-arginine, by the nitric oxide synthase (NOS) isozymes. The arginase isozymes (arginases 1 and 2) convert L-arginine into L-ornithine and urea and thus compete with the NOS isozymes for substrate. Arginase overexpression contributes to airways hyperresponsiveness in asthma, and its expression is further augmented in cigarette smoking asthmatics [51]. It has been recently reported that arginase is upregulated following exposure to O_3 and concentrated ambient particles in murine models of asthma and contributes to the pollution-induced exacerbation of airways responsiveness [52].

The question, whether a diet challenge increases the inflammatory response in the alveolar and the blood compartment in response to carbon nanoparticles (CNP) was investigated by Götz and coworkers [53]. In their study, mice were fed a high-caloric carbohydrate-rich or a fat-rich diet for six weeks and were compared to mice kept on a purified low fat diet, respectively. Bronchoalveolar lavage (BAL) and blood samples were taken 24 h after intratracheal CNP instillation and checked for cellular and molecular markers of inflammation. The authors reported an increase in BAL proinflammatory factors in high-caloric groups and reductions in serum concentrations of anti-inflammatory factors in fat-rich group. They concluded that extended feeding periods, leading to manifest obesity, are necessary to generate an increased susceptibility to particle-induced lung inflammation, although the diet challenge already was efficient in driving proinflammatory systemic events.

Barlow and coworkers [54] assessed the effects of intratracheally instilled PM_{10} collected from London on macrophage clearance in rats *ex vivo*. These authors concluded that acute PM_{10} exposure has an effect on macrophage phagocytosis and chemotaxis that may be deleterious to particle clearance within the alveolar region of the lung. The decrease in chemotactic ability may represent one mechanism that promotes inflammation after increases in ambient PM levels. They also concluded that further investigation is warranted to determine the effects of chronic PM_{10} exposure on macrophage clearance mechanisms.

NPs induce inflammatory responses and oxidative stress but may also have immune-suppressive effects, impairing macrophage function and altering epithelial barrier functions. The question related to whether exposure to NP may increase the risk of pulmonary infection has been recently investigated [55]. It has been demonstrated that Cu NP exposure impaired host defense against bacterial lung infections and induced a dose-dependent decrease in bacterial clearance [55]. Moreover, it has been demonstrated that acute exposure to DEP by inhalation exacerbates lung inflammation induced by lipopolysaccharide [56].

In an interesting study, the impact of pulmonary exposure to carbon black NP on emphysematous lung injury induced by porcine pancreatic elastase (PPE) was investigated in mice [57]. It has been demonstrated that carbon black NP exacerbates PPE-induced pulmonary inflammation and emphysema. This enhancement may be mediated, at least partly, via the increased local expression of proinflammatory molecules.

TiO_2 nanoparticles have several industrial applications, and, as such, also have different sizes, shapes, chemistry, and crystalline structures [58, 59]. TiO_2 occurs in four crystalline polymorphs of which rutile and anatase are most common [60]. Rutile is considered as a more inert form, whereas anatase is an active form of TiO_2. Anatase and rutile TiO_2 particles, delivered at similar surface area doses, increased release of lactate dehydrogenase, interleukin-8, and reactive oxygen species, as well as depressed mitochondrial activity in dissimilar patterns in cultured human epithelial cells [61].

In vivo, it was observed that ultrafine anatase TiO_2 particles produced increases in bronchoalveolar lavage inflammatory indicators, cell proliferation, and histopathology compared to ultrafine rutile TiO_2 particles [62]. However, with both crystalline forms of TiO_2 particles, pulmonary effects were observed at 24 h and resolved by one week after exposure [62]. Furthermore, it has also been demonstrated that the intratracheal instillation of rutile TiO_2 nanorods caused upregulation of lung and systemic inflammation and triggered platelet aggregation [63].

TiO_2-based photocatalysis has attracted extensive interest because of its great advantages in the complete mineralization of organic pollutants in waste water and air [64, 65]. As a popular photocatalyst, TiO_2 has been widely studied because of its various merits, such as optical-electronic properties, low cost, and chemical stability. Characteristics of TiO_2 nanoparticles can be modified by several methods to improve their performance. In this context, TiO_2 nanorods are doped with iron in order to increase their photocatalytic activity [63, 64]. It has been recently demonstrated that exposure to SiO_2-coated rutile TiO_2 nanoparticles ($cnTiO_2$) caused pulmonary neutrophilia, increased expression of tumor necrosis factor-alpha (TNFα) and neutrophil-attracting chemokine CXCL1 in the lung tissue. Uncoated rutile and anatase as well as nanosized SiO_2 did not induce significant inflammation [66]. More recently, pulmonary exposure to well-characterized rutile Fe-TiO_2 promotes pulmonary and systemic inflammation and oxidative stress. It also enhances thrombotic potential, heart rate, and systolic blood pressure (SBP) and induces hepatotoxicity. Moreover, rutile Fe-TiO_2 showed direct toxicity on human lung cancer cells NCI-H460-Luc2 and human hepatoma cells HepG2 [67].

3.1.2. Subacute and Chronic Effects. It has been demonstrated that rats exposed for 6 months to urban air pollution developed secretory cell hyperplasia in the airways and ultrastructural ciliary alterations of the epithelium of the airways, suggesting that chronic exposure to urban levels of air pollution may cause respiratory alterations [68]. Moreover, rats submitted to prolonged exposure to low levels of air pollution experienced deteriorated respiratory defenses against infectious agents [69]. Recently, it has been reported that intranasal instillation of DEP over 60 days increased the expression of Muc5ac in the lungs and the acid mucus content in the nose compared with the 30-day treatment. Moreover, DEP exposure enhanced the total leukocytes in the BAL and the nasal epithelium thickness compared to saline-treated control group [70].

Chronic exposure to $PM_{2.5}$ resulted in prominent inflammatory responses in the lung typified by increased levels of oxidized phospholipid derivatives as well as a systemic inflammatory response [71]. In a subsequent study, the same group has extended some of their observations and reported that exposure to $PM_{2.5}$ resulted in increased T-cell infiltration and increased activation of T-effector cells (evidenced by an increase in $CD4^+CD44^+CD62L^-$ and $CXCR3^+$ T cells in the lungs) and suggests a phenotypic switch to a Th1/Th17 phenotype in lung Teff cells. These results have important implications for how $PM_{2.5}$ may detrimentally modulate pulmonary and systemic immune responses [72].

Chronic obstructive pulmonary disease (COPD) is characterized by not fully reversible airflow obstruction that is usually progressive and associated with an abnormal inflammatory response of the lung to noxious particles or gases. The major etiological factor for COPD is chronic oxidative stress as a result of long-term smoking, use of biomass fuels, and air pollution exposure [73]. Lopes and coworkers recently reported a study in which the effects of chronic exposure (2 months) to ambient levels of PM on development of protease (papain) induced emphysema and pulmonary remodeling were investigated in mice [74]. They found that mean linear intercept and the total amount of collagen fibers in parenchyma were significantly greater in the lungs of mice that were treated with papain and exposed to ambient particles compared to those mice treated with papain and exposed to filtered air for 2 months. These increases in destruction of lung parenchyma and in lung collagen content observed only in the group of mice treated with papain and exposed to ambient particles were associated with an increase in the amount of 8-isoprostane expression in lung tissue, suggesting that the increase in oxidative stress is a possible mechanism to explain these alterations [74].

Different types of NPs can cause various inflammatory reactions in the lung. In mice lungs, the toxicity of single-wall carbon nanotube (SWCNT) in causing epithelioid granulomas and interstitial inflammation 7 and 90 days after intratracheal instillation has been shown to be greater as compared with other NPs, like carbon black or quartz particles [75]. However, the significance of the SWCNT-induced inflammation has been a matter of scientific debate. Initially it has been reported that intratracheally instilled SWCNT in rats causes discrete granulomas that were not dose-responsive, and an absence of signs of inflammation in BAL suggested the possibility that large agglomerates of SWCNT caused the granulomas [76]. A second study in rats, using SWCNT aspiration, also reported slight change in the differentials of BAL and a relative lack of histopathologic evidence of inflammation [77]. Studies in mice demonstrated significant inflammation, confirmed that SWCNT-induced inflammation was often granulomatous, and, most importantly, demonstrated that inflammation was present whether the SWCNTs were inhaled or aspirated [75, 78]. It was concluded that SWCNT inhalation was more effective than aspiration in causing inflammatory response, oxidative stress, collagen deposition, and fibrosis as well as mutations of K-ras gene locus in the lung of C57BL/6 mice [79]. Similarly to SWCNT, multiple wall carbon nanotube (MWCNT) exposures by inhalation at concentrations of 5 mg/m^3 or less for 14 days produced slight evidence of pulmonary inflammation but suppressed T-cell-dependent immune functions [80]. However, the intratracheal instillation of shorter MWCNT failed to show the occurrence of inflammation or fibrosis [81]. Recently, it has been demonstrated that inhalation of MWCNTs for up to 13 weeks caused granulomatous inflammation and pleural thickening at exposure concentrations greater than 6 mg/m^3. However, influx of inflammatory cells

in BAL fluid and interstitial fibrosis wereas demonstrated at exposures above 0.4 mg/m^3 [82].

Pulmonary inflammation caused by NP may also result in changes in membrane permeability, which in turn can result in particle translocation beyond the lung and affecting cardiovascular system [83]. Indeed, it has been shown that NPs have the potential to enter the brain [84] and blood circulation [85, 86] and subsequently other major organs causing inflammation and oxidative stress in these organs.

3.2. Extrapulmonary Effects of Particles

3.2.1. Possible Mechanisms Involved. Despite the consistency of the epidemiologic observations, the pathophysiological mechanisms linking air pollution to adverse cardiovascular events remain unclear. There are three primary hypotheses that are being investigated to explain the extrapulmonary effect of NP [87, 88], and in Figure 3, we summarize the main mechanisms proposed for the systemic effects. The first one relates the effect of particles to their ability to impact the autonomic nervous system. Studies showed that particulate air pollution exposure is associated with rapid changes in autonomic nervous system balance, favoring sympathetic nervous system activation and parasympathetic withdrawal leading to changes in the pattern of breathing, heart rate, and heart rate variability. Decreased heart rate variability indicates the existence of a state of cardiac autonomy dysfunction and is a risk factor for sudden cardiac death because of arrhythmias [89]. The mechanisms responsible for the increase of the sympathetic drive remain unclear but may involve activations of pulmonary neural reflex arcs and direct effects of pollutants on cardiac ion channels [89]. Inhaled particles may affect the cardiovascular system through inflammatory mediators produced in the lungs and released into the circulation [87, 88]. It has been suggested that inhaled particles may lead to systemic inflammatory response through the release of IL-6, TNFα or histamine, and oxidative stress within the lungs and/or systemically [87, 88].

Moreover, several studies have shown that nanoparticles, owing to their small size, could avoid normal phagocytic defenses in the respiratory system and gain access to the systemic circulation and therefore to different extrapulmonary sites [85, 86, 90–93]. The UFP can pass from the lungs into the blood circulation in hamsters [86]. Others [91–94] have also reported extrapulmonary translocation of UFPs after intratracheal instillation or inhalation in other animal species. However, the amount of UFPs that translocated into blood and extrapulmonary organs differed amongst these studies. It has also been shown that, following intranasal delivery, polystyrene microparticles (1.1 μm) can translocate to tissues in the systemic compartment [95]. Recent studies [96–98] have provided morphological data illustrating that inhaled particles are transported into the pulmonary capillary space, presumably by transcytosis. Recently, Elder et al. [91] demonstrated that the olfactory neuronal pathway represents a significant exposure route of central nervous system (CNS) tissue to inhaled UFPs. These authors showed that, in rats, which are obligatory nose breathers, translocation of inhaled nanosized particles along neurons is a more efficient pathway to the CNS than via the blood circulation across the blood-brain barrier. They speculated that given that this neuronal translocation pathway was also demonstrated in nonhuman primates, it is likely to be operative in humans as well [84, 91]. In humans, the literature on the translocation of UFPs from the lungs into the blood circulation is still conflicting [85, 99, 100]. However, given the deep penetration of nanoparticulate matter into the alveoli and close apposition of the alveolar wall and capillary network, such particle translocation seems plausible either as a naked particle or after ingestion by alveolar macrophages [98]. Naked particles have been reported to be taken up (and/or adsorbed) by erythrocytes [101] and can presumably be distributed to various organs. The distribution of radiolabelled ultrafine carbon particles, commonly known as "Technegas", has been investigated after their inhalation by nonsmoking healthy human volunteers [85]. The size of the individualized particles was in the order of 5 to 10 nm, as we confirmed by electron microscopy of the particles. Radioactivity, which was largely particle-bound, as assessed by thin layer chromatography, was detected in blood already after 1 minute, reaching a maximum between 10 and 20 min-, and remaining at this level up to 60 min. Gamma camera images showed substantial radioactivity over the liver and other areas of the body. The presence of radioactivity in the liver is compatible with an accumulation of particles in Kupffer cells, as is known to occur with colloidal particles [102]. More recently, Péry and coworkers [103] developed a physiologically based kinetic model for (99 m) technetium-labelled carbon nanoparticles (Technegas). The model was designed to analyze imaging data obtained from the study of Nemmar and coworkers [85]. It included different translocation rates and kinetics for free technetium and small and large technetium-labelled particles. The authors concluded that the percentage of small particles able to translocate was estimated at 12.7% of total particles, whereas the percentage of unbound technetium was estimated at 6.7% of total technetium [103].

Nurkiewicz and coworkers have studied the effects of inhaled particles and nanoparticles on systemic microvascular endothelium. First, they demonstrated that rats exposed to ROFA or TiO_2 presented a reduction in their capacity to respond to the Ca^{2+} ionophore A23187, which induce arteriolar dilatation [104]. In other studies, the same group has shown that exposure to ROFA or TiO_2 NP, by instillation or inhalation, induce systemic microvascular dysfunction [105, 106]. They also found that the nitric oxide (NO) signaling seems to be involved in the endothelial systemic effects of the particles [107].

3.2.2. Acute Effects. Several studies demonstrated that exposure to UFP or DEP caused pulmonary inflammation and prothrombotic events in ear vein of rats or femoral vein and artery of hamsters [108–112]. Mutlu and coworkers [113], showed that exposure to PM triggers IL-6 production by alveolar macrophages, resulting in reduced clotting times, intravascular thrombin formation, and accelerated carotid artery thrombosis [113]. The occurrence of oxidative stress in

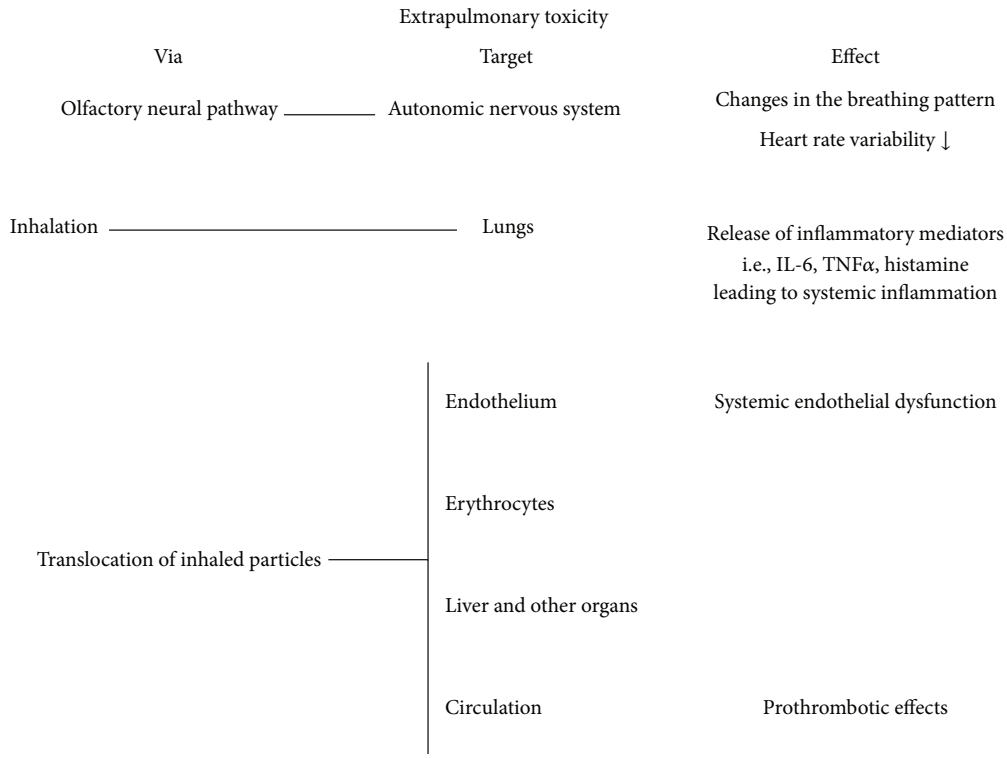

Figure 3: Summary of the main systemic effects associated with particle exposure and the possible mechanisms related to those effects.

the DEP-induced acute thrombotic tendency in pial cerebral venules, activation of circulating blood platelets, and lung inflammation have been reported in mice [25]. Moreover, the same authors showed that the antioxidant pretreatment with cysteine prodrug L-2-oxothiazolidine-4-carboxylic acid prevented DEP-induced inflammatory and the resulting thrombotic complications [25]. More recently, the acute (4 and 18 h) effects of DEP on pulmonary and cardiovascular parameters and the protective effect of thymoquinone were investigated in mice [41]. Four h after DEP administration, there were no significant changes in the cells in BAL, lung histology, or pulmonary function test. However, at 18 h after exposure, both lung inflammation and pulmonary function were significantly affected. Conversely, at both 4 h and 18 h, DEP caused systemic inflammation characterized by leukocytosis, increased IL-6 concentration, and reduced SBP. DEP reduced platelets number and aggravated pial arteriole thrombosis. The addition of DEP (0.1–1 μg/mL) to untreated blood induced platelet aggregation. The cardiovascular effects observed at 4 h after DEP exposure did not appear to result from pulmonary inflammation but possibly from the blood translocation of DEP and/or their associated components [41]. However, at 18 h, DEP-induced significant changes in pulmonary and cardiovascular functions and caused lung inflammation. Pretreatment with thymoquinone effectively prevented DEP-induced cardiorespiratory toxicity [41].

It has been reported that TNFα is a strong agonist for plasminogen activator inhibitor 1 (PAI-1) expression and has been found to play an important role in PAI-1 regulation in a variety of diseases. In a mouse endotoxemia model, TNFα has been found to contribute to the lipopolysaccharide-induced PAI-1 expression [114]. Budinger et al. [115] demonstrated that ambient PM-induced upregulation of PAI-1 disappeared upon treatment of mice with a TNFα inhibitor [115]. In line with the later findings, it has been recently demonstrated that repeated exposure to DEP-induced airway inflammation and hyper-reactivity, systemic inflammation, increased SBP, and accelerated coagulation. TNFα production was increased both in BAL and plasma. Pretreatment with curcumin significantly inhibited the release of TNFα and prevented the respiratory and cardiovascular effects of DEP [116].

An important aspect of the epidemiological associations between air pollution and either morbidity or mortality is that the acute adverse effects appear to be most marked in people with preexisting compromised cardiovascular function, such as hypertension or diabetes [89]. To give credibility for these observations, several experimental studies have been designed to test whether and to what extent the effects of particulate air pollution are aggravated, using an animal model of angiotensin II-induced hypertension. Indeed, exposure particulate matter with diameter ≤ 2.5 μm ($PM_{2.5}$) was found to potentiate angiotensin II-induced hypertension [117, 118]. In addition, $PM_{2.5}$ increased angiotensin II-induced cardiac hypertrophy, collagen deposition, and cardiac and vascular RhoA activation, suggesting that cardiovascular health effects are indeed the results of particulate air pollution exposure [118]. Evidence for exacerbation of thrombotic but not respiratory events was also reported in angiotensin II-induced hypertension in mice [119, 120]. With respect to diabetes mellitus, it has been shown that DEP equally increased

airway resistance and caused infiltration of inflammatory cells in the lung of both diabetic and nondiabetic mice. However, the occurrence of oxidative stress, the presence of lung apoptotic cells, and the increase of total proteins, albumin and TNFα in BAL fluid were only seen in DEP-exposed diabetic mice suggesting an increased respiratory susceptibility to particulate air pollution [121]. Moreover, the same research group has shown that systemic and coagulation events are aggravated by diabetes in mice acutely exposed to DEP [122]. These authors stated that they may be relevant to the exacerbation of cardiovascular morbidity accompanying particulate air pollution in diabetic patients.

Novel evidence that pulmonary deposition of DEP potentiates the renal, systemic, and pulmonary effects of cisplatin-induced acute renal failure (ARF) has been recently reported by Nemmar and colleagues [123]. These findings highlight the importance of environmental factors such as particulate air pollution in aggravating ARF.

Several studies have showed that nanoparticles, owing to their small size, could avoid normal phagocytic defenses in the respiratory system and gain access to the systemic circulation and therefore to different extrapulmonary sites [83, 84, 90–93, 103, 123]. To specifically determine the effect of translocated particles, it has been recently demonstrated in both normotensive and spontaneously hypertensive rats that 24 h following their systemic administration, DEP affected blood pressure and caused pulmonary inflammation assessed by BAL [124, 125]. In a subsequent study in rats, it has been reported that i.v. administration of DEP (0.02 mg/kg) caused acute systemic effects mainly at 6 h and 18 h but not at 48 h or 168 h following particle exposure. While DEPs were found in lungs, heart, liver and kidneys, the histopathological changes were only seen in the lung. This implies that, at the dose and time-points investigated, DEP can cause inflammation in the lungs but not in other organs, suggesting that pulmonary tissue is the predominant site for inflammation based on the mode of delivery of DEP in this study [126]. Furthermore, it has been shown that ultrafine TiO_2 induces acute lung inflammation after i.p. administration and exhibits additive or synergistic effects with LPS, at least partly, via activation of oxidant-dependent inflammatory signaling and the NF-kappaB pathway, leading to increased production of proinflammatory mediators [127]. Geys et al. [128] have investigated the toxicity of quantum dots which have numerous possible applications for *in vivo* imaging. QDs caused marked vascular thrombosis in the pulmonary circulation, especially with carboxyl QDs. QDs were mainly found in lung, liver, and blood. Thrombotic complications were abolished, and P-selectin was not affected by pretreatment of the animals with heparin.

3.2.3. Subacute and Chronic Effect. Akinaga and coworkers [129] reported a study in which mice were continuously exposed, since birth, in two open-top chambers (filtered and nonfiltered for airborne particles $\leq 0.3\,\mu$m) placed 20 m from a street with heavy traffic in downtown Sao Paulo, 24 h per day for 4 months. They found that air pollution induced mild but significant vascular structural alterations in normal individuals, presented as coronary arteriolar fibrosis and elastosis.

PM has been shown to cause significant decreasing patterns of heart rate, body temperature, and physical activity in mice lacking apolipoprotein ($ApoE^{-/-}$) over 5 months of exposure to concentrated ambient PM, with smaller and nonsignificant change for C57 mice [130].

Sun and coworkers demonstrated that $ApoE^{-/-}$ mice exposed to concentrated regional northeastern $PM_{2.5}$ for 6 months (6 h/day for 5 day/week) in conjunction with high-fat chow potentiated plaque development markedly increased vascular inflammation ($CD68^+$ macrophage infiltration and inflammatory nitric oxide synthase (iNOS) expression) and vessel wall markers of oxidative stress [131]. Plaque progression was accompanied by alterations in vasomotor tone, including decreased endothelial-dependent vasodilatory function and heightened vasoconstriction to adrenergic stimuli. The same research group confirmed their findings by another set of experiments which was performed using an identical protocol of exposure but involving an $apoE^{-/-}$ model and a double-knockout (DK) model of $ApoE^{-/-}$ and low-density lipoprotein (LDL) receptor deficient mice (DK mice) to concentrated ambient $PM_{2.5}$ for 6 h a day for 5 days/week for up to 5 months. Although quantitative measurements showed that $PM_{2.5}$ exposure increased atherosclerotic lesions in the $apoE^{-/-}$ mice, changes produced by $PM_{2.5}$ in DK mice were not statistically significant [132]. In subsequent set of experiments, it has been shown that chronic ambient exposure to $PM_{2.5}$ increased tissue factor expression in macrophages and smooth muscle cells in atherosclerosis [133]. They also reported specific recruitment of monocytes into microcirculatory tissue niches (i.e., adipocytes) in response to long-term $PM_{2.5}$ exposure [134]. These experiments suggest a key role for $PM_{2.5}$ in the activation and mobilization of innate immune cell populations.

Long-term cardiovascular effects of inhaled nickel hydroxide NPs (nano-NH) in hyperlipidemic, $ApoE^{-/-}$ mice were investigated by Kang and coworkers [135]. Mice were exposed to nano-NH at either 0 or 79 μg Ni/m^3, via a whole-body inhalation system, for 5 h/day, 5 days/week, for either 1 week or 5 months. Inhaled nano-NH induced significant oxidative stress and inflammation in the pulmonary and extrapulmonary organs, indicated by upregulated mRNA levels of antioxidant enzyme and inflammatory cytokine genes; increased mitochondrial DNA damage in the aorta; significant signs of inflammation in BAL fluid; changes in lung histopathology; and induction of acute-phase response. In addition, after 5-month exposures, nano-NH exacerbated the progression of atherosclerosis in $ApoE^{-/-}$ mice [135].

Emmerechts and coworkers have investigated how continuous traffic-related air pollution exposure affects haemostasis parameters in young and old mice. Young (10 weeks) and old (20 months) mice were placed in an urban roadside tunnel or in a clean environment for 25 or 26 days. They found in old mice that subchronic exposure to polluted air raised platelet numbers, von Willebrand factor, soluble P-selectin, and microvesicles, collectively substantiating

a further elevation of thrombogenicity, already high at old age [136].

There is a potential for neurodegenerative consequence of particle entry to the brain. Histological evidence of neurodegeneration has been reported in both canine and human brains exposed to high ambient PM levels, suggesting the potential for neurotoxic consequences of PM entry [137, 138]. PM-mediated damage may be caused by the oxidative stress pathway which can enhance the susceptibility for neurodegenerative diseases. The relationship between PM exposure and central nervous system degeneration can also be detected under controlled experimental conditions [137, 138]. Morphometric analysis of the central nervous system of $ApoE^{-/-}$ mice exposed to concentrated ambient air pollution showed that the brain is a critical target for particulate air pollution exposure and implicated oxidative stress as affecting factor that links PM exposure and susceptibility to neurodegeneration [137, 138]. Further experimental studies are needed to clarify the effect and mechanisms underlying the neurotoxicity of particulate air pollution.

4. *In Vitro* Studies

In vivo models give a good insight of the toxic effects of particles, and considering the multiple interactions of different cell types in the lung, the complex responses are well documented, but the cellular mechanisms related to the specific responses become very difficult to clarify. In this regard, the *in vitro* models are used as a main tool to evaluate the cellular mechanisms related to the exposure to particles.

There are several approaches to evaluate the toxic effects of particles on cells that have been suggested or pointed as targets of PM and NP. Single cell cultures, cocultures, multiple cocultures, exposure under submerged conditions, and exposure under air-liquid interface are among the main strategies. We are discussing some of the most significant advances on the evaluation of PM *in vitro* toxicology. In Table 2, we summarize the most relevant *in vitro* evidence supporting the observed *in vivo* effects.

4.1. Particle Properties Linked to Primary Cell Interaction. In the lung, the particles may interact with the lung lining fluid and the epithelial cells. In addition the particles may be taken up by macrophages and other immune cells by phagocytosis or pinocytosis. The interaction of particles with the cellular plasma membrane and its receptors and ion channels may directly trigger a biological response. The important DEP-induced reactions often start from constituents leaking from the particles including metals and various PAHs, including derivatives like nitro-PAHs and various oxo-PAH (quinones). The relative position of such components on the particle is most likely of importance since just adding back extracted components may result in less effects than the native particle exerts [139]. Furthermore, the combination of particle constituents like endotoxins and chemicals in organic fraction may elicit more than additive cytokine response effects [15]. On the other hand, with regard to genotoxic effect, the response will be higher in the extracts as more of the carcinogenic PAH will be available to the cells [140, 141].

Table 2: *In vitro* evidence that supports and provides plausible mechanisms for the *in vivo* observed effects induced by PM and NP.

In vitro evidence supporting the observed *in vivo* effects	
In vivo observed effect	*In vitro* evidence
Oxidative stress	ROS increases via NADPH-oxidase in lung epithelial cell exposed to PM.
Local and systemic inflammation	Secretion of IL-1b, IL-6, IL-8, TNFa, MCP-1, and so forth, by lung cells, macrophages, and cocultures.
Hyperplasia	Proliferative stimuli induced by extracts of DEP components.
COPD	Increased cytotoxicity on exposed cell cultures.
Systemic and endothelial dysfunction	Endothelial cell activation by direct contact with particles or indirectly induced in cocultures where pneumocytes, macrophages, and other cell are exposed.
Particle translocation	Changes in the TEER values related to tight junctions Macrophage-dendritic transepithelial cells network alterations in the GJIC.

Although particle uptake in epithelial cells has also been reported to occur [142], most biological responses triggered by particles in these cells do not seem to depend on particle uptake [143]. Particles as such have been reported to trigger biological effects via acellular reactive oxygen species (ROS) formation. However, DEP-induced immune responses in A549 cells were reported to depend on activation of cellular ROS-formation via the NADPH oxidase [144]. Furthermore, emerging evidence suggests that particle constituents are able to bind to or otherwise activate various membrane and cytosolic receptors. Obviously, both AhR-ligand binding as well as reactive electrophilic PAH metabolites covalently binding to DNA are caused by chemical constituents released from the particle [143, 145].

4.2. In Vitro Studies with Implications to Various PM-Induced Cardiovascular Effects and Various Lung Diseases Including Cancer. As we have seen in previous sections, damage of the lung epithelial lining may have important implications with regard to pathogen diseases, asthma, and allergy. Direct or indirect induced chronic inflammation is also considered to be central element in various cardiovascular diseases, COPD, and a likely part of cancer development.

Regarding the latter, there is growing evidence suggesting that air pollution exposure increases risk of lung cancer [146, 147]. The components generally considered being of most interest for such effects are particles in the ultrafine ($PM_{0.1}$) and fine fraction ($PM_{2.5}$) including DEP and wood smoke particles (WSP) [148]. However, more recent *in vitro* evidence indicates that also the larger PM_{10} particles might play a role in cancer development through mechanisms

such as damage to the lung epithelial cells, disruption of tight junction and gap junction, effects of cell proliferation including cytotoxicity, release of inflammatory mediators like chemokines and cytokines, changes in gene expression via receptor binding, and various forms of cellular DNA damage, including epigenetic changes. It is also possible to study *in vitro* effects of particle exposure on the later stages of cancer development like chromosomal instability and cell migration, which are important parts of tumor promotion and metastasis. However, we are not aware of that such studies have been published.

4.2.1. Tight Junction. Tight junctions between the epithelial cells represent an important barrier for the body protecting the rest of tissue and organs from exposure to various pathogenic intruders like virus, bacteria, fungi, air pollution PM, and various particle-bound allergens. Exposure to such components can result in infections and allergic/asthmatic reactions. If combined with PM exposure, the end result may be more chronic inflammatory reactions, which is considered to be an important part of many pulmonary diseases including COPD and cancer development. Geys and coworkers showed that the transepithelial electrical resistance (TEER) is linked to the tight junctions and the correlation between the TEER value and the translocation of particles through cellular monolayers [149]. Using an *in vitro* triple cell culture model consisting of human epithelial cells (16HBE14), monocyte-derived macrophages and dendritic cells, it was recently demonstrated that macrophages, and dendritic cells create a transepithelial network between epithelial cells to capture antigens without disrupting the epithelial tightness [150]. Using a similar model, Lehmann and coworkers [151] observed that a high concentration of DEP (NIST 2975, 125 μg/mL) can modulate the tight junction occluding mRNA in the cells of the epithelial defense system. In this connection, it is also interesting to note that NIST 2975 DEPs have been reported to increase the release of metalloproteinase MMP-1 from human lung epithelial cells (A549 and NCI-H292). MMP-1 is involved in the degradation of collagen and can thus damage the lung epithelial barrier [144]. These findings suggest that DEP can contribute to structural changes in the epithelial lining with inflammatory and possible carcinogenic implications.

4.2.2. Gap Junction Intercellular Communication (GJIC). GJIC is one way of intercellular exchange of low molecular weight molecules between adjacent cells. Chemically induced alterations in this type of communication have been found to result in abnormal cell growth and behavior and is considered to be an interesting assay for *in vitro* studies of chemicals that may act as tumor promoters [152]. Bay/bay-like regions of PAH have been reported to be potent inhibitors of GJIC [153]. Interestingly several high molecular weight PAHs with known strong carcinogenic properties possessed only weak (dibenzopyrenes) or no inhibition potency (dibenzofluoranthenes, naphtho[2,3-a]pyrene, and benzo[a]perylene) [154]. Furthermore, the PAH-induced inhibition of GJIC occurs in the absence of PAH metabolism and aryl hydrocarbon receptor (AhR) binding [155]. More probably, unmetabolized PAH changes GJIC through direct interaction with unknown factor(s) in the cellular membrane. In line with this, DEP has been reported to inhibit GJIC [156–158]. The GJIC-effects of a fractionated DEP extract were found to be due to components in the polar fraction, while the less polar nitro-PAH fraction showed the strongest mutagenic potential (Ames test) [158].

4.2.3. Cell Proliferation and Cytotoxicity. Measuring cellular proliferation and cytotoxicity has been used as one of the primary toxicity tests for particulate matter [15, 16, 159]. With relatively simple methods, differences in the intensity of cytotoxicity have been demonstrated. Equal masses of urban PM collected in different cities, or within a large city, associated with different sources presented differences in cellular proliferation and cytotoxicity [16, 17]. These results were of main interest to evaluate the role of different components of the toxic effects of particles and therefore identifying components such as endotoxin, organic carbon, and some elements, as the components associated to the cytotoxicity [14, 16, 17].

Increased cytotoxicity is often followed by proliferative stimuli considered to be of great importance for both fixation of the primarily DNA lesion as well as for tumor promotion phase. A number of compounds in DEP are cytotoxic; other compounds are known to be DNA damaged thus resulting in G1-arrest and/or accumulation in S-phase due to reduced DNA synthesis [160, 161]. However, DEPs also include compounds which may affect cell proliferation in other ways. Two nitrophenols isolated from DEP 3-methyl-4-nitrophenol (4-nitro-m-cresol, PNMC) and 4-nitro-3-phenylphenol (PNMPP) have been reported to have estrogenic and antiandrogenic activities. Most interestingly, proliferation of MCF-7 cells was stimulated by PNMC, PNMPP, and estradiol-17beta and the antiestrogens 4-hydroxytamoxifen and ICI 182,780 inhibited the proliferation [162]. Crude extract of DEP exhibited both estrogenic and antiestrogenic activities. Estrogenic activity of crude extract and some fractions was induced through estrogen-receptor- (ER-) mediated pathways. In particular, the acid polar fraction of DEPs, which contains phenols, induced high levels of estrogenic activity compared to other fractions [163].

An important part of the known carcinogens found on air pollution particles is various PAHs. Some of these have also been reported to have mitogenic potency. More specifically, weak mitogenic effects have been reported, suggested to occur via increased Ca^{2+}, activation of epidermal growth factor receptor (EGFR) and insulin receptor [164–167]. Furthermore, disruptions of contact inhibition via AhR-dependent induction of JUN-D/cyclin [168] have been observed. This type of effect obviously would also result in increased cell proliferation. Most interestingly, it is known for a while that several of these have so-called "stealth properties" [169–171]. This is a property by which reactive metabolites are able to covalently bind to the DNA without easily being detected by the cells defense system. More specifically, some reactive PAH metabolites bind to DNA without triggering a G1-arrest. An

increase in p53 seems to be induced but not a p21waf1/cip1-inhibition of p53 transcriptional activity. Furthermore, some PAH seems to induce mdm2 which may reduce the p53 activation [172, 173]. AhR-dependent inhibition of E2F1-dependent apoptosis [174] reduced p53 nuclear translocation, stimulation of cell survival signals, and inhibition of DNA damage induced apoptosis have been reported after exposure to certain PAH [175, 176]. Most importantly, such chemicals would change the balance between cell death and cell survival and cell proliferation following a DNA damaging event. If not compensated with increased DNA repair, the end result would necessarily be increased formation of mutation. Furthermore, reactive metabolites that react to a larger degree with DNA than other macromolecules in the cells will have a higher mutagenic potential [177, 178]. In line with this, it has recently been reported that several environmental pollutants including the carcinogenic PAH benzo[a]pyrene may change plasma membrane characteristics, thereby altering cell physiology and the balance between life or death of a cell [179].

4.2.4. Inflammatory Mediators. Several cytokines have been found to function as proliferation and/or survival factors, for example, IL-6, IL-8, and IL-1β [180] and which may have implications for several lung diseases including cancer development. Thus, a number of studies *in vitro* have elucidated the inflammatory potential of various air pollution particles [181]. In studies with BEAS-2B bronchial epithelial lung cells DEP from a pre year 2000 engine increased the release of chemokines such as IL-8 [182]; whereas EURO-4 DEP-induced typically IL-6 and IL-8, but also to a certain degree CCL5, CXCL10, and IL1β [139]. Increased CCL5 (RANTES) after DEP exposure (pre year 2000 engine) has also been reported by Hashimoto et al. [183]. Often the induced expression and release of pro-IL-1β found to be due to a combination of endotoxins and other particle components [184]. In general, oxidative stress is considered an important mechanism of particle-induced toxicity and inflammation [181] in addition to other pathways of particle effects. Direct ROS-formation by DEP may arise from enzymatic metabolism of organic compounds such as PAHs or directly [185, 186]. Possible mechanisms also include a direct activation of the membrane bound NADPH oxidase enzyme, inducing the formation of ROS near the plasma membrane [187]. A correlation between NADPH oxidase activation and proinflammatory response has been reported using both *in vitro* and *in vivo* systems exposed to air particles [188]. As seen typically in studies of air pollution collected from cities, there seems to be large seasonal differences in PM_{10} and $PM_{2.5}$ both with regard to chemical composition and their biological effects as measured as proinflammatory cytokine release and cytotoxicity [184]. The summer PM_{10} exhibited a higher proinflammatory potential, partly due to biological components such as LPS as also previously reported by others [189, 190]. Typically induced cytokines reported include IL-6, IL-8, and IL-1β. However, it should be emphasized that no simple mechanism exists that explains all cellular effects, and in some cases contradictory results have been observed for IL-6 and IL-8 [191]. Furthermore, oxidative stress alone seems to be insufficient to induce proinflammatory responses in lung cells, pointing also to other mechanisms [192, 193]. Moreover, the mechanisms of particle-induced toxicity are likely to change with increasing concentrations.

Of particular interest, recent studies show that DEP may induce Ca^{2+} influx through proteinase-activated receptor-2 (PAR-2) mediated activation of TRPV4 channels in human bronchial epithelial cells. This effect is probably linked to IL-8 responses in bronchial epithelial cells induced by multiple compounds found in ambient air [194]. Studies also suggest that DEP exposure activates EGFR signaling [194]. The activation of EGFR signaling through cleavage and release of membrane bound transforming growth factor (TGF-α) by the metalloproteinase TNFα converting enzyme (TACE or ADAM17) seems to be a universal mechanisms of IL-8 regulation in airway epithelial cells by multiple endogenous and exogenous compounds, including DEP and various air pollution components [194]. It is also possible the particle/DEP-linked formation of reactive metabolites more directly could interfere with various cell signaling pathways or effect organelles, thereby initiating inflammatory reactions.

The vascular endothelium plays a central role in the inflammatory process and cytokine production, and various cellular signaling pathways trigger this response. Considering the evidence that particulate matter can translocate from the lungs within few minutes after exposure [85], the inflammatory signal could reach the vascular endothelium by direct exposure to particles. In this regard, several studies have shown that PM and NP induce endothelial dysfunction after exposure [16, 195–198]. The expression of early (E-Selectin, P-Selectin) and late adhesion molecules (ICAM-1, VCAM-1, PECAM-1) was associated with the presence of endotoxin [199], the size of the particles [200], and the oxidative stress induced by the particles and nanoparticles [201, 202]. Despite the evidence provided by these studies, there is no certainty of the amount of particles that can translocate, and therefore, the experimental conditions of exposure are always of concern.

In vivo, the epithelial cells or macrophages, or any cell that is interacting with a particle, have an interaction with other cell types, and those interactions may exacerbate or inhibit the inflammatory response. Therefore, the single cell cultures have the limitation of not evaluating those interactions. Cocultures of two or more cell types may help to improve the *in vitro* studies. A study using multiple cell cocultures of human lung epithelial cells, macrophages, mast cells, and endothelial cells demonstrated that when cocultures were exposed, a stronger cytokine production was observed in comparison to the responses obtained on single culture [203]. These types of models help to evaluate if the first contact of PM or NP with relevant cells is enough to induce an endothelial activation that may lead to systemic effects. In this regard, a modification of the model described by Alfaro-Moreno et al., using a coculture where the endothelial cells and epithelial cells are seeded on both sides of a membrane, demonstrated that by exposing the epithelial cells, an activation of the endothelial cells was evident within 24 h of exposure [204].

It is interesting to note that inflammatory diseases like asthma and COPD have been suggested to confer an increased risk of lung cancer, although this implication may not be straightforward [199, 200]. The hypothesis is based on that the release of inflammatory mediators (chemokines and cytokines) like IL-1β directly or via increased cytotoxicity (release of DAMP molecules) may result in an increased number of neutrophils/macrophages in the lung. Thus, several *in vivo* studies on other chemicals have reported that the recruitment of such cells will result in increased release of ROS molecules that might exacerbate the increased toxicity and thereby amplify the inflammatory process. Augmented inflammation in a tissue will increase the oxidative/nitrosative stress and lipid peroxidation (LPO), thereby further generating excess ROS, reactive nitrogen species, and DNA-reactive aldehydes. Miscoding etheno- and propano-modified DNA bases are generated interalia by reaction of DNA with these major LPO products [201]. The resulting highly cytotoxic environment will also create surroundings that favor selection of cells with mutations in p53, making them more resistant to cell death [202]. Additional putative mechanisms include impaired or imbalanced DNA repair pathways. In this way, persistent oxidative/nitrosative stress and excess LPO are induced by inflammatory processes in a self-perpetuating process and cause progressive accumulation of DNA damage in target organs including the lung [201].

However, the role of particle-induced inflammation in lung cancer development is very complex. During the latest years, it is becoming increasingly clear that cytokines and chemokines can have a profound role in not only progression, but also rejection of tumors [205].

4.2.5. Changes in Gene Expression via Receptor Binding. Certain changes in phenotypes might give increased probability to development into cancer cells. Regarding exposure to urban air particles, it is well known that some of these like DEP and wood initiate various AhR responses [145, 161, 206]. This is explained by the fact that potent AhR ligands such as PAH and dioxins are released from the particles. The activation of the AhR results in increased metabolism of xenobiotics, and changes in the balance between several metabolic and detoxification pathways are often seen [177]. These types of changes may have important implications for the cells, as more or less reactive metabolites are central for cancer initiation, promotion and for inflammatory reactions. Furthermore, this receptor has also very important physiological functions that extend beyond specific metabolism of xenobiotic, including effects on proliferation, contact inhibition and migration, and immune regulation [145]. All these process may have important implication for cancer development.

4.2.6. Epigenetic Changes. Gene transcription is activated when specific CpG sites are demethylated and histones are acetylated, and, conversely, silenced when sites are methylated and histones deacetylated. Furthermore, in addition to oncogenes, tumor suppressors and miRNAs are the major regulators of signaling in the cancer phenotype [207, 208]. Thus, possible implications of air pollution particle-induced epigenetic changes should clearly be explored *in vitro* systems as these endpoints may become important biological markers for epidemiological studies in the future.

4.2.7. Genotoxicity. It is well documented that different types of particles, their extracts as well as single components attached have genotoxic effects in human and animal studies *in vivo* [209] as well as *in vitro*. After exposure of cells in culture to different types of PM, several studies have shown that cells may be arrested in various parts of the cell cycle [160, 161, 210, 211]. Most often, such effects have been linked to DNA damage. Various forms of DNA damage have been reported after exposure to PM. The DNA damage includes DNA single-strand breaks, alkali-labile single-strand DNA breaks, and various forms of oxidative DNA damage including oxidized guanines measured as 8-oxo-7,8-dihydroguanine (8-oxoGua) and lesions detected as formamidopyrimidine DNA glycosylase (fpg) sites by the comet assay [161, 205]. Often this type of damage is associated with the formation of micronuclei and chromosomal damage. In line with this, positive effects of DEP on chromosome aberration and sister chromatid exchange have been reported in V79 cells without any additional activation system added [212]. The organic extract of $PM_{2.5}$ was reported to generate DNA breakage and micronucleus formation using BEAS-2B cells as a model system. Testing of various fractions in comet assay with fpg in this system suggested a possible role of ROS and that aliphatic/chlorinated hydrocarbons, PAH/alkylderivatives, and nitro-PAH/ketones/quinones may be important causative agents of the genotoxic effects [213]. Furthermore, it should be noted that DEP-extractable organic matter (EOM) has been reported to have a substantial higher capacity than the individual classic carcinogenic PAH with regard to induce oxidative damage to DNA in HepG2 cells [214].

While many reports focus on DNA breaks and/or oxidative-DNA damage with regard to cancer development [209], others link the PM-induced genotoxic and carcinogenic effect to the "classic" carcinogenic PAH giving rise to DNA adducts, often analysed by the ^{32}P postlabelling study [214]. Such PAH needs to be metabolically activated to reactive, electrophilic metabolites that covalently bind to DNA. Both acellular as well as various cells *in vitro* are used. The adduct levels formed are linked to PAH levels in extracts, fractionated extracts, or single PAH compound tested separately [214]. The results from such studies indicate that most DNA adducts detected in cells incubated with extractable organic matter (EOM) from ambient air have their origin in the low concentrations of carcinogenic PAH representing a very low part of EOM total mass (0.03–0.17%; [199]). In general, the bulky DNA adducts are more often associated with high potency to form gene mutations, considered to be of particular important for the initiation phase of cancer development.

An important point in evaluating genotoxic potential is the use of a metabolic activation system with sufficient ability and capacity to activate these carcinogenic PAHs. Certain

types of lung epithelial cells (e.g., Clara and type II) *in vivo* have a relatively high level of CYP enzymes due to exposure to AhR ligands (various PAH, dioxins) linked to ambient air particles. Accordingly, several publications have shown DNA adducts, DNA breaks and oxidative DNA damage(s) after exposure to ambient particles [215–218]. Thus, lung epithelial cells will in the *in vivo* situation have a clear capacity to activate various carcinogenic compounds including PAH. However, in contrast, the various lung epithelial cell lines as well as primary lung cells from laboratory animals used *in vitro* have a much lower capacity to activate such compounds. Such cells are thus, not always, the best choice to use when testing for genotoxic effects of various ambient air particle types. Interestingly, some liver-derived cell lines seem to have a more interesting capacity to metabolic activated PAH somewhat more similar to human *in vivo* situation; although metabolic enzyme profile in liver will be different compared to lung. Such models have nevertheless been suggested to represent better *in vitro* models for investigating the genotoxic potential of complex mixtures containing PAH [214, 219]. Another important aspect is to use a test system that can detect the primary DNA damage of importance. This could include technique such as the ^{32}P postlabeling technique to detect the larger and bulky DNA adducts. In order to detect and evaluate DNA damaging constituents which causes smaller DNA adduct/and other DNA lesions, the comet assay with or without addition of fpg is a good supplement [220].

Although not presently in use, it is possible to test the capacity of particles and their extracts to transform epithelial cells *in vitro*, representing a test of both "initiating" as well as tumor "promoting" properties. In a transformation assay using BALB/c 3T3 cells, DEPs have reported to cause morphological transformation [212]. Similarly, it was reported that DEP and two related compounds, 1-nitropyrene (1-NP) and dibenzo(a,i)pyrene (DBP), are capable of transforming rat tracheal epithelial cells [221]. Various coculture systems also add important information to the problem of a "relevant metabolic activation model" when testing genotoxic effects of PM *in vitro*. In a recent study, results supporting the notion that highly reactive benzo[a]pyrene (B[a]P) derived metabolites produced within human alveolar macrophage could be transferred to a secondary target epithelial cell line were presented [222]. Such findings have in addition important *in vivo* implications when explaining possible mechanisms involved in ambient air induced lung cancer. By using DNA repair capacity *in vitro* many important aspects of the role of DNA repair in maintaining genetic stability and preventing carcinogenesis can be elucidated [223]. Furthermore, studies and analyses of polymorphisms of DNA repair genes involved in nucleotide excision repair (NER) may turn out to be useful biomarkers to identify individuals susceptible to DNA damage resulting from ambient air exposure [224]. Also the level of proteins involved in the DNA response like gamma-H2AX, p53, and p21 (WAF1) protein levels has been analyzed and linked to PM-induced genotoxic and cytotoxic effects [161, 225]. Most interestingly, it has been reported that ambient air PM greatly inhibits nucleotide excision repair (NER) for ultraviolet (UV) light and benzo[a]pyrene diol epoxide (BPDE) induced DNA damage in human lung cells. PM increased both spontaneous and UV-induced mutagenesis, suggesting that the carcinogenicity of PM may act through its combined effect on suppression of DNA repair and enhancement of DNA replication errors [226].

5. Conclusions

Urban air pollution consists of an extremely complex mixture of gaseous and particulate agents. The majority of published studies concur to the statement that whilst gaseous pollutants, such as ozone or SO_2, play a significant role, the unifying element of the adverse health effects of urban air pollution consists of respirable PM [1, 88]. Many studies using animal models have been performed to elucidate PM effects in different organs, in relation to different diseases. With respect to acute effects, most studies have focused on inflammatory responses, and relatively few studies have included more disease-specific responses, perhaps with the exception of studies on allergy-related responses. In contrast more studies on chronic effects have elucidated disease-related processes, such as DNA damage, lung parenchyma destruction, increased plaque volume in arteries, lung fibrosis, or granuloma formation. An increased focus on more direct disease-related parameters in models that closely resemble the human disease pattern would improve the usefulness of the *in vivo* models.

Since the *in vitro* models prove themselves to be most useful to study mechanistic responses, such as initiation events of inflammatory effects or genotoxicity, it would be of interest for the interpretation of results if the *in vivo* studies could also to a greater extent cover mechanistic effects, to discover a possible coherence of results with the *in vitro* studies. Whereas the relationship between some *in vitro* end points, particularly with respect to genotoxicity and indicators of cancer development and disease, has been established; with respect to other end points, this relationship has not been fully developed. Improved *in vitro* models that seek to cover this field need to be further developed.

The *in vitro* models have proven useful in studying the importance of a range of particle sizes and components. For example, evidence suggests that the ultrafine fraction of these particles shows more toxicity at equal mass concentrations compared to larger particles, because of their increased reactivity, surface area, and particle number on a mass basis. Furthermore, a coherence of certain *in vitro* cellular effects and responses in biopsies from human volunteers has been shown for the exposure to diesel exhaust particles [194, 227]. On the other hand, sometimes very high concentrations used in *in vitro* models suggest caution in the interpretation of *in vitro* results and again points to the development of more sensitive models.

Nanotechnology develops products with highly different physical and chemical properties, and they are also used in a variety of areas such as diagnosis, imaging, drug delivery, information, and communication technologies, and their extensive use in the consumer and industrial products is just

beginning to emerge [87]. Thus, in order to cope with such a variation of type of material and use, structure activity and *in vitro* studies will be of help [87].

The increased risk of respiratory and cardiovascular diseases requires additional toxicological studies to be performed and specific measures to be taken for environmental PM and newly developed engineered NP.

Acknowledgment

We want to thank Victor Montalvo for his assistance on preparing and designing the figures.

References

[1] R. D. Brook, S. Rajagopalan, C. A. Pope et al., "Particulate matter air pollution and cardiovascular disease: an update to the scientific statement from the american heart association," *Circulation*, vol. 121, no. 21, pp. 2331–2378, 2010.

[2] B. Nemery, P. H. M. Hoet, and A. Nemmar, "The Meuse Valley fog of 1930: an air pollution disaster," *The Lancet*, vol. 357, no. 9257, pp. 704–708, 2001.

[3] J. G. Townsend, "Investigation of the smog incident in Donora, Pa., and vicinity," *American Journal of Public Health*, vol. 40, no. 2, pp. 183–189, 1950.

[4] W. P. D. Logan, "Mortality in the London fog incident," *The Lancet*, vol. 261, no. 6755, pp. 336–338, 1953.

[5] M. R. Gwinn and V. Vallyathan, "Nanoparticles: health effects—pros and cons," *Environmental Health Perspectives*, vol. 114, no. 12, pp. 1818–1825, 2006.

[6] WHO air quality guidelines, global update. Report on a Working Group meeting, Bonn, Germany, WHO Regional Office for Europe, Copenhagen, Denmark, 2005, http://www.euro.who.int/document/e87950.pdf.

[7] A. Ibald-Mulli, H.-E. Wichmann, W. Kreyling, and A. Peters, "Epidemiological evidence on health effects of ultrafine particles," *Journal of Aerosol Medicine*, vol. 15, no. 2, pp. 189–201, 2002.

[8] "U.S. Environmental Protection Agency, Office of Air Quality Planning and Standards," Revisions to the ambient monitoring regulations: relevancy for the AIRNOW community, 2007.

[9] C. Xiong and S. K. Friedlander, "Morphological properties of atmospheric aerosol aggregates," *Proceedings of the National Academy of Sciences of the United States of America*, vol. 98, no. 21, pp. 11851–11856, 2001.

[10] P. Wåhlin, F. Palmgren, and R. Van Dingenen, "Experimental studies of ultrafine particles in streets and the relationship to traffic," *Atmospheric Environment*, vol. 35, no. 1, pp. S63–S69, 2001.

[11] A. Kocbach, Y. Li, K. E. Yttri, F. R. Cassee, P. E. Schwarze, and E. Namork, "Physicochemical characterisation of combustion particles from vehicle exhaust and residential wood smoke," *Particle and Fibre Toxicology*, vol. 3, article 1, 2006.

[12] R. M. Harrison and J. Yin, "Particulate matter in the atmosphere: which particle properties are important for its effects on health?" *Science of the Total Environment*, vol. 249, no. 1–3, pp. 85–101, 2000.

[13] S. Becker, L. A. Dailey, J. M. Soukup, S. C. Grambow, R. B. Devlin, and Y.-C. T. Huang, "Seasonal variations in air pollution particle-induced inflammatory mediator release and oxidative stress," *Environmental Health Perspectives*, vol. 113, no. 8, pp. 1032–1038, 2005.

[14] J. M. Veranth, T. A. Moss, J. C. Chow et al., "Correlation of *in vitro* cytokine responses with the chemical composition of soil-derived particulate matter," *Environmental Health Perspectives*, vol. 114, no. 3, pp. 341–349, 2006.

[15] I. Rosas Pérez, J. Serrano, E. Alfaro-Moreno et al., "Relations between PM_{10} composition and cell toxicity: a multivariate and graphical approach," *Chemosphere*, vol. 67, no. 6, pp. 1218–1228, 2007.

[16] C. Monn and S. Becker, "Cytotoxicity and induction of proinflammatory cytokines from human monocytes exposed to fine ($PM_{2.5}$) and coarse particles ($PM_{10-2.5}$) in outdoor and indoor air," *Toxicology and Applied Pharmacology*, vol. 155, no. 3, pp. 245–252, 1999.

[17] P. A. Steerenberg, L. Van Amelsvoort, M. Lovik et al., "Relation between sources of particulate air pollution and biological effect parameters in samples from four european cities: an exploratory study," *Inhalation Toxicology*, vol. 18, no. 5, pp. 333–346, 2006.

[18] E. Alfaro-Moreno, L. Martínez, C. García-Cuellar et al., "Biologic effects induced *in vitro* by PM_{10} from three different zones of Mexico City," *Environmental Health Perspectives*, vol. 110, no. 7, pp. 715–720, 2002.

[19] J. M. Soukup and S. Becker, "Human alveolar macrophage responses to air pollution particulates are associated with insoluble components of coarse material, including particulate endotoxin," *Toxicology and Applied Pharmacology*, vol. 171, no. 1, pp. 20–26, 2001.

[20] S. Becker, M. J. Fenton, and J. M. Soukup, "Involvement of microbial components and toll-like receptors 2 and 4 in cytokine responses to air pollution particles," *American Journal of Respiratory Cell and Molecular Biology*, vol. 27, no. 5, pp. 611–618, 2002.

[21] M. R. Wilson, J. H. Lightbody, K. Donaldson, J. Sales, and V. Stone, "Interactions between ultrafine particles and transition metals *in vivo* and *in vitro*," *Toxicology and Applied Pharmacology*, vol. 184, no. 3, pp. 172–179, 2002.

[22] M. Hassellöv, J. W. Readman, J. F. Ranville, and K. Tiede, "Nanoparticle analysis and characterization methodologies in environmental risk assessment of engineered nanoparticles," *Ecotoxicology*, vol. 17, no. 5, pp. 344–361, 2008.

[23] M. G. Perrone, M. Gualtieri, V. Consonni et al., "Particle size, chemical composition, seasons of the year and urban, rural or remote site origins as determinants of biological effects of particulate matter on pulmonary cells," *Environmental Pollution*, vol. 176, pp. 215–227, 2013.

[24] R. Quintana, J. Serrano, V. Gómez et al., "The oxidative potential and biological effects induced by PM_{10} obtained in Mexico City and at a receptor site during the MILAGRO Campaign," *Environmental Pollution*, vol. 159, no. 12, pp. 3446–3454, 2011.

[25] J. I. Levy, D. Diez, Y. Dou, C. D. Barr, and F. Dominici, "A meta-analysis and multisite time-series analysis of the differential toxicity of major fine particulate matter constituents," *American Journal of Epidemiology*, vol. 175, no. 11, pp. 1091–1099, 2012.

[26] P. Schwarze, A. Totlandsdal, and J. I. Herseth, *Importance of Components and Sources for Health Effects of Particulate Air Pollution*, 2010.

[27] I. Rosas, A. Yela, E. Salinas, R. Arreguin, and A. Rodriguez-Romero, "Preliminary assessment of protein associated with airborne particles in Mexico City," *Aerobiologia*, vol. 11, no. 2, pp. 81–86, 1995.

[28] M. Y. Menetrez, K. K. Foarde, R. K. Esch et al., "An evaluation of indoor and outdoor biological particulate matter," *Atmospheric Environment*, vol. 43, no. 34, pp. 5476–5483, 2009.

[29] S. Després, J. A. Huffman, and S. M. Burrows, "Primarybiological aerosol particles in theatmosphere: a review," *Tellus*, vol. 64, pp. 1–58, 2012.

[30] M. Y. Menetrez, K. K. Foarde, and D. S. Ensor, "Fine biological PM: understanding size fractiontransport and exposure potential (Extended Abstract)," in *Proceedings of the The Air and Waste Management Association Specialty Conference (PM '00)*, Particulate Matter and Health—The Scientific Basis for Regulatory Decision-making, Charlestown, SC, USA, 2000.

[31] M. Y. Menetrez, K. K. Foarde, and D. S. Ensor, "An analytical method for the measurement of nonviable bioaerosols," *Journal of the Air and Waste Management Association*, vol. 51, no. 10, pp. 1436–1442, 2001.

[32] R. B. Knox, C. Suphioglu, P. Taylor et al., "Major grass pollen allergen Lol p 1 binds to diesel axhaust particles: implications for asthma and air pollution," *Clinical and Experimental Allergy*, vol. 27, no. 3, pp. 246–251, 1997.

[33] H. Ormstad, "Suspended particulate matter in indoor air: adjuvants and allergen carriers," *Toxicology*, vol. 152, no. 1–3, pp. 53–68, 2000.

[34] A. Adhikari, T. Reponen, S. A. Grinshpun, D. Martuzevicius, and G. Lemasters, "Correlation of ambient inhalable bioaerosols with particulate matter and ozone: a two-year study," *Environmental Pollution*, vol. 140, no. 1, pp. 16–28, 2006.

[35] F. Ferreira, T. Hawranek, P. Gruber, N. Wopfner, and A. Mari, "Allergic cross-reactivity: from gene to the clinic," *Allergy*, vol. 59, no. 3, pp. 243–267, 2004.

[36] C. Monn, "Exposure assessment of air pollutants: a review on spatial heterogeneity and indoor/outdoor/personal exposure to suspended particulate matter, nitrogen dioxide and ozone," *Atmospheric Environment*, vol. 35, no. 1, pp. 1–32, 2001.

[37] P. S. Thorne, "Inhalation toxicology models of endotoxin- and bioaerosol-induced inflammation," *Toxicology*, vol. 152, no. 1–3, pp. 13–23, 2000.

[38] L. Mueller-Annelling, E. Avol, J. M. Peters, and P. S. Thorne, "Ambient endotoxin concentrations in PM_{10} from Southern California," *Environmental Health Perspectives*, vol. 112, no. 5, pp. 583–588, 2004.

[39] H. A. Burge and H. M. Ammann, *Fungal Toxins and (1,3)-b-D-glucan; Bioaerosols: Assessment and Control*, ACGIH, 1999.

[40] U. Singh, T. Reponen, K. J. Cho et al., "Airborne endotoxin and β-D-glucan in PM1 in agricultural and home environments," *Aerosol and Air Quality Research*, vol. 11, no. 4, pp. 376–386, 2011.

[41] A. Nemmar, S. Al-Salam, S. Dhanasekaran, M. Sudhadevi, and B. H. Ali, "Pulmonary exposure to diesel exhaust particles promotes cerebral microvessel thrombosis: protective effect of a cysteine prodrug l-2-oxothiazolidine-4-carboxylic acid," *Toxicology*, vol. 263, no. 2-3, pp. 84–92, 2009.

[42] A. Nemmar, S. Al-Salam, S. Zia et al., "Contrasting actions of diesel exhaust particles on the pulmonary and cardiovascular systems and the effects of thymoquinone," *British Journal of Pharmacology*, vol. 164, no. 7, pp. 1871–1882, 2011.

[43] K.-I. Inoue, H. Takano, M. Sakurai et al., "Pulmonary exposure to diesel exhaust particles enhances coagulatory disturbance with endothelial damage and systemic inflammation related to lung inflammation," *Experimental Biology and Medicine*, vol. 231, no. 10, pp. 1626–1632, 2006.

[44] D. R. Riva, C. B. Magalhães, A. A. Lopes et al., "Low dose of fine particulate matter ($PM_{2.5}$) can induce acute oxidative stress, inflammation and pulmonary impairment in healthy mice," *Inhalation Toxicology*, vol. 23, no. 5, pp. 257–267, 2011.

[45] W. A. Zin, A. G. L. S. Silva, C. B. Magalhães et al., "Eugenol attenuates pulmonary damage induced by diesel exhaust particles," *Journal of Applied Physiology*, vol. 112, no. 5, pp. 911–917, 2012.

[46] K. I. Paraskevas, A. A. Tzovaras, D. D. Briana, and D. P. Mikhailidis, "Emerging indications for statins: a pluripotent family of agents with several potential applications," *Current Pharmaceutical Design*, vol. 13, no. 35, pp. 3622–3636, 2007.

[47] R. P. Young, R. Hopkins, and T. E. Eaton, "Pharmacological actions of statins: potential utility in COPD," *European Respiratory Review*, vol. 18, no. 114, pp. 222–232, 2009.

[48] S. A. Ferraro, J. S. Yakisich, F. T. Gallo, and D. R. Tasat, "Simvastatin pretreatment prevents ambient particle-induced lung injury in mice," *Inhalation Toxicology*, vol. 23, no. 14, pp. 889–896, 2011.

[49] R. Miyata, N. Bai, R. Vincent, D. D. Sin, and S. F. van Eeden, "Novel properties of statins: suppression of the systemic and bone marrow responses induced by exposure to ambient particulate matter (PM_{10}) air pollution," *American Journal of Physiology*, vol. 303, no. 6, pp. L492–L499, 2012.

[50] E. Tamagawa, N. Bai, K. Morimoto et al., "Particulate matter exposure induces persistent lung inflammation and endothelial dysfunction," *American Journal of Physiology*, vol. 295, no. 1, pp. L79–L85, 2008.

[51] M. L. North, N. Khanna, P. A. Marsden, H. Grasemann, and J. A. Scott, "Functionally important role for arginase 1 in the airway hyperresponsiveness of asthma," *American Journal of Physiology*, vol. 296, no. 6, pp. L911–L920, 2009.

[52] M. L. North, H. Amatullah, N. Khanna et al., "Augmentation of arginase 1 expression by exposure to air pollution exacerbates the airways hyperresponsiveness in murine models of asthma," *Respiratory Research*, vol. 12, article 19, 2011.

[53] A. A. Götz, J. Rozman, H. G. Rödel et al., "Comparison of particle-exposure triggered pulmonary and systemic inflammation in mice fed with three different diets," *Particle and Fibre Toxicology*, vol. 8, article 30, 2011.

[54] P. G. Barlow, D. M. Brown, K. Donaldson, J. MacCallum, and V. Stone, "Reduced alveolar macrophage migration induced by acute ambient particle (PM_{10}) exposure," *Cell Biology and Toxicology*, vol. 24, no. 3, pp. 243–252, 2008.

[55] J. S. Kim, A. Adamcakova-Dodd, P. T. O'Shaughnessy, V. H. Grassian, and P. S. Thorne, "Effects of copper nanoparticle exposure on host defense in a murine pulmonary infection model," *Particle and Fibre Toxicology*, vol. 8, article 269, 2011.

[56] K.-I. Inoue, H. Takano, R. Yanagisawa et al., "Effects of inhaled nanoparticles on acute lung injury induced by lipopolysaccharide in mice," *Toxicology*, vol. 238, no. 2-3, pp. 99–110, 2007.

[57] K.-I. Inoue, R. Yanagisawa, E. Koike et al., "Effects of carbon black nanoparticles on elastase-induced emphysematous lung injury in mice," *Basic and Clinical Pharmacology and Toxicology*, vol. 108, no. 4, pp. 234–240, 2011.

[58] J. S. Tsuji, A. D. Maynard, P. C. Howard et al., "Research strategies for safety evaluation of nanomaterials—part 4: risk assessment of nanoparticles," *Toxicological Sciences*, vol. 89, no. 1, pp. 42–50, 2006.

[59] J. J. Li, S. Muralikrishnan, C.-T. Ng, L.-Y. L. Yung, and B.-H. Bay, "Nanoparticle-induced pulmonary toxicity," *Experimental Biology and Medicine*, vol. 235, no. 9, pp. 1025–1033, 2010.

[60] A. K. Madl and K. E. Pinkerton, "Health effects of inhaled engineered and incidental nanoparticles Health effects of inhaled nanoparticles," *Critical Reviews in Toxicology*, vol. 39, no. 8, pp. 629–658, 2009.

[61] C. M. Sayes, R. Wahi, P. A. Kurian et al., "Correlating nanoscale titania structure with toxicity: a cytotoxicity and inflammatory response study with human dermal fibroblasts and human lung epithelial cells," *Toxicological Sciences*, vol. 92, no. 1, pp. 174–185, 2006.

[62] D. B. Warheit, T. R. Webb, K. L. Reed, S. Frerichs, and C. M. Sayes, "Pulmonary toxicity study in rats with three forms of ultrafine-TiO_2 particles: differential responses related to surface properties," *Toxicology*, vol. 230, no. 1, pp. 90–104, 2007.

[63] A. Nemmar, K. Melghit, and B. H. Ali, "The acute proinflammatory and prothrombotic effects of pulmonary exposure to rutile TiO_2 nanorods in rats," *Experimental Biology and Medicine*, vol. 233, no. 5, pp. 610–619, 2008.

[64] K. Melghit and S. S. Al-Rabaniah, "Photodegradation of Congo red under sunlight catalysed by nanorod rutile TiO_2," *Journal of Photochemistry and Photobiology A*, vol. 184, no. 3, pp. 331–334, 2006.

[65] M. Zhou, J. Yu, and B. Cheng, "Effects of Fe-doping on the photocatalytic activity of mesoporous TiO_2 powders prepared by an ultrasonic method," *Journal of Hazardous Materials*, vol. 137, no. 3, pp. 1838–1847, 2006.

[66] E. M. Rossi, L. Pylkkänen, A. J. Koivisto et al., "Airway exposure to silica-coated TiO_2 nanoparticles induces pulmonary neutrophilia in mice," *Toxicological Sciences*, vol. 113, no. 2, pp. 422–433, 2009.

[67] A. Nemmar, K. Melghit, S. Al-Salam et al., "Acute respiratory and systemic toxicity of pulmonary exposure to rutile Fe-doped TiO_2 nanorods," *Toxicology*, vol. 279, no. 1–3, pp. 167–175, 2011.

[68] P. H. N. Saldiva, M. King, V. L. C. Delmonte et al., "Respiratory alterations due to urban air pollution: an experimental study in rats," *Environmental Research*, vol. 57, no. 1, pp. 19–33, 1992.

[69] M. Lemos, A. J. F. C. Lichtenfels, E. Amaro Jr. et al., "Quantitative pathology of nasal passages in rats exposed to urban levels of air pollution," *Environmental Research*, vol. 66, no. 1, pp. 87–95, 1994.

[70] K. Yoshizaki, J. M. Brito, A. C. Toledo et al., "Subchronic effects of nasally instilled diesel exhaust particulates on the nasal and airway epithelia in mice," *Inhalation Toxicology*, vol. 22, no. 7, pp. 610–617, 2010.

[71] T. Kampfrath, A. Maiseyeu, Z. Ying et al., "Chronic fine particulate matter exposure induces systemic vascular dysfunction via NADPH oxidase and TLR4 pathways," *Circulation Research*, vol. 108, no. 6, pp. 716–726, 2011.

[72] J. A. Deiuliis, T. Kampfrath, J. Zhong et al., "Pulmonary T cell activation in response to chronic particulate air pollution," *American Journal of Physiology*, vol. 302, no. 4, pp. L399–L409, 2012.

[73] S. I. Rennard, "COPD: overview of definitions, epidemiology, and factors influencing its development," *Chest*, vol. 113, pp. 235S–241S, 1998.

[74] F. D. T. Q. S. Lopes, T. S. Pinto, F. M. Arantes-Costa et al., "Exposure to ambient levels of particles emitted by traffic worsens emphysema in mice," *Environmental Research*, vol. 109, no. 5, pp. 544–551, 2009.

[75] C.-W. Lam, J. T. James, R. McCluskey, and R. L. Hunter, "Pulmonary toxicity of single-wall carbon nanotubes in mice 7 and 90 days after intractracheal instillation," *Toxicological Sciences*, vol. 77, no. 1, pp. 126–134, 2004.

[76] D. B. Warheit, B. R. Laurence, K. L. Reed, D. H. Roach, G. A. M. Reynolds, and T. R. Webb, "Comparative pulmonary toxicity assessment of single-wall carbon nanotubes in rats," *Toxicological Sciences*, vol. 77, no. 1, pp. 117–125, 2004.

[77] J. B. Mangum, E. A. Turpin, A. Antao-Menezes, M. F. Cesta, E. Bermudez, and J. C. Bonner, "Single-walled carbon nanotube (SWCNT)-induced interstitial fibrosis in the lungs of rats is associated with increased levels of PDGF mRNA and the formation of unique intercellular carbon structures that bridge alveolar macrophages In Situ," *Particle and Fibre Toxicology*, vol. 3, article 15, 2006.

[78] A. A. Shvedova, E. R. Kisin, R. Mercer et al., "Unusual inflammatory and fibrogenic pulmonary responses to single-walled carbon nanotubes in mice," *American Journal of Physiology*, vol. 289, no. 5, pp. L698–L708, 2005.

[79] A. A. Shvedova, E. Kisin, A. R. Murray et al., "Inhalation versus aspiration of single-walled carbon nanotubes in C57BL/6 mice: inflammation, fibrosis, oxidative stress, and mutagenesis," *American Journal of Physiology*, vol. 295, no. 4, pp. L552–L565, 2008.

[80] L. A. Mitchell, J. Gao, R. V. Wal, A. Gigliotti, S. W. Burchiel, and J. D. McDonald, "Pulmonary and systemic immune response to inhaled multiwalled carbon nanotubes," *Toxicological Sciences*, vol. 100, no. 1, pp. 203–214, 2007.

[81] D. Elgrabli, S. Abella-Gallart, F. Robidel, F. Rogerieux, J. Boczkowski, and G. Lacroix, "Induction of apoptosis and absence of inflammation in rat lung after intratracheal instillation of multiwalled carbon nanotubes," *Toxicology*, vol. 253, no. 1–3, pp. 131–136, 2008.

[82] J. Pauluhn, "Multi-walled carbon nanotubes (Baytubes): approach for derivation of occupational exposure limit," *Regulatory Toxicology and Pharmacology*, vol. 57, no. 1, pp. 78–89, 2010.

[83] A. Nemmar, M. F. Hoylaerts, P. H. M. Hoet, and B. Nemery, "Possible mechanisms of the cardiovascular effects of inhaled particles: systemic translocation and prothrombotic effects," *Toxicology Letters*, vol. 149, no. 1–3, pp. 243–253, 2004.

[84] G. Oberdörster, Z. Sharp, V. Atudorei et al., "Translocation of inhaled ultrafine particles to the brain," *Inhalation Toxicology*, vol. 16, no. 6-7, pp. 437–445, 2004.

[85] A. Nemmar, P. H. M. Hoet, B. Vanquickenborne et al., "Passage of inhaled particles into the blood circulation in humans," *Circulation*, vol. 105, no. 4, pp. 411–414, 2002.

[86] A. Nemmar, H. Vanbilloen, M. F. Hoylaerts, P. H. M. Hoet, A. Verbruggen, and B. Nemery, "Passage of intratracheally instilled ultrafine particles from the lung into the systemic circulation in hamster," *American Journal of Respiratory and Critical Care Medicine*, vol. 164, no. 9, pp. 1665–1668, 2001.

[87] G. Oberdörster, E. Oberdörster, and J. Oberdörster, "Nanotoxicology: an emerging discipline evolving from studies of ultrafine particles," *Environmental Health Perspectives*, vol. 113, no. 7, pp. 823–839, 2005.

[88] J. Vermylen, A. Nemmar, B. Nemery, and M. F. Hoylaerts, "Ambient air pollution and acute myocardial infarction," *Journal of Thrombosis and Haemostasis*, vol. 3, no. 9, pp. 1955–1961, 2005.

[89] A. Seaton and K. Donaldson, "Nanoscience, nanotoxicology, and the need to think small," *The Lancet*, vol. 365, no. 9463, pp. 923–924, 2005.

[90] G. Oberdörster, Z. Sharp, V. Atudorei et al., "Extrapulmonary translocation of ultrafine carbon particles following whole-body inhalation exposure of rats," *Journal of Toxicology and Environmental Health Part A*, vol. 65, no. 20, pp. 1531–1543, 2002.

[91] A. Elder, R. Gelein, V. Silva et al., "Translocation of inhaled ultrafine manganese oxide particles to the central nervous system," *Environmental Health Perspectives*, vol. 114, no. 8, pp. 1172–1178, 2006.

[92] W. G. Kreyling, M. Semmler, F. Erbe et al., "Translocation of ultrafine insoluble iridium particles from lung epithelium to extrapulmonary organs is size dependent but very low," *Journal of Toxicology and Environmental Health Part A*, vol. 65, no. 20, pp. 1513–1530, 2002.

[93] J. G. Wallenborn, J. K. McGee, M. C. Schladweiler, A. D. Ledbetter, and U. P. Kodavanti, "Systemic translocation of particulate matter-associated metals following a single intratracheal instillation in rats," *Toxicological Sciences*, vol. 98, no. 1, pp. 231–239, 2007.

[94] S. Takenaka, E. Karg, C. Roth et al., "Pulmonary and systemic distribution of inhaled ultrafine silver particles in rats," *Environmental Health Perspectives*, vol. 109, no. 4, pp. 547–551, 2001.

[95] J. E. Eyles, V. W. Bramwell, E. D. Williamson, and H. O. Alpar, "Microsphere translocation and immunopotentiation in systemic tissues following intranasal administration," *Vaccine*, vol. 19, no. 32, pp. 4732–4742, 2001.

[96] T. Kato, T. Yashiro, Y. Murata et al., "Evidence that exogenous substances can be phagocytized by alveolar epithelial cells and transported into blood capillaries," *Cell and Tissue Research*, vol. 311, no. 1, pp. 47–51, 2003.

[97] N. Kapp, W. Kreyling, H. Schulz et al., "Electron energy loss spectroscopy for analysis of inhaled ultrafine particles in rat lungs," *Microscopy Research and Technique*, vol. 63, no. 5, pp. 298–305, 2004.

[98] M. Geiser, B. Rothen-Rutishauser, N. Kapp et al., "Ultrafine particles cross cellular membranes by nonphagocytic mechanisms in lungs and in cultured cells," *Environmental Health Perspectives*, vol. 113, no. 11, pp. 1555–1560, 2005.

[99] N. L. Mills, N. Amin, S. D. Robinson et al., "Do inhaled carbon nanoparticles translocate directly into the circulation in humans?" *American Journal of Respiratory and Critical Care Medicine*, vol. 173, no. 4, pp. 426–431, 2006.

[100] N. L. Mills, K. Donaldson, P. W. Hadoke et al., "Adverse cardiovascular effects of air pollution," *Nature Clinical Practice Cardiovascular Medicine*, vol. 6, no. 1, pp. 36–44, 2009.

[101] A. Nemmar, S. Zia, D. Subramaniyan, I. Al-Amri, M. A. Al Kindi, and B. H. Ali, "Interaction of diesel exhaust particles with human, rat and mouse erythrocytes *in vitro*," *Cellular Physiology and Biochemistry*, vol. 29, no. 1-2, pp. 163–170, 2012.

[102] B. H. Simon, H. Y. Ando, and P. K. Gupta, "Circulation time and body distribution of 14C-labeled amino-modified polystyrene nanoparticles in mice," *Journal of Pharmaceutical Sciences*, vol. 84, no. 10, pp. 1249–1253, 1995.

[103] A. R. R. Péry, C. Brochot, P. H. M. Hoet, A. Nemmar, and F. Y. Bois, "Development of a physiologically based kinetic model for 99m-Technetium-labelled carbon nanoparticles inhaled by humans Human PBPK model for carbon nanoparticles," *Inhalation Toxicology*, vol. 21, no. 13, pp. 1099–1107, 2009.

[104] T. R. Nurkiewicz, D. W. Porter, M. Barger, V. Castranova, and M. A. Boegehold, "Particulate matter exposure impairs systemic microvascular endothelium-dependent dilation," *Environmental Health Perspectives*, vol. 112, no. 13, pp. 1299–1306, 2004.

[105] T. R. Nurkiewicz, D. W. Porter, M. Barger et al., "Systemic microvascular dysfunction and inflammation after pulmonary particulate matter exposure," *Environmental Health Perspectives*, vol. 114, no. 3, pp. 412–419, 2006.

[106] T. R. Nurkiewicz, D. W. Porter, A. F. Hubbs et al., "Nanoparticle inhalation augments particle-dependent systemic microvascular dysfunction," *Particle and Fibre Toxicology*, vol. 5, article 1, 2008.

[107] T. R. Nurkiewicz, D. W. Porter, A. F. Hubbs et al., "Pulmonary nanoparticle exposure disrupts systemic microvascular nitric oxide signaling," *Toxicological Sciences*, vol. 110, no. 1, pp. 191–203, 2009.

[108] A. Nemmar, M. F. Hoylaerts, P. H. M. Hoet et al., "Ultrafine particles affect experimental thrombosis in an *in vivo* hamster model," *American Journal of Respiratory and Critical Care Medicine*, vol. 166, no. 7, pp. 998–1004, 2002.

[109] A. Nemmar, P. H. M. Hoet, D. Dinsdale, J. Vermylen, M. F. Hoylaerts, and B. Nemery, "Diesel exhaust particles in lung acutely enhance experimental peripheral thrombosis," *Circulation*, vol. 107, no. 8, pp. 1202–1208, 2003.

[110] A. Nemmar, B. Nemery, P. H. M. Hoet, J. Vermylen, and M. F. Hoylaerts, "Pulmonary inflammation and thrombogenicity caused by diesel particles in hamsters: role of histamine," *American Journal of Respiratory and Critical Care Medicine*, vol. 168, no. 11, pp. 1366–1372, 2003.

[111] A. Nemmar, P. H. M. Hoet, J. Vermylen, B. Nemery, and M. F. Hoylaerts, "Pharmacological stabilization of mast cells abrogates late thrombotic events induced by diesel exhaust particles in hamsters," *Circulation*, vol. 110, no. 12, pp. 1670–1677, 2004.

[112] V. M. Silva, N. Corson, A. Elder, and G. Oberdörster, "The rat ear vein model for investigating *in vivo* thrombogenicity of ultrafine particles (UFP)," *Toxicological Sciences*, vol. 85, no. 2, pp. 983–989, 2005.

[113] G. M. Mutlu, D. Green, A. Bellmeyer et al., "Ambient particulate matter accelerates coagulation via an IL-6-dependent pathway," *Journal of Clinical Investigation*, vol. 117, no. 10, pp. 2952–2961, 2007.

[114] M. Yamashita and M. Yamashita, "Tumor necrosis factor alpha is involved in the induction of plasminogen activator inhibitor-1 by endotoxin," *Thrombosis Research*, vol. 87, no. 2, pp. 165–170, 1997.

[115] G. R. S. Budinger, J. L. McKell, D. Urich et al., "Particulate matter-induced lung inflammation increases systemic levels of PAI-1 and activates coagulation through distinct mechanisms," *PLoS ONE*, vol. 6, no. 4, Article ID e18525, 2011.

[116] A. Nemmar, D. Subramaniyan, and B. H. Ali, "Protective effect of curcumin on pulmonary and cardiovascular effects induced by repeated exposure to diesel exhaust particles in mice," *PLoS ONE*, vol. 7, Article ID e39554, 2012.

[117] Q. Sun, P. Yue, Z. Ying et al., "Air pollution exposure potentiates hypertension through reactive oxygen species-mediated activation of Rho/ROCK," *Arteriosclerosis, Thrombosis, and Vascular Biology*, vol. 28, no. 10, pp. 1760–1766, 2008.

[118] Z. Ying, P. Yue, X. Xu et al., "Air pollution and cardiac remodeling: a role for RhoA/Rho-kinase," *American Journal of Physiology*, vol. 296, no. 5, pp. H1540–H1550, 2009.

[119] A. Nemmar, S. Zia, D. Subramaniyan, M. A. Fahim, and B. H. Ali, "Exacerbation of thrombotic events by diesel exhaust particle in mouse model of hypertension," *Toxicology*, vol. 285, no. 1-2, pp. 39–45, 2011.

[120] A. Nemmar, D. Subramaniyan, S. Zia, J. Yasin, and B. H. Ali, "Airway resistance, inflammation and oxidative stress following exposure to diesel exhaust particle in angiotensin II-induced hypertension in mice," *Toxicology*, vol. 292, no. 2-3, pp. 162–168, 2012.

[121] A. Nemmar, S. Al-Salam, D. Subramaniyan et al., "Influence of experimental type 1 diabetes on the pulmonary effects of diesel exhaust particles in mice," *Toxicology Letters*, vol. 217, no. 2, pp. 170–176, 2013.

[122] A. Nemmar, D. Subramaniyan, J. Yasin, and B. H. Ali, "Impact of experimental type 1 diabetes mellitus on systemic and coagulation vulnerability in mice acutely exposed to diesel exhaust particles," *Particle and Fibre Toxicology*, vol. 10, no. 1, article 14, 2013.

[123] A. Nemmar, S. Al-Salam, S. Zia, J. Yasin, I. Al Husseni, and B. H. Ali, "Diesel exhaust particles in the lung aggravate experimental acute renal failure," *Toxicological Sciences*, vol. 113, no. 1, pp. 267–277, 2010.

[124] A. Nemmar, S. Al-Maskari, B. H. Ali, and I. S. Al-Amri, "Cardiovascular and lung inflammatory effects induced by systemically administered diesel exhaust particles in rats," *American Journal of Physiology*, vol. 292, no. 3, pp. L664–L670, 2007.

[125] A. Nemmar, S. Dhanasekaran, J. Yasin et al., "Evaluation of the direct systemic and cardiopulmonary effects of diesel particles in spontaneously hypertensive rats," *Toxicology*, vol. 262, no. 1, pp. 50–56, 2009.

[126] A. Nemmar, S. Al-Salam, S. Zia, S. Dhanasekaran, M. Shudadevi, and B. H. Ali, "Time-course effects of systemically administered diesel exhaust particles in rats," *Toxicology Letters*, vol. 194, no. 3, pp. 58–65, 2010.

[127] C. Moon, H.-J. Park, Y.-H. Choi, E.-M. Park, V. Castranova, and J. L. Kang, "Pulmonary inflammation after intraperitoneal administration of ultrafine titanium dioxide (TiO_2) at rest or in lungs primed with lipopolysaccharide," *Journal of Toxicology and Environmental Health Part A*, vol. 73, no. 5-6, pp. 396–409, 2010.

[128] J. Geys, A. Nemmar, E. Verbeken et al., "Acute toxicity and prothrombotic effects of Quantum dots: impact of surface charge," *Environmental Health Perspectives*, vol. 116, no. 12, pp. 1607–1613, 2008.

[129] L. M. Y. Akinaga, A. J. Lichtenfels, R. Carvalho-Oliveira et al., "Effects of chronic exposure to air pollution from sao paulo city on coronary of swiss mice, from birth to adulthood," *Toxicologic Pathology*, vol. 37, no. 3, pp. 306–314, 2009.

[130] L. C. Chen and J.-S. Hwang, "Effects of subchronic exposures to concentrated ambient particles (CAPs) in mice—4. Characterization of acute and chronic effects of ambient air fine particulate matter exposures on heart-rate variability," *Inhalation Toxicology*, vol. 17, no. 4-5, pp. 209–216, 2005.

[131] Q. Sun, A. Wang, X. Jin et al., "Long-term air pollution exposure and acceleration of atherosclerosis and vascular inflammation in an animal model," *Journal of the American Medical Association*, vol. 294, no. 23, pp. 3003–3010, 2005.

[132] L. C. Chen and C. Nadziejko, "Effects of subchronic exposures to concentrated ambient particles (CAPs) in mice—5. CAPs exacerbate aortic plaque development in hyperlipidemic mice," *Inhalation Toxicology*, vol. 17, no. 4-5, pp. 217–224, 2005.

[133] Q. Sun, P. Yue, R. I. Kirk et al., "Ambient air particulate matter exposure and tissue factor expression in atherosclerosis," *Inhalation Toxicology*, vol. 20, no. 2, pp. 127–137, 2008.

[134] Q. Sun, P. Yue, J. A. Deiuliis et al., "Ambient air pollution exaggerates adipose inflammation and insulin resistance in a mouse model of diet-induced obesity," *Circulation*, vol. 119, no. 4, pp. 538–546, 2009.

[135] G. S. Kang, P. A. Gillespie, A. Gunnison, A. L. Moreira, K.-M. Tchou-Wong, and L.-C. Chen, "Long-term inhalation exposure to nickel nanoparticles exacerbated atherosclerosis in a susceptible mouse model," *Environmental Health Perspectives*, vol. 119, no. 2, pp. 176–181, 2011.

[136] J. Emmerechts, V. De Vooght, S. Haenen et al., "Thrombogenic changes in young and old mice upon subchronic exposure to air pollution in an urban roadside tunnel," *Thrombosis and Haemostasis*, vol. 108, no. 4, pp. 756–768, 2012.

[137] A. Peters, B. Veronesi, L. Calderón-Garcidueñas et al., "Translocation and potential neurological effects of fine and ultrafine particles a critical update," *Particle and Fibre Toxicology*, vol. 3, article 13, 2006.

[138] R. G. Lucchini, D. C. Dorman, A. Elder, and B. Veronesi, "Neurological impacts from inhalation of pollutants and the nose-brain connection," *NeuroToxicology*, vol. 33, pp. 838–841, 2012.

[139] A. I. Totlandsdal, J. I. Herseth, A. K. Bølling et al., "Differential effects of the particle core and organic extract of diesel exhaust particles," *Toxicology Letters*, vol. 208, no. 3, pp. 262–268, 2012.

[140] J. Topinka, A. Milcova, J. Schmuczerova, M. Mazac, M. Pechout, and M. Vojtisek-Lom, "Genotoxic potential of organic extracts from particle emissions of diesel and rapeseed oil powered engines," *Toxicology Letters*, vol. 212, no. 1, pp. 11–17, 2012.

[141] J. Topinka, P. Rossner, A. Milcova, J. Schmuczerova, V. Svecova, and R. J. Sram, "DNA adducts and oxidative DNA damage induced by organic extracts from $PM_{2.5}$ in an acellular assay," *Toxicology Letters*, vol. 202, no. 3, pp. 186–192, 2011.

[142] R. K. Saxena, M. I. Gilmour, and M. D. Hays, "Isolation and quantitative estimation of diesel exhaust and carbon black particles ingested by lung epithelial cells and alveolar macrophages *in vitro*," *BioTechniques*, vol. 44, no. 6, pp. 799–805, 2008.

[143] P. E. Schwarze, J. Øvrevik, R. B. Hetland et al., "Importance of size and composition of particles for effects on cells *in vitro*," *Inhalation Toxicology*, vol. 19, no. 1, pp. 17–22, 2007.

[144] N. Amara, R. Bachoual, M. Desmard et al., "Diesel exhaust particles induce matrix metalloprotease-1 in human lung epithelial cells via a NADP(H) oxidase/NOX4 redox-dependent mechanism," *American Journal of Physiology*, vol. 293, no. 1, pp. L170–L181, 2007.

[145] M. Ciganek, J. Neca, V. Adamec, J. Janosek, and M. Machala, "A combined chemical and bioassay analysis of traffic-emitted polycyclic aromatic hydrocarbons," *Science of the Total Environment*, vol. 334-335, pp. 141–148, 2004.

[146] R. Barouki, M. Aggerbeck, L. Aggerbeck, and X. Coumoul, "The aryl hydrocarbon receptor system," *Drug Metabolism and Drug Interactions*, vol. 27, no. 1, pp. 3–8, 2012.

[147] C. A. Pope III, R. T. Burnett, M. J. Thun et al., "Lung cancer, cardiopulmonary mortality, and long-term exposure to fine particulate air pollution," *Journal of the American Medical Association*, vol. 287, no. 9, pp. 1132–1141, 2002.

[148] P. Vineis, F. Forastiere, G. Hoek, and M. Lipsett, "Outdoor air pollution and lung cancer: recent epidemiologic evidence," *International Journal of Cancer*, vol. 111, no. 5, pp. 647–652, 2004.

[149] J. Geys, L. Coenegrachts, J. Vercammen et al., "*In vitro* study of the pulmonary translocation of nanoparticles: a preliminary study," *Toxicology Letters*, vol. 160, no. 3, pp. 218–226, 2006.

[150] B. Rothen-Rutishauser, F. Blank, C. Muhlfeld, and P. Gehr, "*In vitro* models of the human epithelial airway barrier to study the

toxic potential of particulate matter," *Expert Opinion on Drug Metabolism & Toxicology*, vol. 4, pp. 1075–1089, 2008.

[151] A. D. Lehmann, F. Blank, O. Baum, P. Gehr, and B. M. Rothen-Rutishauser, "Diesel exhaust particles modulate the tight junction protein occludin in lung cells *in vitro*," *Particle and Fibre Toxicology*, vol. 6, article 26, 2009.

[152] H. S. Rosenkranz, N. Pollack, and A. R. Cunningham, "Exploring the relationship between the inhibition of gap junctional intercellular communication and other biological phenomena," *Carcinogenesis*, vol. 21, no. 5, pp. 1007–1011, 2000.

[153] L. M. Weis, A. M. Rummel, S. J. Masten, J. E. Trosko, and B. L. Upham, "Bay or baylike regions of polycyclic aromatic hydrocarbons were potent inhibitors of gap junctional intercellular communication," *Environmental Health Perspectives*, vol. 106, no. 1, pp. 17–22, 1998.

[154] L. Bláha, P. Kapplová, J. Vondrácek, B. Upham, and M. Machala, "Inhibition of gap-junctional intercellular communication by environmentally occurring polycyclic aromatic hydrocarbons," *Toxicological Sciences*, vol. 65, no. 1, pp. 43–51, 2002.

[155] J. J. Sharovskaja, A. V. Vaiman, N. A. Solomatina, and V. A. Kobliakov, "Inhibition of gap junction intercellular communications in cell culture by polycyclic aromatic hydrocarbons (PAH) in the absence of PAH metabolism," *Biochemistry*, vol. 69, no. 4, pp. 413–419, 2004.

[156] J. Song, S. Ye, W. Sheng, and Y. Jiu, "Effects of diesel exhaust particle on gap junction intercellular communication," *Wei Sheng Yan Jiu*, vol. 26, no. 3, pp. 145–147, 1997 (Chinese).

[157] G. M. Alink, M. Sjögren, R. P. Bos, G. Doekes, H. Kromhout, and P. T. Scheepers, "Effect of airborne particles from selected indoor and outdoor environments on gap-junctional intercellular communication," *Toxicology Letters*, vol. 96-97, pp. 209–213, 1998.

[158] E. Rivedal, O. Myhre, T. Sanner, and I. Eide, "Supplemental role of the Ames mutation assay and gap junction intercellular communication in studies of possible carcinogenic compounds from diesel exhaust particles," *Archives of Toxicology*, vol. 77, no. 9, pp. 533–542, 2003.

[159] W. L. Wendy Hsiao, Z.-Y. Mo, M. Fang, X.-M. Shi, and F. Wang, "Cytotoxicity of $PM_{2.5}$ and $PM_{2.5-10}$ ambient air pollutants assessed by the MTT and the Comet assays," *Mutation Research*, vol. 471, no. 1-2, pp. 45–55, 2000.

[160] H. Bayram, K. Ito, R. Issa, M. Ito, M. Sukkar, and K. F. Chung, "Regulation of human lung epithelial cell numbers by diesel exhaust particles," *European Respiratory Journal*, vol. 27, no. 4, pp. 705–713, 2006.

[161] M. Gualtieri, J. Øvrevik, S. Mollerup et al., "Airborne urban particles (Milan winter-PM2.5) cause mitotic arrest and cell death: effects on DNA, mitochondria, AhR binding and spindle organization," *Mutation Research*, vol. 713, no. 1-2, pp. 18–31, 2011.

[162] C. Furuta, A. K. Suzuki, G. Watanabe, C. Li, S. Taneda, and K. Taya, "Nitrophenols isolated from diesel exhaust particles promote the growth of MCF-7 breast adenocarcinoma cells," *Toxicology and Applied Pharmacology*, vol. 230, no. 3, pp. 320–326, 2008.

[163] S. M. Oh, B. T. Ryu, and K. H. Chung, "Identification of estrogenic and antiestrogenic activities of respirable diesel exhaust particles by bioassay-directed fractionation ," *Archives of Pharmacal Research*, vol. 31, no. 1, pp. 75–82, 2008.

[164] S. L. Tannheimer, S. L. Barton, S. P. Ethier, and S. W. Burchiel, "Carcinogenic polycyclic aromatic hydrocarbons increase intracellular Ca^{2+} and cell proliferation in primary human mammary epithelial cells," *Carcinogenesis*, vol. 18, no. 6, pp. 1177–1182, 1997.

[165] S. L. Tannheimer, S. P. Ethier, K. K. Caldwell, and S. W. Burchiel, "Benzo[α]pyrene- and TCDD-induced alterations in tyrosine phosphorylation and insulin-like growth factor signaling pathways in the MCF-10A human mammary epithelial cell line," *Carcinogenesis*, vol. 19, no. 7, pp. 1291–1297, 1998.

[166] M. Plísková, J. Vondrácek, B. Vojtesek, A. Kozubík, and M. Machala, "Deregulation of cell proliferation by polycyclic aromatic hydrocarbons in human breast carcinoma MCF-7 cells reflects both genotoxic and nongenotoxic events," *Toxicological Sciences*, vol. 83, no. 2, pp. 246–256, 2005.

[167] K. Chramostová, J. Vondrácek, L. Sindlerová, B. Vojtesek, A. Kozubík, and M. Machala, "Polycyclic aromatic hydrocarbons modulate cell proliferation in rat hepatic epithelial stem-like WB-F344 cells," *Toxicology and Applied Pharmacology*, vol. 196, no. 1, pp. 136–148, 2004.

[168] Z. Andrysík, J. Vondrácek, M. Machala et al., "The aryl hydrocarbon receptor-dependent deregulation of cell cycle control induced by polycyclic aromatic hydrocarbons in rat liver epithelial cells," *Mutation Research*, vol. 615, no. 1-2, pp. 87–97, 2007.

[169] Q. A. Khan, K. H. Vousden, and A. Dipple, "Cellular response to DNA damage from a potent carcinogen involves stabilization of p53 without induction of p21(waf1/cip1)," *Carcinogenesis*, vol. 18, no. 12, pp. 2313–2318, 1997.

[170] A. Dipple, "DNA reactions, mutagenic action and stealth properties of polycyclic aromatic hydrocarbon carcinogens," *International Journal of Oncology*, vol. 14, no. 1, pp. 103–111, 1999.

[171] Y. Nakanishi, X.-H. Pei, K. Takayama et al., "Polycyclic aromatic hydrocarbon carcinogens increase ubiquitination of p21 protein after the stabilization of p53 and the expression of p21," *American Journal of Respiratory Cell and Molecular Biology*, vol. 22, no. 6, pp. 747–754, 2000.

[172] E. Roudier, O. Mistafa, and U. Stenius, "Statins induce mammalian target of rapamycin (mTOR)-mediated inhibition of Akt signaling and sensitize p53-deficient cells to cytostatic drugs," *Molecular Cancer Therapeutics*, vol. 5, no. 11, pp. 2706–2715, 2006.

[173] M. Malmlöf, G. Pääjärvi, J. Högberg, and U. Stenius, "Mdm2 as a sensitive and mechanistically informative marker for genotoxicity induced by benzo[a]pyrene and dibenzo[a,l]pyrene," *Toxicological Sciences*, vol. 102, no. 2, pp. 232–240, 2008.

[174] J. L. Marlowe, Y. Fan, X. Chang et al., "The aryl hydrocarbon receptor binds to E2F1 and inhibits E2F1-induced apoptosis," *Molecular Biology of the Cell*, vol. 19, no. 8, pp. 3263–3271, 2008.

[175] A. Solhaug, M. Refsnes, M. Låg, P. E. Schwarze, T. Husøy, and J. A. Holme, "Polycyclic aromatic hydrocarbons induce both apoptotic and anti-apoptotic signals in Hepa1c1c7 cells," *Carcinogenesis*, vol. 25, no. 5, pp. 809–819, 2004.

[176] N. E. Landvik, M. Gorria, V. M. Arlt et al., "Effects of nitrated-polycyclic aromatic hydrocarbons and diesel exhaust particle extracts on cell signalling related to apoptosis: possible implications for their mutagenic and carcinogenic effects," *Toxicology*, vol. 231, no. 2-3, pp. 159–174, 2007.

[177] J. A. Holme, B. Trygg, and E. Søderlund, "Species differences in the metabolism of 2-acetylaminofluorene by hepatocytes in primary monolayer cultur," *Cancer Research*, vol. 46, no. 4, pp. 1627–1632, 1986.

[178] U. Rannug, J. A. Holme, J. K. Hongslo, and R. Sram, "An evaluation of the genetic toxicity of paracetamol," *Mutation Research*, vol. 327, no. 1-2, pp. 179–200, 1995.

[179] X. Tekpli, J. A. Holme, O. Sergent, and D. Lagadic-Gossmann, "Importance of plasma membrane dynamics in chemical-induced carcinogenesis," *Recent Patents on Anti-Cancer Drug Discovery*, vol. 6, no. 3, pp. 347–353, 2011.

[180] D. Male, J. Brostoff, D. Roth et al., *Immunology*, Elsevier, Amsterdam, The Netherlands, 2006.

[181] E. Alfaro-Moreno, C. M. García-Cuellar, A. De Vizcaya Ruiz, L. Rojas-Bracho, and A. Osornio-Vargas, "The cellular mechanisms behind particulate matter air pollution related health effects," in *Air Pollution: Health & Environmental Impacts*, B. R. Gurjar, L. T. Molina, and C. S. P. Ojha, Eds., Taylor & Francis, 2010.

[182] H. Takizawa, T. Ohtoshi, S. Kawasaki et al., "Diesel exhaust particles activate human bronchial epithelial cells to express inflammatory mediators in the airways: a review," *Respirology*, vol. 5, no. 2, pp. 197–203, 2000.

[183] S. Hashimoto, Y. Gon, I. Takeshita et al., "Diesel exhaust particles activate p38 MAP kinase to produce interleukin 8 and RANTES by human bronchial epithelial cells and N-acetylcysteine attenuates p38 MAP kinase activation," *American Journal of Respiratory and Critical Care Medicine*, vol. 161, no. 1, pp. 280–285, 2000.

[184] M. Gualtieri, J. Øvrevik, J. A. Holme et al., "Differences in cytotoxicity versus pro-inflammatory potency of different PM fractions in human epithelial lung cells," *Toxicology in Vitro*, vol. 24, no. 1, pp. 29–39, 2010.

[185] A. Baulig, M. Garlatti, V. Bonvallot et al., "Involvement of reactive oxygen species in the metabolic pathways triggered by diesel exhaust particles in human airway epithelial cells," *American Journal of Physiology*, vol. 285, no. 3, pp. L671–L679, 2003.

[186] X. J. Yin, J. Y. C. Ma, J. M. Antonini, V. Castranova, and J. K. H. Ma, "Roles of reactive oxygen species and heme oxygenase-1 in modulation of alveolar macrophage-mediated pulmonary immune responses to Listeria monocytogenes by diesel exhaust particles," *Toxicological Sciences*, vol. 82, no. 1, pp. 143–153, 2004.

[187] A. M. Knaapen, R. P. F. Schins, D. Polat, A. Becker, and P. J. A. Borm, "Mechanisms of neutrophil-induced DNA damage in respiratory tract epithelial cells," *Molecular and Cellular Biochemistry*, vol. 234-235, pp. 143–151, 2002.

[188] R. Becher, A. Bucht, J. Øvrevik et al., "Involvement of NADPH oxidase and iNOS in rodent pulmonary cytokine responses to urban air and mineral particles," *Inhalation Toxicology*, vol. 19, no. 8, pp. 645–655, 2007.

[189] A. Kocbach, J. I. Herseth, M. Låg, M. Refsnes, and P. E. Schwarze, "Particles from wood smoke and traffic induce differential pro-inflammatory response patterns in co-cultures," *Toxicology and Applied Pharmacology*, vol. 232, no. 2, pp. 317–326, 2008.

[190] R. B. Hetland, F. R. Cassee, M. Låg, M. Refsnes, E. Dybing, and P. E. Schwarze, "Cytokine release from alveolar macrophages exposed to ambient particulate matter: heterogeneity in relation to size, city an season," *Particle and Fibre Toxicology*, vol. 2, article 4, 2005.

[191] E. Alfaro-Moreno, V. Torres, J. Miranda et al., "Induction of IL-6 and inhibition of IL-8 secretion in the human airway cell line Calu-3 by urban particulate matter collected with a modified method of PM sampling," *Environmental Research*, vol. 109, no. 5, pp. 528–535, 2009.

[192] K. L. Oslund, L. A. Miller, J. L. Usachenko, N. K. Tyler, R. Wu, and D. M. Hyde, "Oxidant-injured airway epithelial cells upregulate thioredoxin but do not produce interleukin-8," *American Journal of Respiratory Cell and Molecular Biology*, vol. 30, no. 5, pp. 597–604, 2004.

[193] J. Øvrevik, M. Refsnes, P. Schwarze, and M. Låg, "The ability of oxidative stress to mimic quartz-induced chemokine responses is lung cell line-dependent," *Toxicology Letters*, vol. 181, no. 2, pp. 75–80, 2008.

[194] J. Øvrevik, M. Refsnes, A. I. Totlandsdal, J. A. Holme, P. E. Schwarze, and M. Låg, "TACE/TGF-α/EGFR regulates CXCL8 in bronchial epithelial cells exposed to particulate matter components," *European Respiratory Journal*, vol. 38, no. 5, pp. 1189–1199, 2011.

[195] E. Alfaro-Moreno, R. López-Marure, A. Montiel-Dávalos et al., "E-Selectin expression in human endothelial cells exposed to PM10: the role of endotoxin and insoluble fraction," *Environmental Research*, vol. 103, no. 2, pp. 221–228, 2007.

[196] A. Montiel-Dávalos, E. Alfaro-Moreno, and R. López-Marure, "$PM_{2.5}$ and PM_{10} induce the expression of adhesion molecules and the adhesion of monocytic cells to human umbilical vein endothelial cells," *Inhalation Toxicology*, vol. 19, no. 1, supplement, pp. 91–98, 2007.

[197] A. Montiel-Dávalos, M. D. J. Ibarra-Sánchez, J. L. Ventura-Gallegos, E. Alfaro-Moreno, and R. López-Marure, "Oxidative stress and apoptosis are induced in human endothelial cells exposed to urban particulate matter," *Toxicology in Vitro*, vol. 24, no. 1, pp. 135–141, 2010.

[198] A. Montiel-Dávalos, J. L. Ventura-Gallegos, E. Alfaro-Moreno et al., "TiO_2 nanoparticles induce dysfunction and activation of human endothelial cells," *Chemical Research in Toxicology*, vol. 25, no. 4, pp. 920–930, 2012.

[199] A. Rosenberger, H. Bickeböller, V. McCormack et al., "Asthma and lung cancer risk: a systematic investigation by the international lung cancer consortium," *Carcinogenesis*, vol. 33, no. 3, pp. 587–597, 2012.

[200] I. M. Adcock, G. Caramori, and P. J. Barnes, "Chronic Obstructive pulmonary disease and lung cancer: new molecular insights," *Respiration*, vol. 81, no. 4, pp. 265–284, 2011.

[201] H. Bartsch and J. Nair, "Chronic inflammation and oxidative stress in the genesis and perpetuation of cancer: role of lipid peroxidation, DNA damage, and repair," *Langenbeck's Archives of Surgery*, vol. 391, no. 5, pp. 499–510, 2006.

[202] X. Zhou, X. W. Wang, L. Xu et al., "COOH-terminal domain of p53 modulates p53-mediated transcriptional transactivation, cell growth, and apoptosis," *Cancer Research*, vol. 59, no. 4, pp. 843–848, 1999.

[203] E. Alfaro-Moreno, T. S. Nawrot, B. M. Vanaudenaerde et al., "Co-cultures of multiple cell types mimic pulmonary cell communication in response to urban PM10," *European Respiratory Journal*, vol. 32, no. 5, pp. 1184–1194, 2008.

[204] M. D. Ramos-Godínez, B. E. González-Gómez, A. Montiel-Dávalos, R. López-Marure, and E. Alfaro-Moreno, "TiO_2 nanoparticles induce endothelial cell activation in a pneumocyte-endothelial co-culture model," *Toxicology in Vitro*, vol. 27, no. 2, pp. 774–781, 2012.

[205] S. M. Dubinett, J. M. Lee, S. Sharma, and J. J. Mule, "Chemokines: Can effector cells be redirected to the site of the tumor?" *Cancer Journal*, vol. 16, no. 4, pp. 325–335, 2010.

[206] M. D. Meek, "Ah receptor and estrogen receptor-dependent modulation of gene expression by extracts of diesel exhaust

particles," *Environmental Research*, vol. 79, no. 2, pp. 114–121, 1998.

[207] K. A. Pacheco, "Epigenetics mediate environment: gene effects on occupational sensitization," *Current Opinion in Allergy and Clinical Immunology*, vol. 12, no. 2, pp. 111–118, 2012.

[208] P. Vineis and K. Husgafvel-Pursiainen, "Air pollution and cancer: biomarker studies in human populations," *Carcinogenesis*, vol. 26, no. 11, pp. 1846–1855, 2005.

[209] P. Møller, J. K. Folkmann, L. Forchhammer et al., "Air pollution, oxidative damage to DNA, and carcinogenesis," *Cancer Letters*, vol. 266, no. 1, pp. 84–97, 2008.

[210] J. Zhang, A. J. Ghio, M. Gao, K. Wei, G. D. Rosen, and D. Upadhyay, "Ambient particulate matter induces alveolar epithelial cell cycle arrest: role of G1 cyclins," *FEBS Letters*, vol. 581, no. 27, pp. 5315–5320, 2007.

[211] P. H. Danielsen, S. Loft, A. Kocbach, P. E. Schwarze, and P. Møller, "Oxidative damage to DNA and repair induced by Norwegian wood smoke particles in human A549 and THP-1 cell lines," *Mutation Research*, vol. 674, no. 1-2, pp. 116–122, 2009.

[212] M. M. Hasegawa, Y. Nishi, H. Tsuda, N. Inui, and K. Morimoto, "Effects of diesel exhaust particles on chromosome aberration, sister chromatid exchange and morphological transformation in cultured mammalian cells," *Cancer Letters*, vol. 42, no. 1-2, pp. 61–66, 1988.

[213] S. M. Oh, H. R. Kim, Y. J. Park, S. Y. Lee, and K. H. Chung, "Organic extracts of urban air pollution particulate matter (PM2.5)-induced genotoxicity and oxidative stress in human lung bronchial epithelial cells (BEAS-2B cells)," *Mutation Research*, vol. 723, no. 2, pp. 142–151, 2011.

[214] O. Sevastyanova, B. Binkova, J. Topinka et al., "*In vitro* genotoxicity of PAH mixtures and organic extract from urban air particles—part II: human cell lines," *Mutation Research*, vol. 620, no. 1-2, pp. 123–134, 2007.

[215] J. Hukkanen, O. Pelkonen, J. Hakkola, and H. Raunio, "Expression and regulation of xenobiotic-metabolizing cytochrome P450 (CYP) enzymes in human lung," *Critical Reviews in Toxicology*, vol. 32, no. 5, pp. 391–411, 2002.

[216] S. Mollerup, G. Berge, R. Bæra et al., "Sex differences in risk of lung cancer: expression of genes in the PAH bioactivation pathway in relation to smoking and bulky DNA adducts," *International Journal of Cancer*, vol. 119, no. 4, pp. 741–744, 2006.

[217] K. Yang, Y. Huang, G. Zhao, Y. Lei, and K. Wang, "Expression of PAH-DNA adducts in lung tissues of Xuanwei female lung cancer patients," *Chinese Journal of Lung Cancer*, vol. 13, no. 5, pp. 517–521, 2010.

[218] E. Gyorffy, L. Anna, Z. Gyori et al., "DNA adducts in tumour, normal peripheral lung and bronchus, and peripheral blood lymphocytes from smoking and non-smoking patients: correlations between tissues and detection by 32P-postlabelling and immunoassay," *Carcinogenesis*, vol. 25, no. 7, pp. 1201–1209, 2004.

[219] J. A. Holme, M. Gorria, V. M. Arlt et al., "Different mechanisms involved in apoptosis following exposure to benzo[a]pyrene in F258 and Hepa1c1c7 cells," *Chemico-Biological Interactions*, vol. 167, no. 1, pp. 41–55, 2007.

[220] A. Gábelová, Z. Valovicová, G. Bacová et al., "Sensitivity of different endpoints for *in vitro* measurement of genotoxicity of extractable organic matter associated with ambient airborne particles (PM_{10})," *Mutation Research*, vol. 620, no. 1-2, pp. 103–113, 2007.

[221] M.-X. Ensell, W.-Z. Whong, Z.-C. Heng, J. Nath, and T. Ong, "*In vitro* and *in vivo* transformation in rat tracheal epithelial cells exposed to diesel emission particles and related compounds," *Mutation Research*, vol. 412, no. 3, pp. 283–291, 1998.

[222] I. Abbas, G. Garçon, F. Saint-Georges et al., "Polycyclic aromatic hydrocarbons within airborne particulate matter (PM2.5) produced DNA bulky stable adducts in a human lung cell coculture model," *Journal of Applied Toxicology*, vol. 33, no. 2, pp. 109–119, 2011.

[223] A. R. Collins and L. R. Ferguson, "DNA repair as a biomarker," *Mutation Research*, vol. 736, no. 1-2, pp. 2–4, 2012.

[224] B. Binkova, I. Chvatalova, Z. Lnenickova et al., "PAH-DNA adducts in environmentally exposed population in relation to metabolic and DNA repair gene polymorphisms," *Mutation Research*, vol. 620, no. 1-2, pp. 49–61, 2007.

[225] E. Longhin, E. Pezzolato, P. Mantecca et al., "Season linked responses to fine and quasi-ultrafine Milan PM in cultured cells," *Toxicology in Vitro*, vol. 27, pp. 551–559, 2013.

[226] M. Mehta, L.-C. Chen, T. Gordon, W. Rom, and M.-S. Tang, "Particulate matter inhibits DNA repair and enhances mutagenesis," *Mutation Research*, vol. 657, no. 2, pp. 116–121, 2008.

[227] J. Pourazar, A. Blomberg, F. J. Kelly et al., "Diesel exhaust increases EGFR and phosphorylated C-terminal Tyr 1173 in the bronchial epithelium," *Particle and Fibre Toxicology*, vol. 5, article 8, 2008.

Hindawi Publishing Corporation
BioMed Research International
Volume 2013, Article ID 685142, 13 pages
http://dx.doi.org/10.1155/2013/685142

Review Article

Inflammation-Related Effects of Diesel Engine Exhaust Particles: Studies on Lung Cells *In Vitro*

P. E. Schwarze, A. I. Totlandsdal, M. Låg, M. Refsnes, J. A. Holme, and J. Øvrevik

Division of Environmental Medicine, Norwegian Institute of Public Health, Lovisenberggaten 8, 0403 Oslo, Norway

Correspondence should be addressed to P. E. Schwarze; per.schwarze@fhi.no

Received 10 October 2012; Revised 4 January 2013; Accepted 15 January 2013

Academic Editor: Tim Nawrot

Diesel exhaust and its particles (DEP) have been under scrutiny for health effects in humans. In the development of these effects inflammation is regarded as a key process. Overall, *in vitro* studies report similar DEP-induced changes in markers of inflammation, including cytokines and chemokines, as studies *in vivo*. *In vitro* studies suggest that soluble extracts of DEP have the greatest impact on the expression and release of proinflammatory markers. Main DEP mediators of effects have still not been identified and are difficult to find, as fuel and engine technology developments lead to continuously altered characteristics of emissions. Involved mechanisms remain somewhat unclear. DEP extracts appear to comprise components that are able to activate various membrane and cytosolic receptors. Through interactions with receptors, ion channels, and phosphorylation enzymes, molecules in the particle extract will trigger various cell signaling pathways that may lead to the release of inflammatory markers directly or indirectly by causing cell death. *In vitro* studies represent a fast and convenient system which may have implications for technology development. Furthermore, knowledge regarding how particles elicit their effects may contribute to understanding of DEP-induced health effects *in vivo*, with possible implications for identifying susceptible groups of people and effect biomarkers.

1. Introduction

Living close to heavily trafficked roads has been associated with adverse effects on people's health, including increased mortality and morbidity from cardiopulmonary causes [1]. Though the proximity to dense traffic includes exposure to noise and gasses, which may adversely affect health [1, 2], emissions of particle matter (PM) from traffic are estimated to have a major adverse impact on health [1, 3]. Notably, exposure to PM has been associated with adverse effects on the pulmonary as well as cardiovascular system [4, 5]. PM from traffic comprises road dust, vehicle particles, and exhaust particles, which have all been linked to adverse health outcomes [1]. However, most publications focus on the exhaust particles.

Traditionally diesel engines have mostly been used in heavy duty vehicles. However, according to statistics from the European automobile manufacturers' association (ACEA), there has been a large increase in the percentage of newly registered diesel passenger cars in Western Europe, from 13.8% in 1990 to 50.6% in 2010. This is an intended increase as a means to cut CO_2 emissions from transport. However, diesel-fuelled vehicles with pre-EURO 5 technologies or the equivalent US standard are known for their higher PM emissions compared to gasoline-fuelled vehicles, and will dominate the car fleets for several years, considering the average age of the vehicles in operation. As a result of the significant contribution of PM emissions from diesel vehicles for the total concentration of PM in ambient air, extensive research on effects of diesel engine exhaust (DEE) and diesel exhaust particles (DEP) has been carried out.

Inflammation is considered a key step in the development of health effects associated with PM exposure [6–9]. Activated immune cells including neutrophils and macrophages will release cytokines, reactive oxygen species (ROS), lipid mediators, and toxic proteases, which may further amplify and contribute to any DEP-induced epithelial damage. A further increased release of pro-inflammatory mediators from the epithelium and/or induced epithelial cell death may augment as well as prolong the inflammatory reactions, and ultimately result in chronic inflammation if the exposure persists. Furthermore, the increased oxidative stress caused

by activated immune cells, may also contribute to DEP-induced DNA damage, and mutations [10]. Notably, chronic inflammation is also a central part of cancer development [11]. In addition to promoting the development of lung diseases, airway inflammation may be a cardiovascular risk factor. Evidence suggests that inflammation in the lung may lead to systemic inflammation, which may increase the susceptibility to acute cardiovascular disease [12–14].

Cell culture models *in vitro* have been used to characterize various toxic effects of DEP including DNA damage, effects on cell proliferation, release of cytokines and chemokines, differentiation and/or capacity of immune cells to defend against infections cytotoxicity (cellular differentiation), and cytotoxicity. Furthermore, such models have been used to investigate effects of various types of DEP and DEP-components, as well as to study more detailed mechanisms of effect. Since DEP may deposit at various places in the airways [15], different lung epithelial cells as well as immune cells and combinations have been used.

Many factors influence the chemical and physical properties of collected DEP; among them are engine technology, fuel, load, temperature and filtration devices. Thus, a range of different DEP samples with varying composition have been studied. Some studies have also investigated the effect of engine and fuel interventions (Table 1). This paper summarises *in vitro* studies of pro- and anti-inflammatory- and allergy- linked responses of lung cells after exposure to different DEP and associated compounds. Focus will be on mechanisms involved in pro-inflammatory effects. This knowledge will contribute to the understanding of DEP-induced health effects *in vivo* and represent a fast and convenient system for technology development.

2. Expression and Release of Cytokines and Chemokines

Inflammatory reactions *in vivo* involve the production and release of a range of signalling molecules such as cytokines, chemokines, and leukotrienes/prostaglandins and adhesion molecules. These molecules operate in a complex network between epithelial cells and immune cells including macrophages, neutrophils, eosinophils, dendritic cells, and Th-cells [6, 44]. Depending on the cytokines and/or chemokines released, different classes of immune cells will be recruited and affect the outcome of the inflammatory response. In mild to moderate allergic asthma related responses eosinophils are the predominant inflammatory cells, whereas episodes of acute exacerbation of asthma tend to be driven by neutrophilic inflammation [45]. Neutrophils are also believed to be the more important for the development of chronic obstructive pulmonary disease (COPD), because of their ability to release elastase which mediates tissue destruction [46]. Eosinophils express CCR3-chemokine receptors and are primarily activated and recruited by chemokines CCL-chemokines such as CCL5/-7/-11/-16/-24 and -26, whereas neutrophils express CXCR1 and -2 receptors and are primarily activated by CXCL-chemokines including CXCL1-3 and -5-8 [47]. Similarly, other classes of immune cells such as dendritic cells, basophils, B-cells, and various T cells express relatively specific sets of chemokine receptors allowing for targeted activation of different types of immune responses.

At a cellular level, the onset of pro-inflammatory reactions tends to start by release of early-responding cytokines such as interleukin (IL)-1α and-β and tumor necrosis factor (TNF)-α. IL-1α/-β and TNF-α tend to be expressed as inactive proforms in resting cells and may be rapidly cleaved and released without requiring activation of the transcriptional machinery. This enables an immediate response upon encounters with inhaled pathogens or xenobiotics. IL-1α/-β and TNF-α subsequently regulate the expression of a variety of secondary cytokines and chemokines, including IL-6 and CXCL8 (IL-8). However, secondary cytokines may also be activated more directly by DEP (independently of IL-1α/-β and TNF-α) through activation of pro-inflammatory signalling pathways within the cells.

The release of IL-1β is tightly controlled, which seems to requires a dual pathway activation process involving transcriptional activation of the IL-1β gene leading to formation of pro-IL-1β and activation of the NALP3 inflammasome system. This leads to cleavage of the pro-form and subsequent release of active IL-1β [48]. Increased expression of pro-IL-1β is often found after exposure to lipopolysaccharide (LPS), an inflammatory Toll-like receptor (TLR) agonist from bacterial walls. NAPL3 on the other hand responds to so-called danger-associated molecular patterns (DAMPs) released during cellular necrosis, such as uric acid crystals [49]. However, DAMPs and other NALP3 activators do not seem to induce formation of pro-IL-1β. Thus priming with LPS is often required for DAMPs to induce cellular IL-1β release. Interestingly, in the absence of LPS, an increased expression of IL-1β in alveolar epithelial lung cells (A549) was found in an air-liquid exposure system to freshly generated DEP [42]. Also, in THP-1 monocytes NIST-2975 DEP induced an increase in IL-1β release, independently of the presence of LPS [20]. In a coculture of BEAS-2B cells and primary human monocytes, NIST 2975 DEP enhanced the cytokine release of IL-8 after pre-treatment with LPS. [26]. However, this response does not seem to occur through a "classic" activation of the NALP3-inflammasome complex. NIST 2975 DEP is also reported to reduce an IL-1β-induced IL-8 response in the BEAS-2B and monocytes co-culture [26]. Furthermore, central elements of the NALP3-inflammasome did not seem to be needed in responses to DEP in transgenic mice [50].

TNF-α is expressed as a membrane bound proform that is released upon cleavage by the metalloprotease TNF-α converting enzyme (TACE), also known as ADAM-17 [51]. Thus, DEP may induce pro-inflammatory effects dependent on TACE-mediated TNF-α cleavage. DEP have been reported to induce TNF-α responses in primary monocyte-derived macrophages, and cytokine responses in endothelial cells exposed to conditioned media from DEP-exposed macrophages was suppressed by TNF-α-inhibition [52]. Diesel-enriched PM has also been found to induce TNF-α in monocyte-derived dendritic cells [53]. In contrast, studies in human and murine alveolar macrophages have reported

Table 1: Origin of diesel particles used in the different studies, test systems, concentrations and effects on different end-points. The arrows give a rough indication of the magnitude of effects judged from the results presented (small: ↑; moderate: ↑↑; strong ↑↑↑).

Diesel type	Test system	Concentrations	Endpoints	Citation
Heavy duty machine NIST 1650	Cell-free	Not relevant	ROS (malondialdehyde) ↑↑	Ball et al. [16]
Heavy duty machine NIST 1650	Bronchial epithelial cells (16HBE cell line), Primary human nasal epithelial cells	10–30 μg/cm^2	ROS-formation (DCF-fluoroscence) ↑↑, CYPIAI mRNA and EROD-activity ↑↑; NADPH quinone oxidodreductase-1 mRNA ↑↑; translocation of transcription factor Nrf2 ↑↑	Baulig et al., [17, 18]
Heavy duty machine NIST 1650	16-HBE (bronchial epithelial cells)	10 μg/cm^2	GM-CSF ↑↑, NFκ-B activity ↑↑, CYP1A1 mRNA ↑↑, Phosphorylation of MAPK Erk and p38 ↑↑	Bonvallot et al., [19]
Heavy duty machine NIST 1650	THP-1 monocyte and A549 epithelial cell co-culture	10–40 μg/cm^2	IL-6 ↑; IL-8 ↑; TNFα	Kocbach et al., [20]
Heavy duty machine NIST 1650	A549 epithelial cells	0.1 to 20 ppm	IL-8 ↑; CRP ↑	Patel et al., [21]
Heavy duty machine NIST 1650	RAW monocyte/macrophages	5–20 μg/mL	NO-production ↑↑	Saxena et al., [22]
Heavy duty machine NIST 1650	BEAS-2B, (bronchial epithelial cells)	~4–60 μg/cm^2	Increased cytotoxicity	Totlandsdal et al., [23]
Forklift NIST 2975	Cell-free,	Not relevant	ROS (malondialdehyde) ↑	Ball et al. [16]
Forklift NIST 2975	Primary human epithelial cells	50 μg/mL	Phosphorylation of Stat3, EGF-receptor ↑↑	Cao et al., [24]
Forklift NIST 2975	BEAS-2B Bronchial epithelial cells	10 μg/cm^2	STAT3; src; EGFR necessary for p21 ↑↑; inhibition of proliferation	Cao et al., [25]
Forklift NIST 2975	BEAS-2B Bronchial epithelial cells + primary monocytes	50 μg/mL	IL-1	Chaudhuri et al., [26]
Forklift NIST 2975	HEK-293 epidermal cells, primary mouse neurons	77–770 μg/mL	TRPA-1 activation ↑	Deering-Rice et al., [27]
Forklift NIST 2975	16-HBE, monocytes, dendritic cells, triple co-culture	125 μg/mL (cells on insert)	Reduction and altered distribution of occluding, minor effect in epithelial cells, stronger in other cell types	Lehmann et al., [28]
Forklift NIST 2975	A549 and NCI-H292 cells	5–10 μg/cm^2	MMP-1	Amara et al., [29]
Forklift NIST 2975	Primary murine tracheal cells	25 μg/cm^2	Small effects on LDH, HO-1 Alveolar lung cell line GSH/GSSG ratio	Manzo et al., [30]
Forklift NIST 2975	Primary human macrophages Suspension culture,	100 μg/mL	No significant increase in TNF or IL-8; DEP reduced cytokine release induced by LPS	Sawyer et al., [31]
Forklift NIST 2975	BEAS-2B (bronchial epithelial cells)	Only extracts tested	IL.6 ↑; IL-8 ↑	Swanson et al., [32]
Forklift NIST 2975	BEAS-2B cells (bronchial epithelial cells), HAEC cells	10 μg/cm^2	IL-8 mRNA ↑↑, N-DEP effect NFκB dependent	Tal et al., [33]
NIST, not specified	A549 epithelial cells and primary rat airway epithelial cells	20 μg/cm^2	Transepithelial conductance ↑ Occluding ↓	Caraballo et al., [34]
C-DEP, EPA diesel (2005)	Primary human epithelial cells	50 μg/mL	Phosphorylation of Stat3 ↑↑↑	Cao et al., [24]
A-DEP, diesel from Sagai et al., [35]	BEAS-2B (bronchial epithelial cells)	10 μg/cm^2	IL-8 mRNA ↑↑↑	Tal et al., [33]

Table 1: Continued.

Diesel type	Test system	Concentrations	Endpoints	Citation
A-DEP, diesel from Sagai et al., [35]	BEAS-2B (bronchial epithelial cells)	5–50 μg/mL	HSP70 ↑↑ at 10 μg/mL	Jung et al., [36]
2.7 L Isuzu diesel; A-DEP diesel from Sagai et al., [35]	BEAS-2B (bronchial epithelial cells) and primary peripheral airway cells	5 and 25 μg/mL	IL-8 ↑↑	Kawasaki et al., [37]
2.7 L Isuzu diesel; A-DEP before year 2000	BEAS-2B (bronchial epithelial cells)	5–100 μg/mL	IL-8 ↑↑, GM-CSF ↑↑, Depending on NFκB, reduced by NAC	Takizawa et al., [38, 39]
2.7 L Isuzu diesel; A-DEP before year 2000	BEAS-2B (bronchial epithelial cells)	5–100 μg/mL	IL-8 ↑↑, RANTES ↑↑; dependent on p38, reduced by NAC	Hashimoto et al., [40]
Deutz unloaded 2.2 L; EURO 4 (2009)	BEAS-2B (bronchial epithelial cells)	~4–60 μg/cm^2	IL-6 ↑↑; IL-8 ↑↑; CYP1A1 ↑↑↑ (at 0.004 μg/cm^2); COX-2 ↑↑↑; p38 ↑ and NFκB ↑	Totlandsdal et al., [23]
DEP_A (from EPA)	Primary murine tracheal cells	5–200 μg/cm^2	LDH ↑ at 100 μg/cm^2 Alveolar lung cell line HO-1 ↑↑	Manzo et al., [30]
1.6 L Volkswagen diesel; from EPA (1992)	Primary human bronchial epithelial cells; human primary monocytes differentiated to dendritic cells;	3 μg/cm^2	Epithelial cells TSLP ↑↑ Dendritic cells OX40L ↑↑;	Bleck et al., [41]
Heavy duty 9.2 L; DEP freshly generated	A549 epithelial cells, Air-liquid interface exposure	Low 0.1 mg/m^3 High 0.8 mg/m^3	IL-1β only at one conc of high NO_2, reduced viability	Tsukue et al., [42]
2.2 L Honda EURO 4 machine DEP + rape seed biodiesel (±DPF)	BEAS-2B (bronchial epithelial cells)	~6 to 200 μg/mL	IL-6 Most effect in μg/mL B50 DPF ≫ B0DPF > B50 > B0	Gerlofs-Nijland et al., submitted
2.2 L Honda EURO 4 machine, Golf. Corolla cars DPF, diesel biodiesel	Cell-free	Not relevant	Correlation of DTT consumption with EC/Water insoluble OC/OC	Ka et al., [43]
US 2004 machine (black smoker)	HEK-293 epidermal cells, primary mouse neurons	77–770 μg/mL	TRPA-1 activation ↑↑	Deering-Rice et al., [27]
Soy bean biodiesel 2005	BEAS-2B (bronchial epithelial cells)	Only extracts tested	Stronger effects of biodiesel (soy bean)	Swanson et al., [32]

that DEP rather suppress TNF-α responses [54–56]. To the best of our knowledge, no effects of DEP or DEP-extracts on TNF-α response have been reported from pulmonary epithelial cells. However, DEP have been found to induce TNF-α responses in middle-ear epithelial cells [57], but not in human keratinocytes [58]. In total, TNF-α-release does not seem to be a prerequisite for DEP to induce pro-inflammatory responses *in vitro*. In line with this, *in vivo* studies with TNF-α knock-out mice suggest that DEP-induced inflammation is triggered independently of TNF-α [59].

Many *in vitro* studies on lung epithelial cells have reported that DEP induce the release of a number of cytokines and chemokines that are involved in both innate and/or adaptive immunity inflammatory responses [60]. Innate immunity cytokines such as IL-6 and IL-8 have often been included in investigations of DEP effects. In studies with BEAS-2B bronchial epithelial lung cells DEP from a pre-year-2000 engine increased the release of chemokines such as IL-8 [33, 38]. In a comparison of different DEP, the older DEPs from Japan [35] and the NIST 2975 were considerably more potent than the more recently produced DEP from EPA (Table 1). However, not all studies report increased IL-8 levels after DEP exposure, despite increased IL-8 RNA levels [23]. In a broader analysis on the mRNA level of EURO-4 DEP-induced cytokines in BEAS-2B cells, Totlandsdal and coworkers observed increased levels of CCL5 (RANTES), CXCL10, and IL-1β among others, in addition to high levels of IL-6 and IL-8 [23]. However, only the last two reached statistical significance. Increased RANTES after DEP-exposure (pre-year-2000 engine) has also been reported by Hashimoto and co-workers [40].

Thymic stromal lymphopoietin (TSLP) is an an IL-7-like cytokine which has received considerable attention as a possible "master-switch" in allergic disease. TSLP from epithelial barrier surfaces suppress p40 and induce OX40L expression by dendritic cells (DCs), which suppress Th1 and promote Th2 responses, respectively [61]. Exposure to pre-year-2000 DEP has been shown to induce TSLP release from human bronchial epithelial cells (BEAS-2B) subsequently leading to maturation and polarisation of DCs [41]. The DEP-dependent release of TSLP from the epithelial cells also caused the DCs to express OX40L ligand and Jagged-1 [62].

Thus effects of DEP on epithelial lung cells may promote the induction of Th2 responses, often associated with adaptive immunity and allergic asthma. The ability of DEP to stimulate adaptive immune responses has been corroborated by a study in transgenic mice [63].

An increase in granulocyte macrophage colony-stimulating factor (GM-CSF), that stimulates monocyte multiplication, has also been observed after DEP exposure [17, 38]. DEP-enriched particulate matter sampled in a tunnel stimulated cytokine release (IL-12, TNF-α, IL-6, and interferon (IFN)-γ) from primary monocyte-derived dendritic cells [53]. This indicates that other cell types can contribute to a pro-inflammatory pattern of cytokines and chemokines in concert with macrophages and epithelial cells. Moreover, conditioned medium from macrophages exposed to DEP (NIST 2975) stimulated primary human endothelial cells (HUVEC) to release cytokines and chemokines through a TNF-α dependent mechanism, indicating that pulmonary inflammatory markers may influence systemic cells [52]. Similar observations have also been reported from studies with carbon black particles [64].

3. Other Inflammation-Related Proteins

In addition to cytokines and chemokines, a variety of other signalling molecules are involved in the orchestration of inflammatory responses. ICAM-1 plays a critical role in the adhesion of inflammatory cells to reach the place of an inflammatory response. BEAS-2B cells have been shown to increase expression of this molecule on their surfaces upon exposure to pre-year-2000 DEP [39].

Epithelial cells can form a tight monolayer that presents a barrier to prevent the external agents from entering the circulation. NIST DEP can increase transepithelial electrical conductance and loosening of the tight junctions, thus increasing the possibility of leakage of proteins and perhaps particles to the vascular system [34]. In a triple coculture model (bronchial epithelial 16HBe140 cells, monocyte derived macrophages, and dendritic cells) Lehmann et al. observed that NIST 2975 modulated occludin RNA levels which may have implications for tight junction function. However the effect was only observed at the highest concentration [28]. In this connection, it is interesting to note that NIST 2975 DEP have been reported to increase the release of metalloproteinase MMP-1 from human lung epithelial cells (A549 and NCI-H292). MMP-1 is involved in the degradation of collagen and can thus damage the lung epithelial barrier, probably involving an oxidative mechanism that includes NOX4 [29]. These findings suggest that DEP not only can induce pro-inflammatory responses, but also contribute to structural changes with inflammatory implications.

Prostaglandins function as attractants of inflammatory cells. Studies have found that EURO-4 DEP increased the levels of COX-2 in BEAS-2B cells, a key enzyme in prostaglandin production [23]. This response was also observed with three different DEP (Table 1). DEP have also been reported to enhance COX-2- and prostaglandin E2-responses in monocyte-derived macrophages primed with TLR2 and -4 ligands [65].

Heat shock proteins HSP70 and HSP40 and two other proteins involved in the protein unfolding response were induced after exposure of BEAS-2B cells to pre-year-2000 DEP extracts. This response was accompanied by an increase in IL-6 and IL-8 and possibly related to DEP-induced oxidative stress [36].

Many studies have reported that DEP induce the expression of phase I and II xenobiotic metabolising enzymes through activation of the AhR and Nrf2 transcription factors, respectively [18, 23, 66–68]. Thus, AhR- and Nrf2-regulated gene expression may represent indirect biomarkers of exposure to DEP. Furthermore, phase I enzymes are involved in metabolic activation of various xenobiotics to reactive electrophilic metabolites including ROS, possible triggering molecules of inflammatory reactions following DEP-exposure. This may occur not only directly with regard to triggering of cytokines/chemokine release, but also indirectly via increased cellular toxicity and release of inflammatory DAMP molecules. Thus, changes in the balance between activation and detoxification of the metabolism of xenobiotic in the lung cells may have important inflammatory implications. The phase I enzyme CYP 1A1 is reported to be induced at concentrations of about 0.1 μg/mL or 0.004 μg/cm^2 [23]. However, the increase in CYP1A1 was greatly reduced at higher concentrations, when inflammatory cytokines and chemokines were prominent [23]. The data indicate a reciprocal relationship between the AhR/Arnt-dependent CYP1A1 induction and cytokine production, apparently because AhR has an inhibitory role in the control of inflammation [69–71]. Also the stimulation of the expression of phase II detoxification enzymes by DEP extracts seemed to reduce the cytokine response [72].

4. Particle Considerations

There seems to be obvious differences in the composition of DEP of different age and source. Some older DEP-preparations are apparently less potent than some newer ones (e.g., EURO 4 DEP), although these differences do not seem to correlate with "classic", carcinogenic polycyclic aromatic hydrocarbons (PAH) content (unpublished results from our lab). DEP typically consists of agglomerates of primary carbon particles 15–30 nm in diameter and nucleation mode particles of condensed hydrocarbons and sulphate [73]. However, differences in engine and emission-cleansing technologies may affect the ratio of these two main particle fractions in diesel exhaust emissions and has also considerable impact on the amount and composition of chemicals adhered to the surface of the emitted DEP [74].

4.1. Importance of Soluble Organic Fraction of DEP. In general, both the particulate as well as the organic components of DEP are of importance for DEP-induced effects [75–77]. However, some *in vitro* studies comparing effects induced by organic DEP extracts and corresponding residual particles (subjected to extraction) have demonstrated that the organic

fractions of DEP may be of particular importance for pro-inflammatory responses [19, 78, 79]. It is yet unclear to what extent these responses to the organic extracts could be attributed to the presence of specific groups of compounds. Recent studies indicate that polar organic extracts of PM were found to induce cytotoxicity and IL-6 responses in BEAS-2B cells, while nonpolar organic PM-extracts had no apparent effect [80]. In accordance with this, observations from our lab indicate that compounds eluting in the polar fraction of methanol-extracts of DEP may be of particular importance. Notably, the effects of the polar fraction could not be attributed to identified PAH and PAH-derivatives in the extract (Totlandsdal et al., unpublished results).

Suppressive effects of DEP and DEP organic extracts on various immune responses have also been reported. More specifically, DEP and DEP organic extracts have been found to reduce alveolar macrophage function as demonstrated by reduced production of cytokines (IL-1, TNF-α) and ROS in response to a variety of biological agents (LPS, interferon-γ and bacteria) [54–56, 76]. Different fractions of organic DEP-extracts have been tested for the ability to suppress NO production from BCG-stimulated macrophages [22]. The polar fractions seemed more inhibitory than the less polar fractions [22]. Recent observations from our lab also suggest that high-polar organic DEP-extracts supress IL-8 responses in BEAS-2B cells, despite stimulating IL-6 responses (Totlandsdal et al. unpublished results). Similar findings have been reported for polar extracts of ambient PM [80]. Furthermore, it has been shown that the organic content of DEP, which was in the rank order NIST 2975 < compressor diesel (EPA) < automobile diesel, did not correlate with the immune responses [33]. Thus, obviously there are specific compounds of the organic fraction of DEP, differing with regard to DEP-age, -fuel type, and/or engine, that are of particular importance for cellular responses.

With respect to allergy-related responses there are to our knowledge no *in vitro* studies that investigate the difference between DEP and corresponding DEP organic extracts and residual DEP. However, a study in mice has indicated that the organic fraction rather than the washed particles may be responsible for the enhancement of allergy-related responses, although a role for the solid core of the carbonaceous particles could not be excluded [81].

4.2. Biodiesel. A major reason for the interest in biodiesel fuel has been environmental benefits in terms of decreased global warming impacts and reduced emissions. Increased use of biodiesel in Europe represents an important step for the European Union in order to meet its emission reduction targets and a variety of biofuels are already being introduced into wider use in heavy-duty diesel engines such as those installed in buses and trucks in cities. However, according to a previous review, biodiesel exhaust emission has been extensively characterized under field and laboratory conditions, but there have been limited studies on the effects of biodiesel exhaust in biologic systems [82].

More recently, it has been demonstrated by human inhalation studies that biodiesel (soy bean ethyl esters, SEE: B50 and B100 (50 and 100% biodiesel, resp.)) was equally or more toxic than fossil diesel in promoting cardiovascular alterations as well as pulmonary and systemic inflammation [83]. Coherent with the inflammatory potential of biodiesel demonstrated in this *in vivo* study, recent *in vitro* work from our lab demonstrates a greater toxic and pro-inflammatory capacity in human bronchial epithelial BEAS-2B cells of DEP with biodiesel (rape seed oil methyl esters, RME) than ordinary DEP, especially in the presence of a diesel particle filter (Gerlofs-Nijland et al. unpublished results). Moreover, extracts of biodiesel (blend of SEE and SME) have been reported to induce cytokine responses in BEAS-2B cells at lower concentrations than extracts of petroleum diesel [32]. In contrast, Jalava and colleagues [84] observed that biodiesel DEP were as potent as ordinary DEP, or less potent, depending on the end point (pro-inflammatory response, cell death, DNA damage, or oxidative potential in a mouse macrophage-like cell line (RAW264.7)). In a separate study, only pure fossil diesel and not B20-blends of RME or animal fat methyl esters (AFME) was found to induce ICAM-1 and VCAM-1 expression in primary human umbilical cord cells (HUVECs), and none of the tested DEPs affected IL-8 and CCL2 expression significantly in the human monocytic cell line, THP-1 [85]. Whether these apparent discrepancies in the pro-inflammatory potential of biodiesel are due to cell specific effects or differences in the chemical composition of the DEPs used in the different studies remains to be clarified. Importantly, as pointed out by Brito and colleagues [83], biodiesel may from a commercial point of view be considered as a cleaner, less toxic, and more biodegradable fuel. Thus, the above findings clearly highlight the importance of further studies to elucidate how and to what extent biodiesel fuels affect pro-inflammatory compared to conventional fossil fuel.

5. Biological Mechanisms of DEP-Induced Proinflammatory and Cytotoxic Effects

The genotoxicity of DEP is to a large extent considered to be due to chemicals found in the organic DEP-extracts, such as PAH. In particular, nitro-PAH seem to be important for the mutagenicity of DEP [86, 87]. Also the pro-inflammatory DEP-effects seem mainly to be mediated by constituents in organic DEP-extracts [19, 37, 78, 79]. Most interestingly, DEP with different amount of soluble organic materials may induce IL-8 responses through different mechanisms [33]. DEP with high organic content induced IL-8 through activation of AP-1, while DEP with low organic content induced IL-8 through nuclear factor (NF)-κB. The reason for this difference is unclear, but since activation of the AhR may lead to suppression of NF-κB signaling [69, 71], it is conceivable that the effects could be related to a higher content of AhR-activating compounds in the organic-rich DEP. In any case, the observation is of particular importance as it underscores that DEP from different sources may induce inflammation through different mechanisms, triggered by different DEP-constituents. It should also be considered that even with a single-source DEP it seems unlikely, given the multitude of chemical components adhered to the particle

surface, that there exists a simple mechanism explaining the cellular effects. Moreover, as the concentration-effect course of toxicity by different DEP-constituents most probably differs, the complexity of DEP-induced toxicity is also likely to increase by increasing concentrations, as more and more DEP-constituents enter toxic levels. As a consequence, mechanisms of effects observed at high DEP-concentrations in *in vitro* studies may not necessarily be directly relevant for the effects of low-level DEP-concentrations in real-life exposure.

As within most fields of particle toxicity, oxidative stress is considered a main mechanism of DEP-induced toxicity and inflammation [7, 88, 89]. DEP-induced ROS-formation may activate redox-sensitive transcription factors involved in regulation of pro-inflammatory genes, such as NF-κB and Nrf2 [18, 19]. ROS may interfere with various cell signaling pathways by inhibition of phosphatases through binding/oxidation of important thiol groups subsequently leading to increased phosphorylation/activation of protein kinases. In line with this, genotype variation in antioxidant enzymes, such as glutathione-s-transferases (GSTs), has been associated with susceptibility towards DEP-induced allergic inflammation in humans [90]. However, since GSTs are phase II metabolizing enzymes, also involved in detoxification of organic chemicals present in DEP, it cannot be excluded that the protective role of GSTs in DEP-induced inflammation extends beyond ROS-scavenging.

Direct ROS formation by DEP may arise from enzymatic metabolism of organic compounds such as PAH [18, 91]. However, several studies show that DEP also exert oxidative effects in acellular model systems. In a study of DEP produced by 4 different engine technologies (Euro1 to Euro 4), the antioxidant (DTT) consumption as a measure of oxidative capacity showed a correlation with the content of elemental carbon, water-insoluble carbon, and organic carbon [43]. Moreover, the two different reference-DEP, NIST 1650 and 2975, have been found to exhibit different oxidative capacity in cell free systems, possibly due to difference in chemical composition [16]. Furthermore, Mudway and colleagues [92] showed that DEP depleted lung lining fluid antioxidant levels *in vitro*. In contrast, a comparable effect of DEP was not observed in the airways of healthy subjects; and in a cell culture model *in vitro* the ratio of oxidised to nonoxidised glutathione did not change significantly after exposure to two different diesels, DEPa and NIST 2975 [30]. Thus, possibly the antioxidant defence in the lung lining fluid [92] and lung epithelial cells of healthy individuals are capable of dealing with the oxidative challenge posed by DEP at environmentally relevant concentrations. In a recent study of DEP from different fuel types, produced in the presence or absence of particle filter technology (PDF-treatment), we did not observe any correlation between a cellular DEP-induced ROS formation and DEP-induced cytokine responses in human bronchial epithelial BEAS-2B cells (Gerlofs-Nijland et al. unpublished results). This observation resembles previous results of studies on mineral particles showing no clear correlation between acellular ROS-formation and pro-inflammatory responses in *in vitro* cell culture models [93, 94].

DEP may also stimulate cellular generation of ROS as well as reactive nitrogen species (RNS) through activation of nitric oxide synthetase (iNOS) [29, 95, 96]. Moreover, DEP-induced MMP-1 responses in human alveolar type-2 like A549 cells appeared to be dependent on activation of cellular ROS-formation by the NADPH-oxidase analogue NOX4 [29]. NADPH-oxidase-mediated ROS formation also seems to regulate DEP-induced TNF-α responses in isolated rat brain capillaries [97], and toxicity of DEP in dopaminergic neurons [98]. Moreover, the DEP-component 1,2-naphthoquinone (1,2-NQ) was reported to induce IL-8 responses in human bronchial epithelial BEAS-2B cells, through mitochondrial H_2O_2-production [99]. Thus, it is conceivable that much of the reported suppressive effects of antioxidants on DEP-induced pro-inflammatory responses may be due to interference with DEP-induced cellular ROS-generation, rather than the direct particle-derived ROS production observed in acellular systems. If this is the case, oxidative stress should be considered a cellular response to DEP exposure and not a direct DEP property. However, findings obtained by use of antioxidants need to be interpreted with caution. While antioxidants may attenuate DEP-induced inflammation, the role of oxidative stress in cellular responses is inherently difficult to interpret. Antioxidants like N-acetyl cysteine (NAC) may also detoxify other reactive electrophilic DEP-constituents that potentially could trigger inflammatory reactions. Furthermore, ROS is an important and natural second messenger in most signaling pathways [100–102]. Thus, use of antioxidants is likely to interfere with a variety of cellular responses irrespective of oxidative stress. Few, if any, studies using antioxidants to assess the role of oxidative stress in particle induced effects have included proper controls to clarify these issues. It has also been pointed out that *in vitro* ROS-formation may have limited value in predicting pathological effects, because almost all particles elicit oxidative stress in cells, given a sufficient concentration [103]. Finally, oxidative stress alone may not be sufficient to induce pro-inflammatory responses in lung cells [104, 105], thus other and/or additional mechanisms are likely involved in DEP-induced inflammation.

Of particular interest, recent studies show that pre-year-2000 DEP may induce Ca^{2+}-signaling through activation of transient receptor potential (TRP) cation-channels in primary and transformed human bronchial epithelial cells (NHBE and BEAS-2B cells). Li and colleagues [106] have shown that DEP triggered Ca^{2+}-influx through proteinase-activated receptor-2 (PAR-2) mediated activation of TRPV4 channels on the surface of human bronchial epithelial cells leading to increased expression of matrix metalloproteinase-1 (MMP-1). Ca^{2+}-signaling appears to be central to IL-8 responses in bronchial epithelial cells induced by multiple compounds found in ambient air [107]. Therefore, it seems likely that DEP-induced PAR-2/TRPV4-activation is not restricted to MMP-1 regulation, but also involved in cytokine responses. In support of this, recent results from our lab show that silencing of PAR-2 by siRNA attenuated DEP-induced IL-6 responses in bronchial epithelial BEAS-2B cells (Øvrevik et al., unpublished results). Whether DEP activates

PAR-2 receptors directly remains to be clarified. However, in line with previous studies on DEP-induced inflammation the effects appeared to be due to the soluble organic fraction of the particles [106]. These authors also showed that a TRPV4 polymorphism ($TRPV4_{P19S}$) associated with increased susceptibility to COPD significantly enhanced DEP-induced Ca^{2+}-signaling and MMP-1 responses, thus providing a possible link between COPD pathogenesis and DEP-exposure. In parallel to these observations, Deering-Rice and co-workers [27] found that DEP (black smoker, Table 1) induced Ca^{2+}-signaling by activating TRPA1 receptors in sensory nerve cells. This effect was attributed to electrophilic components of DEP, including various aldehydes and quinones [27]. In further support of these findings, the DEP-component 1,2-NQ has been found to activate TRPV1 (vanilloid receptor-1) in guinea pig trachea [108]. However, this study suggests that TRPV1 was indirectly activated by 1,2-NQ through transactivation of protein tyrosine kinases such as the epidermal growth factor receptor (EGFR).

It is interesting to note that cellular signaling through RAGE (receptors for advanced glycation end-products) was suggested to have a role in DEP-induced NF-κB-activation and chemokine responses (MCP-1 and CINC-1) in a type-I-like epithelial cell line (R3/1) [109]. In line with this, DEP-exposure also enhanced RAGE-expression in R3/1 cells and primary human small airway epithelial cells (SAECs), possibly providing a positive feedback mechanism for DEP-induced inflammation [109]. However, as with the studies on PAR-2 and TRP-channels, it is still unclear whether DEP activated RAGE directly or whether DEP or DEP-components caused formation of RAGE-ligands in the exposed cells.

Studies also suggest that DEP exposure activates EGFR-signaling [24, 107, 110, 111]. Of notice, the EGFR does not seem to be a direct target of DEP or DEP-components, but is more likely a downstream response to some DEP-triggered effect. Activation of EGFR-signaling through cleavage and release of membrane bound transforming growth factor (TGF-α) by the metalloproteinase TNF-α converting enzyme (TACE or ADAM17) seems to be a universal mechanisms of IL-8 regulation in airway epithelial cells by multiple endogenous and exogenous compounds, including DEP and various air pollution components [107, 112, 113]. In coherence with reported *in vitro* effects increased EGFR-expression and activation have been observed in biopsies of bronchial epithelium from volunteers exposed to freshly generated DEP [114]. Moreover, TACE and EGFR are overexpressed in pulmonary epithelium of asthmatics and COPD patients and this correlates with increased expression of IL-8, which is a key activator of neutrophils [115]. Thus, increased TACE and EGFR-expression may be important susceptibility factors for neutrophilic inflammation by air pollutants.

Considerable progress has been made to elucidate the mechanisms of DEP-induced inflammation, beyond the mere oxidative stress effects. Whether any of the above mentioned receptors are direct targets of DEP or organic chemicals from DEP remains to be clarified. However, depending on the further research, these receptors may turn out as important susceptibility factors for adverse effects of DEP-exposure. Such knowledge may also substantiate any possible role of biomarkers of effect as measured by gene-array. Another important aspect to consider is that if DEP-induced pro-inflammatory responses are regulated by different cell surface receptors, this is likely to give rise to cell specific effects, since receptor expression may be highly cell-type dependent. Similarly, expression of metabolizing enzymes involved in bioactivation or ROS-formation from adhered hydrocarbons may also vary between different cell-types and affect the outcome of exposure. It is conceivable that this may explain apparent discrepancies in effects obtained by different *in vitro* models, such as the reported biodiesel effects discussed above. For the same reason, care should be taken when interpreting the importance of results obtained by a single cell model.

6. Challenges and Concluding Remarks

Diesel engine exhaust represents a complex and variable air pollution mixture, of which the physicochemical characteristics are highly dependent on the fuel used and the type of engine [43, 116]. Recently, Hesterberg and colleagues have stressed this important issue, by questioning the relevance of certain samples or exhaust exposures that currently are used in experimental studies, for risk-assessment of particulate matter from new technology diesel exhaust [74]. As shown in Table 1, a large proportion of the *in vitro* studies have used the standard reference diesel material from the National Institute of Standards and Technology (NIST, USA), which were collected from a fork lift truck several years ago. Although a thoroughly characterised material may be very useful for investigating the role of the physicochemical composition for the effects, one may question whether it is time to produce and agree on a commercial reference diesel sample which is more representative to current diesel emissions.

In vitro studies represent a fast and convenient system which may have implications for technology development. *In vitro* studies are also of key importance for increasing our knowledge about the underlying biological mechanisms of effects. Interestingly, several of the proteins investigated in *in vitro* studies of mechanisms of signal transduction, have also been observed activated in bronchial biopsies from human volunteers exposed to diesel exhaust particles in clinical studies [15, 114, 117, 118]. Thus there is in many cases a coherence of *in vitro* and *in vivo* findings.

With respect to *in vitro* research on the pulmonary effects of diesel engine exhaust emissions on inflammatory reactions, a large diversity of *in vitro* models has been applied, and a range of effect parameters have been investigated. In addition, several different types of DEP samples have been used, subjected to different treatments for exposure. The various models have their advantages and disadvantages, but the diversity can be seen as strength, though it challenges the process of generating overall conclusions. Furthermore, for a complete evaluation of DEP effects also genotoxic and other outcomes should be taken into consideration.

A well-known limitation of *in vitro* studies is the general use of exposure concentrations that are on the high

side, compared to real world situations. The exact levels to which pulmonary cells are likely to be exposed to *in vivo* are difficult to estimate, based on the complexity of the deposition pattern. However, according to estimations of Li and colleagues, a biologically relevant tissue culture concentration of DEP ranges from 0.2 to 20 ug/cm^2 [119]. Although the concentrations used in several studies fall within this range, and certain effects also have been detected at concentrations below this range, it would be important to optimize and increase the sensitivity of current *in vitro* models. Of notice, direct exposure to freshly generated DEP of cells at the air/liquid interface (ALI) has been performed [42, 120–122]. Results reported from these rather complicated models support results obtained by exposing traditional submerged cell cultures with DEP collected on filters. This may be due to similar amounts of organic components being released independently of the aggregation/agglomeration state. However, some studies suggest that response to ALI exposure may occur at lower DEP-doses that by conventional exposure of submerged cell cultures [120–122]. These are important observations considering that *in vitro* studies often are criticized for using too high particle concentrations.

The inflammatory effects of DEP seem to be attributable to the soluble organic fraction, but questions still remain with respect to what fraction and components that are most important for the inflammatory responses. The mechanisms are still unclear, but receptors in the plasma membrane, including the PAR-2 receptor, vanilloid-1 receptor, RAGE-receptor, and the EGF-receptor, seem to be involved. DEP are known to induce acellular as well as cell-mediated ROS-formation, oxidative stress and deplete the levels of antioxidants, which seem to be involved in the inflammatory effects of DEP. At what stage the oxidative tonus exerts its major effect(s) in the signalling pathways leading to inflammation remains to be further clarified.

Of notice, engine and fuel technology have been rapidly changing resulting in reduced emissions. The question arises whether this reduction in DEP from modern engines has resulted in an equivalent reduction in harmful properties of the emissions. Moreover, increased use of biodiesel to meet demands for CO_2-neutral fuels warrants further studies on how different fuels affect the pro-inflammatory properties of DEP.

References

[1] WHO, *Health Effects of Transport-Related Air Pollution*, World Health Organization, Copenhagen, Denmark, 2005.

[2] E. van Kempen and W. Babisch, "The quantitative relationship between road traffic noise and hypertension: a meta-analysis," *Journal of Hypertension*, vol. 30, no. 6, pp. 1075–1086, 2012.

[3] A. J. Cohen, H. R. Anderson, B. Ostro et al., "The global burden of disease due to outdoor air pollution," *Journal of Toxicology and Environmental Health*, vol. 68, no. 13-14, pp. 1301–1307, 2005.

[4] J. O. Anderson, J. G. Thundiyil, and A. Stolbach, "Clearing the air: a review of the effects of particulate matter air pollution on human health," *Journal of Medical Toxicology*, vol. 8, no. 2, pp. 166–175, 2012.

[5] R. D. Brook, S. Rajagopalan, C. A. Pope III et al., "Particulate matter air pollution and cardiovascular disease: an update to the scientific statement from the American Heart Association," *Circulation*, vol. 121, no. 21, pp. 2331–2378, 2010.

[6] S. Salvi and S. T. Holgate, "Mechanisms of particulate matter toxicity," *Clinical and Experimental Allergy*, vol. 29, no. 9, pp. 1187–1194, 1999.

[7] K. Donaldson and V. Stone, "Current hypotheses on the mechanisms of toxicity of ultrafine particles," *Annali dell'Istituto Superiore di Sanita*, vol. 39, no. 3, pp. 405–410, 2003.

[8] F. J. Kelly and J. C. Fussell, "Air pollution and airway disease," *Clinical and Experimental Allergy*, vol. 41, no. 8, pp. 1059–1071, 2011.

[9] Z. D. Ristovski, B. Miljevic, N. C. Surawski et al., "Respiratory health effects of diesel particulate matter," *Respirology*, vol. 17, no. 2, pp. 201–212, 2012.

[10] A. Emmendoerffer, M. Hecht, T. Boeker, M. Mueller, and U. Heinrich, "Role of inflammation in chemical-induced lung cancer," *Toxicology Letters*, vol. 112-113, pp. 185–191, 2000.

[11] H. Bartsch and J. Nair, "Chronic inflammation and oxidative stress in the genesis and perpetuation of cancer: role of lipid peroxidation, DNA damage, and repair," *Langenbeck's Archives of Surgery*, vol. 391, no. 5, pp. 499–510, 2006.

[12] K. Donaldson, V. Stone, A. Seaton, and W. MacNee, "Ambient particle inhalation and the cardiovascular system: potential mechanisms," *Environmental Health Perspectives*, vol. 109, no. 4, pp. 523–527, 2001.

[13] M. W. Frampton, "Systemic and cardiovascular effects of airway injury and inflammation: ultrafine particle exposure in humans," *Environmental Health Perspectives*, vol. 109, no. 4, pp. 529–532, 2001.

[14] W. Q. Gan, S. F. P. Man, A. Senthilselvan, and D. D. Sin, "Association between chronic obstructive pulmonary disease and systemic inflammation: a systematic review and a meta-analysis," *Thorax*, vol. 59, no. 7, pp. 574–580, 2004.

[15] J. Pourazar, I. S. Mudway, J. M. Samet et al., "Diesel exhaust activates redox-sensitive transcription factors and kinases in human airways," *American Journal of Physiology*, vol. 289, no. 5, pp. L724–L730, 2005.

[16] J. C. Ball, A. M. Straccia, W. C. Young, and A. E. Aust, "The formation of reactive oxygen species catalyzed by neutral, aqueous extracts of NIST ambient particulate matter and diesel engine particles," *Journal of the Air and Waste Management Association*, vol. 50, no. 11, pp. 1897–1903, 2000.

[17] A. Baulig, M. Sourdeval, M. Meyer, F. Marano, and A. Baeza-Squiban, "Biological effects of atmospheric particles on human bronchial epithelial cells. Comparison with diesel exhaust particles," *Toxicology in Vitro*, vol. 17, no. 5-6, pp. 567–573, 2003.

[18] A. Baulig, M. Garlatti, V. Bonvallot et al., "Involvement of reactive oxygen species in the metabolic pathways triggered by diesel exhaust particles in human airway epithelial cells," *American Journal of Physiology*, vol. 285, no. 3, pp. L671–L679, 2003.

[19] V. Bonvallot, A. Baeza-Squiban, A. Baulig et al., "Organic compounds from diesel exhaust particles elicit a proinflammatory response in human airway epithelial cells and induce cytochrome p450 1A1 expression," *American Journal of Respiratory Cell and Molecular Biology*, vol. 25, no. 4, pp. 515–521, 2001.

[20] A. Kocbach, J. I. Herseth, M. Låg, M. Refsnes, and P. E. Schwarze, "Particles from wood smoke and traffic induce differential pro-inflammatory response patterns in co-cultures,"

Toxicology and Applied Pharmacology, vol. 232, no. 2, pp. 317–326, 2008.

[21] H. Patel, S. Eo, and S. Kwon, "Effects of diesel particulate matters on inflammatory responses in static and dynamic culture of human alveolar epithelial cells," *Toxicology Letters*, vol. 200, no. 1-2, pp. 124–131, 2011.

[22] Q. B. Saxena, R. K. Saxena, P. D. Siegel, and D. M. Lewis, "Identification of organic fractions of diesel exhaust particulate (DEP) which inhibit nitric oxide (NO) production from a murine macrophage cell line," *Toxicology Letters*, vol. 143, no. 3, pp. 317–322, 2003.

[23] A. I. Totlandsdal, F. R. Cassee, P. Schwarze, M. Refsnes, and M. Låg, "Diesel exhaust particles induce CYP1A1 and pro-inflammatory responses via differential pathways in human bronchial epithelial cells," *Particle and Fibre Toxicology*, vol. 7, article 41, 2010.

[24] D. Cao, P. A. Bromberg, and J. M. Samet, "COX-2 expression induced by diesel particles involves chromatin modification and degradation of HDAC1," *American Journal of Respiratory Cell and Molecular Biology*, vol. 37, no. 2, pp. 232–239, 2007.

[25] D. Cao, P. A. Bromberg, and J. M. Samet, "Diesel particle-induced transcriptional expression of p21 involves activation of EGFR, Src, and Stat3," *American Journal Respiratory Cell Molecular Biology*, vol. 42, no. 1, pp. 88–95, 2010.

[26] N. Chaudhuri, C. Paiva, K. Donaldson, R. Duffin, L. C. Parker, and I. Sabroe, "Diesel exhaust particles override natural injury-limiting pathways in the lung," *American Journal of Physiology*, vol. 299, no. 2, pp. L263–L271, 2010.

[27] C. E. Deering-Rice, E. G. Romero, D. Shapiro et al., "Electrophilic components of diesel exhaust particles (DEP) activate transient receptor potential ankyrin-1 (TRPA1): a probable mechanism of acute pulmonary toxicity for DEP," *Chemical Research in Toxicology*, vol. 24, no. 6, pp. 950–959, 2011.

[28] A. D. Lehmann, F. Blank, O. Baum, and P. Gehr B. M, "Rothen-Rutishauser: diesel exhaust particles modulate the tight junction protein occludin in lung cells in vitro," *Particle and Fibre Toxicology*, vol. 6, article 26, 2009.

[29] N. Amara, R. Bachoual, M. Desmard et al., "Diesel exhaust particles induce matrix metalloprotease-1 in human lung epithelial cells via a NADP(H) oxidase/NOX4 redox-dependent mechanism," *American Journal of Physiology*, vol. 293, no. 1, pp. L170–L181, 2007.

[30] N. D. Manzo, R. Slade, J. H. Richards, J. K. McGee, L. D. Martin, and J. A. Dye, "Susceptibility of inflamed alveolar and airway epithelial cells to injury induced by diesel exhaust particles of varying organic carbon content," *Journal of Toxicology and Environmental Health*, vol. 73, no. 8, pp. 565–580, 2010.

[31] K. Sawyer, S. Mundandhara, A. J. Ghio, and M. C. Madden, "The effects of ambient particulate matter on human alveolar macrophage oxidative and inflammatory responses?" *Journal of Toxicology and Environmental Health Part A*, vol. 73, no. 1, pp. 41–57, 2010.

[32] K. J. Swanson, N. Y. Kado, W. E. Funk, J. D. Pleil, M. C. Madden, and A. J. Ghio, "Release of the pro-inflammatory markers by BEAS-2B cells following in vitro exposure to biodiesel extracts," *Open Toxicology Journal*, vol. 3, pp. 8–15, 2009.

[33] T. L. Tal, S. O. Simmons, R. Silbajoris et al., "Differential transcriptional regulation of IL-8 expression by human airway epithelial cells exposed to diesel exhaust particles," *Toxicology and Applied Pharmacology*, vol. 243, no. 1, pp. 46–54, 2010.

[34] J. C. Caraballo, C. Yshii, W. Westphal, T. Moninger, and A. P. Comellas, "Ambient particulate matter affects occludin distribution and increases alveolar transepithelial electrical conductance," *Respirology*, vol. 16, no. 2, pp. 340–349, 2011.

[35] M. Sagai, H. Saito, T. Ichinose, M. Kodama, and Y. Mori, "Biological effects of diesel exhaust particles. I. In vitro production of superoxide and in vivo toxicity in mouse," *Free Radical Biology and Medicine*, vol. 14, no. 1, pp. 37–47, 1993.

[36] E. J. Jung, N. K. Avliyakulov, P. Boontheung, J. A. Loo, and A. E. Nel, "Pro-oxidative DEP chemicals induce heat shock proteins and an unfolding protein response in a bronchial epithelial cell line as determined by DIGE analysis," *Proteomics*, vol. 7, no. 21, pp. 3906–3918, 2007.

[37] S. Kawasaki, H. Takizawa, K. Takami et al., "Benzene-extracted components are important for the major activity of diesel exhaust particles: effect on interleukin-8 gene expression in human bronchial epithelial cells," *American Journal of Respiratory Cell and Molecular Biology*, vol. 24, no. 4, pp. 419–426, 2001.

[38] H. Takizawa, T. Ohtoshi, S. Kawasaki et al., "Diesel exhaust particles activate human bronchial epithelial cells to express inflammatory mediators in the airways: a review," *Respirology*, vol. 5, no. 2, pp. 197–203, 2000.

[39] H. Takizawa, S. Abe, T. Ohtoshi et al., "Diesel exhaust particles up-regulate expression of intercellular adhesion molecule-1 (ICAM-1) in human bronchial epithelial cells," *Clinical and Experimental Immunology*, vol. 120, no. 2, pp. 356–362, 2000.

[40] S. Hashimoto, Y. Gon, I. Takeshita et al., "Diesel exhaust particles activate p38 MAP kinase to produce interleukin 8 and RANTES by human bronchial epithelial cells and N-acetylcysteine attenuates p38 MAP kinase activation," *American Journal of Respiratory and Critical Care Medicine*, vol. 161, no. 1, pp. 280–285, 2000.

[41] B. Bleck, D. B. Tse, M. A. Curotto De Lafaille, F. Zhang, and J. Reibman, "Diesel exhaust particle-exposed human bronchial epithelial cells induce dendritic cell maturation and polarization via thymic stromal lymphopoietin," *Journal of Clinical Immunology*, vol. 28, no. 2, pp. 147–156, 2008.

[42] N. Tsukue, H. Okumura, T. Ito, G. Sugiyama, and T. Nakajima, "Toxicological evaluation of diesel emissions on A549 cells," *Toxicology in Vitro*, vol. 24, no. 2, pp. 363–369, 2010.

[43] L. C. Ka, A. Polidori, L. Ntziachristos et al., "Chemical characteristics and oxidative potential of particulate matter emissions from gasoline, diesel, and biodiesel cars," *Environmental Science and Technology*, vol. 43, no. 16, pp. 6334–6340, 2009.

[44] D. E. Davies and S. T. Holgate, "Asthma: the importance of epithelial mesenchymal communication in pathogenesis: inflammation and the airway epithelium in asthma," *International Journal of Biochemistry and Cell Biology*, vol. 34, no. 12, pp. 1520–1526, 2002.

[45] P. Bogaert, K. G. Tournoy, T. Naessens, and J. Grooten, "Where asthma and hypersensitivity pneumonitis meet and differ: noneosinophilic severe asthma," *American Journal of Pathology*, vol. 174, no. 1, pp. 3–13, 2009.

[46] E. R. Sutherland and R. J. Martin, "Airway inflammation in chronic obstructive pulmonary disease: comparisons with asthma," *Journal of Allergy and Clinical Immunology*, vol. 112, no. 5, pp. 819–828, 2003.

[47] Y. H. Oo and D. H. Adams, "The role of chemokines in the recruitment of lymphocytes to the liver," *Journal of Autoimmunity*, vol. 34, no. 1, pp. 45–54, 2010.

[48] O. Gross, C. J. Thomas, G. Guarda, and J. Tschopp, "The inflammasome: an integrated view," *Immunological Reviews*, vol. 243, no. 1, pp. 136–151, 2011.

[49] V. Pétrilli, C. Dostert, D. A. Muruve, and J. Tschopp, "The inflammasome: a danger sensing complex triggering innate immunity," *Current Opinion in Immunology*, vol. 19, no. 6, pp. 615–622, 2007.

[50] S. Provoost, T. Maes, N. S. Pauwels et al., "NLRP3/caspase-1-independent IL-1beta production mediates diesel exhaust particle-induced pulmonary inflammation," *Journal of Immunology*, vol. 187, no. 6, pp. 3331–3337, 2011.

[51] M. Gooz, "ADAM-17: the enzyme that does it all," *Critical Reviews in Biochemistry and Molecular Biology*, vol. 45, no. 2, pp. 146–169, 2010.

[52] C. A. Shaw, S. Robertson, M. R. Miller et al., "Diesel exhaust particulate—exposed macrophages cause marked endothelial cell activation," *American Journal of Respiratory Cell and Molecular Biology*, vol. 44, no. 6, pp. 840–851, 2011.

[53] M. Porter, M. Karp, S. Killedar et al., "Diesel-enriched particulate matter functionally activates human dendritic cells," *American Journal of Respiratory Cell and Molecular Biology*, vol. 37, no. 6, pp. 706–719, 2007.

[54] H. M. Yang, J. Y. C. Ma, V. Castranova, and J. K. H. Ma, "Effects of diesel exhaust particles on the release of interleukin-1 and tumor necrosis factor-alpha from rat alveolar macrophages," *Experimental Lung Research*, vol. 23, no. 3, pp. 269–284, 1997.

[55] W. Dong, J. Lewtas, and M. I. Luster, "Role of endotoxin in tumor necrosis factor α expression from alveolar macrophages treated with urban air particles," *Experimental Lung Research*, vol. 22, no. 5, pp. 577–592, 1996.

[56] K. Amakawa, T. Terashima, T. Matsuzaki, A. Matsumaru, M. Sagai, and K. Yamaguchi, "Suppressive effects of diesel exhaust particles on cytokine release from human and murine alveolar macrophages," *Experimental Lung Research*, vol. 29, no. 3, pp. 149–164, 2003.

[57] J. J. Song, J. D. Lee, B. D. Lee, S. W. Chae, and M. K. Park, "Effect of diesel exhaust particles on human middle ear epithelial cells," *International Journal of Pediatric Otorhinolaryngology*, vol. 76, no. 3, pp. 334–338, 2012.

[58] H. Ushio, K. Nohara, and H. Fujimaki, "Effect of environmental pollutants on the production of pro-inflammatory cytokines by normal human dermal keratinocytes," *Toxicology Letters*, vol. 105, no. 1, pp. 17–24, 1999.

[59] A. T. Saber, J. Bornholdt, M. Dybdahl et al., "Tumor necrosis factor is not required for particle-induced genotoxicity and pulmonary inflammation," *Archives of Toxicology*, vol. 79, no. 3, pp. 177–182, 2005.

[60] P. E. Schwarze, A. I. Totlandsdal, J. I. Herseth et al., "Importance of sources and components of particulate air pollution for cardio-pulmonary inflammatory responses," in *Air Pollution*, V. V. Rijeka, Ed., pp. 47–54, Sciyo, 2010.

[61] S. F. Ziegler and D. Artis, "Sensing the outside world: TSLP regulates barrier immunity," *Nature Immunology*, vol. 11, no. 4, pp. 289–293, 2010.

[62] B. Bleck, D. B. Tse, T. Gordon, M. R. Ahsan, and J. Reibman, "Diesel exhaust particle-treated human bronchial epithelial cells upregulate Jagged-1 and OX40 ligand in myeloid dendritic cells via thymic stromal lymphopoietin," *Journal of Immunology*, vol. 185, no. 11, pp. 6636–6645, 2010.

[63] S. Provoost, T. Maes, M. A. M. Willart, G. F. Joos, B. N. Lambrecht, and K. G. Tournoy, "Diesel exhaust particles stimulate adaptive immunity by acting on pulmonary dendritic cells," *Journal of Immunology*, vol. 184, no. 1, pp. 426–432, 2010.

[64] A. I. Totlandsdal, M. Refsnes, T. Skomedal, J. B. Osnes, P. E. Schwarze, and M. Låg, "Particle-induced cytokine responses in cardiac cell cultures—the effect of particles versus soluble mediators released by particle-exposed lung cells," *Toxicological Sciences*, vol. 106, no. 1, pp. 233–241, 2008.

[65] T. P. J. Hofer, E. Bitterle, I. Beck-Speier et al., "Diesel exhaust particles increase LPS-stimulated COX-2 expression and PGE_2 production in human monocytes," *Journal of Leukocyte Biology*, vol. 75, no. 5, pp. 856–864, 2004.

[66] M. Gualtieri, J. Øvrevik, S. Mollerup et al., "Airborne urban particles (Milan winter-PM2.5) cause mitotic arrest and cell death: effects on DNA, mitochondria, AhR binding and spindle organization," *Mutation Research*, vol. 713, no. 1-2, pp. 18–31, 2011.

[67] N. Li, M. I. Venkatesan, A. Miguel et al., "Induction of heme oxygenase-1 expression in macrophages by diesel exhaust particle chemicals and quinones via the antioxidant-responsive element," *Journal of Immunology*, vol. 165, no. 6, pp. 3393–3401, 2000.

[68] N. Li, J. Alam, M. I. Venkatesan et al., "Nrf2 is a key transcription factor that regulates antioxidant defense in macrophages and epithelial cells: protecting against the proinflammatory and oxidizing effects of diesel exhaust chemicals," *Journal of Immunology*, vol. 173, no. 5, pp. 3467–3481, 2004.

[69] Y. Tian, A. B. Rabson, and M. A. Gallo, "Ah receptor and NF-κB interactions: mechanisms and physiological implications," *Chemico-Biological Interactions*, vol. 141, no. 1-2, pp. 97–115, 2002.

[70] B. N. M. Zordoky and A. O. S. El-Kadi, "Role of NF-κB in the regulation of cytochrome P450 enzymes," *Current Drug Metabolism*, vol. 10, no. 2, pp. 164–178, 2009.

[71] I. Monteleone, T. T. MacDonald, F. Pallone, and G. Monteleone, "The aryl hydrocarbon receptor in inflammatory bowel disease: linking the environment to disease pathogenesis," *Current Opinion in Gastroenterology*, vol. 28, no. 4, pp. 310–313, 2012.

[72] S. A. Ritz, J. Wan, and D. Diaz-Sanchez, "Sulforaphane-stimulated phase II enzyme induction inhibits cytokine production by airway epithelial cells stimulated with diesel extract," *American Journal of Physiology*, vol. 292, no. 1, pp. L33–L39, 2007.

[73] M. Matti Maricq, "Chemical characterization of particulate emissions from diesel engines: a review," *Journal of Aerosol Science*, vol. 38, no. 11, pp. 1079–1118, 2007.

[74] T. W. Hesterberg, C. M. Long, S. N. Sax et al., "Particulate matter in new technology diesel exhaust (NTDE) is quantitatively and qualitatively very different from that found in traditional diesel exhaust (TDE)," *Journal of the Air & Waste Management Association*, vol. 61, no. 9, pp. 894–913, 2011.

[75] J. Y. C. Ma and J. K. H. Ma, "The dual effect of the particulate and organic components of diesel exhaust particles on the alteration of pulmonary immune/inflammatory responses and metabolic enzymes," *Journal of Environmental Science and Health*, vol. 20, no. 2, pp. 117–147, 2002.

[76] P. D. Siegel, R. K. Saxena, Q. B. Saxena et al., "Effect of diesel exhaust particulate (DEP) on immune responses: contributions of particulate versus organic soluble components," *Journal of Toxicology and Environmental Health*, vol. 67, no. 3, pp. 221–231, 2004.

[77] H. Takano, R. Yanagisawa, and K. I. Inoue, "Components of diesel exhaust particles diversely enhance a variety of respiratory diseases related to infection or allergy: extracted organic chemicals and the residual particles after extraction differently affect respiratory diseases," *Journal of Clinical Biochemistry and Nutrition*, vol. 40, no. 2, pp. 101–107, 2007.

[78] A. I. Totlandsdal, J. I. Herseth, A. K. Bolling et al., "Differential effects of the particle core and organic extract of diesel exhaust particles," *Toxicology Letters*, vol. 208, no. 3, pp. 262–268, 2012.

[79] A. L. Holder, D. Lucas, R. Goth-Goldstein, and C. P. Koshland, "Inflammatory response of lung cells exposed to whole, filtered, and hydrocarbon denuded diesel exhaust," *Chemosphere*, vol. 70, no. 1, pp. 13–19, 2007.

[80] E. Fuentes-Mattei, E. Rivera, A. Gioda, D. Sanchez-Rivera, F. R. Roman-Velazquez, and B. D. Jimenez-Velez, "Use of human bronchial epithelial cells (BEAS-2B) to study immunological markers resulting from exposure to PM2.5 organic extract from Puerto Rico," *Toxicology and Applied Pharmacology*, vol. 243, no. 3, pp. 381–389, 2010.

[81] R. Yanagisawa, H. Takano, K. I. Inoue et al., "Components of diesel exhaust particles differentially affect Th1/Th2 response in a murine model of allergic airway inflammation," *Clinical and Experimental Allergy*, vol. 36, no. 3, pp. 386–395, 2006.

[82] K. J. Swanson, M. C. Madden, and A. J. Ghio, "Biodiesel exhaust: the need for health effects research," *Environmental Health Perspectives*, vol. 115, no. 4, pp. 496–499, 2007.

[83] J. M. Brito, L. Belotti, A. C. Toledo et al., "Acute cardiovascular and inflammatory toxicity induced by inhalation of diesel and biodiesel exhaust particles," *Toxicological Sciences*, vol. 116, no. 1, pp. 67–78, 2010.

[84] P. I. Jalava, M. Tapanainen, K. Kuuspalo et al., "Toxicological effects of emission particles from fossil- and biodiesel-fueled diesel engine with and without DOC/POC catalytic converter," *Inhalation Toxicology*, vol. 22, supplement 2, pp. 48–58, 2010.

[85] J. G. Hemmingsen, P. Moller, J. K. Nojgaard, M. Roursgaard, and S. Loft, "Oxidative stress, genotoxicity, and vascular cell adhesion molecule expression in cells exposed to particulate matter from combustion of conventional diesel and methyl ester biodiesel blends," *Environmental Science & Technology*, vol. 45, no. 19, pp. 8545–8551, 2011.

[86] K. Hayakawa, A. Nakamura, N. Terai, R. Kizu, and K. Ando, "Nitroarene concentrations and direct-acting mutagenicity of diesel exhaust particulates fractionated by silica-gel column chromatography," *Chemical and Pharmaceutical Bulletin*, vol. 45, no. 11, pp. 1820–1822, 1997.

[87] I. Salmeen, A. M. Durisin, and T. J. Prater, "Contribution of 1-nitropyrene to direct-acting Ames assay mutagenicities of diesel particulate extracts," *Mutation Research*, vol. 104, no. 1–3, pp. 17–23, 1982.

[88] R. P. F. Schins, "Mechanisms of genotoxicity of particles and fibers," *Inhalation Toxicology*, vol. 14, no. 1, pp. 57–78, 2002.

[89] Y. J. Li, H. Takizawa, and T. Kawada, "Role of oxidative stresses induced by diesel exhaust particles in airway inflammation, allergy and asthma: their potential as a target of chemoprevention," *Inflammation and Allergy*, vol. 9, no. 4, pp. 300–305, 2010.

[90] F. D. Gilliland, Y. F. Li, A. Saxon, and D. Diaz-Sanchez, "Effect of glutathione-S-transferase M1 and P1 genotypes on xenobiotic enhancement of allergic responses: randomised, placebo-controlled crossover study," *The Lancet*, vol. 363, no. 9403, pp. 119–125, 2004.

[91] X. J. Yin, J. Y. C. Ma, J. M. Antonini, V. Castranova, and J. K. H. Ma, "Roles of reactive oxygen species and heme oxygenase-1 in modulation of alveolar macrophage-mediated pulmonary immune responses to *Listeria monocytogenes* by diesel exhaust particles," *Toxicological Sciences*, vol. 82, no. 1, pp. 143–153, 2004.

[92] I. S. Mudway, N. Stenfors, S. T. Duggan et al., "An in vitro and in vivo investigation of the effects of diesel exhaust on human airway lining fluid antioxidants," *Archives of Biochemistry and Biophysics*, vol. 423, no. 1, pp. 200–212, 2004.

[93] J. Øvrevik, R. B. Hetland, R. P. Schins, T. Myran, and P. E. Schwarze, "Iron release and ROS generation from mineral particles are not related to cytokine release or apoptosis in exposed A549 cells," *Toxicology Letters*, vol. 165, no. 1, pp. 31–38, 2006.

[94] A. Clouter, D. Brown, D. Höhr, P. Borm, and K. Donaldson, "Inflammatory effects of respirable quartz collected in workplaces versus standard DQ12 quartz: particle surface correlates," *Toxicological Sciences*, vol. 63, no. 1, pp. 90–98, 2001.

[95] H. Zhao, M. W. Barger, J. K. H. Ma, V. Castranova, and J. Y. C. Ma, "Cooperation of the inducible nitric oxide synthase and cytochrome P450 1A1 in mediating lung inflammation and mutagenicity induced by diesel exhaust particles," *Environmental Health Perspectives*, vol. 114, no. 8, pp. 1253–1258, 2006.

[96] Y. Zhao, P. V. Usatyuk, I. A. Gorshkova et al., "Regulation of COX-2 expression and IL-6 release by particulate matter in airway epithelial cells," *American Journal of Respiratory Cell and Molecular Biology*, vol. 40, no. 1, pp. 19–30, 2009.

[97] A. M. S. Hartz, B. Bauer, M. L. Block, J. S. Hong, and D. S. Miller, "Diesel exhaust particles induce oxidative stress, proinflammatory signaling, and P-glycoprotein up-regulation at the blood-brain barrier," *The FASEB Journal*, vol. 22, no. 8, pp. 2723–2733, 2008.

[98] M. L. Block, X. Wu, Z. Pei et al., "Nanometer size diesel exhaust particles are selectively toxic to dopaminergic neurons: the role of microglia, phagocytosis, and NADPH oxidase," *The FASEB Journal*, vol. 18, no. 13, pp. 1618–1620, 2004.

[99] W. Y. Cheng, J. Currier, P. A. Bromberg, R. Silbajoris, S. O. Simmons, and J. M. Samet, "Linking oxidative events to inflammatory and adaptive gene expression induced by exposure to an organic particulate matter component," *Environmental Health Perspectives*, vol. 120, no. 2, pp. 267–274, 2012.

[100] H. Sauer, M. Wartenberg, and J. Hescheler, "Reactive oxygen species as intracellular messengers during cell growth and differentiation," *Cellular Physiology and Biochemistry*, vol. 11, no. 4, pp. 173–186, 2001.

[101] M. Torres and H. J. Forman, "Redox signaling and the MAP kinase pathways," *BioFactors*, vol. 17, no. 1–4, pp. 287–296, 2003.

[102] T. J. Guzik, R. Korbut, and T. Adamek-Guzik, "Nitric oxide and superoxide in inflammation and immune regulation," *Journal of Physiology and Pharmacology*, vol. 54, no. 4, pp. 469–487, 2003.

[103] K. Donaldson, P. J. A. Borm, V. Castranova, and M. Gulumian, "The limits of testing particle-mediated oxidative stress in vitro in predicting diverse pathologies; relevance for testing of nanoparticles," *Particle and Fibre Toxicology*, vol. 6, article 13, 2009.

[104] K. L. Oslund, L. A. Miller, J. L. Usachenko, N. K. Tyler, R. Wu, and D. M. Hyde, "Oxidant-injured airway epithelial cells upregulate thioredoxin but do not produce interleukin-8," *American Journal of Respiratory Cell and Molecular Biology*, vol. 30, no. 5, pp. 597–604, 2004.

[105] J. Øvrevik, M. Refsnes, P. Schwarze, and M. Låg, "The ability of oxidative stress to mimic quartz-induced chemokine responses is lung cell line-dependent," *Toxicology Letters*, vol. 181, no. 2, pp. 75–80, 2008.

[106] J. Li, P. Kanju, M. Patterson et al., "TRPV4-mediated calcium influx into human bronchial epithelia upon exposure to diesel exhaust particles," *Environmental Health Perspectives*, vol. 119, no. 6, pp. 784–793, 2011.

[107] J. Ovrevik, M. Refsnes, A. I. Totlandsdal, J. A. Holme, P. E. Schwarze, and M. Lag, "TACE/TGF-alpha/EGFR regulates CXCL8 in bronchial epithelial cells exposed to particulate matter components," *European Respiratory Journal*, vol. 38, no. 5, pp. 1189–1199, 2011.

[108] S. Kikuno, K. Taguchi, N. Iwamoto et al., "1,2-Naphthoquinone activates vanilloid receptor 1 through increased protein tyrosine phosphorylation, leading to contraction of guinea pig trachea," *Toxicology and Applied Pharmacology*, vol. 210, no. 1-2, pp. 47–54, 2006.

[109] P. R. Reynolds, K. M. Wasley, and C. H. Allison, "Diesel particulate matter induces receptor for advanced glycation end-products (RAGE) expression in pulmonary epithelial cells, and RAGE signaling influences NF-κB-mediated inflammation," *Environmental Health Perspectives*, vol. 119, no. 3, pp. 332–336, 2011.

[110] S. Blanchet, K. Ramgolam, A. Baulig, F. Marano, and A. Baeza-Squiban, "Fine particulate matter induces amphiregulin secretion by bronchial epithelial cells," *American Journal of Respiratory Cell and Molecular Biology*, vol. 30, no. 4, pp. 421–427, 2004.

[111] T. L. Tal, P. A. Bromberg, Y. Kim, and J. M. Samet, "Epidermal growth factor receptor activation by diesel particles is mediated by tyrosine phosphatase inhibition," *Toxicology and Applied Pharmacology*, vol. 233, no. 3, pp. 382–388, 2008.

[112] J. L. Koff, M. X. G. Shao, I. F. Ueki, and J. A. Nadel, "Multiple TLRs activate EGFR via a signaling cascade to produce innate immune responses in airway epithelium," *American Journal of Physiology*, vol. 294, no. 6, pp. L1068–L1075, 2008.

[113] I. Kuwahara, E. P. Lillehoj, W. Lu et al., "Neutrophil elastase induces IL-8 gene transcription and protein release through p38/NF-κB activation via EGFR transactivation in a lung epithelial cell line," *American Journal of Physiology*, vol. 291, no. 3, pp. L407–L416, 2006.

[114] J. Pourazar, A. Blomberg, F. J. Kelly et al., "Diesel exhaust increases EGFR and phosphorylated C-terminal Tyr 1173 in the bronchial epithelium," *Particle and Fibre Toxicology*, vol. 5, article 8, 2008.

[115] P. R. Burgel and J. A. Nadel, "Epidermal growth factor receptor-mediated innate immune responses and their roles in airway diseases," *European Respiratory Journal*, vol. 32, no. 4, pp. 1068–1081, 2008.

[116] P. I. Jalava, P. Aakko-Saksa, T. Murtonen et al., "Toxicological properties of emission particles from heavy duty engines powered by conventional and bio-based diesel fuels and compressed natural gas," *Particle and Fibre Toxicology*, vol. 9, no. 1, p. 37, 2012.

[117] C. Nordenhäll, J. Pourazar, A. Blomberg, J. O. Levin, T. Sandström, and E. Ädelroth, "Airway inflammation following exposure to diesel exhaaust: a study of time kinetics using induced sputum," *European Respiratory Journal*, vol. 15, no. 6, pp. 1046–1051, 2000.

[118] S. S. Salvi, C. Nordenhall, A. Blomberg et al., "Acute exposure to diesel exhaust increases IL-8 and GRO-α production in healthy human airways," *American Journal of Respiratory and Critical Care Medicine*, vol. 161, no. 2, pp. 550–557, 2000.

[119] N. Li, M. Hao, R. F. Phalen, W. C. Hinds, and A. E. Nel, "Particulate air pollutants and asthma: a paradigm for the role of oxidative stress in PM-induced adverse health effects," *Clinical Immunology*, vol. 109, no. 3, pp. 250–265, 2003.

[120] A. L. Holder, D. Lucas, R. Goth-goldstein, and C. P. Koshland, "Cellular response to diesel exhaust particles strongly depends on the exposure method," *Toxicological Sciences*, vol. 103, no. 1, pp. 108–115, 2008.

[121] J. Li, A. J. Ghio, S. H. Cho, C. E. Brinckerhoff, S. A. Simon, and W. Liedtke, "Diesel exhaust particles activate the matrix-metalloproteinase-1 gene in human bronchial epithelial in a β-arrestin-dependent manner via activation of RAS," *Environmental Health Perspectives*, vol. 117, no. 3, pp. 400–409, 2009.

[122] D. J. Cooney and A. J. Hickey, "Cellular response to the deposition of diesel exhaust particle aerosols onto human lung cells grown at the air-liquid interface by inertial impaction," *Toxicology in Vitro*, vol. 25, no. 8, pp. 1953–1965, 2011.

Hindawi Publishing Corporation
BioMed Research International
Volume 2013, Article ID 734137, 15 pages
http://dx.doi.org/10.1155/2013/734137

Research Article

The CULTEX RFS: A Comprehensive Technical Approach for the *In Vitro* Exposure of Airway Epithelial Cells to the Particulate Matter at the Air-Liquid Interface

Michaela Aufderheide,[1] Beat Halter,[2] Niklas Möhle,[1] and Dieter Hochrainer[3]

[1] *Cultex Laboratories GmbH, Feodor-Lynen-Straße 21, 30625 Hannover, Germany*
[2] *Halter Engineering GmbH, Huebstraße 16, 9100 Herisau, Switzerland*
[3] *Von der Hardt 16, 57392 Oberkirchen, Germany*

Correspondence should be addressed to Michaela Aufderheide; m.aufderheide@cultex-laboratories.com

Received 8 October 2012; Revised 23 November 2012; Accepted 16 December 2012

Academic Editor: Abderrahim Nemmar

The EU Regulation on Registration, Evaluation, Authorization and Restriction of Chemicals (REACH) demands the implementation of alternative methods for analyzing the hazardous effects of chemicals including particulate formulations. In the field of inhalation toxicology, a variety of *in vitro* models have been developed for such studies. To simulate the *in vivo* situation, an adequate exposure device is necessary for the direct exposure of cultivated lung cells at the air-liquid interface (ALI). The CULTEX RFS fulfills these requirements and has been optimized for the exposure of cells to atomized suspensions, gases, and volatile compounds as well as micro- and nanosized particles. This study provides information on the construction and functional aspects of the exposure device. By using the Computational Fluid Dynamics (CFD) analysis, the technical design was optimized to realize a stable, reproducible, and homogeneous deposition of particles. The efficiency of the exposure procedure is demonstrated by exposing A549 cells dose dependently to lactose monohydrate, copper(II) sulfate, copper(II) oxide, and micro- and nanoparticles. All copper compounds induced cytotoxic effects, most pronounced for soluble copper(II) sulfate. Micro- and nanosized copper(II) oxide also showed a dose-dependent decrease in the cell viability, whereby the nanosized particles decreased the metabolic activity of the cells more severely.

1. Introduction

Provoked by public pressure and triggered by an increasing number of lethal lung diseases over the last few decades [1, 2], more and more studies in the field of inhalation toxicology now concentrate on the understanding of particle-lung interactions. Investigations of the toxicological effects of inhalable substances on the respiratory tract mainly focus on results from animal experiments based on the OECD guideline 403 on acute inhalation toxicology. So far, only a few *in vitro* alternatives to animal inhalation tests for toxicology have been described [3, 4]. However, none of them is validated or officially accepted by the authorities.

Recent changes in the EU chemical policy, namely, the new Registration, Evaluation, Authorization and Restriction of Chemicals directive (REACH; EC no. 1907/2006), and complaints about the immense number of animals needed to fulfill the requirements of REACH [6] demand the development and implementation of novel *in vitro* technologies—also in the field of inhalation toxicology. In order to evaluate the effects of relevant particulate substances, only classic methodological approaches are available using either suspended or dissolved particles under submerged conditions in cell culture experiments [4, 7]. The main concerns about these test methods are (1) the unrealistic behavior of suspended particles and (2) culture and exposure conditions which do not reflect the situation in the lung. The fact of losing nanosized particles by agglomeration or the uncontrollable behavior of nanosized particles in suspensions may lead to uncertainties in the results [8].

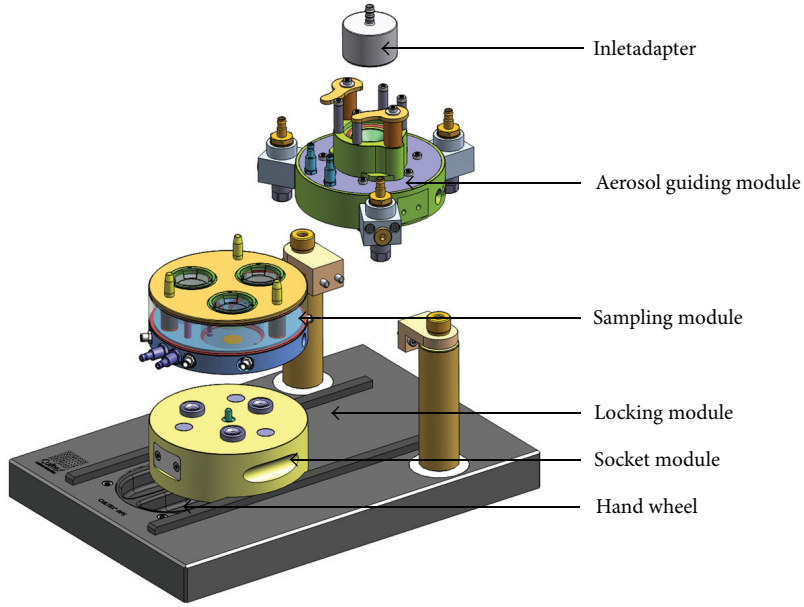

Figure 1: Overview image of the modular CULTEX RFS exposure system. The device is composed of the following components: (1) inlet adapter, (2) aerosol guiding module, (3) sampling module and socket module, and (4) locking module with a hand wheel.

Another major point of the discussion is the transferability of data from animal experiments to the human organism due to species-specific reactions and the generation of false positive or negative results [9].

One of the "first" approaches for direct cell exposure came from Tarkington et al. [10] who conducted the atmosphere via a vertical stream directly over the cultivated test organisms. The system is also based on a biphasic cell culture exposed at an air-liquid interface [11]. The basic idea is to mimic the inhalation cycle *in vitro* by taking into consideration the most important biological and technical aspects. The selection of an appropriate cell model and its cultivation at the air-liquid interface are the basic prerequisites for such a system. On the other hand, the technical implementation should guarantee the direct contact of the test substances with the cells, as well as the homogeneous exposure of the entire cell layer without interfering with the cell viability.

These theoretical concepts led to the development of the CULTEX exposure module in 1999 by Aufderheide and Mohr [12] for the exposure of cultivated cells at the air-liquid interface. The test aerosol is conducted directly over the cells through specially designed inlet nozzles. This setup guarantees a close contact between the test aerosol and the cells without any interference of the cell culture media. The first CULTEX exposure devices were used for the exposure to complex mixtures like cigarette smoke and gases, or in a modified version to analyze the mutagenic potency of airborne materials in the AMES assay [13].

Nowadays, a large number of other air-liquid interface exposure systems are available, ranging from the exposure of two-cell culture plates (6-well), like the ALICE exposure device [14] or a flow-through system [15] to a radial multiwell module [16]. All of these modules have certain advantages and disadvantages and may therefore only be used for a limited test assembly.

The results obtained from exposure studies with the CULTEX RFS module have shown that the interactions between cells and particles are closely linked to the physical and chemical properties of these compounds and have advanced the redesign of the handmade CULTEX glass modules.

The CULTEX Radial Flow System (RFS) presented here overcomes the limitations of its predecessor model and includes all features that are required to realize the exposure of cultivated cells to airborne particles under realistic conditions.

2. Material and Methods

2.1. Technical Description. The CULTEX RFS module was designed for exposing adherent growing cells at the air-liquid interface and is a precision instrument, characterized by a modular construction (Figure 1).

The basic CULTEX RFS consists of the following parts: (1) the inlet adapter which connects the aerosol generation and aerosol guiding module (Figure 1), (2) the aerosol guiding module to conduct and distribute the particles to be deposited on the cell culture inserts in the sampling module (Figures 2(a) and 2(b)), and (3) the sampling and socket module with three exposure chambers where the cell culture inserts or Petri dishes are located (Figures 1 and 2(c)).

The aerosol guiding module as well as the sampling module can be heated to the appropriate temperature (e.g., 37°C) by the connection to an external water bath. The socket module (4) guides the sampling module on the slide rails of the locking device (5) and serves as a spacer for integrating

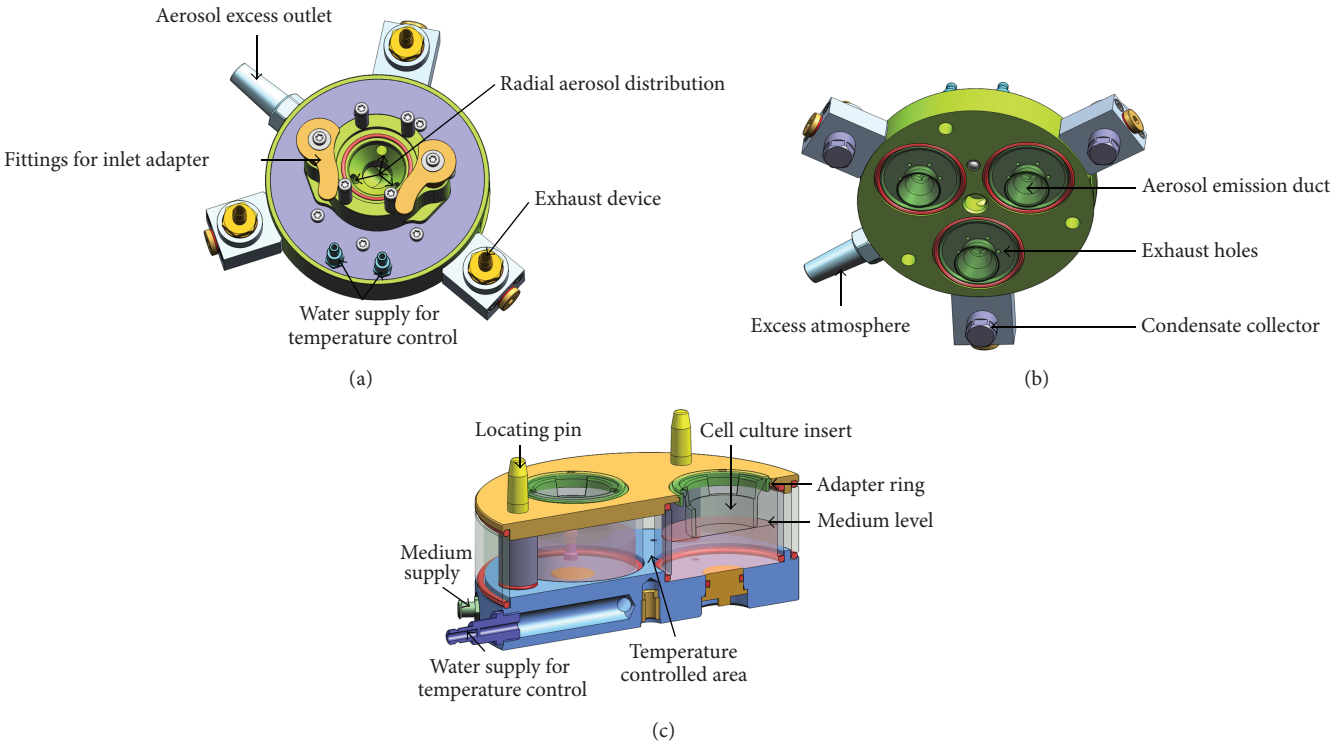

Figure 2: Aerosol guiding module of the CULTEX RFS: (a) top view, (b) bottom view, and (c) sampling module.

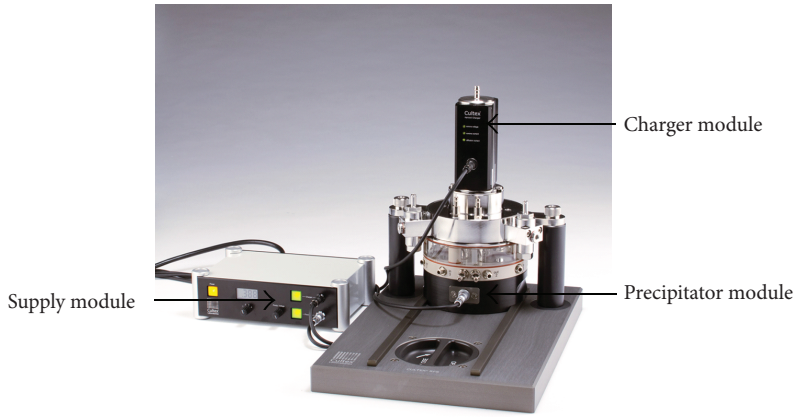

Figure 3: The CULTEX RFS exposure device extended with an electrical deposition device (Cultex EDD) for the increased particle deposition efficiency.

additional functions, like a control unit for electrostatic precipitation.

In addition to the above-mentioned modular components, the system can also be equipped with special adapters to enable the use of commercial inserts from different suppliers and of different sizes or for Petri dishes. The aerosol emission ducts are adapted correspondingly.

To increase the particle deposition efficiency, notably for nanosized particles, the electrical deposition device (Cultex EDD) can further be integrated into the technical setup (Figure 3).

2.2. Test Materials. Dry powder atmospheres were prepared from the substances listed in Tables 1 and 2 and used for the exposure studies.

The substances were pressed into powder cakes by the CULTEX HyP-Hydraulic Press (Cultex Laboratories GmbH,

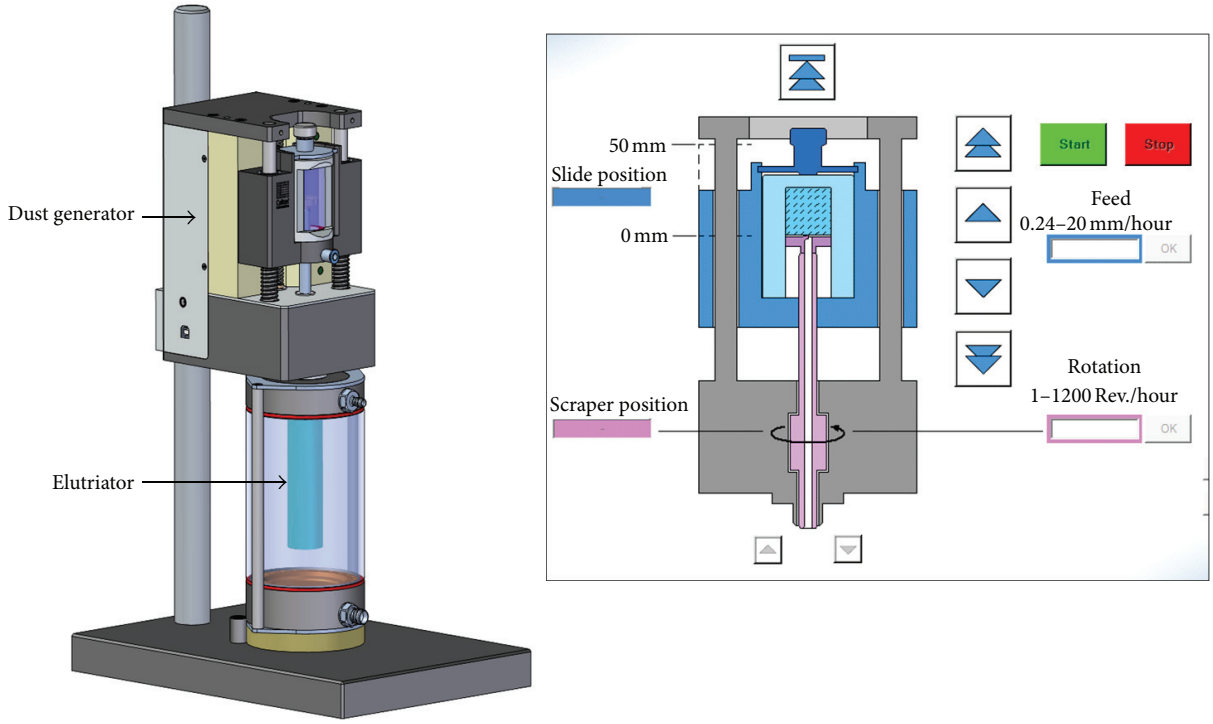

Figure 4: The CULTEX DG (Dust Generator) (Cultex Laboratories GmbH, Germany) enables the generation of aerosols from a powder cake according to Wright [5].

Table 1: Substances used for the generation of dry powder atmospheres.

Substance	Producer/catalogue number	Primary particle size
Lactose monohydrat	Fluka/61341	Not available
Copper(II) oxide nano	Ionic Liquids Technologies GmbH/NO-0031-HP	40–80 nm
Copper(II) oxide mikro	Sigma Aldrich/20844-1	5 μm
Copper(II) sulfat	Sigma Aldrich/12852	Not available

Table 2: Conditions for the generation of powder cakes and particulate atmospheres.

Substance	Powder cake generation	Particle generation	
	Pressure (bar)	Scraper (rev/h)	Feed rate (mm/h)
Lactose monohydrat	110	800	10.0
Copper(II) oxide nano	82	800	2.5
Copper(II) oxide micro	82	800	2.0
Copper(II) sulfate	82	800	4.5

Germany), which allows electronically controlled compression of a high variety of powders by a pneumo-hydraulic cylinder.

2.3. Aerosol Generation. The aerosol was generated from the prepared powder cakes with the CULTEX DG (Dust Generator) (Cultex Laboratories GmbH) according to Wright [5] (Figure 4). The fully computerized generator is able to provide uniform airborne concentrations of dust over a long period of time.

The highly compressed substances are scraped off by a rotating scraper under standardized controlled conditions (feed rate 0.24 to 20 mm/h, rotation 1 to 800 revs/h). The total exposure time is varied from 15, 30, to 60 minutes to generate different particle concentrations on the cell culture membranes without changing the aerosol generation or any other physical or chemical parameter.

The generated particles were transported to the integrated elutriator by a constant air stream (8 L/min). The elutriator retains undesired large particles (> approx. 8 μm) and serves as a reservoir for a uniform aerosol which is finally drawn through the CULTEX RFS.

The complete experimental setup is shown in Figure 5 consisting of the particle generation unit, two CULTEX RFS devices, and two pumps for the medium supply. The cells are exposed to the test aerosol and clean air (process control) in parallel, in order to preclude process-related reactions which might interfere with the substance-specific effects.

2.4. CFD Analysis. The aerosol flow within the experimental setup was simulated and optimized by means of Computational Fluid Dynamics (CFD) software (ANSYS CFX, ANSYS Incorporated).

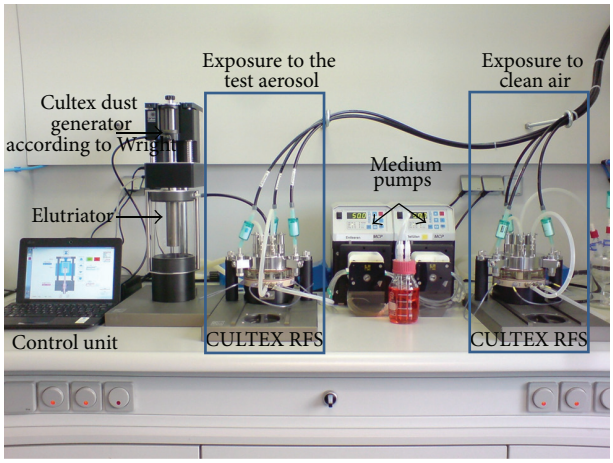

FIGURE 5: Experimental setup for exposing cultivated cells at the air-liquid interface to particles. The components of the exposure station are the particle generator according to Wright, the elutriator, two CULTEX RFS devices for exposure to particles and clean air and medium pumps for the automatic nutrient supply.

2.5. Particle Number and Mass Distribution. The determination of the particle number and mass distribution was conducted with an *Aerodynamic Particle Sizer* APS (3321/TSI Incorporated) in the size range of 0.5 to 20 μm. By accelerating particles through a nozzle and optical time-of-flight measurement of the particles, they are classified into 51 logarithmic size ranges between 0.523 and 20 μm.

2.6. Particle Deposition. The deposition of the particles was analyzed by gravimetric methods, using the precision balance (SE2-F filter ultra-microbalance, Sartorius).

In preliminary tests, the particle mass concentration within the exposure system was analyzed at three sampling points (sampling point 1: 200 seconds, sampling point 2 + 3: 60 minutes) to determine appropriate exposure times for the corresponding test particles (Figure 6) and to check for uniform particle distribution. The first sampling point was located directly after the elutriator, the second at the outlet port of the aerosol emission duct to estimate the particle mass entering the exposure chamber, and the third at the insert membrane surface to measure the particle mass deposited on the cultivated cells. The particle mass was determined by collecting the particles on filter pads (glass fiber filter/GF-A/Macherey-Nagel), which were weighed before and after the exposure over a constant period (15 minutes). This approach allows the analysis of the deposition efficiency of each test atmosphere within the exposure module. Under these experimental conditions, the deposited particle numbers on the cell cultures can only be calculated by taking into consideration the measurements of the *Aerodynamic Particle Sizer* APS (3321/TSI Incorporated) and the system-specific deposition capacities (Aufderheide et al. [17], Supplementary Material).

2.7. Cell Cultivation and Exposure. For particle exposure experiments, the human lung adenocarcinoma epithelial cell line A549 (ATCC number: CCL-185) was used [18, 19]. The cells were grown in Dulbecco's MEM (Biochrom FG 0145, Germany) supplemented with 10% fetal calf serum and gentamicin (5 μg/mL).

A549 cells were seeded onto microporous membranes (growth area: 4.2 cm^2) of cell culture inserts (0.4 μm pore size, BD Biosciences) with a density of $1*10^5$ cells/cm^2 and cultivated submerged in a cell culture medium. After 24 hours, the apical medium was removed from the confluent cell layers and the direct exposure at the air-liquid interface with the CULTEX RFS was started. The cells were exposed either to the test substances (deposition rate: 25 $\mu g/cm^2$/15 min) or clean air (process control) for 15, 30, and 60 minutes. The incubator control cultures were cultivated at the air-liquid interface in the incubator during the exposure period.

2.8. WST Assay. The aim of our study was the characterization of the exposure device, limited to the functional description of the system. Accordingly, we used only one biological endpoint, the metabolic activity of the cells, to demonstrate dose-dependent cytotoxic reactions, not investigating further into the mechanisms behind these effects.

After a postincubation time of 24 hours (air-liquid interface; 37°C/5% CO_2), the particle-exposed cells and the control cultures (incubator control: unexposed cells, process control: clean air-exposed cells) were analyzed for cell viability by using the WST-1 assay for the mitochondrial activity according to the manufacturer's instructions (Roche Diagnostics, Germany). The data of the exposed cells were normalized to the values of the clean air control. The incubator controls were not considered, because they did not show significant differences to the clean air controls.

2.9. Statistical Analysis. The results of three independent tests with three samples each is expressed as mean ± SD. A Student's *t*-test was performed to analyze whether the differences between the mean values of the three exposure times are significant [20].

3. Results

3.1. Deposition Efficiency. The CULTEX RFS was designed for exposing adherent cells at the air-liquid interface to airborne materials like gases, complex mixtures, and particles. When dealing with particulate matter especially, questions arise concerning the deposition efficiency of such an exposure device.

The basic and theoretical considerations forming the basis of the efficiency of the system are already described by Aufderheide et al. ([17], Electronic Supplementary Material).

3.2. CFD Analysis—Flow Conditions within the System. When developing the CULTEX RFS and its peripheral devices, a key to achieve uniform particle deposition on the cell cultures was the simulation and optimization of the particle flow within the system by means of CFD analysis (Figures 7 to 9).

Figure 7 shows a cross-section through the elutriator (a) and a streamline velocity plot (b) of the CFD analysis. The

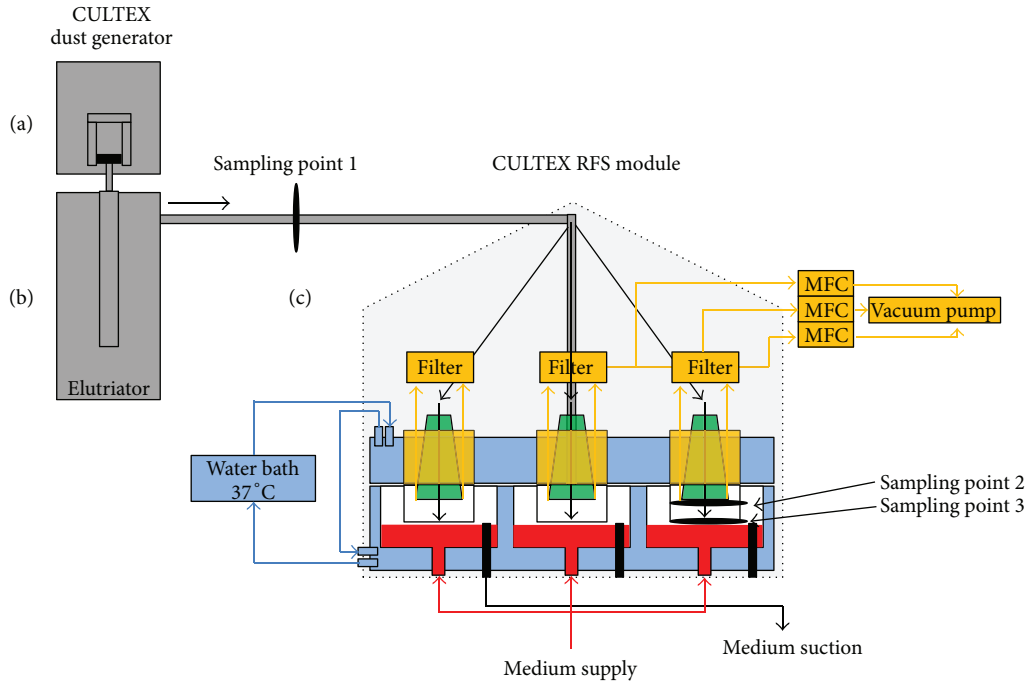

Figure 6: Schematic overview of the CULTEX system for exposing cultivated cells to particles at the air-liquid interface. Components of the exposure station: (a) particle generator according to Wright (CULTEX Dust Generator); (b) elutriator: glass tube with vertical upward flow, where large particles are removed from the aerosol due to sedimentation; (c) CULTEX RFS modules for exposure to particles and synthetic air. The sampling points (1–3) for the test aerosols in the overall stream are marked.

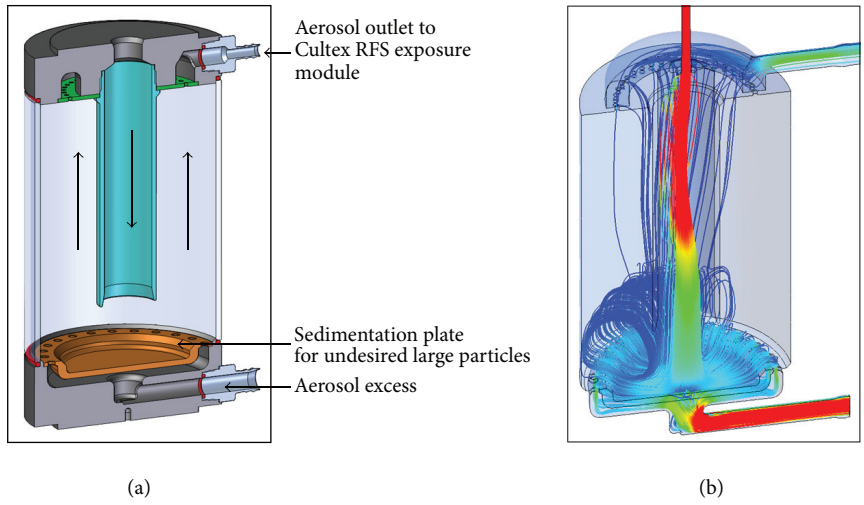

Figure 7: Sectional view of the elutriator (a) and streamline plot calculated by CFD Analysis (b).

basic principle of an elutriator consists of separating small (light) from large (heavy) particles in a vertically upward directed stream. The elutriator features an additional outlet at the bottom for discharging excess aerosol, as aerosol generation may require higher flow rates (e.g., 8 L/min) than those for the CULTEX RFS exposure module (e.g., 1.6 L/min). The streamline plot shows a curl in the lower zone of the device but a uniform upstream above, which is essential for a reliable particle separation. The results are based on flow rates of 8.0 L/min at the inlet, 1.09 L/min at the outlet, and

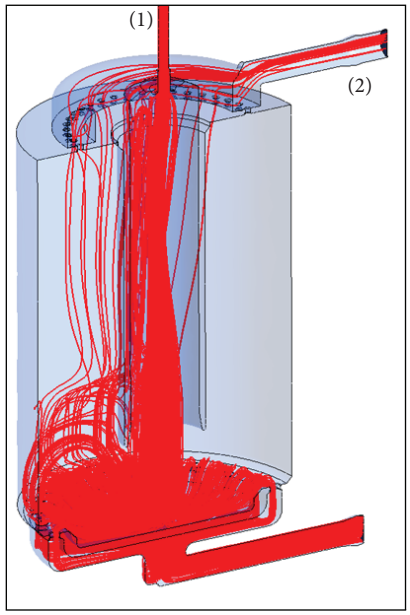

(a)

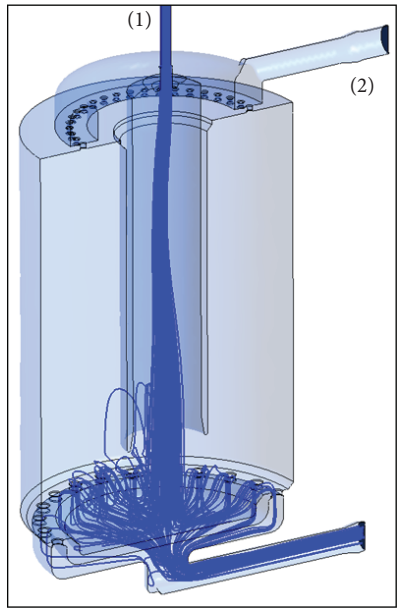

(b)

Figure 8: Particle track simulation for 2 μm (a) and 10 μm (b) particles. 8 L/min inlet flow rate (1) and 1.09 L/min outlet low rate (2).

6.91 L/min at the aerosol excess outlet. Further calculations with the same flow rate at the inlet but 1.59 L/min at the aerosol outlet showed no substantial differences.

Figure 8 shows particle trajectory simulations with particle sizes of 2 μm (a) and 10 μm (b). While small particles are transported upwards to the aerosol outlet and the Cultex RFS module, large particles remain in the elutriator. The major portion of the particles is carried to the excess outlet, as a flow rate of only 1.09 L/min from totally 8 L/min was conducted to the module in this simulation.

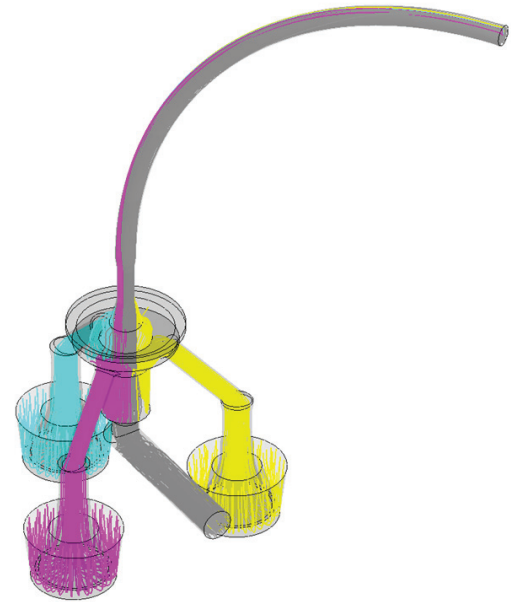

(a)

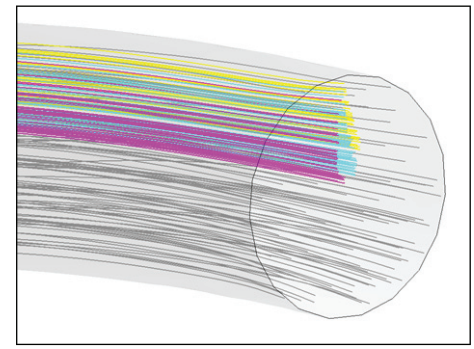

(b)

Figure 9: (a) Backtracking of flow lines from deposition chambers and excess outlet to the beginning of the aerosol feeding tube. (b) Flow lines running to the deposition chambers start at specific locations at the beginning of the feeding tube.

When testing prototypes of the Cultex RFS module, the distribution patterns between the three deposition chambers and within the individual chambers showed considerable differences. CFD calculations of the gas flow lines and particle trajectories resulted in the following essential findings.

Figure 9(a) shows the aerosol flow channels within the Cultex RFS module including a curved aerosol feeding tube with 6 mm diameter and 200 mm length. The flow lines represent an aerosol flow of 1590 mL/min in the feeding tube, which is divided into three minor flows of 30 mL/min leading to the deposition chambers and an excess flow of 1500 mL/min. Backtracking a defined number of particles from the deposition chamber to the beginning of the curved aerosol feeding tube (which is equal to the elutriator outlet) showed that these particles originate from specific locations in the tube profile (Figure 9(b)). Further calculations showed that the specific locations are sensitive to changes in tube bending radius, tube length, or flow rate. As the particle

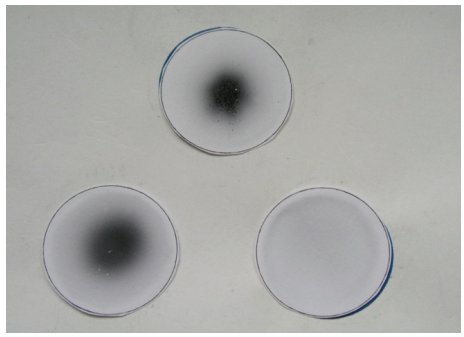

(a)

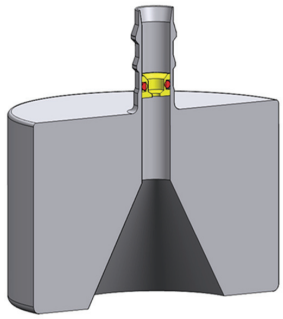

(b)

(c)

Figure 10: (a) Unequal deposition of copper(II) oxide microparticles on filter membranes after a 60 min exposure. (b) Inlet-adapter with an integrated jet nozzle to avoid unequal particle deposition within the CULTEX RFS module. (c) Uniform deposition of copper(II) oxide on filter membranes after a 60 min exposure with a jet nozzle.

concentration and particle size distribution at the beginning of the feeding tube is usually nonuniform across the tube profile, the distribution pattern in the deposition chambers are consequently also nonuniform.

An optimal solution to completely avoid these undesired effects was the integration of a jet nozzle into the inlet adapter of the Cultex RFS module. Figure 10(a) shows the deposition of copper(II) oxide micro on insert membranes without using a jet nozzle. The integration of a jet nozzle into the inlet adapter (Figure 10(b)) resulted in a homogenous distribution of the particles on the insert membranes (Figure 10(c), Table 3).

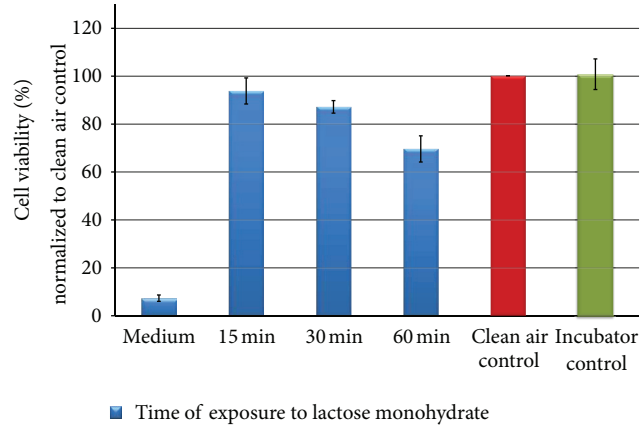

Figure 11: Relative cell viability of A549 cells after exposure to lactose monohydrate particles normalized to the clean air control dependent on time (15, 30, and 60 min).

Table 3: Deposition of copper(II) oxide microparticles on filter membranes after an exposure time of 60 minutes with a jet nozzle in the inlet adapter.

60 minutes exposure of copper(II) oxide	Chamber 1	Chamber 2	Chamber 3
Weight gain of filter paper (μg)	530	529	549
Weight gain of filter paper (μg)	529	537	521
Weight gain of filter paper (μg)	548	553	548

3.3. Dose-Response Relationship. After optimizing the deposition characteristics within the CULTEX RFS module, A549 cells were exposed to lactose monohydrate (process control), copper(II) sulfate (soluble substance), copper(II) oxide micro as well as copper(II) oxide nanoparticles (insoluble) for 15, 30, and 60 minutes. The particle generation was adjusted for each substance to result in a particle deposition of 25 μg/cm^2 (low dose) during an exposure time of 15 minutes. The concentration (low effect level, LOEL) is based on an interdisciplinary European project in which the cytotoxic potency of a variety of particles was analyzed with different cell types under submersed culture conditions [21]. The conditions for the particle generation had to be adjusted in preliminary experiments due to substance-specific variations. 24 hours after exposure, the cell viability was measured. The values obtained for the particle-exposed cultures were normalized to the clean air-exposed cells.

The results are shown in Figures 11, 12, 13, 14, 15, 16, 17, and 18. Generally the clean air-exposed cells (process control) showed no significant reduction in the cell viability in comparison with the incubator control. Accordingly, the exposure process itself had no influence on the metabolic activity of the cells.

The exposure of the cell cultures to the test compounds showed, dependent on the chemical and physical properties of the particulate atmosphere, considerable differences in

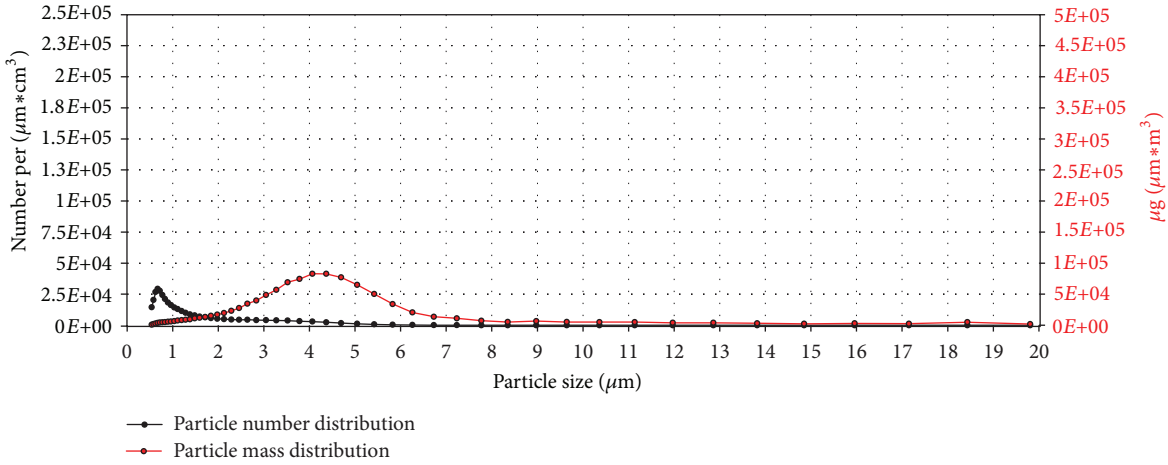

Figure 12: Particle number (black line) and particle mass distribution (red line) of the generated lactose monohydrate aerosol entering the exposure module. The analysis was performed with an Aerodynamic Particle Sizer (TSI Inc.).

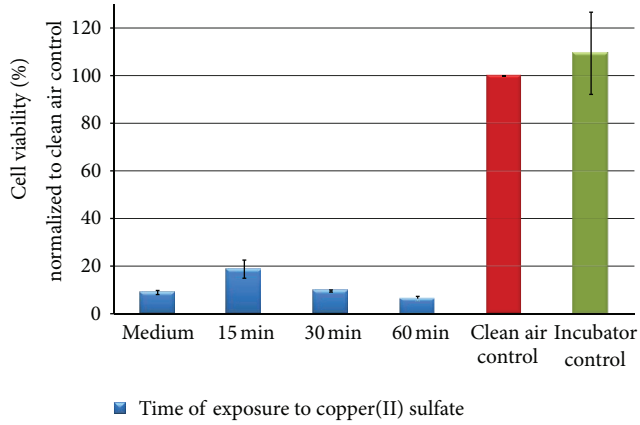

Figure 13: Relative cell viability of A549 cells after exposure to copper(II) sulfate particles normalized to the clean air control dependent on time (15, 30, and 60 min).

the cytotoxic response among the three exposure times. The comparison of the 15, 30, and 60 minutes exposures in a Student's t-test demonstrates significant differences with a 5% error probability. No significant differences could be obtained for lactose monohydrate (30 minutes compared to 15 minutes) and copper(II) oxide micro-sized (60 minutes compared to 30 minutes) due to the low number of tests.

The exposure of A549 cells to lactose monohydrate (negative substance) led to a slight decrease in the cell viability of the cells after 15 minutes (94% of the clean air control). By increasing the exposure time to 60 minutes, the metabolic activity of the cells was reduced by 30% in comparison to the clean air control. At that point, the cultures were covered by a dense layer of the particulate matter thus pointing to an overload effect.

The particle number (black line) and mass distribution (red line) of the lactose monohydrate aerosol dependent on particle size are shown in Figure 12. The units number, respectively, mass per $\mu m*cm^3$ may be unfamiliar at first glance. As the curves are based on particle counts, classified to 51 particle size intervals, the counts have to be divided not only through the volume but also through the interval width to get the required values for particle distribution curves.

The particle number distribution curve exhibits its peak value at a particle size of 0.7 μm while the particle *mass* distribution curve shows its peak value at a particle size of 4.2 μm due to the greater mass of larger particles.

The exposure of the cell populations to copper(II) sulfate led to a pronounced decrease in the cell viability after 15 minutes 19% of the clean air control. By increasing the time to 60 minutes, the metabolic activity was reduced by more than 91% compared to the clean air control.

The peak for the particle number distribution was at 0.9 μm and the peak for the particle mass distribution was at 3.8 μm (Figure 14). Both particle number and particle mass were about five times higher than for lactose monohydrate.

The results after the exposure of A549 cells to copper(II) oxide micro also indicated a dose-dependent decrease of the metabolic activity over the exposure time (Figure 15). The decrease of cell viability after 60 minutes exposure (61% reduction in comparison to the synthetic air control) is significantly higher than for lactose monohydrate but not as clear as for copper(II) sulfate.

In comparison with copper(II) sulfate, the particle number distribution of copper(II) oxide micro also showed a peak at 0.9 μm, but with a more than four times lower number of particles (Figure 16). The values for the particle mass distribution were about 25% lower compared to copper(II) sulfate, indicating that the substances mostly differ in their content of small particles.

The cell viability of the A549 cells was significantly reduced after the exposure to copper(II) oxide nanoparticles. After 15 minutes, the metabolic activity was reduced to less than 50% compared to the clean air and incubator control. A particle mass of 100 $\mu g/cm^2$ (60 minutes) led to a reduction in the metabolic activity of 85%, indicating a higher cytotoxic effect by the nanopowder compared to the micro.

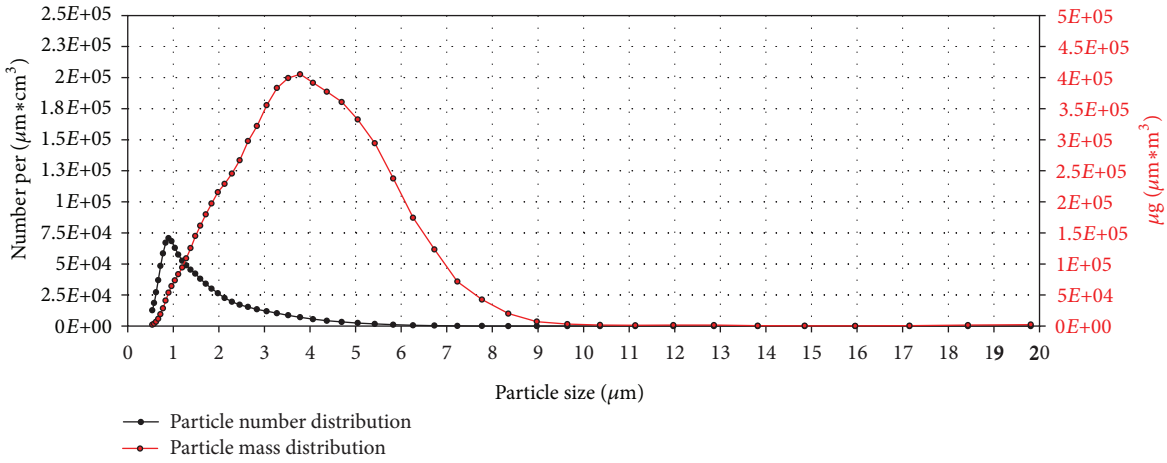

Figure 14: Particle number (black line) and particle mass distribution (red line) of the generated copper(II) sulfate aerosol entering the exposure module. The analysis was performed with an Aerodynamic Particle Sizer (TSI Inc.).

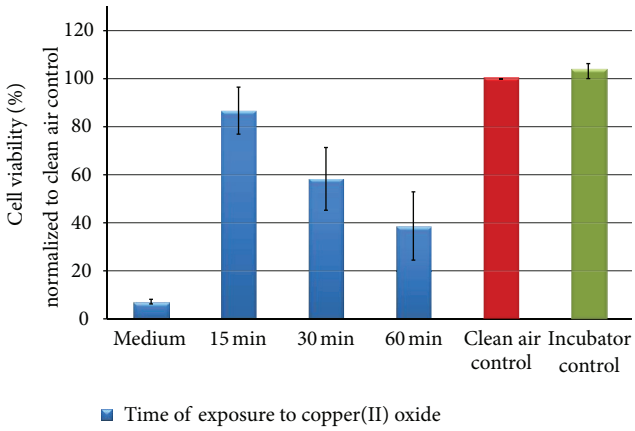

Figure 15: Relative cell viability of A549 cells after exposure to copper(II) oxide microparticles normalized to the clean air control dependent on time (15, 30, and 60 min).

Copper(II) oxide nano does not differ strongly from copper(II) oxide micro in numbers of sub-μm particles. The nanopowder exhibits much lower mass distribution values, however, due to few particles in the size range over 1 μm.

4. Discussion

Due to changes in the EU regulations concerning the approval of chemical substances (Regulation (EU) no. 1907/2006) and the ongoing demand for alternative methods, new cell systems and exposure techniques were developed and characterized, also in the field of inhalation toxicology. The latter should meet special requirements with regard to the cell type and the type of exposure.

The biological test systems include bronchial (Calu-3, 16HBE14o-, BEAS-2B) and alveolar epithelial (A549) cell lines, mostly from tumors as well as human primary cells isolated from different regions of the respiratory tract [22–25]. At the moment primary cell cultures are mostly studied under mechanistic aspects (differentiation, cellular interactions) [26] and are not used routinely for screening methods to address acute toxicity. Therefore, the studies are mostly performed with cell lines like the alveolar epithelial cell line A549, which allows the generation of stable cultures (undifferentiated). The advantage of these cultures is the delivery of stable, reproducible, and significant data for the calculation of dose-response curves as well as the definition of key values (effective dose: EC_{50}).

The exposure of cultivated cells from the respiratory tract for studying the effects of airborne substances represents a challenge with regard to the experimental design. The exposure of cells under conventional submerged conditions, mostly with soluble test substances, shows a variety of shortcomings like the interference of the test atmosphere with medium components, unrealistic exposure conditions including uncertain effective doses for gases and particles. Therefore, several approaches have been made for the development of exposure systems (Table 4) at the air-liquid interface [3, 12, 14, 17, 27–35]. Under such conditions, the cells are in direct contact with the test aerosol, which is conducted through the exposure device to the cells. The exposure systems have to fulfill cell-specific requirements, meaning the maintenance of the cell cultures during the exposure process by medium supply and the establishment of a cell-specific environment (pH value, 37°C).

All described systems have taken into consideration those basic requirements. The inserts are located in medium-containing chambers, connected with a medium supply for intermittent or continuous medium exchange. In the system described by Adamson et al. [36], 4 culture vessels are placed together in a chamber filled up with medium to the bottom of the cell culture inserts. In the CULTEX RFS, and also the CULTEX glass modules [27, 28], the inserts are housed separately and are supplied individually with nutrients, as independent exposure chambers within one module. The medium level is adjusted via an overflow tube to establish comparable conditions in all three chambers.

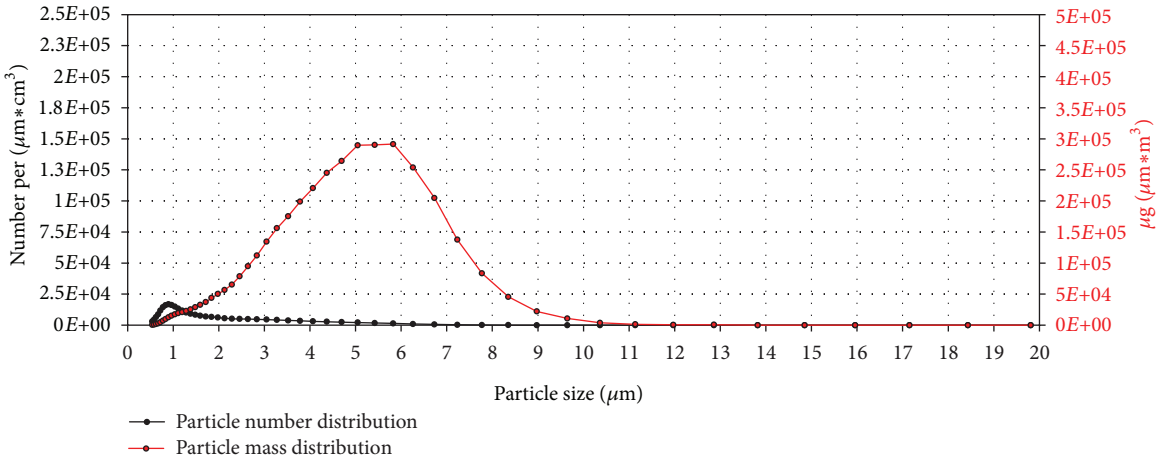

Figure 16: Particle number (black line) and particle mass distribution (red line) of the generated copper(II) oxide microaerosol entering the exposure module. The analysis was performed with an Aerodynamic Particle Sizer (TSI Inc.).

Table 4: Exposure systems for exposing cultivated cells at the air-liquid interface.

Exposure system	Electrostatic precipitation	Cell type	Test atmosphere	Literature
Cultex CG	No	LK004 HFBE-21 CHO-K1 A549 BEAS-2B	Cigarette smoke Diesel exhaust Ozone and nitrogene dioxide Phosgene Volatile organic compounds Pharmaceuticals Trichloramine Fly ash Particles	Aufderheide and Mohr 1999 [12] Ritter et al. 2001 [46] Knebel et al. 2002 [47] Diabaté et al. 2008 [48] Pariselli et al. 2009 [49] Deschl et al. 2011 [50] Schmalz et al. 2011 [51] Wijte et al. 2011 [52] Nara et al. [53] Elihn et al. 2012 [54]
Cultex RFS	Yes	A549 16HBE14o-	Cigarette smoke	Aufderheide et al. 2011 [17]
ALICE	No	A549	Carbon black nanoparticles Zinc oxide nanoparticles Gold nanoparticles	Lenz et al. 2009 [14]
NACIVT	Yes	BEAS-2B Porcine lung macrophages	Secondary organic aerosols Polystyrene particles	Gaschen et al. 2010 [55] Savi et al. 2008 [16]
Vitrocell	No	A549	Laser printer emissions Volatile organic compounds Carbon nanotubes	Tang et al. 2012 [56] Frohlich et al. 2012 [57] Anderson et al. 2010 [58] Gminski et al. 2011 [59]
BAT	No	NCI-H292	Cigarette smoke	Phillips et al. 2005 [35]
EAVES	Yes	A549	Polystyrene particles Diesel exhaust Coarse ambient particles	de Bruijne et al. 2009 [15] Volckens et al. 2009 [60]

The basic principle of cellular exposure to airborne materials is based on the treatment of the cultivated cells at the air-liquid interface (ALI). The experimental setup to realize a direct contact between the cells and the test atmosphere differs considerably in the different systems, which are listed in Table 4. A limited number of devices favor the exposure of the cultures to an aerosol passing through a box or exposure chamber [35, 36], but most of the exposure systems prefer a stream directed towards the cell culture to realize a close contact between the test atmosphere and the cell surface for depositing particles. Gaseous compounds can be studied in all systems due to the homogeneous distribution of their test atmosphere, whereas the exposure of particulate materials is based mostly on a directed aerosol flow. A comparative study of the different test systems is limited due to the limited availability of the modules and the absence of information.

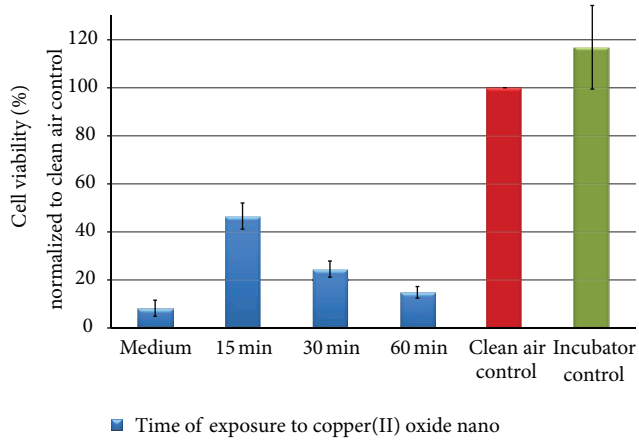

Figure 17: Relative cell viability of A549 cells after exposure to copper(II) oxide nanoparticles normalized to the clean air control dependent on time (15, 30, and 60 min).

The CULTEX glass modules as well as the RFS are designed to establish an incoming flow which is directed immediately via emission ducts to the surface of the cells to guarantee a close contact with the test atmosphere, both qualitatively and quantitatively. In comparison with the glass modules, the aerosol guiding module of the RFS has been optimized concerning the uniform distribution of the incoming test atmosphere to the three exposure chambers, thus stabilizing the whole exposure process. In the glass modules, the aerosol is guided linearly above the module and the sampling points for the test atmosphere are arranged in succession. In the case of gaseous compounds, the homogeneous distribution of the atmosphere is not limited, but airborne particles belong to another category, especially with regard to their aerosol physical properties. A linear flow path above the glass module leads to a concentration gradient, which may result, due to the sequentially arranged sampling points, at different exposure levels. In contrast, the CULTEX RFS module is characterized by a central inlet for the test atmosphere into the exposure device, wherefrom the aerosol is distributed into the chambers and the particles deposited on the cell cultures. The resulting data are characterized by a small standard deviation within a test or for multiple experiments. Another relevant advantage of the new system is the adjustment of the medium level, which ensures a comparable microenvironment for all cultures. The level in the Cultex RFS is controlled by special overflow tubes to stabilize the sensitive microclimate around the cells. An autonomous medium supply for each cell culture insert offers the opportunity to test different medium additives without interaction between the three test chambers. The new modular design of the Cultex RFS guarantees a high flexibility in working with different types of cell culture inserts or even Petri dishes (for the AMES assay) by using special adapters.

The efficiency of the exposure process depends on the deposition efficiency and represents, especially in the case of fine and ultrafine particles (nano particles), one of the main challenges [17]. The deposition efficiency of the particles in most air-liquid interface systems is based on sedimentation and diffusion. Accordingly, a characterization of the test aerosol with regard to the particle number and particle mass dependent on the particle size is one of the main requirements to judge the biological activity of the airborne material. Due to changes within the aerosol during the generation process and due to particle-particle interactions, the primary particle size should only be used as a basic indication. In this context, particle loss within the system and agglomeration of the particles has to be taken into account.

In the literature, the deposition efficiency rate of *in vitro* exposure devices is described inconsistently. Theoretical considerations and experimental exposure data with ultrafine carbonaceous model particles with a CMD of 95 nm resulted in an efficiency of 2% [37].

The combination of such air-liquid interface exposure systems with an electrical charger and precipitator could improve particle deposition. Experimental data from Savi et al. [16] showed that the deposition efficiency can be increased to 30% with this type of setup without causing a cytotoxic effect on the exposed cells. First results obtained with the Cultex RFS in combination with an electrical deposition device (Cultex EDD) indicated that the efficiency for particles which are not deposited by sedimentation or diffusion can be increased up to 95% (data not shown).

The outstanding importance of particle size and mass for the deposition efficiency highlights the importance of a controlled and stable generation of particulate atmospheres as well as the behavior of such particles in an exposure device.

To obtain more insights into the flow conditions within our Cultex RFS module, CFD analysis was conducted by taking into consideration all components of the experimental setup. CFD simulations included the particle distribution in the tubing system (connection between the elutriator and the exposure module) and the exposure module itself. Here, we found that inhomogeneous particle distributions propagate over long distances due to laminar flow conditions. The integration of a jet nozzle into the inlet adapter enabled a homogeneous particle distribution and deposition on the insert membranes as shown in Figure 10 at the example of copper(II) oxide micro. The CFD analysis provides a good method to simulate the trajectories of the particles from generation to deposition. The consideration of different experimental conditions like the air flow rate or dimensions of the connecting tubes allows the selection of the appropriate experimental design to enhance the efficiency of the exposure system.

Besides the experimental setup, the chemical and physical properties of the particles highly influence their deposition efficiency. To compare the biological activity of the different copper compounds, the particle mass concentration per area was adjusted for each substance to establish a comparable particle mass deposition (deposition rate: 25 $\mu g/cm^2$/15 min). A549 cells were exposed for 15, 30, and 60 minutes at the air-liquid interface to the different test atmospheres and the metabolic activity of the cells was analyzed as an estimate for cytotoxicity. In comparison to the incubator control, the cells that were exposed to clean air showed no reduction in the cell viability, indicating that

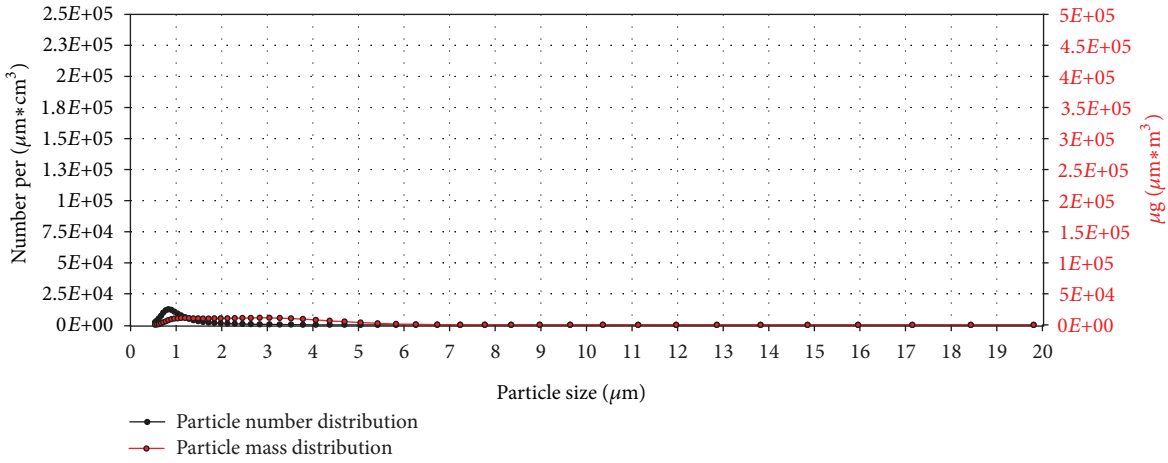

Figure 18: Particle number (black line) and particle mass distribution (red line) of the generated copper(II) oxide nano aerosol entering the exposure module. The analysis was performed with an Aerodynamic Particle Sizer (TSI Inc.).

the exposure procedure itself had *no effect* on this analyzed endpoint. As a negative substance control we used lactose, which induced no considerable cell damage (13% after an exposure time of 30 minutes). At the end of the exposure period, the cultures were covered by a dense particle layer and a further reduction in cell viability (37% of the clean air control) was measured probably due to an overload effect.

In comparison with lactose monohydrate, all copper compounds induced significant dose-related effects. The cytotoxic signal correlated strongly with the chemical and physical properties of the test compound. Copper(II) sulfate, as soluble compound, induced a pronounced cytotoxic effect already after an exposure time of 15 minutes (reduction of cell viability of 80%). Comparable effects could also be observed for the insoluble copper(II) oxide compounds, but to a lesser extent. As described by Karlsson and coworkers [38], the exposure of the cells to both substances resulted in a dose-dependent decrease in the cell viability by increasing the particle concentration, whereby the copper(II) oxide nanomaterial appeared to be more harmful to the cells than copper(II) oxide micro, based on the exposed particle mass. In the literature, nanoparticles are repeatedly described to be more potent in causing a cellular damage than microparticles [38–40], but there is also evidence that there is no difference in their biological activity [41–43]. In agreement with the above-mentioned studies, our direct exposure studies with nanosized copper(II) oxide exhibited a stronger cytotoxicity than the micro-sized particles. Most of the studies on micro- or nanosized particles have been conducted under submersed conditions. Ahamed and coworkers also used A549 cells, which were treated with CuO nanoparticles (NP) suspended in medium (0, 10, 25, and 50 μg/mL for 24 hours) [44]. CuO NPs significantly decreased cell viability in a dose-dependent manner. The highest concentration (50 μg/mL) induced a reduction in viability of 52%, whereas the directly exposed A549 cells showed a decrease of more than 75%, pointing to a more efficient contact and interaction between deposited particles and the lung cells. Investigations of Karlsson et al. support this assessment [38, 45].

Concerning the number of particles per cm^2 for each substance, A549 cells were exposed in the case of copper(II) oxide nano to more particles in comparison to copper(II) oxide micro. Accordingly, the higher cytotoxicity may also be a result of the higher number of smaller particles coming into contact with the surface of the cells.

In summary, our results show that an efficient and stable cell exposure system like the Cultex RFS module allows a reproducible analysis of dose-dependent reactions to airborne materials. The cell cultures can be exposed to the generated particulate atmospheres, characterized with regard to particle size and mass distribution, under controlled conditions thus favoring the generation of valid data for the calculation of key values (effective dose). These data can be compared with animal or clinical data and offer the possibility to verify the relevance and meaningfulness of these *in vitro* studies.

Disclosure

M. Aufderheide and N. Möhle are employees of Cultex Laboratories GmbH. B. Halter and D. Hochrainer are consultants.

References

[1] P. J. Barnes, "New therapies for chronic obstructive pulmonary disease," *Medical Principles and Practice*, vol. 19, no. 5, pp. 330–338, 2010.

[2] A. D. Lopez and C. C. J. L. Murray, "The global burden of disease, 1990–2020," *Nature Medicine*, vol. 4, no. 11, pp. 1241–1243, 1998.

[3] K. Bérubé, M. Aufderheide, D. Breheny et al., "*In vitro* models of inhalation toxicity and disease. The report of a FRAME workshop," *Alternatives to Laboratory Animals*, vol. 37, no. 1, pp. 89–141, 2009.

[4] S. May, B. Jensen, M. Wolkenhauer, M. Schneider, and C. M. Lehr, "Dissolution techniques for *in vitro* testing of dry powders for inhalation," *Pharmaceutical Research*, vol. 29, no. 8, pp. 2157–2166, 2012.

[5] B. M. Wright, "A new dust-feed mechanism," *Journal of Scientific Instruments*, vol. 27, no. 1, pp. 12–15, 1950.

[6] C. Rovida and T. Hartung, "Re-evaluation of animal numbers and costs for *in vivo* tests to accomplish REACH legislation requirements for chemicals—a report by the transatlantic think tank for toxicology (t(4))," *ALTEX*, vol. 26, no. 3, pp. 187–208, 2009.

[7] D. O. Raemy, R. N. Grass, W. J. Stark, C. M. Schumacher, M. J. Clift et al., "Effects of flame made zinc oxide particles in human lung cells—a comparison of aerosol and suspension exposures," *Particle and Fibre Toxicology*, vol. 9, article 33, 2012.

[8] L. K. Limbach, Y. Li, R. N. Grass et al., "Oxide nanoparticle uptake in human lung fibroblasts: effects of particle size, agglomeration, and diffusion at low concentrations," *Environmental Science and Technology*, vol. 39, no. 23, pp. 9370–9376, 2005.

[9] T. Hartung, "Thoughts on limitations of animal models," *Parkinsonism & Related Disorders*, vol. 14, supplement 2, pp. S81–S83, 2008.

[10] B. K. Tarkington, R. Wu, W. M. Sun, K. J. Nikula, D. W. Wilson, and J. A. Last, "*In vitro* exposure of tracheobronchial epithelial cells and of tracheal explants to ozone," *Toxicology*, vol. 88, no. 1–3, pp. 51–68, 1994.

[11] C. Voisin, C. Aerts, E. Jakubczak, J. L. Houdret, and T. B. Tonnel, "Effects of nitrogen dioxide on alveolar macrophages surviving in the gas phase. A new experimental model for the study of *in vitro* cytotoxicity of toxic gases (author's transl)," *Bulletin Européen de Physiopathologie Respiratoire*, vol. 13, no. 1, pp. 137–144, 1977.

[12] M. Aufderheide and U. Mohr, "CULTEX–a new system and technique for the cultivation and exposure of cells at the air/liquid interface," *Experimental and Toxicologic Pathology*, vol. 51, no. 6, pp. 489–490, 1999.

[13] M. Aufderheide and U. Mohr, "A modified CULTEX system for the direct exposure of bacteria to inhalable substances," *Experimental and Toxicologic Pathology*, vol. 55, no. 6, pp. 451–454, 2004.

[14] A. G. Lenz, E. Karg, B. Lentner, V. Dittrich, C. Brandenberger et al., "A dose-controlled system for air-liquid interface cell exposure and application to zinc oxide nanoparticles," *Particle and Fibre Toxicology*, vol. 6, article 32, 2009.

[15] K. de Bruijne, S. Ebersviller, K. G. Sexton et al., "Design and testing of Electrostatic Aerosol *In Vitro* Exposure System (EAVES): an alternative exposure system for particles," *Inhalation Toxicology*, vol. 21, no. 2, pp. 91–101, 2009.

[16] M. Savi, M. Kalberer, D. Lang et al., "A novel exposure system for the efficient and controlled deposition of aerosol particles onto cell cultures," *Environmental Science and Technology*, vol. 42, no. 15, pp. 5667–5674, 2008.

[17] M. Aufderheide, S. Scheffler, N. Mohle, B. Halter, and D. Hochrainer, "Analytical *in vitro* approach for studying cyto- and genotoxic effects of particulate airborne material," *Analytical and Bioanalytical Chemistry*, vol. 401, no. 10, pp. 3213–3220, 2011.

[18] D. J. Giard, S. A. Aaronson, G. J. Todaro et al., "*In vitro* cultivation of human tumors: establishment of cell lines derived from a series of solid tumors," *Journal of the National Cancer Institute*, vol. 51, no. 5, pp. 1417–1423, 1973.

[19] M. Lieber, B. Smith, A. Szakal et al., "A continuous tumor-cell line from a human lung carcinoma with properties of type II alveolar epithelial cells," *International Journal of Cancer*, vol. 17, no. 1, pp. 62–70, 1976.

[20] F. Kohlrausch, *Praktische Physik: zum Gebrauch für Unterricht, Forschung und Technik*, V. Kose, S. Wagner, Ed., 24. Aufl., B. G. Teubner, Stuttgart, Germany, 1996.

[21] NanoCare, "Health related aspects of nanomaterials," Project Report, 2009.

[22] B. Forbes, A. Shah, G. P. Martin, and A. B. Lansley, "The human bronchial epithelial cell line 16HBE14o- as a model system of the airways for studying drug transport," *International Journal of Pharmaceutics*, vol. 257, no. 1-2, pp. 161–167, 2003.

[23] C. I. Grainger, L. L. Greenwell, D. J. Lockley, G. P. Martin, and B. Forbes, "Culture of Calu-3 cells at the air interface provides a representative model of the airway epithelial barrier," *Pharmaceutical Research*, vol. 23, no. 7, pp. 1482–1490, 2006.

[24] A. Penn, G. Murphy, S. Barker, W. Henk, and L. Penn, "Combustion-derived ultrafine particles transport organic toxicants to target respiratory cells," *Environmental Health Perspectives*, vol. 113, no. 8, pp. 956–963, 2005.

[25] B. Rothen-Rutishauser, F. Blank, C. Muhlfeld, and P. Gehr, "*In vitro* models of the human epithelial airway barrier to study the toxic potential of particulate matter," *Expert Opinion on Drug Metabolism and Toxicology*, vol. 4, no. 8, pp. 1075–1089, 2008.

[26] A. C. Gray, J. D. McLeod, and R. H. Clothier, "A review of *in vitro* modelling approaches to the identification and modulation of squamous metaplasia in the human tracheobronchial epithelium," *Alternatives to Laboratory Animals*, vol. 35, no. 5, pp. 493–504, 2007.

[27] M. Aufderheide, "Direct exposure methods for testing native atmospheres," *Experimental and Toxicologic Pathology*, vol. 57, supplement 1, pp. 213–226, 2005.

[28] M. Aufderheide, "An efficient approach to study the toxicological effects of complex mixtures," *Experimental and Toxicologic Pathology*, vol. 60, no. 2-3, pp. 163–180, 2008.

[29] M. Aufderheide and U. Mohr, "CULTEX—an alternative technique for cultivation and exposure of cells of the respiratory tract to airborne pollutants at the air/liquid interface," *Experimental and Toxicologic Pathology*, vol. 52, no. 3, pp. 265–270, 2000.

[30] E. Bitterle, E. Karg, A. Schroeppel et al., "Dose-controlled exposure of A549 epithelial cells at the air-liquid interface to airborne ultrafine carbonaceous particles," *Chemosphere*, vol. 65, no. 10, pp. 1784–1790, 2006.

[31] Y. Fukano, M. Ogura, K. Eguchi, M. Shibagaki, and M. Suzuki, "Modified procedure of a direct *in vitro* exposure system for mammalian cells to whole cigarette smoke," *Experimental and Toxicologic Pathology*, vol. 55, no. 5, pp. 317–323, 2004.

[32] S. Mülhopt, H. R. Paur, S. Diabate, and H. F. Krug, "In-vitro testing of inhalable fly ash at the air liquid interface," in *Environmental Monitoring*, Y. J. Kim, Ed., pp. 402–414, Springer, Dordrecht, The Netherlands, 2008.

[33] B. Rothen-Rutishauser, F. Blank, C. Mühlfeld, and P. Gehr, "Nanoparticle-cell membrane interactions," in *Particle-Lung Interactions*, P. Gehr, C. Mühlfeld, B. Rothen-Rutishauser, and F. Blank, Eds., pp. 226–242, Informa Healtscare, New York, NY, USA, 2009.

[34] B. Rothen-Rutishauser, R. N. Grass, F. Blank et al., "Direct combination of nanoparticle fabrication and exposure to lung cell cultures in a closed setup as a method to simulate accidental nanoparticle exposure of humans," *Environmental Science and Technology*, vol. 43, no. 7, pp. 2634–2640, 2009.

[35] J. Phillips, B. Kluss, A. Richter, and E. D. Massey, "Exposure of bronchial epithelial cells to whole cigarette smoke: assessment

of cellular responses," *Alternatives to Laboratory Animals*, vol. 33, no. 3, pp. 239–248, 2005.

[36] J. Adamson, D. Azzopardi, G. Errington, C. Dickens, J. McAughey et al., "Assessment of an *in vitro* whole cigarette smoke exposure system: the Borgwaldt RM20S 8-syringe smoking machine," *Chemistry Central Journal*, vol. 5, article 50, 2011.

[37] A. Tippe, U. Heinzmann, and C. Roth, "Deposition of fine and ultrafine aerosol particles during exposure at the air/cell interface," *Journal of Aerosol Science*, vol. 33, no. 2, pp. 207–218, 2002.

[38] H. L. Karlsson, J. Gustafsson, P. Cronholm, and L. Möller, "Size-dependent toxicity of metal oxide particles—a comparison between nano- and micrometer size," *Toxicology Letters*, vol. 188, no. 2, pp. 112–118, 2009.

[39] K. Donaldson and C. L. Tran, "Inflammation caused by particles and fibers," *Inhalation Toxicology*, vol. 14, no. 1, pp. 5–27, 2002.

[40] G. Oberdörster, "Pulmonary effects of inhaled ultrafine particles," *International Archives of Occupational and Environmental Health*, vol. 74, no. 1, pp. 1–8, 2001.

[41] S. Park, Y. K. Lee, M. Jung et al., "Cellular toxicity of various inhalable metal nanoparticles on human alveolar epithelial cells," *Inhalation Toxicology*, vol. 19, supplement 1, pp. 59–65, 2007.

[42] J. M. Veranth, E. G. Kaser, M. M. Veranth, M. Koch, and G. S. Yost, "Cytokine responses of human lung cells (BEAS-2B) treated with micron-sized and nanoparticles of metal oxides compared to soil dusts," *Particle and Fibre Toxicology*, vol. 4, article 2, 2007.

[43] D. B. Warheit, T. R. Webb, V. L. Colvin, K. L. Reed, and C. M. Sayes, "Pulmonary bioassay studies with nanoscale and fine-quartz particles in rats: toxicity is not dependent upon particle size but on surface characteristics," *Toxicological Sciences*, vol. 95, no. 1, pp. 270–280, 2007.

[44] M. Ahamed, M. A. Siddiqui, M. J. Akhtar, I. Ahmad, A. B. Pant, and H. A. Alhadlaq, "Genotoxic potential of copper oxide nanoparticles in human lung epithelial cells," *Biochemical and Biophysical Research Communications*, vol. 396, no. 2, pp. 578–583, 2010.

[45] H. L. Karlsson, P. Cronholm, J. Gustafsson, and L. Möller, "Copper oxide nanoparticles are highly toxic: a comparison between metal oxide nanoparticles and carbon nanotubes," *Chemical Research in Toxicology*, vol. 21, no. 9, pp. 1726–1732, 2008.

[46] D. Ritter, J. W. Knebel, and M. Aufderheide, "*In vitro* exposure of isolated cells to native gaseous compounds—development and validation of an optimized system for human lung cells," *Experimental and Toxicologic Pathology*, vol. 53, no. 5, pp. 373–386, 2001.

[47] J. W. Knebel, D. Ritter, and M. Aufderheide, "Exposure of human lung cells to native diesel motor exhaust—development of an optimized *in vitro* test strategy," *Toxicology in Vitro*, vol. 16, no. 2, pp. 185–192, 2002.

[48] S. Diabaté, S. Mülhopt, H. R. Paur, and H. F. Krug, "The response of a co-culture lung model to fine and ultrafine particles of incinerator fly ash at the air-liquid interface," *Alternatives to Laboratory Animals*, vol. 36, no. 3, pp. 285–298, 2008.

[49] F. Pariselli, M. G. Sacco, and D. Rembges, "An optimized method for *in vitro* exposure of human derived lung cells to volatile chemicals," *Experimental and Toxicologic Pathology*, vol. 61, no. 1, pp. 33–39, 2009.

[50] U. Deschl, J. Vogel, and M. Aufderheide, "Development of an *in vitro* exposure model for investigating the biological effects of therapeutic aerosols on human cells from the respiratory tract," *Experimental and Toxicologic Pathology*, vol. 63, no. 6, pp. 593–598, 2011.

[51] C. Schmalz, H. G. Wunderlich, R. Heinze, F. H. Frimmel, C. Zwiener et al., "Application of an optimized system for the well-defined exposure of human lung cells to trichloramine and indoor pool air," *Journal of Water and Health*, vol. 9, no. 3, pp. 586–596, 2011.

[52] D. Wijte, M. J. Alblas, D. Noort, J. P. Langenberg, and H. P. van Helden, "Toxic effects following phosgene exposure of human epithelial lung cells *in vitro* using a CULTEX system," *Toxicology in Vitro*, vol. 25, no. 8, pp. 2080–2087, 2011.

[53] H. Nara, Y. Fukano, T. Nishino, and M. Aufderheide, "Detection of the cytotoxicity of water-insoluble fraction of cigarette smoke by direct exposure to cultured cells at an air-liquid interface," *Experimental and Toxicologic Pathology*. In press.

[54] K. Elihn, P. Cronholm, H. L. Karlsson, K. Midander, I. Odnevall Wallinder et al., "Cellular dose of partly soluble Cu particle aerosols at the air-liquid interface using an *in vitro* lung cell exposure system," *Journal of Aerosol Medicine and Pulmonary Drug Delivery*. In press.

[55] A. Gaschen, D. Lang, M. Kalberer et al., "Cellular responses after exposure of lung cell cultures to secondary organic aerosol particles," *Environmental Science and Technology*, vol. 44, no. 4, pp. 1424–1430, 2010.

[56] T. Tang, R. Gminski, M. Konczol, C. Modest, B. Armbruster et al., "Investigations on cytotoxic and genotoxic effects of laser printer emissions in human epithelial A549 lung cells using an air/liquid exposure system," *Environmental and Molecular Mutagenesis*, vol. 53, no. 2, pp. 125–135, 2012.

[57] E. Frohlich, G. Bonstingl, A. Hofler, C. Meindl, G. Leitinger et al., "Comparison of two *in vitro* systems to assess cellular effects of nanoparticles-containing aerosols," *Toxicology in Vitro*, vol. 27, no. 1, pp. 409–417, 2012.

[58] S. E. Anderson, L. G. Jackson, J. Franko, and J. R. Wells, "Evaluation of dicarbonyls generated in a simulated indoor air environment using an *in vitro* exposure system," *Toxicological Sciences*, vol. 115, no. 2, pp. 453–461, 2010.

[59] R. Gminski, K. Decker, C. Heinz et al., "Genotoxic effects of three selected black toner powders and their dimethyl sulfoxide extracts in cultured human epithelial A549 lung cells *in vitro*," *Environmental and Molecular Mutagenesis*, vol. 52, no. 4, pp. 296–309, 2011.

[60] J. Volckens, L. Dailey, G. Walters, and R. B. Devlin, "Direct particle-to-cell deposition of coarse ambient particulate matter increases the production of inflammatory mediators from cultured human airway epithelial cells," *Environmental Science and Technology*, vol. 43, no. 12, pp. 4595–4599, 2009.

Hindawi Publishing Corporation
BioMed Research International
Volume 2013, Article ID 161687, 16 pages
http://dx.doi.org/10.1155/2013/161687

Review Article

Early Alzheimer's and Parkinson's Disease Pathology in Urban Children: Friend versus Foe Responses—It Is Time to Face the Evidence

Lilian Calderón-Garcidueñas,[1] Maricela Franco-Lira,[2] Antonieta Mora-Tiscareño,[3] Humberto Medina-Cortina,[3] Ricardo Torres-Jardón,[4] and Michael Kavanaugh[1]

[1] *Center for Structural and Functional Neurosciences, The University of Montana, 32 Campus Drive, Skaggs Building 287, Missoula, MT 59812, USA*
[2] *Departamento de Investigación, Hospital Central Militar, Secretaria de la Defensa Nacional, 11649 México, DF, Mexico*
[3] *Departamentos de Radiología y Patología Experimental, Instituto Nacional de Pediatria, 04530 México, DF, Mexico*
[4] *Centro de Ciencias de la Atmósfera, Universidad Nacional Autónoma de México, 04510 México, DF, Mexico*

Correspondence should be addressed to Lilian Calderón-Garcidueñas; lilian.calderon-garciduenas@umontana.edu

Received 7 November 2012; Revised 1 January 2013; Accepted 1 January 2013

Academic Editor: Tim Nawrot

Chronic exposure to particulate matter air pollution is known to cause inflammation leading to respiratory- and cardiovascular-related sickness and death. Mexico City Metropolitan Area children exhibit an early brain imbalance in genes involved in oxidative stress, inflammation, and innate and adaptive immune responses. Early dysregulated neuroinflammation, brain microvascular damage, production of potent vasoconstrictors, and perturbations in the integrity of the neurovascular unit likely contribute to progressive neurodegenerative processes. The accumulation of misfolded proteins coincides with the anatomical distribution observed in the early stages of both Alzheimer's and Parkinson's diseases. We contend misfolding of hyperphosphorylated tau (HPπ), alpha-synuclein, and beta-amyloid could represent a compensatory early protective response to the sustained systemic and brain inflammation. However, we favor the view that the chronic systemic and brain dysregulated inflammation and the diffuse vascular damage contribute to the establishment of neurodegenerative processes with childhood clinical manifestations. Friend turns Foe early; therefore, implementation of neuroprotective measures to ameliorate or stop the inflammatory and neurodegenerative processes is warranted in exposed children. Epidemiological, cognitive, structural, and functional neuroimaging and mechanistic studies into the association between air pollution exposures and the development of neuroinflammation and neurodegeneration in children are of pressing importance for public health.

1. Introduction

Air pollution is a significant health problem in megacities around the world [1–3]. In a scenario where the projected world population will have a further increase of 2 to 4.5 billion in the first 50 years of this century [4], the issue of deteriorating environments and their health impact is critical. The problem of air pollution is not confined to large urban centers, it also affects small cities and rural areas. Particulate matter (PM) air pollution is a public health problem affecting millions of people worldwide.

Recent works have shed new light on the etiology of Alzheimer's and Parkinson's diseases (AD and PD), with a growing body of evidence that oxidative stress and neuroinflammation are at the core of their etiopathogenesis and that there is a close interplay between environmental factors and neurodegeneration [5–8]. We also know the most beneficial neuroprotective effects might only be achieved in the very early stages of the detrimental processes. As such, a great effort has been made in establishing the associations between particulate air pollution, neuroinflammation, and neurodegeneration in highly exposed megacity children and young

adults. The first part of this paper deals briefly with the current state of air pollution in Mexico City Metropolitan Area (MCMA) and with the several areas of investigation in our laboratory that exemplify how seemingly clinically healthy children are responding to the sustained exposures to air pollutants. The second part of the paper turns to a more troublesome challenge. How do you formulate the neuropathology and gene brain expression findings in *clinically healthy children and young adults* and establish the links with the current mainstream concepts of neurodegeneration. This principled problem thus addresses the relation between neuroinflammation, neurodegeneration, and air pollution exposures with an emphasis on compensatory responses. Dealing with this problem invites the development of linking hypotheses between the domains and the need for intervention, issues addressed in the third part of the paper.

2. Air Pollution Background and Clinical Issues in Metropolitan Mexico City Clinically Health Children

2.1. Air Pollution in Mexico City Metropolitan Area (MCMA). Although there is significant air pollution associated with ozone in MCMA, in this work, we will focus on particulate matter (PM) broadly defined by the diameter of the aerodynamic particles and classified into coarse particles (<10 μm; PM_{10}), fine particles (<2.5 μm; $PM_{2.5}$), and ultrafine particles (<100 nm; UFPM). Fine and ultrafine PM are of particular interest given their capability to reach the brain [9]. The smaller the particle, the greater its penetration, diffusion, and deposition into the respiratory tract and its direct translocation into the brain [9–11].

MCMA, the largest urban center in North America, is an example of extreme urban growth and environmental pollution [12]. The metropolitan area of over 2000 square kilometers is home to over 20 million inhabitants including 8 million children. The energy demand of this population and over 40000 industries and 4 million vehicles consumes more than 40 million liters of petroleum fuels per day resulting in an annual emission of approximately 2.6 tons of pollutants including coarse and fine particulate matter, gaseous pollutants, polycyclic aromatic hydrocarbons, and lipopolysaccharides [12]. The MCMA is located in the southwestern portion of an elevated basin 2240 m above sea level that is surrounded on three sides by mountain ridges at 19° N 99° W. The high altitude and tropical insolation of the basin facilitate ozone production all year and contribute to the formation of secondary PM. Air quality is generally worse in the winter when thermal inversions are more frequent [13].

Even with the substantial reductions in the concentrations of some criteria pollutants (such as lead, CO, and SO_2) achieved during the past fifteen years, MCMA residents remain exposed to concentrations of airborne pollutants exceeding current ambient air quality standards for PM and ozone [14]. High concentrations of $PM_{2.5}$ as well as significant levels of PM_{10} associated with lipopolysaccharides (PM-LPS) have been registered historically in Mexico City's air, and marked regional differences in the air pollutants concentrations and composition have been reported within MCMA [12, 15–19].

Figure 1 shows the trend of 24-hour average PM_{10} concentrations for MCMA (1995–2011). PM_{10} concentrations had shown a clear reduction up to 2007; however, concentrations have been slowly back on the rise in the last 5 years. $PM_{2.5}$ data from the monitoring network [20] in Figure 2 show the 90th percentile of the 24-hour average concentrations per year have been above the respective air quality standard of 35 $\mu g/m^3$. MCMA residents are also exposed to UFPM from ambient air and workplaces. These nano sized PM include combustion sources (e.g., diesel exhaust particles, welding fumes) and manufactured or engineered nanoparticles (NPs). It is not widely appreciated that nano-sized materials are also present in many consumer products to which large segments of the population are exposed (e.g., toothpastes, cosmetics, sunscreens, food additives, and laser printer emissions) [21, 22].

In this massive exposure chamber, 8 million children and teens <18 y are receiving the impact of the involuntary exposure to the polluted air.

2.2. Detrimental NonCNS Effects in Exposed Children. It is important to emphasize that PM exposure has been epidemiologically associated to a wide spectrum of cardiovascular, pulmonary, and CNS effects [10, 11, 23–25]. Exposure to fine PM over a few hours to weeks can trigger cardiovascular disease-related mortality and nonfatal events [10]. Longer-term exposure increases the risk for cardiovascular mortality to an even greater extent than exposures over a few days [10]. In the cardiovascular literature "*credible pathological mechanisms have been elucidated that lend biological plausibility to* (detrimental) *findings*" [10]. Two mechanistic pathways applied to the cardiovascular and lung effects fit precisely the detrimental pathways in place in MCMA children [8]. These pathways include: pulmonary and systemic oxidative stress, and inflammation and direct effects of PM or its constituents on the vasculature and/or blood elements after translocation from the lung [10].

The pediatric studies from our laboratory cited in this work were performed in Mexico City clinically healthy children with no known risk factors for pulmonary, cardiovascular, and CNS pathology or cognitive deficits. MCMA children are selected from nonsmoking families and their results compared to age, gender, and socioeconomic status (SES) matched children residing in low polluted places. The detrimental nonCNS effects associated to residency in MC include the following.

(i) Systemic inflammation with increased concentrations of proinflammatory cytokines, chemokines, and potent vasoconstrictors (i.e., endothelin-1, ET-1). The concentrations of inflammatory mediators and ET-1 correlate positively with cumulative exposures to $PM_{2.5}$ and outdoor exposure hours [26]. Chronic inflammation involving the upper and lower respiratory tracts has been identified as a link between air pollution and brain damage [26–33]. Continuous

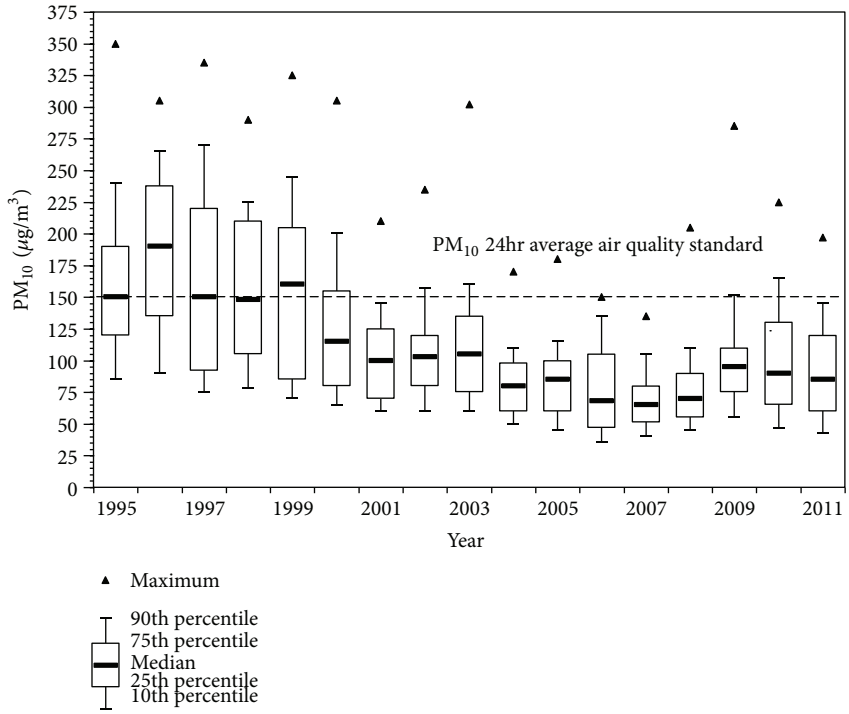

Figure 1: Trend of the PM_{10} 24-hour average concentrations from all monitoring stations in the MCMA from 1995 to 2011. The dashed line shows the U.S. EPA PM_{10} 24 hr average air quality standard (data from the SMA-GDF).

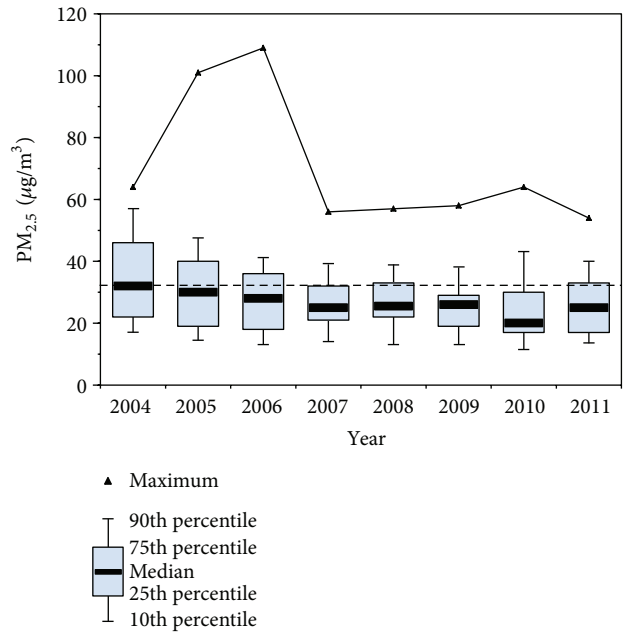

Figure 2: Trend of the $PM_{2.5}$ 24-hour average concentrations from all monitoring stations in the MCMA from 2004 to 2011. The dashed line shows the U.S. EPA $PM_{2.5}$ 24 hr average air quality standard (data from the SMA-GDF).

expression of inflammatory mediators capable of reaching the CNS promotes the formation of reactive oxygen species (ROS) [8]. Activation of innate immune responses within the brain may follow the interactions between circulating cytokines and the constitutively expressed cytokine receptors of brain endothelial cells. Such responses may, in turn, be followed by activation of cells involved in adaptive immunity [30, 34, 35]. Monocytes are the main innate immune response mediator cells, producing and secreting TNF-α, interleukin-6 (IL-6), and IL-1β, which in turn recruit and increase the activity of other immune cells [34]. Sustained exposures to fine and ultrafine PM likely start a chain of events leading to brain endothelial cell activation, disruption of the neurovascular unit, altered response of the innate immune system, neuroinflammation, and neurodegeneration [8, 30, 34–36].

(ii) Altered immune responses include significant decreases in the numbers of natural killer cells and increased numbers of mCD14+ monocytes and CD8+ cells. The reduction in the number of NK cells goes along with the low concentrations of interferon gamma (IFN-γ) [28]. MCMA children have monocytic mCD14 upregulation—a key membranous receptor involved in lipopolysaccharide (LPS) binding. The CD14 upregulation represents the early step in cell activation by LPS involving the innate immune initial host response to Gram negative bacterial infections [37]. MCMA children are historically exposed to endotoxin associated with PM [17, 28, 32, 38]. The issue is very important because we have shown there is a significant frontal upregulation of inflammasome-associated genes in MCMA children

and young adults [30]. Moreover, particle exposure has been associated to pathogen sensors and the signaling by ROS drives inflammasome intracellular signaling complexes activation [39–41]. Even very low doses of LPS elicit an augmented response to subsequent endotoxin challenge with a violent immune response [42]. The priming phenomenon could play a role in the neuroinflammatory responses observed in MCMA children [30, 35].

(iii) Pulmonary changes in MCMA children living in tobacco free homes include bilateral hyperinflation and increased linear markings observed in chest radiographs and mild bronchial wall thickening, prominent central airways, air trapping and pulmonary nodules identified by computed tomography scans. Abnormal lung function tests based on predicted values are seen in 7.8% of MCMA children. Higher concentrations of endothelin-1 correlate with elevations of mean pulmonary artery pressure, average hours per day spent outdoors, and 7 day cumulative concentrations of fine $PM_{2.5}$ [26, 27].

(iv) Cardiovascular effects include a significant right ventricle upregulation of IL-1β, TNF-α, IL-10, and CD14, and a left ventricle difference in TNF-α, and IL-10 in South versus North Mexico City residents, a key point in relation to the marked difference in pollutant profiles determined by the residence MCMA location [43].

2.3. Detrimental CNS Effects in Exposed Children. MCMA children with no known risk factors for neurological or cognitive disorders exhibit significant deficits in a combination of fluid and crystallized cognition tasks versus control children [29]. Fifty-six percent of MCMA children showed prefrontal white matter hyperintense (WMH) lesions by MRI and similar lesions were observed in MCMA dogs (57%) [29]. One control child out of 13 tested exhibited a single white matter lesion, and this child was an APOE 3/4 carrier [29]. Critical to this paper, MC breed animal facility dogs had frontal lesions with vascular subcortical pathology associated with neuroinflammation, enlarged Virchow-Robin spaces, gliosis, and ultrafine particulate matter deposition [29]. The dogs MRI findings were the same as the children, including their prefrontal location [29]. The data suggested the prefrontal cortex was a target anatomical region in exposed children and its damage could have contributed to their cognitive dysfunction. We next tested whether patterns of brain growth, cognitive deficits, and WMH were associated with exposures to MCMA air pollution [44]. Baseline and 1-year followup measurements of global and regional brain MRI volumes, cognitive abilities (Wechsler Intelligence Scale for Children-Revised, WISC-R), and serum inflammatory mediators were collected in 20 MCMA children (10 with white matter hyperintensities, WMH (+), and 10 without, WMH (−)) and 10 matched controls (CTL). There were significant differences in white matter volumes between CTL and MCMA children—both WMH (+) and WMH (−)—in right parietal and bilateral temporal areas. Both WMH (−) and WMH (+) MC children showed progressive deficits, compared to CTL children, on the WISC-R Vocabulary and Digit Span subtests. Interestingly, the cognitive deficits in MCMA children matched the localization of the volumetric differences detected over the 1 year followup [44].

When we analyzed the WMH lesions in relation to the profile of cytokines and chemokines [32], MCMA WMH (−) children displayed the profile of classical proinflammatory defensive responses: high interleukin 12, production of powerful proinflammatory cytokines, and low concentrations of key cytokines and chemokines associated with neuroprotection. In contrast, MC WMH (+) children exhibited a response involved in resolution of inflammation, immunoregulation, and tissue remodeling. The MC WMH (+) group responded to the air pollution-associated brain volumetric alterations with white and grey matter volume increases in temporal, parietal, and frontal regions and better cognitive performance compared to MC WMH (−).

These findings suggest a complex modulation of cytokines and chemokines influencing children's white matter hyperintensities, volumetric white matter responses and cognitive outcomes as a result of environmental pollution exposures.

3. Neuroinflammation and Neuropathology in Mexico City Children and Young Adults and Comparative Studies

In 2002, we published a dog study pointing to the nasal cavity as a major portal of entry of xenobiotics to the brain [45]. The study evaluated 32 healthy mongrel MCMA dogs, versus 8 dogs from Tlaxcala, a low polluted control city. MCMA dogs exhibited expression of nuclear neuronal NF-kappa B and iNOS in cortical endothelial cells at ages 2 and 4 weeks with subsequent damage to the blood-brain barrier (BBB), deposition of Apolipoprotein E (APOE)-positive lipid droplets in smooth muscle cells and pericytes, diffuse amyloid plaques, and neurofibrillary tangles [45]. Nasal respiratory and olfactory epithelium were clearly found to be early pollutant targets, as evidenced by the significant apurinic/apyrimidinic (AP) sites in MCMA dogs versus controls [46]. Moreover, olfactory bulb and hippocampal AP sites were also significantly higher in MCMA animals and nickel (Ni) and vanadium (V) were present in a gradient from olfactory mucosa > olfactory bulb > frontal cortex [46]. Striking findings in our canine studies included the presence of diffuse amyloid plaques in 11-month-old dogs and the presence of oil combustion PM-associated metals Ni and V in brain target areas. The dog studies are critical as they showed Alzheimer pathology beginning early in life with air pollutants playing a crucial role. Healthy young dogs exhibit a striking acceleration of Alzheimer's pathology when they live in a highly polluted place. It is well known that dogs are a good aging model and AD-type pathology and cognitive deficits are seen in older animals [47–49].

3.1. Neuroinflammation and Vascular Damage in MCMA Children and Young Adults. A very critical component of air

pollution exposure is neuroinflammation [8, 50–52]. MCMA young urbanites exhibit an important frontal imbalance in genes essential for inflammation, innate and adaptive immune responses, oxidative stress, cell proliferation and apoptosis, when compared to age-matched residents in low pollution cities [30]. Measurements of mRNA cyclooxygenase-2, interleukin-1beta, and CD14 in target brain regions from 12 controls and 35 MC residents aged 25.1 ± 1.5 years showed upregulation of cyclooxygenase-2, IL-1β, and CD14 in supra, and infratentorial regions and cranial nerves including: olfactory bulb, frontal cortex, substantia nigrae, and the vagus nerve [35].

The entry of activated lymphocytes, mast cells, and macrophages into the brain parenchyma is a hallmark of chronic inflammatory processes [34, 53–56]. Clusters of mononuclear cells around blood vessels and activated microglia in the frontal and temporal cortex, subicular area, and the brain stem (Figure 3(a)) were present in all MCMA children and were extremely rare in control children [30, 35]. These mononuclear cells are positive for CD68, CD163, Iba-1 (Figure 3(a)), and HLA-DR (Figure 3(b)) [57]. Intact and degranulated mast cells identified by means of tryptase monoclonal antibodies are seen in perivascular locations in frontal (Figure 3(c)) and temporal cortices, as well in trigeminal ganglia, and in peripheral autonomic nerves innervating the lungs and hearts in MCMA subjects, whereas in the controls mast cells were rare and intact. Blood vessels exhibit vacuolated endothelial cells and marginal WBCs, both indicative of endothelial damage and activation (Figure 3(d)). While the presence of abundant lipofuscin in endothelial cells (Figure 3(e))—usually associated with aging and indicative of a highly oxidized and covalently cross-linked aggregate of proteins—is evidence of a dysfunctional lysosomal degradation not expected in children or young adults.

There was extensive vascular damage in the olfactory bulb and in the frontal cortex. In the prefrontal cortex, the vascular damage affects predominantly white matter (Figure 3(f)). The main vascular findings included thickened walls, abundant perivascular macrophages, and focal enlargement of the Virchow-Robin spaces (Figure 3(g)). Young dogs show similar lesions to children with significant endothelial cell hyperplasia markedly reducing the vessel lumen (Figure 3(h)). The extensive prefrontal vascular damage is accompanied by white matter focal damage that in some children is significant (Figure 3(i)). Extensive leaking of blood vessels involves supra and infratentorial regions (Figures 3(j) and 3(k)). Olfactory bulb arterioles also show marked focal thickening of the vessel walls, indicative of a chronic reparative process (Figure 3(l)).

Ultrafine particles are likely players in the endothelial cell activation and are found in various CNS regions, including the Olfactory bulb (Figure 3(m)). UFPM are also seen in erythrocytes with the formation of patterned discrete contact points between endothelial cells and RBCs in the CNS, trigeminal ganglia, and lung capillaries of highly exposed people [35].

3.2. Alzheimer's and Parkinson's Diseases Hallmarks. A growing body of epidemiologic and experimental data point to particulate matter components of air pollution as well as nanoparticles in the environment as risk factors for neurodegenerative diseases [51, 52, 58–63]. Indeed, exposure to different size and composition PM produce molecular hallmarks of neurodegeneration, including the production and deposit of misfolded protein aggregates (amyloid, alpha synuclein, hyperphosphorylated tau), oxidative stress, cell damage and death in susceptible neuronal populations [51, 52, 64–66]. Neuronal oxidative stress is prominent even in small MCMA children [35]. Extensive cytoplasmic accumulation of 8OHdG in key neuronal complexes (Figure 4(a)) correlates with oxidative stress and damage to DNA. Nitrotyrosine, a marker for inflammation and nitric oxide (NO) production, is also present in frontal neurons and infratentorial neuronal groups (Figure 4(b)). Nitrotyrosine positive inclusions are also seen in glial cells, microglia, and perivascular macrophages [35].

3.2.1. Cortical Neurodegeneration Hallmarks. In young MCMA residents, amyloid beta42 (Aβ42) frontal (Figure 4(c)), olfactory bulb, and/or hippocampal immunoreactivity was observed in 58.8% of Apolipoprotein E (APOE) 3/3 <25 y, and 100% of the APOE 4 subjects (Figure 4(d)), whereas α-synuclein was seen in 23.5% of <25 y subjects [29]. In a different MCMA cohort, aged 18.3 ± 6.9 years, 40% exhibited tau hyperphosphorylation with pretangle material (Figures 4(e) and 4(f)) and 51% had Aβ42 diffuse frontal plaques compared with 0% in controls [30]. Thus, diffuse amyloid plaques and pretangle hyperphosphorilated tau are common frontal findings in highly exposed children, while low pollution controls are negative.

3.2.2. Brainstem Neurodegeneration Hallmarks. Infratentorial involvement is also present in exposed children thus neuropathology is seen in the brainstems of children age 96.3 ± 8.5 months from highly polluted (n = 34) versus a low polluted city (n = 17) [67]. Figure 5(a) shows medial superior olivary neurons with strong oxidative stress as evidenced by their 8-hydroxyguanosine immunoreactivity. MC children have auditory and vestibular abnormal findings [67]. The pathology involves every level of the brainstem from the midbrain to the lower medulla. The substantia nigrae pars compacta displays IBA-1 microglia. The number of activated microglia also varies significantly between control and MCMA children (Figures 5(b) and 5(c)). Activated microglia are found throughout the brainstem in exposed children (Figures 5(c), 5(d), and 5(e)), along with reactive glial fibrillary acidic protein (GFAP) positive astrocytes, indicative of responsive glia to cell damage (Figure 5(f)). Accumulation of α-synuclein, activated microglia, extracellular neuromelanin, and pigment-laden macrophages are seen from the dorsal motor nucleus of the vagus level (Figure 5(g)) to the substantia nigrae midbrain sections (Figures 5(h) and 5(i)). There is a punctuated cytoplasmic accumulation of α-synuclein in affected neurons, while α-syn positive neurites are also seen in the neuropil.

3.2.3. Olfactory Bulb Neurodegeneration. The olfactory bulb pathology deserves special attention because large segments

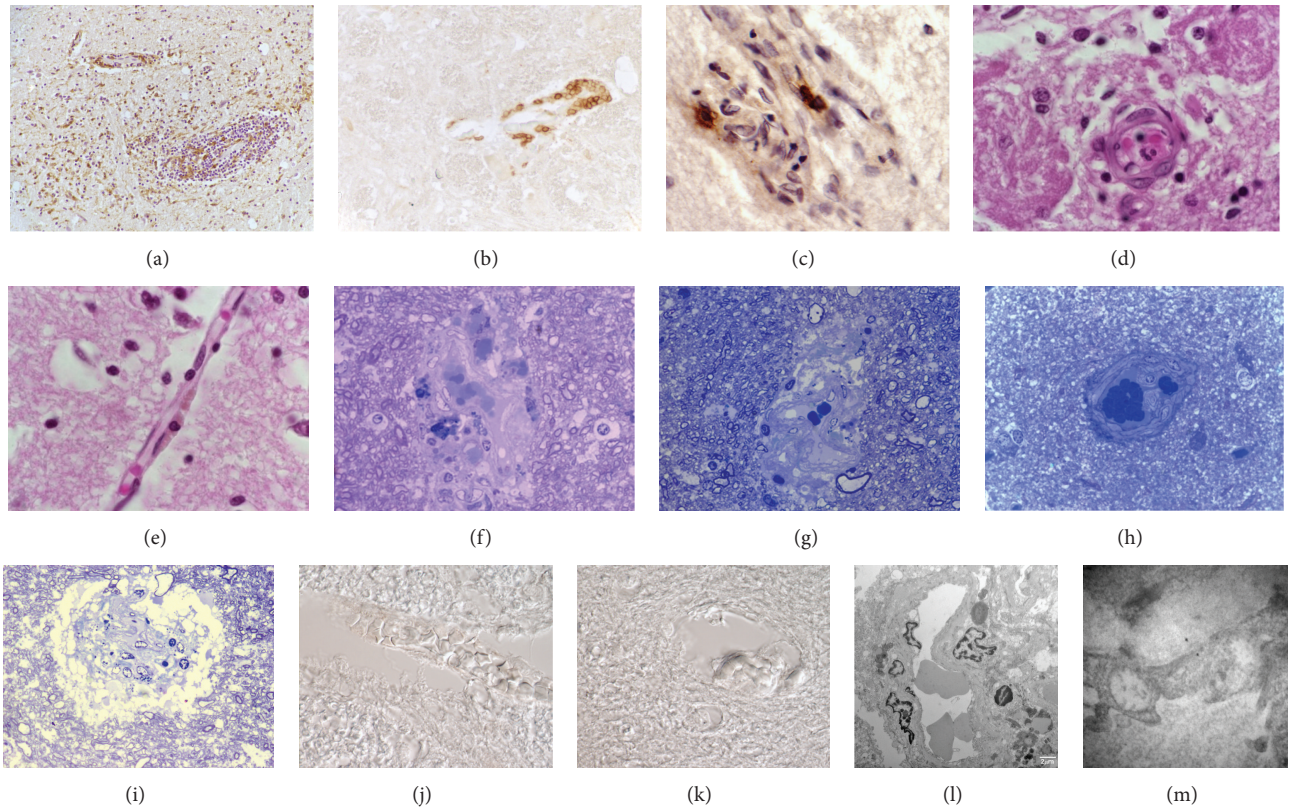

Figure 3: (a) Eleven year old MCMA girl with abundant ionized calcium binding adaptor molecule 1 (Iba-1)-positive microglia. Approximately 50% of the perivascular cells are Iba-1+ (Iba-1 antibody with DAB + brown product). (b) Eleven year old MCMA girl with brainstem perivascular accumulation of HLA-DR positive cells (HLA-DR antibody and DAB + brown product). (c) Frontal cortex in a MCMA 24 y old male with perivascular partially degranulated tryptase positive cells (Tryptase Ab with DAB + brown product). (d) Olfactory bulb blood vessel in a 14 year old MCMA boy. Notice a vacuolated endothelial cell and a polymorphonuclear leucocyte (PMN) attached to the vessel wall. Two glomeruli are adjacent to the damaged vessel. H&E. (e) Olfactory bulb blood vessel in a 14-year-old MCMA male APOE 3/3. Endothelial cells in the delicate vessel exhibit abundant lipofuscin, a highly oxidized and covalently cross-linked aggregate of proteins associated with aging. H&E. (f) Frontal cortex white matter from a MCMA 33 year old healthy subject with a cluster of blood vessels displaying perivascular numerous macrophages with lisosomal bodies and lipofuscin. The larger vessel displays abundant cell debris within the wall. One micron toluidine blue section. (g) Fourteen year old MCMA girl prefrontal white matter with an abnormal blood vessel displaying perivascular macrophages with lisosomal bodies and lipofuscin, abundant cell debri within the wall, apoptotic nuclei and focal enlargement of the Virchow-Robin space. One micron toluidine blue section. (h) Vascular lesions are also seen in young MCMA dogs. This 19 month dog exhibits a frontal white matter arteriole with hyperplastic endothelial cells partially reducing the lumen. One micron toluidine blue section. (i) The prefrontal cortex exhibits extensive vascular white matter damage, illustrated in this 13 y old MCMA girl. The arteriole shows extensive perivascular accumulation of macrophages with abundant lisosomal bodies. A striking enlargement of the Virchow-Robin space is seen with focal white matter damage. One micron toluidine blue section. (j) Seventeen year old MCMA teen brainstem blood vessel with extensive leaking expanding the Virchow-Robin space. (k) Same child as (j), the breakdown of the neurovascular unit also affects smaller blood vessels. (l) Electron micrograph of an olfactory bulb arteriole in a 17 y old MCMA boy. There is marked focal thickening of the vessel wall, numerous perivascular macrophages with lisosomal bodies and lipofuscin and vacuolization of endothelial cells. (m) Nanosized particles are seen in endothelial cells in many brain regions. This electron micrograph from a 17 y old MCMA male shows an arteriole in the olfactory bulb with two sharply defined particles in the endothelial cell cytoplasm and its basement membrane. The particles are 16 to 20 nanometers. EM ×50,000.

of the world population are exposed to a myriad of toxic substances on a daily basis that have the potential for harming the olfactory system and penetrating the brain via the olfactory epithelium (OE) [68–71]. Extreme instances of such exposures in the USA include the massive dust cloud following the September 11, 2001, terrorist attack in New York City, smoke and debris from wildfires, exposures to airborne herbicides and pesticides in farming communities, and pollutants from vehicle exhaust and manufacturing enterprises in major metropolitan areas. The issue is very important because olfactory dysfunction is among the earliest "preclinical" features of AD and PD, occurring in ~90% of early onset cases [72–76].

In MCMA residents, the severe pathological changes in the nasal respiratory epithelium go hand and hand with a marked decrease in olfactory neurons, significant changes in Bowman's glands, and pathologic Alzheimer and Parkinson's early stage changes within the olfactory bulbs (OBs) [77]. In one study comparing the OBs of 35 young MCMA residents versus 9 controls (20.8 ± 8.5 years) from a minimally

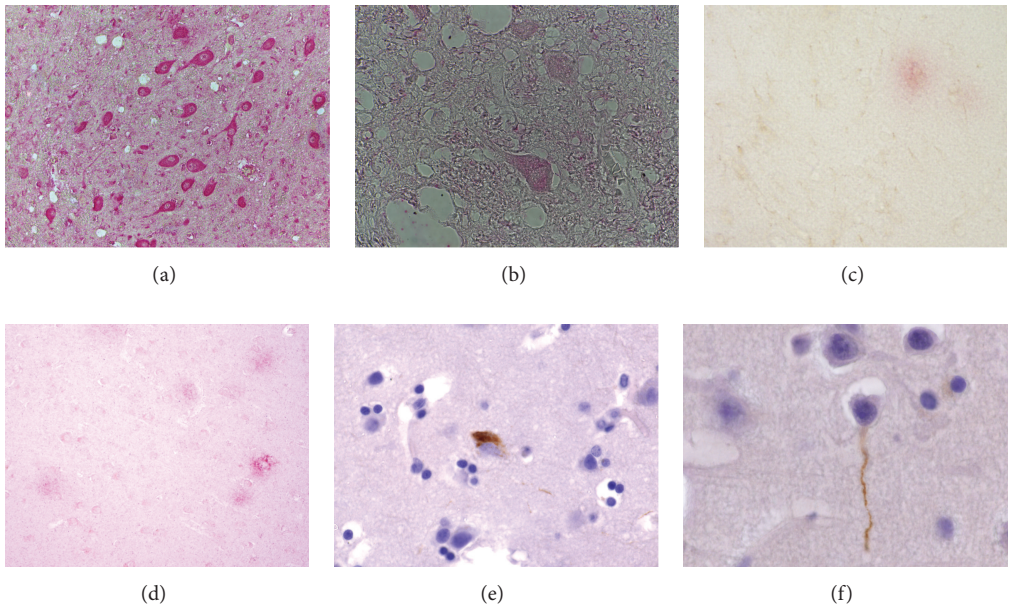

Figure 4: (a) Eleven year MCMA girl dorsal motor nucleus of the vagus stained with anti-8-OHdG showing immunohistochemical staining of oxidized nucleoside in neurons. 8-hydroxyguanosine is a modified base that occurs in DNA due to attack by hydroxyl radicals that are formed as byproducts and intermediates of aerobic metabolism and during oxidative stress. 8-OHdG immunohistochemistry red product. (b) Same 11 y old girl as in Figure 4(a) showing caudal pontine reticular nucleus neuronal protein oxidation marked by nitrotyrosine immunoreactivity. (c) Frontal cortex in an APOE 3/3 17 y old MCMA teen. A diffuse amyloid plaque (red product) is seen surrounded by glial cells negative for reactive astrocytes as detected by their reaction to the glial fibrillary acidic protein (GFAP). Dual immunohistochemistry for amyloid beta 1–42 and GFAP (DAB + brown product). (d) Frontal cortex in a 36 y old MCMA male APOE 3/4. This subject shows numerous diffuse and mature amyloid beta 1–42 plaques. (e) Frontal cortex in a 15 y old MCMA APOE 3/3 boy. Abnormal tau protein positive with the Tau 8 antibody (Innogenetics, Belgium), both in the neuronal body and in neuritis. (f) Frontal cortex in a 15 y old MCMA APOE 3/4 boy. A clear Tau 8 positive neurite is seen.

polluted city, the MC residents exhibited significant amounts of particles in OB glomerular neurons (Figure 6(a)), while reactive astrocytes were prominent in young children (Figure 6(b)). Immunoreactivity to alpha-synuclein, a hallmark of Parkinson's disease was present in OB neurons of MCMA teens and young adult (Figures 6(c), 6(d), and 6(e)) [77]. While neuronal accumulation of Aβ42 was present in young children regardless of APOE genotype (Figure 6(f)). The basic laminar OB organization of the glomerular, external plexiform, mitral cell, internal plexiform, and granular cell layers of the controls were generally intact (Figure 6(g)). In contrast, ill-defined and fragmented organization of the olfactory bulb layers, including small acellular glomeruli characterized MCMA youngsters (Figure 6(h)). The changes were extreme in APOE 4 carriers (Figures 6(i) and 6(j)). The early olfactory deficits appear to be associated with the aforementioned presence of beta amyloid, alpha synuclein, particulate matter in glomerular structures and the massive distortion of the OB organization.

3.3. The Role of the APOE Genotype in the Brain Effects of Air Pollution. The Apolipoprotein E (APOE) 4 polymorphism influences aging and age-related diseases including the risk for Alzheimer's disease [78–80]. The differential effects of ApoE isoforms on AD risk are given at least in part by the ability to affect Aβ aggregation and clearance in the brain, effects on synaptic plasticity, cell signaling, lipid transport and metabolism, and neuroinflammation [78]. APOE receptors influence both the CNS effects of APOE as well as Aβ metabolism and toxicity. The APOE 4 genotype (in contrast to APOE 3) is associated with oxidative stress and chronic inflammation [78]. In traumatic brain injury, APOE 4 carriers may be more predisposed to brain cellular damage as measured by S-100B and NSE concentrations [79]. APOE4 also influences plasma lipid concentrations, increases the risk of type 2 diabetes mellitus (particularly among obese subjects and smokers), conditions associated with high oxidative stress, neuroinflammation, and brain vascular damage [80]. In keeping with the current literature suggesting APOE 4 carriers have disadvantages in terms of brain repair, management of Aβ metabolism and toxicity and increased oxidative stress and chronic inflammation, we have shown MCMA APOE4 carriers have greater hyperphosphorylated tau and diffuse Aβ plaques versus E3 carriers ($Q = 7.82$, $P = 0.005$) [30]. This observation is important because based on our data, air pollution moderates the association between APOE genotype and neurodegenerative changes, that is, an APOE 4 carrier residing in a highly polluted environment will have an acceleration of neurodegenerative changes towards AD [35]. This information is critical when planning the neuroprotection of susceptible populations exposed to air pollutant components.

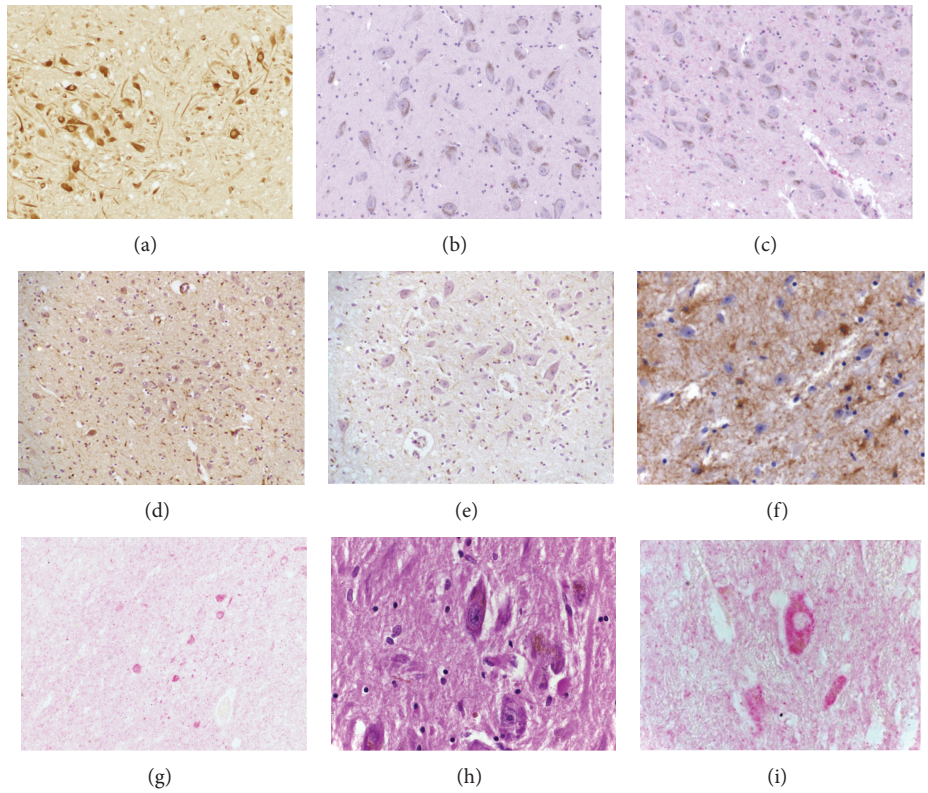

Figure 5: (a) Medial superior olive neurons from an 11 year old MCMA girl exhibit strong positivity for 8-hydroxyguanosine indicative of oxidative stress. 8-OHdG immunohistochemistry DAB brown product. (b) Substantia nigrae, pars compacta in a 17 y old Control teen. The section has been stained for the ionized calcium binding adaptor molecule 1 (IBA-1). There are very few positive cells. IBA-1 antibody with red product. (c) In contrast, this is the substantia nigrae, pars compacta in a 14 y old MCMA teen stained for IBA-1. Numerous positive cells are seen among the pigmented neurons and in perivascular locations. IBA-1 antibody with red product. (d) The same child has numerous positive IBA-1 activated microglia in her vestibular nuclei. IBA-1 antibody with brown product. (e) Same child as previous picture. Positive IBA-1 activated microglia in her dorsal motor nucleus of the vagus. IBA-1 antibody with brown product. (f) Reactive astrocytes are part of the response of glial cells to cell damage. Reactive astrocytes positive for GFAP surround the dorsal motor nucleus of the vagus neurons in this MCMA teen. GFAP with DAB brown product. (f) The dorsal motor nucleus of the vagus displays positive α synuclein neurons in the same child as 5F. α-Synuclein with red product. (h) The substantia nigrae is an early target in highly exposed teens. In this 11 y old girl there are partially degranulated pigmented neurons with a few macrophages containing the pigmented granules. An elongated microglia-like cell contains such brown granules in the vicinity of a neuronal shadow. H&E. (i) Substantia nigrae pigmented neuron is positive for alpha-synuclein in this 14 y old MCMA girl. α-Synuclein with red product.

4. Compensatory Responses versus Neurotoxic and Neurodegenerative Changes. Friend or Foe?

In our pediatric studies, the early clinical olfactory deficits appear to be associated with the presence of misfolded proteins, reactive gliosis and vascular damage in the olfactory bulb and the frontal cortex [77]. There is no doubt the extensive olfactory bulb pathology likely affects OB proteins with critical functions [81]. Likewise, the prefrontal cortex differential regulation of key gene networks; that is, IL1, NFκB, TNF, IFN, and TLRs are likely players in the significant cognitive deficits observed in children with no risk factors for neurological or cognitive deficits, other than their residency in a highly polluted megacity [29, 32, 33, 77]. In the same stream of thought, the central delay in the brainstem auditory evoked potentials and the significant white matter volumetric changes described after 1-year followup of MCMA versus control children could be related to the accumulation of abnormal proteins in key neuronal groups and the significant neuroinflammation involving both gray and white matter [30, 35, 67].

In view of the cognitive, olfactory, auditory, vestibular, and volumetric white matter changes described in exposed children, a series of critical questions arise:

(1) What is the role of PM in the neuroinflammatory process described in highly exposed children?

(2) What is the relationship between clinical and electrophysiological changes and the described neuropathology?

(3) How to interpret the neuropathology hallmarks of AD and PD in a 10 year old child with no family history of neurological diseases?

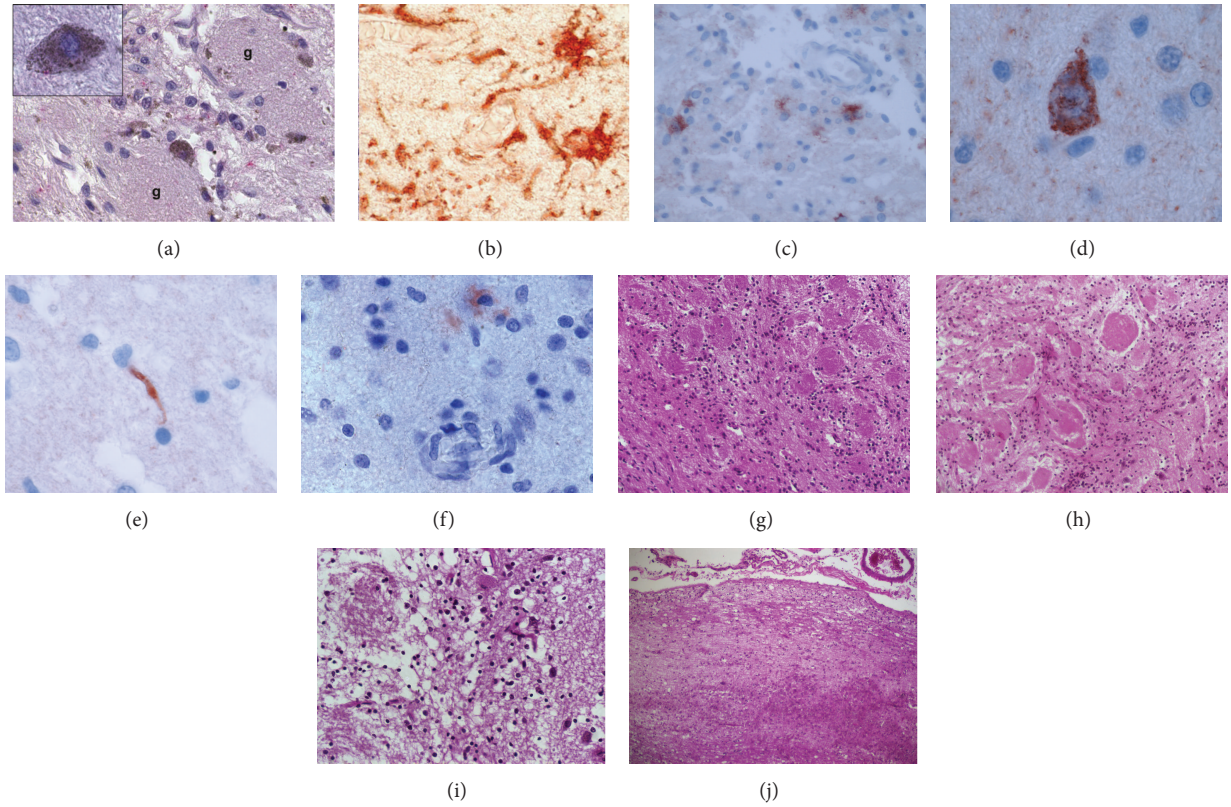

Figure 6: (a) Fourteen year old MCMA boy with abundant particulate material in neurons in the glomerular region. The insert shows a close-up of one such neuron with abundant particles and positive red cytoplasmic stain for Aβ42. Aβ42 immunohistochemistry and hematoxilin counterstain. (b) Reactive astrocytes are seen in the olfactory bulbs of MC children and teens. This is a 14 y old MCMA boy with reactive olfactory bulb astrocytes strongly staining for GFAP. GFAP immunohistochemistry with red product. (c) Olfactory bulb in an 11 y old MCMA boy APOE 3/3. Numerous neurons display positive cytoplasmic granular staining. α-Synuclein with red product. (d) A close-up of an olfactory bulb neuron with abundant α-Synuclein. (e) A close-up of a Lewy neurite is seen. α-Synuclein with red product. (f) Eleven year old MCMA male with β-amyloid 1–42 in olfactory bulb neurons. Aβ42 immunohistochemistry and hematoxilin counterstain. (g) This is the olfactory bulb of a control 20 year old male from a low polluted city. The glomerular structures are organized and exhibit normal cellular components. H&E. (h) In contrast, this is the olfactory bulb of an 11 year old MC boy APOE 3/3 with abnormal, loose and low cellular glomeruli. H&E. (i) Even more striking changes are seen in this 32 y old MC APOE 4/4 female. There are no remaining normal glomeruli, the few structures remaining are ill-defined with very few cells o no cells at all. It is expected this individual had significant olfactory deficits. H&E. (j) Same case as (i). The olfactory bulb shows extensive premature accumulation of corporae amylacea: glycoproteinaceous inclusions in astrocytic processes associated with astrocytic injury and gliosis. Premature accumulation of corpora amylacea plays an important role in the sequestration of toxic cellular metabolites. H&E.

Let us begin with the issue of particulate matter: Mexico City residents have been chronically exposed to concentrations of particulate matter above the USA standards for the last 26 years [1, 12, 13, 16]. A considerable fraction of the $PM_{2.5}$ consists of organic compounds including biologic components from bacteria and fungi, and transition metals with neurotoxic properties [17–19]. Environmental endotoxins—from open field waste areas, waste water treatment plants, open sewer channels, and daily outdoor deposits of 500 metric tons of animal and human fecal material—are an important part of the organic portion of $PM_{2.5}$.

Why is PM important for MCMA children? Because fine and ultrafine particles reach their brain by uptake through olfactory neurons and cranial nerves, trafficking of macrophage-like cells loaded with PM from the lung capillary bed to the systemic circulation, and by a direct transfer of ultrafine particles from the systemic circulation and/or red blood cells to brain endothelial cells [30, 35]. Our data and those of others suggest that exposure to PM can activate pathogen sensors, and that signaling by ROS can drive inflammatory processes [82–86]. Asbestos and silica activate the NALP 3 inflammasome and NALP3 deficient mice have a significant reduction of their lung inflammatory responses [41]. The innate immune system rapidly detects invading pathogenic microbes and eliminates them. We have shown an upregulation of 27/84 frontal inflammasome associated genes, including NOD-like receptors and proinflammatory caspases [30], so it is biologically plausible that PM with lipopolysaccharides (PM-LPS) initiates an inflammatory brain response. Toll-like receptors sense "extracellular microbes" (e.g., PM-LPS) and trigger anti-pathogen signaling cascades [84]. Both LPS responses and systemic inflammation are important for the understanding of how the sensing of "*microbial invaders*" could translate into signaling pathways that culminate in

the transcriptional regulation of immune responsive genes and how the activation of inflammasomes [84] could be a contributing factor for CNS inflammatory responses. The inflammasome activation results in caspase 1 activation leading to processing and secretion of proinflammatory cytokines like IL1β to engage innate immune defenses [86]. Indeed, this pathway is clearly active in MCMA children: the activation of inflammasomes turns on the protease caspase-1. Caspase-1 cleaves prointerleukin-1β into an active form. We have repeatedly shown IL-1β in frontal cortex, olfactory bulb, hippocampus, and the dorsal vagal complex is upregulated in highly exposed children, dogs and mice compared to low pollution controls [30, 35, 87]. There is a clear need for better understanding of the role of inflammasome activation in urban children's brains and the defense against *pathogens* that do not really exist (only components of them, e.g., PM-LPS), and neuroinflammation. This is of particular importance as neuroprotective strategies are being explored.

The relationship between clinical and electrophysiological changes and the described neuropathology is of deep interest to pediatricians working in polluted urban centers. We mentioned olfaction deficits and abnormal UPSIT (University of Pennsylvania Smell Identification Test) scores present in 35.5% of the MCMA teens versus 12% of age matched controls [77]. Moreover, highly exposed APOE 4 carriers failed 2.4 ± 0.54 of the 10 UPSIT items identified in one study as being most strongly related to AD [88], while APOE 2/3 and 3/3 subjects failed only 1.36 ± 0.16 such items ($P = 0.01$). The olfactory bulb neuropathology associated with urban exposures is very similar to the one described in early stages of AD and PD [89–96].

The central delayed brainstem auditory evoked potentials (BAEPs), auditory impairment and vestibular dysfunction could relate to the extensive brainstem inflammation with accumulation of β amyloid and alpha synuclein in key olfactory nuclei [67]. Neurodegenerative changes in the dorsal motor nucleus of the vagus, the nucleus of the solitary tract, arcuate nucleus, raphe midline, and extra-raphe medial and lateral tegmental neurons [67] are similar to the PD stages I and II of Braak et al. [90, 91, 96].

It is difficult to establish the association between cognitive deficits, frontal tau hyperphosphorylation, and amyloid-β diffuse plaques in the absence of cognitive and brain MRI data in the demised children. However, we have shown a strong relationship between residency, brain structural changes and cognitive deficits [32]. MCMA children with WMH (+) are responding to the air pollution exposures with white and grey matter volume increases in temporal, parietal, and frontal regions and better cognitive performance compared to WMH negative children [32]. WMH in elderly people are associated with clinical symptoms related to disruption of fiber tracts, cognitive impairment risk, cerebral ischemia, neurodegeneration, cardiovascular, and metabolic diseases [97–106]. WMH partially identify underlying white matter pathology and may be associated with widespread white matter changes, the novel concept of white matter hyperintensities penumbra [107]. Disruption of fiber tracts in the developing brain could result in cortical cholinergic and monoaminergic deafferentation and impact attention, emotion and goal-directed behavior [99]. The characterization of WMH in young urbanites is critical and knowledge about the complex modulation of cytokines and chemokines in the setting of air pollution are important because they may shed light into the etiopathogenesis of well-characterized risk factors for neurodegeneration, vascular, and cognitive disorders and disability [106, 107].

A difficult question to answer is how to interpret the early neuropathology hallmarks of Alzheimer's and Parkinson's diseases in children with no family history of neurological diseases.

In the Alzheimer's brain, tau is abnormally hyperphosphorylated and it is aggregated into paired helical filaments forming neurofibrillary tangles, a histopathological hallmark of the disease [108]. Tau phosphorylation could be protective (e.g., hibernation) or toxic (e.g., hyperphosphorylation and aggregation of tau) [109]. Hyperphosphorylated tau in epitopes characteristic of AD has been identified by immunohistochemistry in 62.5% of APOE 4 and 33% of APOE 3 young MCMA carriers [30].

Is tau phosphorylation in children detrimental or protective in the setting of severe air pollution? [109–114]. The aggregation of HP tau species has been proposed to represent a compensatory neuronal response against oxidative stress and to serve at least initially as a protector against cell death [111, 113]. The tau protective or toxic function could be related to different conformational molecular changes [109]. The formation of tangles is a quick process as it was demonstrated by De Calignon et al. [112] using *in vivo* multiphoton imaging in living tau transgenic mice. Caspase activation precedes tangle formation by hours to days, tangles form quickly but persist apparently indefinitely, thus cleavage of tau is enough to cause misfolding of tau followed by nucleation and recruitment of additional tau molecules to the neuronal cell body. Is our description of HPτ in MCMA children's brains an isolated observation in the literature? The answer is no, Braak and Del Tredeci [93] examined 42 young brains (4–29 years) with a wide range of pathologies described pretangle HPτ using AT8 in 38/42 cases with no extracellular amyloid β protein deposition or neuritic plaques with the 4G8 antibody. Although these subjects were not healthy, there was no APOE genotyping or a recorded history of environmental exposures, we fully agree with Braak and Del Tredeci [93] that these findings may indicate Alzheimer's disease-related pathological process leading to neurofibrillary tangle formation start quite early, before puberty or in early young adulthood.

There are very few arguments about the role of abnormal tau hyperphosphorylation in AD, related tauopathies and under experimental conditions [108, 109, 114–118]. A subject to be explored in air pollution animal models ought to be the characterization of the HPτ and if indeed represents a compensatory neuronal response against oxidative stress. At this time, however, we are of the opinion that given the factors (chronic oxidative stress, neuroinflammation, presence of nanosize particles in critical brain units and anatomical regions) potentially accounting for the aggregation of tau, tau phosphorylation could represent an early sensor of oxidative stress with all the subsequent detrimental effects if the exposure persist.

Likewise, Aβ42 is capable of aggregation and misfolding leading to progressive neurodegeneration that develops insidiously over a lifetime. A key issue has to be addressed in this scenario: APOE4 carriers not only have HPτ, but also exhibit significant numbers of Aβ 6E10 diffuse plaques (P = 0.005) in comparison to APOE 3 carriers. Recent work by Cerf et al. [119] suggests that APOE4 strongly stabilizes Aβ oligomers, the pathological species responsible for AD; thus we suggest APOE4 carriers are potentially at a higher risk of developing AD if residing in a highly polluted environment. This information is critical given that ~18% of the MCMA population carries an APOE 4 allele [30].

Alpha-synuclein aggregation is associated to the pathogenesis of Parkinson's disease and exposure to a myriad of environmental agents, including agrochemicals increases the PD risk [120, 121]. Mitochondrial dysfunction and oxidative stress constitute key PD pathogenic events. Alpha-synuclein prevents cytochrome c release and apoptosis through inhibition of the MAPK signaling pathway, suggesting that endogenous concentrations of α-synuclein confer resistance to oxidative stress downstream of free radical production and scavenging [122]. Recent evidence also suggests misfolded α-synuclein directly activates microglia inducing the production and release of the proinflammatory cytokine, TNF-α, and increasing antioxidant enzyme expression [123]. Béraud et al. emphasized the importance of protein misfolding, oxidative stress, and inflammation in PD as a potential locus for the development of novel therapeutics focused on induction of the Nrf2-directed antioxidant pathway and inhibition of protein misfolding [123].

It is important to note that α-synuclein in MCMA children is present in key regions associated with PD pathology including olfactory bulb, the midbrain, and the lower sections of the brainstem, for example, the medulla oblongata [67, 77]. MCMA teens exhibit already olfactory disturbances [77] and autonomic dysfunction (syncope in MCMA children personal communication of Dr. Maricela Franco-Lira), the latter severe enough to require pediatric care. The issue of MCMA children already showing symptoms seen in the premotor stages of PD has to be well thoughtout [73, 74] given the neurodegenerative process begins earlier in the olfactory bulb and lower brain stem and the fact there is a delay of several decades between the onset of dopaminergic denervation and the appearance of motor signs [96]. There is no question olfactory dysfunction is an early "preclinical" sign of Parkinson's disease [73, 74]. Damage to cholinergic, serotonergic, and noradrenergic components of the olfactory pathway likely involved to explain the olfactory dysfunction [73, 74]. The presence of up-regulated inflammatory cytokines, α-synuclein- and HPπ-related olfactory bulb pathology in young highly exposed children is an ominous sign possibly associated with a number of other nonmotor symptoms related to PD, such as dysautonomia and sleep disturbances. Epidemiological studies addressing nonmotor PD symptoms in highly exposed young urbanites are warranted.

4.1. Looking Forward and Limitations. Despite controversy regarding the mechanistic pathways involved in the CNS damage associated with exposure to air pollutants, specifically fine and ultrafine particles of diverse origin, animal models and tissue culture studies have greatly improved our understanding of the mechanistic processes [39, 41, 42, 48–52, 58–66, 69–71]. We are looking forward to bridging the gap between early neuroinflammation and neurodegeneration observed in childhood and early adulthood and experimental air pollution animal models. There is a strong need for collaborations between those who investigate humans and those who study experimental animal models to derive therapies that may be neuroprotective. There is also a need for looking into the neuropathology in diverse populations residing in megacities across the globe and sharing the results of the investigations. This is critical since the responses to air pollutants depend not only on the components of air pollution and concentrations, but also on the genetic background of the exposed populations and on a large list of environmental factors including dietary risk factors, obesity, alcohol intake, and lifelong experiences for example, educational and occupational attainment [124]. Our results are potentially limited by the characteristics of the air pollutants in MCMA and the populations we are studying, namely ethnic groups with a complex admixture of ancestral populations as seen with Mexican mestizos. Nevertheless, the significant differences in clinical and neuropathology findings between high and low pollution exposed subjects warrants extensive investigations in exposed populations from countries around the world.

5. Summary

MCMA children experience a chronic, intense state of oxidative stress resulting from lifelong exposures to a severely polluted environment. Children exhibit an early brain imbalance in genes involved in oxidative stress, inflammation, innate and adaptive immune responses, cell proliferation and apoptosis. Neuroinflammation, endothelial activation, endothelial cell hyperplasia, the attachment of white blood cells to the endothelial damaged walls with the reduction of the lumen vessel, high blood concentrations of endothelin-1, and the breakdown of the BBB clearly contribute to cognitive impairment and pathogenesis and pathophysiology of neurodegenerative states [125, 126]. Environmental and genetic factors play a key role in their CNS responses as evidenced by the acceleration of neurodegenerative AD pathology in children carrying an APOE 4 allele.

The neuronal accumulation of misfolded proteins in exposed children coincides with the anatomical distribution observed in the early stages of both AD and PD with early clinical evidence of olfactory and cognitive deficits, brain volumetric changes, white matter hyperintense lesions, altered brainstem evoked auditory potentials and autonomic disbalance. There is a complex modulation of cytokines and chemokines influencing structural and volumetric brain responses and cognitive deficits.

We contend that misfolding of critical proteins could be a defensive early response to the sustained systemic and CNS inflammation. However, the sustained oxidative stress associated with dysregulated inflammation, both systemic

and in the CNS contribute to the establishment of neurodegenerative processes with clinical early counterparts. We strongly support the contention that the nasal (olfactory and trigeminal), cardiorespiratory and gastrointestinal (vagus) pathways-along with the systemic direct transport of particles to the brain and the dysregulated systemic inflammation are critical in explaining the brain pathology in highly exposed MCMA children. Moreover, these children are at risk of developing Alzheimer's and Parkinson's diseases as adults.

We have a 50-year window of opportunity between the early brain changes observed in children and the time when the patient with mild cognitive impairment or dementia will show up at the neurologist's door. Facing the current pediatric clinical and pathology evidence is imperative if we are aiming our efforts to identify and mitigate environmental factors that influence AD and PD pathogenesis.

One thing is clear: early implementation of neuroprotective measures to ameliorate or stop the inflammatory and neurodegenerative processes in children is warranted [43, 87]. Identification of biomarkers associating systemic inflammation to brain growth is also critical for detecting children at higher risk for cognitive deficits and neurodegeneration.

It is important to remember there is a severe and woeful deficit of progress in the development of both AD and PD-modifying therapy [127, 128]. Since fine and ultrafine PM likely play a key role in the development of neuroinflammation and neurodegeneration, it is very noteworthy that in the US alone, as of December 2012, more than 74 million people are being exposed to concentrations of $PM_{2.5}$ above the 2006 standards ($PM_{2.5}$ annual standard of 15 $\mu g/m^3$) [129]. An appeal to research supporting institutions may be made to strongly invest in defining the CNS pathology associated with exposure to air pollutants in children and young adults and as Castellani and Perry suggested, consider a systems biology approach and an early preventive pathway [128].

Epidemiological, cognitive, and mechanistic studies into the association between air pollution exposures and the development of CNS damage in children are of pressing importance for public health and quality of life.

Acknowledgments

This work was supported in part by ITHS UL1RR025014, P20RR015583 and Canada-Latin America and the Caribbean Research Exchange Grants Program (LACREG 2011).

References

[1] L. T. Molina and M. J. Molina, "Improving air quality in megacities: Mexico City case study," *Annals of the New York Academy of Sciences*, vol. 1023, pp. 142–158, 2004.

[2] B. Chen and H. Kan, "Air pollution and population health: a global challenge," *Environmental Health and Preventive Medicine*, vol. 13, no. 2, pp. 94–101, 2008.

[3] D. D. Parrish and T. Zhu, "Clean air for megacities," *Science*, vol. 326, no. 5953, pp. 674–675, 2009.

[4] D. E. Bloom, "7 Billion and counting," *Science*, vol. 333, no. 6042, pp. 562–569, 2011.

[5] R. Rodrigues, M. A. Smith, X. Wang et al., "Molecular neuropathogenesis of Alzheimer's disease: an interaction model stressing the central role of oxidative stress," *Future Neurology*, vol. 7, pp. 287–305, 2012.

[6] A. Nunomura, P. I. Moreira, R. J. Castellani et al., "Oxidative damage to RNA in aging and neurodegenerative disorders," *Neurotoxicity Research*, vol. 22, pp. 231–248, 2012.

[7] E. C. Hirsch, P. Jenner, and S. Przedborski, "Pathogenesis of Parkinson's disease," *Movement Disorders*. In press.

[8] M. L. Block and L. Calderón-Garcidueñas, "Air pollution: mechanisms of neuroinflammation and CNS disease," *Trends in Neurosciences*, vol. 32, no. 9, pp. 506–516, 2009.

[9] G. Oberdörster, A. Elder, and A. Rinderknecht, "Nanoparticles and the brain: cause for concern?" *Journal of Nanoscience and Nanotechnology*, vol. 9, no. 8, pp. 4996–5007, 2009.

[10] R. D. Brook, S. Rajagopalan, C. A. Pope III et al., "American Heart Association Council on Epidemiology and Prevention, Council on the Kidney in Cardiovascular Disease, and Council on Nutrition, Physical Activity and Metabolism. Particulate matter air pollution and cardiovascular disease: an update to the scientific statement from the American Heart Association," *Circulation*, vol. 121, pp. 2331–2378, 2010.

[11] T. Kampfrath, A. Maiseyeu, Z. Ying et al., "Chronic fine particulate matter exposure induces systemic vascular dysfunction via NADPH oxidase and TLR4 pathways," *Circulation Research*, vol. 108, no. 6, pp. 716–726, 2011.

[12] L. T. Molina, C. E. Kolb, B. de Foy et al., "Air quality in North America's most populous city—overview of the MCMA-2003 campaign," *Atmospheric Chemistry and Physics*, vol. 7, no. 10, pp. 2447–2473, 2007.

[13] L. T. Molina, S. Madronich, J. S. Gaffney et al., "An overview of the MILAGRO 2006 Campaign: Mexico City emissions and their transport and transformation," *Atmospheric Chemistry and Physics*, vol. 10, no. 18, pp. 8697–8760, 2010.

[14] J. Evans, J. Levy, J. Hammitt et al., "Health benefits of air pollution control," in *Air Quality in the Mexico Megacity: An Integrated Assessment*, L. T. Molina and M. J. Molina, Eds., pp. 103–136, Kluwer Academic Publishers, 2002.

[15] E. Ezcurra and M. Mazari-Hiriart, "Are megacities viable? A cautionary tale from Mexico City," *Environment*, vol. 38, no. 1, pp. 6–15, 1996.

[16] H. Bravo-Alvarez and R. Torres-Jard*a*n, "Air pollution levels and trends in the México City metropolitan area," in *Urban Air Pollution and Forest: Resources at Risk in the Mexico City Air Basin*, M. Fenn, L. de Bauer, and T. Hernández, Eds., vol. 156 of *Ecological Studies*, chapter 6, pp. 121–159, Springer, New York, NY, USA, 2002.

[17] A. R. Osornio-Vargas, J. C. Bonner, E. Alfaro-Moreno et al., "Proinflammatory and cytotoxic effects of Mexico City air pollution particulate matter in vtro are dependent on particle size and composition," *Environmental Health Perspectives*, vol. 111, no. 10, pp. 1289–1293, 2003.

[18] I. Rosas Pérez, J. Serrano, E. Alfaro-Moreno et al., "Relations between PM_{10} composition and cell toxicity: a multivariate and graphical approach," *Chemosphere*, vol. 67, no. 6, pp. 1218–1228, 2007.

[19] X. Querol, J. Pey, M. C. Minguill*a*n et al., "PM speciation and sources in Mexico during the MILAGRO-2006 Campaign," *Atmospheric Chemistry and Physics*, vol. 8, pp. 111–128, 2008.

[20] SMA-GDF (Secretaria del Medio Ambiente del Gobierno del Distrito Federal), "Sistema de Monitoreo Atmosférico. Secretaría del Medio Ambiente," http://www.calidadaire.df.gob.mx/calidadaire/index.php.

[21] T. Tang, Hurraß, R. Gminski, and V. Mersch-Sundermann, "Fine and ultrafine particles emitted from laser printers as indoor air contaminants in German offices," *Environmental Science and Pollution Research*, vol. 19, no. 9, pp. 3840–3849, 2012.

[22] E. Fröhlich and E. Roblegg, "Models for oral uptake of nanoparticles in consumer products," *Toxicology*, vol. 291, no. 1–3, pp. 10–17, 2012.

[23] R. W. Atkinson, I. M. Carey, A. J. Kent, T. P. van Staa, H. R. Anderson, and D. G. Cook, "Long-term exposure to outdoor air pollution and incidence of cardiovascular disease," *Epidemiology*, vol. 24, pp. 44–53, 2013.

[24] Z. F. Zhang, S. Z. Yu, and G. D. Zhou, "Indoor air pollution of coal fumes as a risk factor of stroke, Shanghai," *American Journal of Public Health*, vol. 78, no. 8, pp. 975–977, 1988.

[25] P. J. Villeneuve, J. Y. Johnson, D. Pasichnvk, J. Lowes, S. Kirkland, and B. H. Rowe, "Short-term effects of ambient air pollution on stroke: who is most vulnerable?" *Science of the Total Environment*, vol. 430, pp. 193–201, 2012.

[26] L. Calderón-Garcidueñas, R. Vincent, A. Mora-Tiscareño et al., "Elevated plasma endothelin-1 and pulmonary arterial pressure in children exposed to air pollution," *Environmental Health Perspectives*, vol. 115, pp. 1248–1253, 2007.

[27] L. Calderón-Garcidueñas, A. Mora-Tiscareño, L. A. Fordham et al., "Respiratory damage in children exposed to urban pollution," *Pediatric Pulmonology*, vol. 36, no. 2, pp. 148–161, 2003.

[28] L. Calderón-Garcidueñas, M. Macias-Parra, H. J. Hoffmann et al., "Immunotoxicity and environment: immunodysregulation and systemic inflammation in children," *Toxicologic Pathology*, vol. 37, pp. 161–169, 2009.

[29] L. Calderón-Garcidueñas, A. Mora-Tiscareño, E. Ontiveros et al., "Air pollution, cognitive deficits and brain abnormalities: a pilot study with children and dogs," *Brain and Cognition*, vol. 68, pp. 117–127, 2008.

[30] L. Calderón-Garcidueñas, M. Kavanaugh, M. L. Block et al., "Neuroinflammation, hyperphosphorilated tau, diffuse amyloid plaques and down- regulation of the cellular prion protein in air pollution exposed children and adults," *Journal of Alzheimer Disease*, vol. 28, pp. 93–107, 2012.

[31] L. Calderón-Garcidueñas, A. Serrano-Sierra, R. Torres-Jardón et al., "The impact of environmental metals in young urbanites' brains," *Experimental and Toxicologic Pathology*. In press.

[32] L. Calderón-Garcidueñas, A. Mora-Tiscareón, M. Styner et al., "White matter hyperintensities, systemic inflammation, brain growth and cognitive functions in children exposed to air pollution," *Journal of Alzheimer's Disease*, vol. 31, no. 1, pp. 183–191, 2012.

[33] L. Calderón-Garcidueñas and R. Torres-Jardón, "Air pollution, socioeconomic status and children's cognition in megacities: the Mexico City Scenario," *Frontiers in Psychology*, vol. 3, article 217, 2012.

[34] S. Rivest, S. Lacroix, L. Vallières, S. Nadeau, J. Zhang, and N. Laflamme, "How the blood talks to the brain parenchyma and the paraventricular nucleus of the hypothalamus during systemic inflammatory and infectious stimuli," *Proceedings of the Society for Experimental Biology and Medicine*, vol. 223, no. 1, pp. 22–38, 2000.

[35] L. Calderón-Garcidueñas, A. C. Solt, C. Henríquez-Roldán et al., "Long-term air pollution exposure is associated with neuroinflammation, an altered innate immune response, disruption of the blood-brain barrier, ultrafine particulate deposition, and accumulation of amyloid β-42 and α-synuclein in children and young adults," *Toxicologic Pathology*, vol. 36, no. 2, pp. 289–310, 2008.

[36] N. R. Saunders, S. A. Liddelow, and K. M. Dziegielewska, "Barrier mechanisms in the developing brain," *Frontiers in Psychology*, vol. 3, article 46, 2012.

[37] D. Heumann and T. Roger, "Initial responses to endotoxins and Gram-negative bacteria," *Clinica Chimica Acta*, vol. 323, no. 1-2, pp. 59–72, 2002.

[38] J. C. Bonner, A. B. Rice, P. M. Lindroos et al., "Induction of the lung myofibroblast PDGF receptor system by urban ambient particles from Mexico City," *American Journal of Respiratory Cell and Molecular Biology*, vol. 19, no. 4, pp. 672–680, 1998.

[39] E. J. Yang, S. Kim, J. S. Kim, and J. H. Choi, "Inflammasome formation and IL1β release by human blood monocytes in response to silver nanoparticles," *Biomaterials*, vol. 33, pp. 6858–6867, 2012.

[40] G. Guarda, C. Dostert, F. Staehli et al., "T cells dampen innate immune responses through inhibition of NLRP1 and NLRP3 inflammasomes," *Nature*, vol. 460, no. 7252, pp. 269–273, 2009.

[41] C. Dostert, V. Pétrilli, R. van Bruggen, C. Steele, B. T. Mossman, and J. Tschopp, "Innate immune activation through Nalp3 inflammasome sensing of asbestos and silica," *Science*, vol. 320, no. 5876, pp. 674–677, 2008.

[42] M. Morris and L. Li, "Molecular mechanisms and pathological consequences of endotoxin tolerance and priming," *Archivum Immunologiae Et Therapiae Experimentalis*, vol. 60, pp. 13–18, 2012.

[43] R. Villarreal-Calderón, G. Dale, R. Delgado-Chavez et al., "Intra-city differences in cardiac expression of inflammatory genes and inflammasomes in young urbanites: a pilot study," *Journal of Toxicologic Pathology*, vol. 25, pp. 163–173, 2012.

[44] L. Calderón-Garcidueñas, R. Engle, A. Mora-Tiscareño et al., "Exposure to severe urban pollution influences cognitive outcomes, brain volume and systemic inflammation in clinically healthy children," *Brain Cognition*, vol. 77, pp. 345–355, 2011.

[45] L. Calderón-Garcidueñas, B. Azzarelli, H. Acuña et al., "Air pollution and brain damage," *Toxicologic Pathology*, vol. 30, pp. 373–389, 2002.

[46] L. Calderón-Garcidueñas, R. R. Maronpot, R. Torres-Jardon, C. Henríquez-Roldán, R. Schoonhoven, and H. Acuña-Ayala, "DNA damage in nasal and brain tissues of canines exposed to air pollutants is associated with evidence of chronic brain inflammation and neurodegeneration," *Toxicologic Pathology*, vol. 31, pp. 524–538, 2003.

[47] J. K. Chambers, M. Mutsuga, K. Uchida, and H. Nakayama, "Characterization of AβpN3 deposition in the brains of dogs of various ages and other animal species," *Amyloid*, vol. 18, no. 2, pp. 63–71, 2011.

[48] C. H. Yu, G. S. Song, J. Y. Yhee et al., "Histopathological and immunohistochemical comparison of the brain of human patients with Alzheimer's disease and the brain of aged dogs with cognitive dysfunction," *Journal of Comparative Pathology*, vol. 145, no. 1, pp. 45–58, 2011.

[49] C. W. Cotman and E. Head, "The canine (dog) model of human aging and disease: dietary, environmental and immunotherapy approaches," *Journal of Alzheimer's Disease*, vol. 15, no. 4, pp. 685–707, 2008.

[50] A. Campbell, J. A. Araujo, H. Li, C. Sioutas, and M. Kleinman, "Particulate matter induced enhancement of inflammatory markers in the brains of apolipoprotein E knockout mice," *Journal of Nanoscience and Nanotechnology*, vol. 9, no. 8, pp. 5099–5104, 2009.

[51] S. Levesque, M. J. Surace, J. McDonald, and M. L. Block, "Air pollution and the brain: subchronic diesel exhaust exposure causes neuroinflammation and elevates early markers of neurodegenerative disease," *Journal of Neuroinflammation*, vol. 8, article 105, 2011.

[52] S. Levesque, T. Taetzsch, M. E. Lull et al., "Diesel exhaust activates and primes microglia: air pollution, neuroinflammation and regulation of dopaminergic neurotoxicity," *Environmental Health Perspectives*, vol. 119, pp. 1149–1155, 2011.

[53] S. Rivest, "Regulation of innate immune responses in the brain," *Nature Reviews Immunology*, vol. 9, no. 6, pp. 429–439, 2009.

[54] A. R. Simard and S. Rivest, "Role of inflammation in the neurobiology of stem cells," *NeuroReport*, vol. 15, no. 15, pp. 2305–2310, 2004.

[55] K. Fassbender, S. Walter, S. Kühl et al., "The LPS receptor (CD14) links innate immunity with Alzheimer's disease," *The FASEB Journal*, vol. 18, no. 1, pp. 203–205, 2004.

[56] M. D. Nguyen, J. P. Julien, and S. Rivest, "Innate immunity: the missing link in neuroprotection and neurodegeneration?" *Nature Reviews Neuroscience*, vol. 3, no. 3, pp. 216–227, 2002.

[57] W. K. Kim, X. Alvarez, J. Fisher et al., "CD163 identifies perivascular macrophages in normal and viral encephalitic brains and potential precursors to perivascular macrophages in blood," *American Journal of Pathology*, vol. 168, no. 3, pp. 822–834, 2006.

[58] J. Wu, C. Wang, J. Sun, and Y. Xue, "Neurotoxicity of silica nanoparticles: brain localization and dopaminergic neurons damage pathways," *ACS Nano*, vol. 5, no. 6, pp. 4476–4489, 2011.

[59] H. S. Sharma and A. Sharma, "Neurotoxicity of engineered nanoparticles from metals," *CNS & Neurological Disorders*, vol. 11, pp. 65–80, 2012.

[60] W. J. Trickler, S. M. Lantz, A. M. Schrand et al., "Effects of copper nanoparticles on rat cerebral microvessel endothelial cells," *Nanomedicine*, vol. 7, pp. 835–846, 2012.

[61] T. T. Win-Shwe and H. Fujimaki, "Nanoparticles and neurotoxicity," *International Journal of Molecular Sciences*, vol. 12, pp. 6267–6280, 2011.

[62] Y. S. Ho, X. Yang, S. C. Yeung et al., "Cigarette smoking accelerated brain aging and induced pre-Alzheimer-like neuropathology in rats," *PLoS One*, vol. 7, no. 5, Article ID e36752, 2012.

[63] R. G. Lucchini, D. C. Dorman, A. Elder, and B. Veronesi, "Neurological impacts from inhalation of pollutants and the nose-brain connection," *Neurotoxicology*, vol. 33, pp. 838–841, 2012.

[64] L. Qin, X. Wu, M. L. Block et al., "Systemic LPS causes chronic neuroinflammation and progressive neurodegeneration," *GLIA*, vol. 55, no. 5, pp. 453–462, 2007.

[65] A. M. S. Hartz, B. Bauer, M. L. Block, J. S. Hong, and D. S. Miller, "Diesel exhaust particles induce oxidative stress, proinflammatory signaling, and P-glycoprotein up-regulation at the blood-brain barrier," *The FASEB Journal*, vol. 22, no. 8, pp. 2723–2733, 2008.

[66] S. M. MohanKumar, A. Campbell, M. Block, and B. Veronesi, "Particulate matter, oxidative stress and neurotoxicity," *Neurotoxicology*, vol. 29, no. 3, pp. 479–488, 2008.

[67] L. Calderón-Garcidueñas, A. D'Angiulli, R. J. Kulesza et al., "Air pollution is associated with brainstem auditory nuclei pathology and delayed brainstem auditory evoked potentials," *International Journal of Developmental Neuroscience*, vol. 29, no. 4, pp. 365–375, 2011.

[68] H. Tjälve, J. Henriksson, J. Tallkvist, B. S. Larsson, and N. G. Lindquist, "Uptake of manganese and cadmium from the nasal mucosa into the central nervous system via olfactory pathways in rats," *Pharmacology and Toxicology*, vol. 79, no. 6, pp. 347–356, 1996.

[69] H. Tjalve and J. Henriksson, "Uptake of metals in the brain via olfactory pathways," *NeuroToxicology*, vol. 20, no. 2-3, pp. 181–195, 1999.

[70] D. C. Dorman, M. F. Struve, M. W. Marshall, C. U. Parkinson, R. A. James, and B. A. Wong, "Tissue manganese concentrations in young male rhesus monkeys following subchronic manganese sulfate inhalation," *Toxicological Sciences*, vol. 92, no. 1, pp. 201–210, 2006.

[71] Y. Wang, B. Wang, M. T. Zhu et al., "Microglial activation, recruitment and phagocytosis as linked phenomena in ferric oxide nanoparticle exposure," *Toxicology Letters*, vol. 205, no. 1, pp. 26–37, 2011.

[72] R. L. Doty, "Symposium overview: do environmental agents enter the brain via the olfactory mucosa to induce neurodegenerative diseases," *Annals of the New York Academy of Sciences*, vol. 1170, pp. 610–614, 2009.

[73] R. L. Doty, "Olfactory dysfunction in Parkinson's disease," *Nature Reviews Neurology*, vol. 8, pp. 329–339, 2012.

[74] R. L. Doty, "Olfaction in Parkinson's disease and related disorders," *Neurobiology of Disease*, vol. 46, pp. 527–552, 2012.

[75] P. W. Schofield, H. Ebrahimi, A. L. Jones, G. A. Bateman, and S. R. Murray, "An olfactory "stress test" may detect preclinical Alzheimer's disease," *BMC Neurology*, vol. 12, article 24, 2012.

[76] S. Rahayel, J. Frasnelli, and S. Joubert, "The effects of Alzheimer's disease and Parkinson's disease on olfaction: a meta-analysis," *Brain Research*, vol. 1442, pp. 55–65, 2012.

[77] L. Calderón-Garcidueñas, M. Franco-Lira, C. Henríquez-Roldán et al., "Urban air pollution: influences on olfactory function and pathology in exposed children and young adults," *Experimental and Toxicologic Pathology*, vol. 62, no. 1, pp. 91–102, 2010.

[78] D. M. Holtzman, J. Herz, and G. Bu, "Apolipoprotein e and apolipoprotein e receptors: normal biology and roles in Alzheimer disease," *Cold Spring Harbor Perspectives in Medicine*, vol. 2, no. 3, Article ID a006312, 2012.

[79] Z. Olivecrona and L. O. Koskinen, "The release of S-100B and NSE in severe traumatic head injury is associated with ApoE 4," *Acta Neurochirurgica*, vol. 154, pp. 675–680, 2012.

[80] R. Chaudhary, A. Likidlilid, and T. Peerapatdit, "Apolipoprotein E gene polymorphism: effects on plasma lipids and risk of type 2 diabetes and coronary artery disease," *Cardiovascular Diabetology*, vol. 11, article 36, 2012.

[81] J. Fernández-Irigoyen, F. J. Corrales, and E. Santamaria, "Proteomic atlas of the human olfactory bulb," *Journal of Proteomics*, vol. 75, no. 13, pp. 4005–4016, 2012.

[82] K. Schroder, V. Sagulenko, A. Zamoshnikova et al., "Acute lipopolysaccharide priming boosts inflammasome activation independently of inflammasome sensor induction," *Immunobiology*, vol. 217, no. 12, pp. 1325–1329, 2012.

[83] M. Lamkanfi and V. M. Dixit, "Inflammasomes and their roles in health and disease," *Annual Review of Cell and Developmental Biology*, vol. 28, pp. 137–161, 2012.

[84] F. Martinon, "Signaling by ROS drives inflammasome activation," *European Journal of Immunology*, vol. 40, no. 3, pp. 616–619, 2010.

[85] R. Hanamsagar, M. L. Hanke, and T. Kielian, "Toll-like receptor (TLR) and inflammasome actions in the central nervous system," *Trends in Immunology*, vol. 33, pp. 333–342, 2012.

[86] E. Latz, "The inflammasomes: mechanisms of activation and function," *Current Opinion in Immunology*, vol. 22, no. 1, pp. 28–33, 2010.

[87] R. Villarreal-Calderon, R. Torres-Jardón, J. Palacios-Moreno et al., "Urban air pollution targets the dorsal vagal complex and

dark chocolate offers neuroprotection," *International Journal of Toxicology*, vol. 29, no. 6, pp. 604–615, 2010.

[88] M. H. Tabert, X. Liu, R. L. Doty et al., "A 10-item smell identification scale related to risk for Alzheimer's disease," *Annals of Neurology*, vol. 58, no. 1, pp. 155–160, 2005.

[89] H. Braak and E. Braak, "Neuropathological stageing of Alzheimer-related changes," *Acta Neuropathologica*, vol. 82, no. 4, pp. 239–259, 1991.

[90] H. Braak, K. Del Tredici, U. Rüb, R. A. I. de Vos, E. N. H. Jansen Steur, and E. Braak, "Staging of brain pathology related to sporadic Parkinson's disease," *Neurobiology of Aging*, vol. 24, no. 2, pp. 197–211, 2003.

[91] H. Braak, U. Rüb, W. P. Gai, and K. Del Tredici, "Idiopathic Parkinson's disease: possible routes by which vulnerable neuronal types may be subject to neuroinvasion by an unknown pathogen," *Journal of Neural Transmission*, vol. 110, no. 5, pp. 517–536, 2003.

[92] H. Braak, D. R. Thal, E. Ghebremedhin, and K. Del Tredici, "Stages of the pathologic process in Alzheimer disease: age categories from 1 to 100 years," *Journal of Neuropathology & Experimental Neurology*, vol. 70, no. 11, pp. 960–969, 2011.

[93] H. Braak and K. Del Tredici, "The pathological process underlying Alzheimer's disease in individuals under thirty," *Acta Neuropathologica*, vol. 121, no. 2, pp. 171–181, 2011.

[94] K. Jellinger, H. Braak, E. Braak, and P. Fischer, "Alzheimer lesions in the entorhinal region and isocortex in Parkinson's and Alzheimer's diseases," *Annals of the New York Academy of Sciences*, vol. 640, pp. 203–209, 1991.

[95] K. A. Jellinger, "Interaction between pathogenic proteins in neurodegenerative disorders," *Journal of Cellular and Molecular Medicine*, vol. 16, pp. 1166–1183, 2012.

[96] W. G. Meissner, "When does Parkinson's disease begin? From prodromal disease to motor signs," *Revue Neurologique*, vol. 168, no. 11, pp. 809–814, 2012.

[97] A. L. Jefferson, J. M. Massaro, P. A. Wolf et al., "Inflammatory markers are associated with total brain volume: the Framingham Heart Study," *Neurology*, vol. 68, pp. 1032–1038, 2007.

[98] A. L. Jefferson, J. M. Massaro, A. S. Beiser et al., "Inflammatory markers and neuropsychological functioning: the Framingham Heart Study," *Neuroepidemiology*, vol. 37, no. 1, pp. 21–30, 2011.

[99] N. I. Bohnen, M. L. T. M. Miiller, H. Kuwabara, G. M. Constantine, and S. A. Studenski, "Age-associated leukoaraiosis and cortical cholinergic deafferentation," *Neurology*, vol. 72, no. 16, pp. 1411–1416, 2009.

[100] N. I. Bohnen and R. L. Albin, "White matter lesions in Parkinson disease," *Nature Reviews Neurology*, vol. 7, no. 4, pp. 229–236, 2011.

[101] L. C. Silbert, D. B. Howieson, H. Dodge, and J. A. Kaye, "Cognitive impairment risk: white matter hyperintensity progression matters," *Neurology*, vol. 73, no. 2, pp. 120–125, 2009.

[102] A. M. Brickman, A. Zahra, J. Muraskin et al., "Reduction in cerebral blood flow in areas appearing as white matter hyperintensities on magnetic resonance imaging," *Psychiatry Research*, vol. 172, no. 2, pp. 117–120, 2009.

[103] M. E. Murray, M. L. Senjem, R. C. Petersen et al., "Functional impact of white matter hyperintensities in cognitively normal elderly subjects," *Archives of Neurology*, vol. 67, no. 11, pp. 1379–1385, 2010.

[104] A. A. Gouw, A. Seewann, W. M. van der Flier et al., "Heterogeneity of small vessel disease: a systematic review of MRI and histopathology correlations," *Journal of Neurology, Neurosurgery and Psychiatry*, vol. 82, no. 2, pp. 126–135, 2011.

[105] D. Bunce, K. J. Anstey, N. Cherbuin et al., "Cognitive deficits are associated with frontal and temporal lobe white matter lesions in middle-aged adults living in the community," *PLoS ONE*, vol. 5, no. 10, Article ID e13567, 2010.

[106] A. Wallin and T. Fladby, "Do white matter hyperintensities on MRI matter clinically?" *British Medical Journal*, vol. 341, Article ID c3400, 2010.

[107] P. Maillard, E. Fletcher, D. Harvey et al., "White matter hyperintensity penumbra," *Stroke*, vol. 42, no. 7, pp. 1917–1922, 2011.

[108] J. Z. Wang, Y. Y. Xia, I. Grundke-Iqbal, and K. Iqbal, "Abnormal hyperphosphorylation of tau: sites, regulation and molecular mechanism of neurofibrillary degeneration," *Journal of Alzheimer's Disease*. In press.

[109] J. Avila, G. León-Espinosa, E. García, V. Garcia-Escudero, F. Hernández, and J. Defelipe, "Tau phosphorilation by GSK3 in different conditions," *International Journal of Alzheimer's Disease*, vol. 2012, Article ID 578373, 7 pages, 2012.

[110] D. J. Bonda, R. J. Castellani, X. Zhu et al., "A novel perspective on Tau in Alzheimer's disease," *Current Alzheimer Research*, vol. 8, no. 6, pp. 639–642, 2011.

[111] H. G. Lee, G. Perry, P. I. Moreira et al., "Tau phosphorylation in Alzheimer's disease: pathogen or protector?" *Trends in Molecular Medicine*, vol. 11, no. 4, pp. 164–169, 2005.

[112] A. De Calignon, L. M. Fox, R. Pitstick et al., "Caspase activation precedes and leads to tangles," *Nature*, vol. 464, no. 7292, pp. 1201–1204, 2010.

[113] L. Buée, L. Troquier, S. Burnouf et al., "From tau phosphorylation to tau aggregation: what about neuronal death?" *Biochemical Society Transactions*, vol. 38, no. 4, pp. 967–972, 2010.

[114] J. Avila, "Intracellular and extracellular tau," *Frontiers in Neuroscience*, vol. 4, article 49, 2010.

[115] D. P. Hanger and S. Wray, "Tau cleavage and tau aggregation in neurodegenerative disease," *Biochemical Society Transactions*, vol. 38, no. 4, pp. 1016–1020, 2010.

[116] B. Cui, L. Zhu, X. She et al., "Chronic noise exposure causes persistence of tau hyperphosphorilation and formation of NFT tau in the rat hippocampus and prefrontal cortex," *Experimental Neurology*, vol. 238, pp. 122–129, 2012.

[117] N. Lénárt, V. Szegedi, G. Juhász et al., "Increased Tau phosphorilation and impaired presynaptic function in hypertriglyceridemic ApoB-100 transgenic mice," *PLOS ONE*, vol. 7, no. 9, Article ID e46007, 2012.

[118] C. W. Lee, Y. S. Shih, S. Y. Wu, T. Yang, C. Lin, and Y. M. Kuo, "Hypoglycemia induces tau hyperphosphorilation," *Current Alzheimer Research*. In press.

[119] E. Cerf, A. Gustot, E. Goormaghtigh, J. M. Ruysschaert, and V. Raussens, "High ability of apolipoprotein E4 to stabilize amyloid-β peptide oligomers, the pathological entities responsible for Alzheimer's disease," *The FASEB Journal*, vol. 25, no. 5, pp. 1585–1595, 2011.

[120] B. A. Silva, L. Breydo, A. L. Fink, and V. N. Uversky, "Agrochemicals, α-synuclein and Parkinson's disease," *Molecular Neurobiology*. In press.

[121] R. Perfeito, T. Cunha-Oliveira, and A. C. Rego, "Revisiting oxidative stress and mitochondrial dysfunction in the pathogenesis of Parkinson's disease-resemblance to the effect of amphetamine drugs of abuse," *Free Radical Biology & Medicine*, vol. 53, pp. 1791–1806, 2012.

[122] R. E. Musgrove, A. E. King, and T. C. Dickson, "a-Synuclein protects neurons from apoptosis downstream of free-radical production through modulation of the MAPK signaling pathway," *Neurotoxicity Research*. In press.

[123] D. Béraud, H. A. Hathaway, J. Trecki et al., "Microglial activation and antioxidant responses induced by the Parkinson's disease protein a-synuclein," *Journal of NeuroImmune Pharmacology*. In press.

[124] Y. Stern, "Cognitive reserve in aging and Alzheimer's disease," *Lancet Neurology*, vol. 11, pp. 1006–1012, 2012.

[125] H. Jian, W. Yi-Fang, L. Qi, H. Xiai-Song, and Z. Gui-Yun, "Cerebral blood flow and metabolic changes in hippocampalregions of a modified rat model with chronic cerebral hypoperfusion," *Acta Neurologica Belgica*. In press.

[126] A. E. Roher, J. P. Debbins, M. Malek-Ahmadi et al., "Cerebral blood flow in Alzheimer's disease," *Journal of Vascular Health and Risk Management*, vol. 8, pp. 599–611, 2012.

[127] J. C. De la Torre, "A turning point for Alzheimer's disease?" *Biofactors*, vol. 38, pp. 78–83, 2012.

[128] R. J. Castellani and G. Perry, "Pathogenesis and disease-modifying therapy in Alzheimer's disease: the flat line of progress," *Archives of Medical Research*, vol. 43, no. 8, pp. 694–698, 2012.

[129] http://www.epa.gov/oaqps001/greenbk/.

Hindawi Publishing Corporation
BioMed Research International
Volume 2013, Article ID 158093, 9 pages
http://dx.doi.org/10.1155/2013/158093

Research Article

Release of IL-1β Triggered by Milan Summer PM_{10}: Molecular Pathways Involved in the Cytokine Release

Rossella Bengalli,[1] Elisabetta Molteni,[2] Eleonora Longhin,[1] Magne Refsnes,[3] Marina Camatini,[1] and Maurizio Gualtieri[1,4]

[1] *Polaris Research Centre, Department of Environmental Sciences and Earth Sciences, University of Milano-Bicocca, Piazza della Scienza 1, 20126 Milano, Italy*
[2] *Department of Biology and Biotecnology, University of Pavia, Via Ferrata 1, 27100 Pavia, Italy*
[3] *Division of Environmental Medicine, Norwegian Institute of Public Health, P.O. Box 4404, Nydalen, 0403 Oslo, Norway*
[4] *UTTS Saluggia, ENEA, Strada Crescentino, 13040 Saluggia, Italy*

Correspondence should be addressed to Maurizio Gualtieri; maurizio.gualtieri@unimib.it

Received 2 October 2012; Revised 22 December 2012; Accepted 3 January 2013

Academic Editor: Per Schwarze

Particulate matter (PM) exposure is related to pulmonary and cardiovascular diseases, with increased inflammatory status. The release of the proinflammatory interleukin- (IL-) 1β, is controlled by a dual pathway, the formation of inactive pro-IL-1β, through Toll-like receptors (TLRs) activation, and its cleavage by NLRP3 inflammasome. THP-1-derived macrophages were exposed for 6 h to 2.5 μg/cm^2 of Milan PM_{10}, and the potential to promote IL-1β release by binding TLRs and activating NLRP3 has been examined. Summer PM_{10}, induced a marked IL-1β response in the absence of LPS priming (50-fold increase compared to unexposed cells), which was reduced by caspase-1 inhibition (91% of inhibition respect summer PM_{10}-treated cells) and by TLR-2 and TLR-4 inhibitors (66% and 53% of inhibition, resp.). Furthermore, summer PM_{10} increased the number of early endosomes, and oxidative stress inhibition nearly abolished PM_{10}-induced IL-1β response (90% of inhibition). These findings suggest that summer PM_{10} contains constituents both related to the activation of membrane TLRs and activation of the inflammasome NLPR3 and that TLRs activation is of pivotal importance for the magnitude of the response. ROS formation seems important for PM_{10}-induced IL-1β response, but further investigations are needed to elucidate the molecular pathway by which this effect is mediated.

1. Introduction

In the last decade great effort has been paid to understand the mechanisms involved in particulate matter (PM) induced adverse health effects. Epidemiological evidence shows an association between exposure to air pollution and the occurrence of respiratory pathologies (chronic bronchitis, COPD) and exacerbation of allergic conditions such as asthma [1–3]. Furthermore, many studies also show an association between PM atherothrombotic effects, cardiovascular morbidity, and mortality [4–6].

PM is a heterogeneous pollutant composed of particles of different chemical composition and different sizes (defined as PM_{10}, $PM_{2.5}$, and $PM_{0.1}$ for their aerodynamic diameter). Although the size determines the site of deposition of PM in the respiratory tract [7], the chemical composition of the inhaled particles is considered of primary importance in determining the adverse biological effects [8, 9]. The chemical properties of PM are strongly related to the sources of emission of the particles, and this is known to be crucial for the differences of the PM effects from different sampling sites [10–13].

The fine fraction ($PM_{2.5}$) is generally composed of primary particles derived from combustion processes, mostly consisting of primary particles with mean diameter lower than 100 nm ($PM_{0.1}$, ultrafine particles) and secondary aerosol deriving from chemical reaction of free compounds in the atmosphere. The particle composition reflects the sources of emission; indeed fine PM has usually higher content in organic compounds (such as PAHs) and elemental carbon (the soot core of the particles) than the coarse PM.

The coarse fraction ($PM_{10-2.5}$) is on the contrary dominated by particles derived from abrasion processes, such as the erosion of crustal material, resuspension of deposited particles, and biological components. We have previously shown that the season of PM sampling strongly influences the chemical and biological composition of both coarse and fine PMs [14, 15]. In fact summer and winter PM_{10} fractions showed a completely different composition in chemical and biological constituents, the latter being higher in summer PM_{10} [11, 16, 17].

Moreover, the chemical characterization showed that the PM_{10} contained crystal silica and other elements which can contribute to its inflammatory potential.

A lot of studies have shown that PM_{10} exposure promotes inflammation in the lung which is associated with a systemic inflammatory response. Macrophages and lung epithelial cells incubated with PM_{10} release significantly increased amounts of cytokines and chemokines, including granulocyte-macrophage colony-stimulating factor (GM-CSF), interleukin IL-1β, IL-6, and IL-8, and macrophage chemo-attractant protein (MCP)-1 [18]. An increased lung inflammation is known to be fundamental for the development of different lung diseases, such as COPD [19–21]. However, despite the increased evidence that the coarse fraction of PM is potent in inducing lung inflammation, a model explaining its effects has not been completely understood.

A critical property of the innate immune system is its ability to discriminate microbes from "self" by the recognition of invariant microbial structure called pathogen-associated recognition patterns (PAMPs) such as lipopolysaccharides (LPS) [22]. The sensing of these PAMPs is usually mediated by the membrane-bounded Toll-like receptors (TLRs), such as TLR-2 and TLR-4 [23, 24]. Commonly these receptors trigger the activation of the NF-kB pathway which determines the release of different proinflammatory proteins, such as pro-IL-1β. Another set of pattern recognition receptors are the cytoplasm Nod-like receptors. These receptors have been demonstrated to be key proteins in the activation of pro-caspase-1, through the formation of the caspase-1 activating platforms, the inflammasomes. The inflammasomes control in turn the cleavage and secretion of potent proinflammatory interleukins such as IL-1β and IL-18. Among the different inflammasomes, the NLRP3 (or NALP3) is the most characterized. This complex is composed of a basic scaffold, the adaptor molecule apoptosis-associated speck-like protein containing a caspase recruitment domain (ASC), and the caspase-1. The activation of this complex has been related to the exposure of different PAMPs as well as host-derived molecules [25].

IL-1β is released at the site of injury, or immunological challenge is coordinating inflammatory responses, such as the recruitment of other cells to the site of infection or injury [26], and is known to be crucial in development of different diseases, including silicosis [27, 28]. IL-1β is also, however, known to regulate sleep, appetite, and body temperature. Due to its potent activities, it is not surprisingly that IL-1β activity is rigorously controlled throughout its entire release pathway, from expression to maturation and final secretion.

The activation of the inflammasome machinery has been related to different mechanisms which have been reviewed in [25]. However for the release of IL-1β a priming stimulus is required for the formation of pro-IL-1β as reported in [29].

It has been shown that particles occurring in ambient PM, such as crystalline silica, as well as different nanoparticles, may induce inflammasome activation [20, 30–33]. The potential role of the inflammasome in PM-induced inflammation is however not known. Reactive oxygen substances (ROS) are known to be involved in PM_{10}-induced inflammation [34, 35] and also in silica-induced inflammasome activation [21, 36]. Potentially ROS might be involved in the pro-IL-1β formation as well as the inflammasome activation [37, 38].

In the present study it was hypothesized that PM_{10} due to its chemical and physical nature might induce IL-1β release. Summer Milan PM_{10} contains both endotoxins, which might activate TLR receptors, and elemental and crustal constituents, which might activate the inflammasome mechanism. Furthermore, it is hypothesized that ROS is involved in PM_{10}-induced IL-1β responses.

2. Materials and Methods

2.1. Cell Culture and Treatments. The human monocytes cell line, THP-1, was maintained in Opti-MEM medium supplemented with 10% FBS and 100 U/100 mL Penicillin/Streptomycin at 37°C, 5% CO_2. THP-1 cells were differentiated into macrophage-like cells by incubation with phorbol myristate acetate (PMA, 20 nM) (Sigma Aldrich) for 24 h. PMA was then removed and cells were washed and incubated in Opti-MEM (Invitrogen, Italy) medium supplemented with 20% FBS o/n. Cells were treated in 10% FBS medium with summer PM_{10} at different concentrations (1 μg/cm^2, 2.5 μg/cm^2, and 5 μg/cm^2) for different times of exposure (30 min, 2 h, 4 h, and 6 h). Winter PM_{10} and carbon black (CB, 2–12 μm, Sigma Aldrich, Italy) were used (5 μg/cm^2) as comparison and reference particles, respectively. In order to investigate TLR-2, TLR-4 and caspase-1 involvement in IL-1β release, cells were pre-treated for 1 h with inhibitors of TLR-2 and TLR-4 (0, 1 μg/mL, R&D Systems) and caspase-1 (z-YVAD-fmk, 10 μM, Calbiochem) and then exposed to summer PM_{10} (2.5 μg/cm^2). Summer and winter PM_{10} particles have been characterised as previously reported in [39] and [40] respectively. ROS involvement in IL-1β release was assessed by treating PM_{10} exposed cells with N-acetylcysteine (NAC, 15 mM, 30 min prior to PM exposure).

2.2. IL-1β Release. Supernatants from control and PM_{10}-exposed cells were collected and stored at −80°C. Supernatants were assayed for IL-1β with ELISA kits (Invitrogen Srl) according to manufacturer's instructions.

2.3. Endocytic Pathway Analysis

2.3.1. Immunostaining. After 30 min exposure to summer PM_{10}, cells were washed in phosphate-buffered saline 1X (PBS), fixed in paraformaldehyde 4% for 20 min, and washed

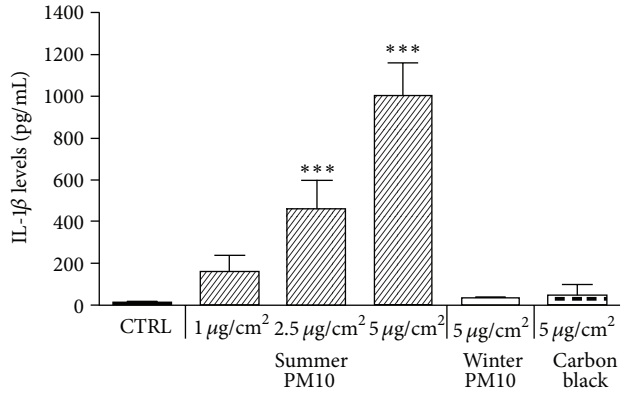

Figure 1: IL-1β release by THP-1-derived macrophages exposed for 6 h to different PM_{10} and carbon black (CB). The cells were exposed to increasing concentrations of summer Milan PM_{10}, and one concentration (5 $\mu g/cm^2$) of winter PM_{10} and CB. CTRL: unexposed cells. Results are the mean and s.d. of three independent experiments and presented as pg/mL released in the culture medium. $^{***}P < 0.001$ versus CTRL.

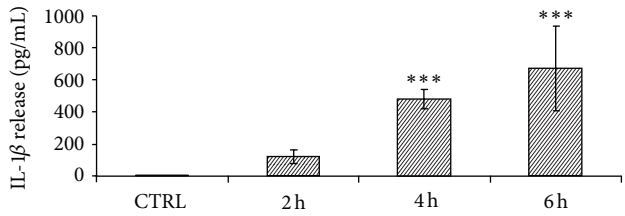

Figure 2: Time-dependent release of IL-1β in THP-1-derived macrophages cells treated for 2, 4, and 6 h with summer Milan PM_{10} at a concentration of 2.5 $\mu g/cm^2$. CTRL: untreated cells. Results are the mean and s.d. of at least three independent experiments and presented as pg/mL released in the culture medium. $^{***}P < 0.001$ versus CTRL.

twice in PBS. Fixed cells were permeabilized with 0.1% Triton X-100 (Sigma Aldrich), 0.1% Tween (Sigma Aldrich), and 2% BSA (Sigma Aldrich) in PBS and incubated o/n with the rabbit anti-human early endosome antibody 1 (EEA1 Antibody, Cell Signaling Technology; dilution 1 : 100). Cells were then washed in PBS and incubated with Alexa fluor-488 (Invitrogen Molecular Probes Srl; dilution 1 : 1000) for 2 h. Samples were mounted on a slide with ProLong mount (Invitrogen Srl) and observed by Axio Observer inverted microscope (Zeiss, Germany).

2.3.2. Western Blot. After exposure to summer PM_{10} cells were washed in PBS and stored at −80°C. Cells were then lysed in RIPA buffer (50 mM Tris-HCl pH 8; 150 mM NaCl; 1% NP-40; 0.5% sodium deoxycholate; 0.1% SDS; Sigma Ladrich Italy) and then sonicated three times for 30 sec on ice. Cell lysates were then separated by 8% SDS-PAGE and transferred on nitrocellulose membranes. Blots were incubated with rabbit polyclonal antibody against human EEA1

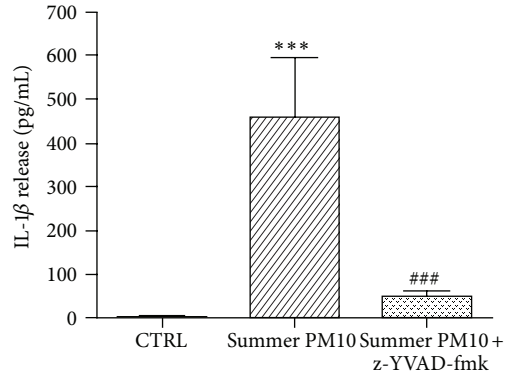

Figure 3: PM_{10}-induced IL-1β release dependent on caspase-1 activation in THP-1-derived macrophages cells. The cells were pretreated with the caspase-1 inhibitor, z-YVAD-fmk (10 μM) for 1 h, and exposed to summer PM_{10} for 6 h. Results are the mean and s.d. of three independent experiments. CTRL: untreated cells. $^{***}P < 0.001$ versus CTRL, $^{###}P < 0.001$ versus summer PM_{10}.

(Cell Signaling Technology; dilution 1 : 1000) o/n or anti-actin antibody (Sigma Aldrich, Italy; dilution 1 : 2000). After washes, the membranes were incubated with secondary antibody anti-rabbit IgG (Fab2 fragment-Alkaline Phosphatase, Sigma Aldrich; dilution 1 : 10000) and subsequently incubated with SIGMA FAST BCIP/NBT alkaline phosphatase substrate (Sigma Aldrich) for 10 min for detection. Fold increase data over control, obtained by acquisition of membrane and densitometry analysis with dedicated software (UVP, US), were normalized to the actin content.

2.4. Cells-Particles Interaction

2.4.1. Haematoxylin-Eosin Staining. THP-1-derived macrophage untreated and treated with summer PM_{10} for 24 h at the concentration of 2.5 $\mu g/cm^2$, were fixed in paraformaldehyde 4% for 20 min and then stained following haematoxylin-eosin protocol and then observed under an Axiolab light microscope (Zeiss, Germany).

2.4.2. Transmission Electron Microscopy. Samples were prepared for transmission electron microscopy (TEM) using standard procedures. At the end of exposure the cells were fixed in 2.5% glutaraldehyde for 20 min at 4°C and postfixed with 1% osmium tetroxide for 1 h, followed by dehydration using a scale of graded ethanol. Cells were then embedded in Epon resin, and semithin and ultrathin sections were prepared by an ultramicrotome (Ultracut Jung E, Reichert Germany). Ultrathin slides were mounted on copper grids and counterstained by lead citrate and uranyl acetate prior to examination by Jeol JEM 1220 microscope operating at 80 kV and digital images were taken with a Gatan CCD camera.

2.5. Statistical Analysis. Results are reported as mean ± standard deviation of at least three independent experiments. Statistical differences were analysed by the software SigmaStat

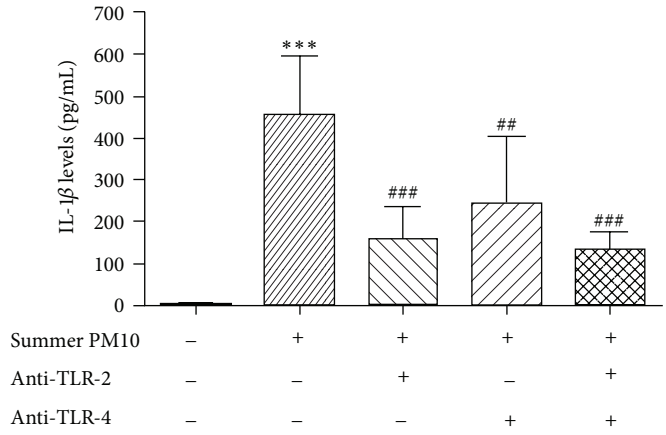

Figure 4: Inhibition of PM_{10}-induced IL-1β release in THP-1-derived macrophages by TLR-2 and TLR-4 antagonist molecules. The cells were pretreated with TLR-2 and TLR-4 inhibitors (0.1 μg/mL) for 1 h and then incubated in the presence (+) or absence (−) of summer PM_{10} (2.5 μg/cm^2) for 6 h. Results are the mean and s.d. of three independent experiments. $^{***}P < 0.001$ versus CTRL, $^{###}P < 0.001$ versus summer PM_{10}, and $^{##}P < 0.01$ versus summer PM_{10}.

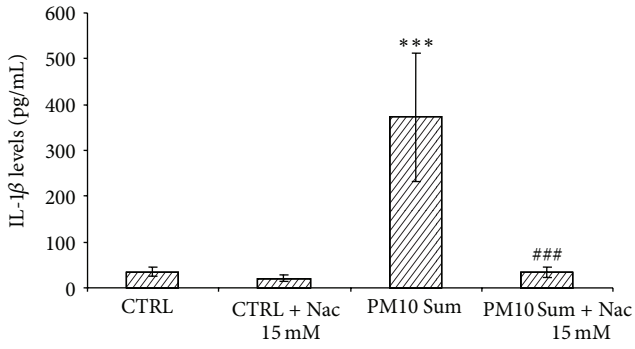

Figure 5: Inhibition of PM_{10}-induced IL-1β release in THP-1-derived macrophages by NAC. The cells were pretreated with 15 mM NAC (+) and then incubated with summer PM_{10} (2.5 μg/cm^2) for 6 h. Results are the mean and s.d. of at least three independent experiments. $^{***}P < 0.001$ versus CTRL, $^{###}P < 0.001$ versus summer Milan PM_{10}.

3.1 performing ANOVA test with post hoc analysis (Dunn's); if required a parametric statistical analysis was performed.

3. Results

3.1. Release of IL-1β from Human Macrophage-Like Cell after Summer Milan PM_{10} Exposure. THP-1-derived macrophages were treated as reported with summer Milan PM_{10} and with winter PM_{10} and CB. The experiments showed that IL-1β was dose-dependently increased after summer Milan PM_{10} treatment, with a progressive increase from 1 to 5 μg/cm^2. In contrast, winter Milan PM_{10} and CB did not induce significant release of the interleukin (Figure 1). Cells were then exposed to 2.5 μg/cm^2 of summer Milan PM_{10}, chosen as the first dose of effects, to investigate the time-course release of IL-1β. The IL-1β release showed a progressive increase from 2 to 6 h (Figure 2).

3.2. IL-1β Release and Inhibition of Caspase-1, TLR-2/-4 and Oxidative Stress. THP-1-derived macrophages were pretreated for 1 h with the caspase-1 inhibitor z-YVAD (10 μM) and then treated with summer PM_{10} (2.5 μg/cm^2) for 6 h, or only with z-YVAD. Cells preexposed with z-YVAD showed IL-1β release similar to the control (data not shown). The experiments showed that z-YVAD significantly reduced summer PM_{10}-induced release of IL-1β (approximately 90%), compared to PM_{10} treatment alone (Figure 3).

Subsequently THP-1-derived macrophages were pretreated with TLR-2 and TLR-4 inhibitors (0.1 μg/mL) for 1 h before exposure to summer PM_{10} (2.5 μg/cm^2 for 6 h). The inhibition of the TLR receptors significantly reduced the release of IL-1β induced by summer Milan PM_{10} (Figure 4). The TLR-2 inhibitor was more potent than the TLR-4 inhibitor. Furthermore, combining the two inhibitors gave the maximal reduction of IL-1β release. The TLR inhibitors did not affect the IL-1β release from control cells (data not shown).

Treatment with NAC, an inhibitor of oxidative stress, reduced the release of IL-1β in THP-1-derived macrophages treated with PM_{10} to control levels (Figure 5).

3.3. Cells-Particles Interaction: Endocytosis Pathway. We focused our study also on the molecular mechanisms involved in summer Milan PM_{10}-induced IL-1β release.

The activity of early endosomes after the exposure to summer PM_{10} was examined by analysing the expression of the early endosome antigen 1 (EEA1) in THP-1-derived macrophages. The cells were exposed to summer PM_{10} for 30 min and then assessed by EEA1 immunostaining. We

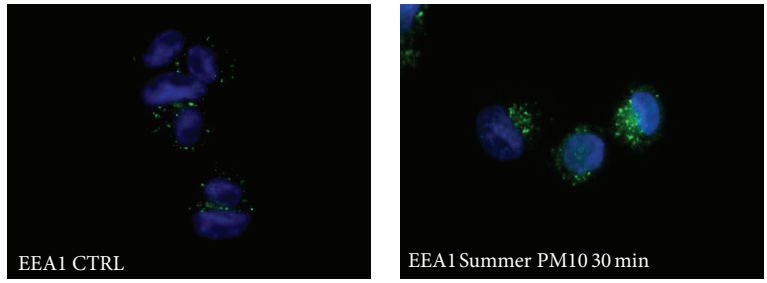

Figure 6: PM_{10}-induced overexpression of early endosomes in THP-1-derived macrophages. The cells were treated with summer Milan PM_{10} at the concentration of 2.5 μg/cm^2 for 30 min and then stained for the early endosome antigen EEA1 (green). Nuclei are stained with DAPI (blue): representative images.

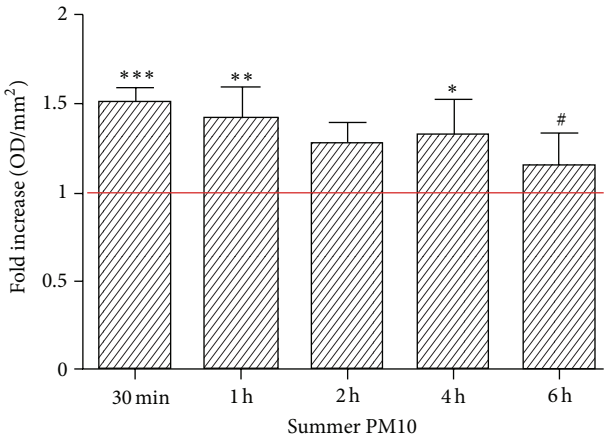

Figure 7: Early endosome antigen 1 EEA1 protein expression in THP-1-derived macrophages exposed to summer Milan PM_{10}. The cells were treated with summer PM_{10} (2.5 μg/cm^2) for 30 min, 1 h, 2 h, 4 h, and 6 h and then assessed for EEA1 expression by Western analysis. Mean and s.d. of at least three independent experiments. $^{***}P < 0.001$ versus CTRL, $^{**}P < 0.01$ versus control, $^{*}P < 0.05$ versus CTRL, and $^{\#}P < 0.05$ versus 30 min.

observed that EEA1 expression after 30 min was remarkably increased compared to the control (Figure 6). This result is also confirmed by immunoblotting of EEA1. The cells were treated with summer PM_{10} (2.5 μg/cm^2) for 2 to 6 h and assessed for EEA1 expression by Western analysis. The data show that the EEA1 is overexpressed from 30 min to 4 h, but was approximately similar to the control at 6 h (Figure 7). These results suggest that THP-1-derived macrophages are able to phagocytise summer PM_{10} and its internalization involves early endosomes.

3.4. Cell Particles Interaction. The interaction between summer Milan PM_{10} and THP-1-derived macrophages was determined by haematoxylin-eosin staining and electron transmission microscopy (TEM). Haematoxylin-eosin-stained macrophages exposed to summer PM_{10} (for 6 h) showed a high number of particles attached to the cells (Figures 8(b) and 8(c)). TEM picture demonstrated the internalization of summer PM_{10} particles in cytoplasm vesicles and also translocation of small aggregates in the nucleus (Figure 8(d)). The TEM picture showed also a clear interaction of summer PM_{10} with plasma membranes with the formation of phagocyte structures (Figure 8(e)).

4. Discussion

Recently PM_{10} was demonstrated to induce IL-1β release via an inflammasome mechanism as revealed by caspase-1 inhibition and siRNA against NALP3 in THP-1 cells and by NALP3 knockout mice. The potential of PM_{10} was however relatively slight, about 3-fold using 500 μg/mL [35]. Compared to this we report that PM_{10} collected in the summer in Milan induced a massive IL-1β response (a 50-fold increase, at 10-fold lower concentrations) in THP-1-derived macrophages. However, PM_{10} collected in Milan in the winter showed only a slight IL-1β response, underlining the importance of the PM_{10} sources. Our study also indicates the importance of an inflammasome mechanism, as the response was reduced by caspase- 1 inhibition. It is however suggested that the summer Milan PM_{10}-induced activation of TLR-2 and TLR-4 receptors, leading to synthesis of pro-IL-1β, is the major determinant for the massive response induced by summer Milan PM_{10}. Furthermore, our study showed a role for oxidative stress in the PM_{10}-induced IL-1β release.

Most of the in vitro studies of particle-induced IL-1β responses have primed the cells with the endotoxins like LPS to increase the pool of pro-IL-1β before exposing to different agents capable of inducing the inflammasome mechanism. Indeed, for both crystalline and amorphous silica particles [20, 30], the priming of exposed cells with bacterial LPS is essential for the release of IL-1β following the activation of the inflammasome. It is now emerging in a lot of studies that different nanoparticles and other agents might activate the inflammasome mechanism, and induce large IL-1β responses in LPS-primed cells [30, 41]. In the present study it is also shown that the activation of the inflammasome is a crucial mechanism for the PM_{10}-induced IL-1β response, as the caspase-1 inhibitor z-YVAD reduced the interleukin release. Furthermore, PM_{10} induced a marked increase in endosomes

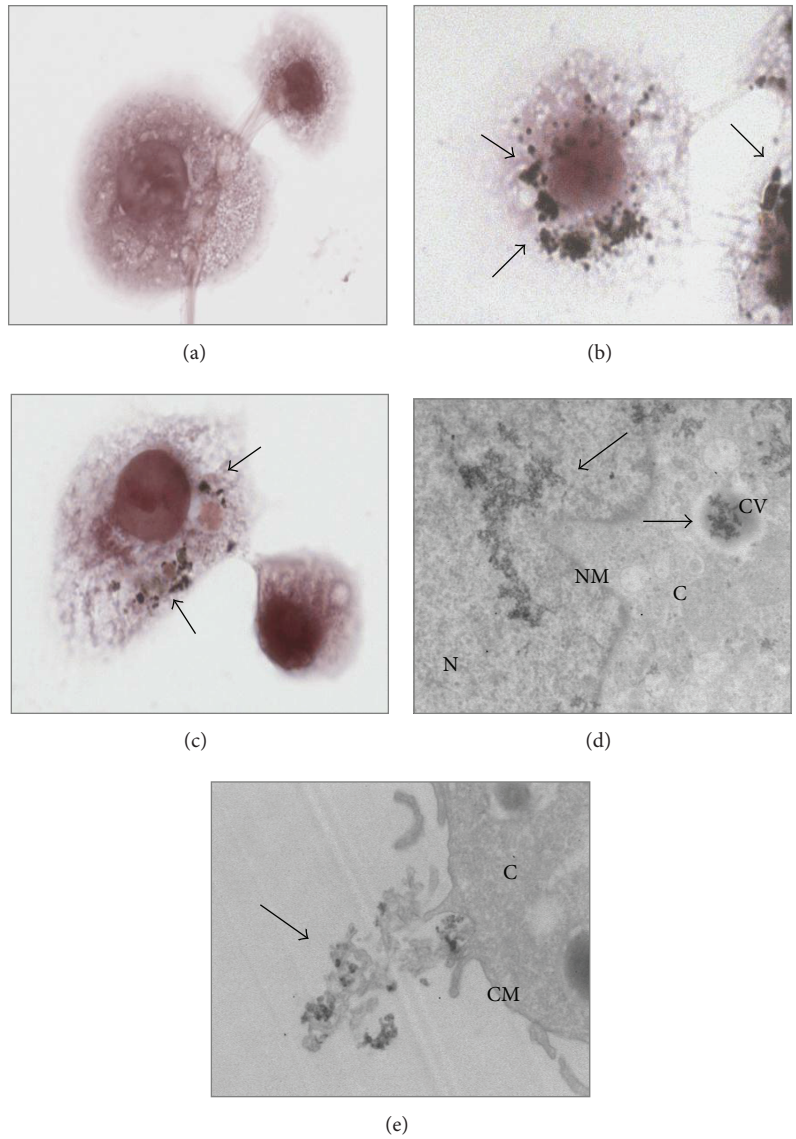

FIGURE 8: PM_{10} interaction with THP-1-derived macrophages. The cells were exposed to summer PM_{10} at the concentration of 2.5 $\mu g/cm^2$ for 4 h (b) and 6 h (c) and stained by haematoxylin eosin and compared with the control (a). An increased number of particles associated with the cells is indicated by black arrows. TEM images of the cells exposed to summer PM_{10} after 6 h are showed in (d, e), showing particles internalised in cytoplasm vesicles as well as particles into the nucleus (d). Particles interaction with the cell membrane are presented in (e). N: nucleus; NM: nuclear membrane; C: cytoplasm; CV: cytoplasmic vesicle; CM: cellular membrane. Magnification = 10 K.

internalization that has been shown to be involved in the inflammasome pathway [22, 42]. The most striking in this study is however that the marked IL-1β response is observed in the absence of LPS-priming. This suggest that summer Milan PM_{10} contains constituents (endotoxins capable of the activation of TLR-2 and/or TLR-4) which lead to pro-IL-1β formation; in support of this, the suppression of TLRs activation by pretreating the cells with anti-TLR-2 and TLR-4 molecules induced a significant reduction of IL-1β release. Both the TLR-2 and 4 are receptors which role in recognition and binding of LPS, and other bacterial PAMPs have been extensively described [43, 44]. Since airways macrophages seldom recognize bacterial components individually, the response to different bacterial PAMPs is usually orchestrated by a combination of different TLRs. In fact we demonstrated that the combination of the two inhibitors seems to give the maximal reduction of IL-1β release after PM_{10} exposure. However, our data may indicate that other biological components or PAMPs and/or other membrane receptors may be involved in the priming of cells, since the reduction of TLR-2 and 4 activities did not abolish completely the final release of IL-1β. Indeed is has been reported that the activation of the different TRLs might be promoted by different molecules which can be found in PM [45]. The inhibition of TLR2 and 4 indicates the importance of these two receptors in summer Milan PM_{10}-related effects, but the involvement of

other TLRs cannot be excluded. Furthermore we have already reported [41] the presence of crustal elements in summer Milan PM_{10} which can promote proinflammatory responses.

Also, in the study of Hirota [35], a PM_{10}-induced release of IL-1β is observed without LPS priming, but to a much less extent than for PM_{10} collected in Milan in the summer. In accordance with Hirota, we found a modest IL-1β response upon treatment to winter Milan PM_{10}. The differential effects can presumably be attributed to the content of endotoxins in the PM_{10}. In fact, we have previously reported that coarse fraction of summer PM_{10} is rich in Gram-negative bacteria, expressing LPS, in addition to crustal elements among which also silica [39, 46]. Interestingly, with respect to other endpoints, like DNA damage and apoptotic cell death, we have shown that winter Milan PM_{10} is more potent than summer Milan PM_{10}.

Oxidative stress seems to be crucial for the PM_{10}-induced IL-1β response, as demonstrated by inhibition by the inhibitor NAC. In addition to generation of ROS by a cell-free mechanism, ROS may be generated via the mitochondrial pathway [47]. Upon rupturing the lysosome membrane, the ROS may also be released to the cytoplasm [21]. A critical question is whether the ROS exerts its effect on IL-1β release after PM_{10} treatment by affecting the lysosome pathway or the pathway from TLR activation to pro-IL-1β formation. The increased number of endosomes subsequent to PM_{10} exposure reported in this study could indicate a release of ROS via this pathway that may be linked to inflammasome mechanism. However, ROS scavengers, such as NAC, have been reported to interact more with the priming of the NLRP3 rather than its activation [48]. A better understanding of the importance of ROS in the TLR-activation, subsequent NF-kB activation, and synthesis of pro-IL-1β, versus activation of the inflammasome, is thus needed.

4.1. Concluding Remarks. Since IL-1β has been related to a number of human diseases, including different pulmonary pathologies [49], and PM is known to increase the development of lung disease [50], it is crucial to increase the understanding of the pathways involved. Our findings, with very marked effect of PM_{10} in absence of exogenous addition of LPS, suggest that summer Milan PM_{10} contains constituents both related to the activation of membrane TLRs and activation of the inflammasome NLPR3. Furthermore, our study suggests that the activation of TLRs is of much importance for explaining the magnitude of the PM_{10}-induced IL-1β response. Thus, PM_{10} containing less biological components (PM_{10} sampled in winter) induces only a minor IL-1β response. The present study indicates an important role for ROS in PM_{10}-induced IL-1β formation, but further investigations are needed to elucidate the origin of the ROS (by lysosomes rupture or other pathways), and to what extent the effect is mediated by inhibition of the NLP3 activation or the TLR-pro-IL-1β pathway, or a combination of both these pathways.

Conflict of Interests

The authors do not have any conflict of interests.

Authors' Contribution

R. Bengalli, E. Molteni, and E. Longhin contributed equally to the in vitro experimental part. M. Gualtieri and R. Magne planned the in vitro experiments and contributed to the revision of the paper. M. Camatini and M. Gualtieri supervised the research activities during the Tosca Project.

Acknowledgment

M. Camatini and M. Gualtieri greatly thank Cariplo Foundation for financing the Tosca Project during which this research was performed.

References

[1] R. W. Atkinson, H. R. Anderson, J. Sunyer et al., "Acute effects of particulate air pollution on respiratory admissions: results from APHEA 2 project," *American Journal of Respiratory and Critical Care Medicine*, vol. 164, no. 10, pp. 1860–1866, 2001.

[2] B. Brunekreef and B. Forsberg, "Epidemiological evidence of effects of coarse airborne particles on health," *European Respiratory Journal*, vol. 26, no. 2, pp. 309–318, 2005.

[3] K. Donaldson and W. MacNee, "Potential mechanisms of adverse pulmonary and cardiovascular effects of particulate air pollution (PM_{10})," *International Journal of Hygiene and Environmental Health*, vol. 203, no. 5-6, pp. 411–415, 2001.

[4] R. D. Brook, S. Rajagopalan, C. A. Pope III et al., "Particulate matter air pollution and cardiovascular disease: an update to the scientific statement from the american heart association," *Circulation*, vol. 121, pp. 2331–2378, 2010.

[5] C. A. Pope III, M. Ezzati, and D. W. Dockery, "Fine-particulate air pollution and life expectancy in the United States," *The New England Journal of Medicine*, vol. 360, no. 4, pp. 376–386, 2009.

[6] A. Seaton, A. Soutar, V. Crawford et al., "Particulate air pollution and the blood," *Thorax*, vol. 54, no. 11, pp. 1027–1032, 1999.

[7] M. Lippmann, D. B. Yeates, and R. E. Albert, "Deposition, retention, and clearance of inhaled particles," *British Journal of Industrial Medicine*, vol. 37, no. 4, pp. 337–362, 1980.

[8] P. I. Jalava, R. O. Salonen, A. S. Pennanen et al., "Heterogeneities in inflammatory and cytotoxic responses of RAW 264.7 macrophage cell line to urban air coarse, fine, and ultrafine particles from six European sampling campaigns," *Inhalation Toxicology*, vol. 19, no. 3, pp. 213–225, 2007.

[9] M. S. Happo, R. O. Salonen, A. I. Hälinen et al., "Dose and time dependency of inflammatory responses in the mouse lung to urban air coarse, fine, and ultrafine particles from six European cities," *Inhalation Toxicology*, vol. 19, no. 3, pp. 227–246, 2007.

[10] E. Brüggemann, H. Gerwig, T. Gnauk, K. Müller, and H. Herrmann, "Influence of seasons, air mass origin and day of the week on size-segregated chemical composition of aerosol particles at a kerbside," *Atmospheric Environment*, vol. 43, no. 15, pp. 2456–2463, 2009.

[11] M. G. Perrone, M. Gualtieri, L. Ferrero et al., "Seasonal variations in chemical composition and in vitro biological effects of fine PM from Milan," *Chemosphere*, vol. 78, no. 11, pp. 1368–1377, 2010.

[12] J. Pey, X. Querol, and A. Alastuey, "Discriminating the regional and urban contributions in the North-Western Mediterranean:

PM levels and composition," *Atmospheric Environment*, vol. 44, no. 13, pp. 1587–1596, 2010.

[13] S. Kudo, K. Sekiguchi, K. H. Kim, and K. Sakamoto, "Spatial distributions of ultrafine particles and their behavior and chemical composition in relation to roadside sources," *Atmospheric Environment*, vol. 45, pp. 6403–6413, 2011.

[14] P. A. Steerenberg, L. van Amelsvoort, M. Lovik et al., "Relation between sources of particulate air pollution and biological effect parameters in samples from four european cities: an exploratory study," *Inhalation Toxicology*, vol. 18, no. 5, pp. 333–346, 2006.

[15] M. S. Happo, M. R. Hirvonen, A. I. Hälinen et al., "Seasonal variation in chemical composition of size-segregated urban air particles and the inflammatory activity in the mouse lung," *Inhalation Toxicology*, vol. 22, no. 1, pp. 17–32, 2010.

[16] M. Gualtieri, E. Longhin, M. Mattioli et al., "Gene expression profiling of A549 cells exposed to Milan PM2.5," *Toxicology Letters*, vol. 209, pp. 136–145, 2012.

[17] E. Longhin, E. Pezzolato, P. Mantecca et al., "Season linked responses to fine and quasi-ultrafine Milan PM in cultured cells," *Toxicology in Vitro*, vol. 27, pp. 551–559, 2012.

[18] R. B. Hetland, F. R. Cassee, M. Låg, M. Refsnes, E. Dybing, and P. E. Schwarze, "Cytokine release from alveolar macrophages exposed to ambient particulate matter: heterogeneity in relation to size, city an season," *Particle and Fibre Toxicology*, vol. 2, article 4, 2005.

[19] K. F. Chung and I. M. Adcock, "Multifaceted mechanisms in COPD: inflammation, immunity, and tissue repair and destruction," *European Respiratory Journal*, vol. 31, no. 6, pp. 1334–1356, 2008.

[20] V. Hornung, F. Bauernfeind, A. Halle et al., "Silica crystals and aluminum salts activate the NALP3 inflammasome through phagosomal destabilization," *Nature Immunology*, vol. 9, no. 8, pp. 847–856, 2008.

[21] C. Dostert, V. Pétrilli, R. van Bruggen, C. Steele, B. T. Mossman, and J. Tschopp, "Innate immune activation through Nalp3 inflammasome sensing of asbestos and silica," *Science*, vol. 320, no. 5876, pp. 674–677, 2008.

[22] L. Franchi, T. Eigenbrod, R. Muñoz-Planillo, and G. Nuñez, "The inflammasome: a caspase-1-activation platform that regulates immune responses and disease pathogenesis," *Nature Immunology*, vol. 10, no. 3, pp. 241–247, 2009.

[23] M. A. Kovach and T. J. Standiford, "Toll like receptors in diseases of the lung," *International Immunopharmacology*, vol. 11, pp. 1399–1406, 2011.

[24] S. Becker, L. Dailey, J. M. Soukup, R. Silbajoris, and R. B. Devlin, "TLR-2 is involved in airway epithelial cell response to air pollution particles," *Toxicology and Applied Pharmacology*, vol. 203, no. 1, pp. 45–52, 2005.

[25] K. Schroder and J. Tschopp, "The Inflammasomes," *Cell*, vol. 140, no. 6, pp. 821–832, 2010.

[26] P. Rider, Y. Carmi, O. Guttman et al., "IL-1α and IL-1β recruit different myeloid cells and promote different stages of sterile inflammation," *Journal of Immunology*, vol. 187, no. 9, pp. 4835–4843, 2011.

[27] S. L. Cassel, S. C. Eisenbarth, S. S. Iyer et al., "The Nalp3 inflammasome is essential for the development of silicosis," *Proceedings of the National Academy of Sciences of the United States of America*, vol. 105, no. 26, pp. 9035–9040, 2008.

[28] K. D. Srivastava, W. N. Rom, J. Jagirdar, Y. I. E. Ting-An, T. Gordon, and K. M. Tchou-Wong, "Crucial role of interleukin-1β and nitric oxide synthase in silica-induced inflammation and apoptosis in mice," *American Journal of Respiratory and Critical Care Medicine*, vol. 165, no. 4, pp. 527–533, 2002.

[29] H. B. Yu and B. B. Finlay, "The caspase-1 inflammasome: a pilot of innate immune responses," *Cell Host and Microbe*, vol. 4, no. 3, pp. 198–208, 2008.

[30] W. J. Sandberg, M. Låg, J. A. Holme et al., "Comparison of non-crystalline silica nanoparticles in IL-1ß release from macrophages," *Particle and Fibre Toxicology*, vol. 9, article 32, 2012.

[31] A. S. Yazdi, G. Guarda, N. Riteau et al., "Nanoparticles activate the NLR pyrin domain containing 3 (Nlrp3) inflammasome and cause pulmonary inflammation through release of IL-1α and IL-1β," *Proceedings of the National Academy of Sciences of the United States of America*, vol. 107, no. 45, pp. 19449–19454, 2010.

[32] T. Morishige, Y. Yoshioka, H. Inakura et al., "The effect of surface modification of amorphous silica particles on NLRP3 inflammasome mediated IL-1β production, ROS production and endosomal rupture," *Biomaterials*, vol. 31, no. 26, pp. 6833–6842, 2010.

[33] E.-J. Yang, S. Kim, J. S. Kim, and I.-H. Choi, "Inflammasome formation and IL-1β release by human blood monocytes in response to silver nanoparticles," *Biomaterials*, vol. 33, no. 28, pp. 6858–6867, 2012.

[34] N. Li, T. Xia, and A. E. Nel, "The role of oxidative stress in ambient particulate matter-induced lung diseases and its implications in the toxicity of engineered nanoparticles," *Free Radical Biology and Medicine*, vol. 44, no. 9, pp. 1689–1699, 2008.

[35] J. A. Hirota, S. A. Hirota, S. M. Warner et al., "The airway epithelium nucleotide-binding domain and leucine-rich repeat protein 3 inflammasome is activated by urban particulate matter," *Journal of Allergy and Clinical Immunology*, vol. 129, pp. 1116–1125, 2012.

[36] E. J. Park and K. Park, "Oxidative stress and pro-inflammatory responses induced by silica nanoparticles in vivo and in vitro," *Toxicology Letters*, vol. 184, no. 1, pp. 18–25, 2009.

[37] R. Zhou, A. S. Yazdi, P. Menu, and J. Tschopp, "A role for mitochondria in NLRP3 inflammasome activation," *Nature*, vol. 469, pp. 221–225, 2011.

[38] A. Rubartelli, M. Gattorno, M. G. Netea, and C. A. Dinarello, "Interplay between redox status and inflammasome activation," *Trends in Immunology*, vol. 32, no. 12, pp. 559–566, 2011.

[39] M. Gualtieri, A. Franzetti, P. Mantecca et al., "In vitro effects of chemical and microbiological characterized Milan particulate matter," *Procedia Environmental Sciences*, vol. 4, pp. 192–197, 2011.

[40] M. Gualtieri, J. Øvrevik, J. A. Holme et al., "Differences in cytotoxicity versus pro-inflammatory potency of different PM fractions in human epithelial lung cells," *Toxicology in Vitro*, vol. 24, no. 1, pp. 29–39, 2010.

[41] J. L. Kang, C. Moon, H. S. Lee et al., "Comparison of the biological activity between ultrafine and fine titanium dioxide particles in RAW 264.7 cells associated with oxidative stress," *Journal of Toxicology and Environmental Health A*, vol. 71, no. 8, pp. 478–485, 2008.

[42] C. Schorn, B. Frey, K. Lauber et al., "Sodium overload and water influx activate the NALP3 Inflammasome," *Journal of Biological Chemistry*, vol. 286, no. 1, pp. 35–41, 2011.

[43] C. Alexander and E. T. Rietschel, "Bacterial lipopolysaccharides and innate immunity," *Journal of Endotoxin Research*, vol. 7, no. 3, pp. 167–202, 2001.

[44] J. A. Mitchell, M. J. Paul-Clark, G. W. Clarke, S. K. McMaster, and N. Cartwright, "Critical role of toll-like receptors and nucleotide oligomerisation domain in the regulation of health and disease," *Journal of Endocrinology*, vol. 193, no. 3, pp. 323–330, 2007.

[45] L. E. Plummer, S. Smiley-Jewell, and K. E. Pinkerton, "Impact of air pollution on lung inflammation and the role of Toll-like receptors," *International Journal of Interferon, Cytokine and Mediator Research*, vol. 4, pp. 43–57, 2012.

[46] A. Franzetti, I. Gandolfi, E. Gaspari, R. Ambrosini, and G. Bestetti, "Seasonal variability of bacteria in fine and coarse urban air particulate matter," *Applied Microbiology and Biotechnology*, vol. 90, pp. 745–753, 2011.

[47] E. Naik and V. M. Dixit, "Mitochondrial reactive oxygen species drive proinflammatory cytokine production," *Journal of Experimental Medicine*, vol. 208, no. 3, pp. 417–420, 2011.

[48] F. Bauernfeind, E. Bartok, A. Rieger, L. Franchi, G. Núñez, and V. Hornung, "Cutting edge: reactive oxygen species inhibitors block priming, but not activation, of the NLRP3 inflammasome," *Journal of Immunology*, vol. 187, no. 2, pp. 613–617, 2011.

[49] W. P. Arend, "The balance between IL-1 and IL-1Ra in disease," *Cytokine and Growth Factor Reviews*, vol. 13, no. 4-5, pp. 323–340, 2002.

[50] M. Strak, N. A. H. Janssen, K. J. Godri et al., "Respiratory health effects of airborne particulate matter: the role of particle size, composition, and oxidative potential—the RAPTES project," *Environmental Health Perspectives*, vol. 120, no. 8, pp. 1183–1189, 2012.

Hindawi Publishing Corporation
BioMed Research International
Volume 2013, Article ID 521728, 13 pages
http://dx.doi.org/10.1155/2013/521728

Research Article

Air Pollutant Characterization in Tula Industrial Corridor, Central Mexico, during the MILAGRO Study

G. Sosa, E. Vega, E. González-Avalos, V. Mora, and D. López-Veneroni

Investigación y Posgrado, Instituto Mexicano del Petróleo, Eje Central Lázaro Cárdenas Núm 152 Colonia San Bartolo Atepehuacan, Delegación Gustavo A. Madero, 07730 México, DF, Mexico

Correspondence should be addressed to E. Vega; evega@imp.mx

Received 4 September 2012; Revised 22 November 2012; Accepted 6 December 2012

Academic Editor: Ernesto Alfaro-Moreno

Pollutant emissions and their contribution to local and regional air quality at the industrial area of Tula were studied during a four-week period as part of the *MILAGRO* initiative. A recurrent shallow stable layer was observed in the morning favoring air pollutants accumulation in the lower 100 m atmospheric layer. In the afternoon the mixing layer height reached 3000 m, along with a featuring low level jet which was responsible of transporting air pollutants at regional scales. Average PM_{10} at Jasso (JAS) and Tepeji (TEP) was 75.1 and 36.8 $\mu g/m^3$, respectively while average $PM_{2.5}$ was 31.0 and 25.7 $\mu g/m^3$. JAS was highly impacted by local limestone dust, while TEP was a receptor of major sources of combustion emissions with 70% of the PM_{10} constituted by $PM_{2.5}$. Average hourly aerosol light absorption was 22 Mm^{-1}, while aerosol scattering (76 Mm^{-1}) was higher compared to a rural site but much lower than at Mexico City. $\delta^{13}C$ values in the epiphyte *Tillandsia recurvata* show that the emission plume directly affects the SW sector of Mezquital Valley and is then constrained by a mountain range preventing its dispersion. Air pollutants may exacerbate acute and chronic adverse health effects in this region.

1. Introduction

Recent research initiatives in Mexico have focused on the measurement of air pollutants, with particular emphasis on ozone and suspended particles, with the objective of establishing pollution controls on most industries. Major studies in central Mexico include the *Mexico City Air Quality Research Initiative* (MARI) in 1990 [1], the *Investigacion sobre Materia Particulada y Deterioro Atmosferico-Aerosol and Visibility Evaluation Research* (IMADA-AVER) in 1997 [2], the *MCMA-2003* [3, 4], and the *Megacity Initiative: Local and Global Research Observations* (MILAGRO) in 2006. As part of the MILAGRO project, atmospheric pollutant concentrations and chemical composition were measured intensively in Tula (in the State of Hidalgo) during four weeks to determine the potential impact of contaminant emissions of Tula on the northern sector of Mexico City.

Mezquital Valley, localized some 60 km northwest of Mexico City Metropolitan Area (MCMA), is site of the Tula-Vito-Apasco industrial corridor where intensive anthropogenic activity, including oil refining, electrical generation, limestone extraction, and cement, textile and chemical production take place. In this site, both the biggest refinery in Mexico and the adjacent thermoelectric power plant use fuel oil, and it has been estimated that together they contribute with over 90% of the pollution in the valley [5, 6]. Characterization of suspended particles in the area has shown an important contribution of soil fugitive dust by agricultural activity and limestone mincing; and particle emissions from the refinery and thermoelectric power plant complex (RTPPC) covering a considerable area regardless of wind direction [6]. Additionally, the cement industry contributes with particle emissions during material extraction in open pit mines, mincing, transportation, and high temperature incineration. The SE and NE sectors of the valley are used for agriculture, most of which is irrigated with residual waters from MCMA via the Tula River. Overall, the valley is site of considerable soil, water, and air pollution.

Several lines of evidence have associated air pollution with health effects. A direct correlation between particulate matter (PM) concentration and cardiovascular and respiratory diseases have been demonstrated [7, 8]. Recent studies

have shown positive association of PM chemical composition and mortality [9, 10]. Epidemiological and toxicological studies found that the cytokine secretion patterns are influenced by the size and chemical composition of PM in Mexico City [11, 12]. A recent study evaluated the association between PM and cases of mortality, acute respiratory infections, and asthma in the Tula-Tepeji region [13].

The high emissions, complex topography, wind circulation, and its closeness to MCMA have prompted the monitoring and modeling of plume dispersion from the Miguel Hidalgo Oil Refinery and the Francisco Perez Rios Power Plant and their effects on the northern sector of the MCMA. In particular, it has been estimated that nearly 50% of the SO_2 concentrations in MILAGRO Supersite T1 (NE Mexico City) are attributable to these two industries [5, 14, 15]. A similar influence of other contaminants would thus be expected.

This paper documents a four-week daily data set on the concentrations of $PM_{2.5}$, PM_{10}, submicrometric particles, black carbon, light scattering, and criteria contaminants in addition to meteorological variables to further support the characterization of Tula emissions as a potential source of pollutants to Mexico City and nearby cities (Tepeji and Jasso). In addition, stable carbon isotopes in the epiphyte *Tillandsia recurvata* collected in Mezquital Valley during the study are used here as a proxy of the long-term trajectory of the emission plume.

2. Study Area and Experimental

2.1. Sampling Sites and Measurements. The Miguel Hidalgo refinery is the second largest refinery in Mexico, processing 3×10^5 barrels of crude oil per day, and it supplies the 50×10^6 liters per day of gasoline-equivalent (all fuels included) to Mexico City [16]. In turn, the Francisco Pérez Ríos power plant has 1.5 GW of capacity and it mainly supplies the electricity demand for Central Mexico. The power plant has four major units fueled primarily by fuel oil (4% sulfur by weight) and five small combined cycle units burning natural gas. In comparison, urban emissions due to transport and service/commerce activities in nearby localities (Tula de Allende, Atotonilco, Atitalaquia and Tepeji) represent a small contribution to local air pollution [17].

Three sampling sites within the Tula-Vito-Apasco corridor were selected to measure PM, and upper and surface meteorological parameters (Table 1).

2.1.1. Tula (TUL) Upper Air Monitoring Station. Tula (TUL) located inside the Instituto Mexicano del Petróleo facilities adjacent to the refinery (99.27°W, 20.05°N). This site was selected as an upper air monitoring station to determine the diurnal evolution of the mixing height (MH) as well as other meteorological variables, such as wind direction (WD) and wind speed (WS). These variables are essential in air quality studies to determine the vertical extension in which pollutants are mixed, dispersed, and transported [18].

A Vaisala radiosonde system (Model SPS-220) was used for upper air sounding measurements of pressure, temperature, relative humidity, and the horizontal wind vector, at different altitudes. Vertical profiles were determined by launching four rawinsondes everyday at 08:00, 12:00, 15:00, and 18:00 h CST. Additionally, surface meteorological parameters, temperature (T), ambient pressure (P), relative humidity (RH), wind direction (WD), wind speed (WS), and solar radiation (SR) were also measured using a regular meteorological station. These measurements took place from 18 March to 17 April, 2006.

Table 1: Equipment deployed at each site and frequency of measurements.

Equipment	Site	Frequency
Rawinsondes	TUL	8, 12, 15, 18 h
Surface meteorology	TUL, JAS, TEP	6 min
Minivols ($PM_{2.5}$, PM_{10})	JAS, TEP	24 hrs
Denuders	JAS, TEP	24 hrs
SMPS + DMA	JAS	15 min
Nephelometer	JAS	1 min
Aethalometer	JAS	1 min
Criteria pollutants (CO, O_3, NO_2, SO_2)	JAS TEP	1 min
MiniDOAS	Mobile	Continuous
Pilot balloons	TUL	1 hr from 10 to 18 h

SMPS: scanning mobility particle sizer; DMA: differential mobility analyzer.

2.1.2. Jasso (JAS) and Tepeji (TEP) Surface Stations. JAS and TEP were considered as core sites where several equipments were installed to simultaneously measure criteria pollutants (CO, NO_2, O_3, and SO_2), PM, and submicrometric particles. These sites are influenced by both urban and major industrial sources. JAS (99.31°W, 20.02°N) is located about 5 km SW from the refinery and the power plant, whereas major urban intercounty heavy traffic roads are located south and west. This site is close to a major limestone area where mining for cement materials occurs. TEP (99.29°W, 19.86°N) is located 21 km S away from the refinery, far from urban areas but close to a major highway. This site is also close to the major cement plant and near limestone mining areas.

2.2. Meteorology and Criteria Pollutants. Surface meteorological parameters and criteria pollutants were measured from 22 March to 21 April 2006 at TEP, and from 25 March to 22 April at JAS. Measured variables included temperature, pressure, relative humidity, wind speed and wind direction, and SR (T, P, RH, WS, WD, and solar radiation, resp.). Criteria pollutants were measured using a mobile laboratory equipped with conventional analyzers (Monitor Labs). Methods used to determine criteria pollutants were NOM-034-SEMARNAT-1993 using dispersive spectroscopy for CO, NOM-037-SEMARNAT-1993 using chemoluminescence for NO_x, USEPA-EQOA-0193-091 using UV photometry for O_3, and USEPA–EQSA-0193-092 using pulse fluorescence for SO_2.

2.3. Particulate Matter (PM). PM samples were collected daily from 00:00 to 24:00 h using portable low volume MiniVol samplers (Airmetrics, Springfield, USA) at a flow

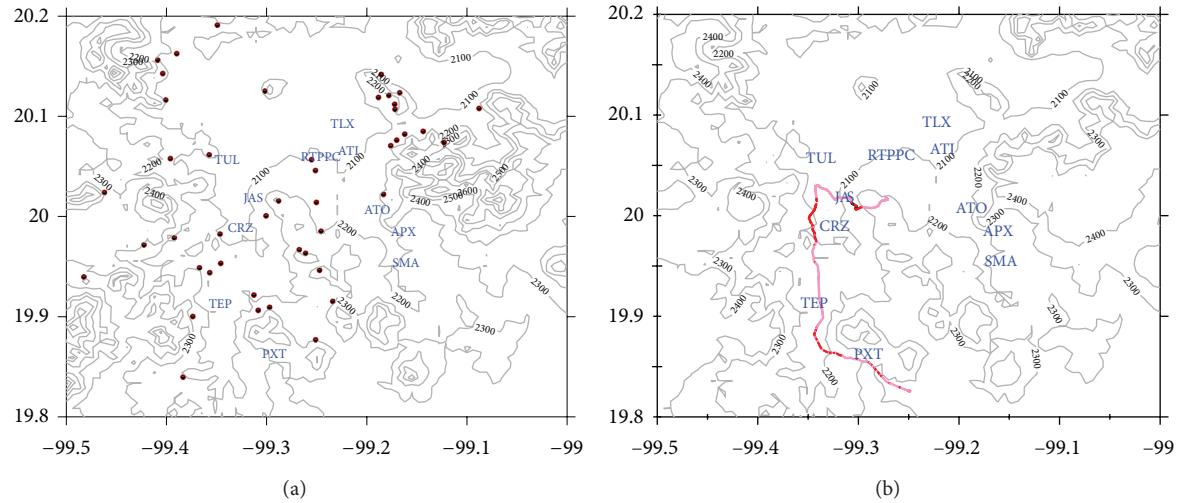

Figure 1: (a) Mezquital Valley topography with sampling sites (circles), major population centers, and the refinery-thermoelectrical plant complex. (b) Trajectory of the SO_2 dispersion plume in SE direction observed on April 4, 2006 at 16:00 and 17:00 hours. APX: Apaxco, ATO: Atoyac, ATI: Atitalaquia, CRZ: Cruz Azul, JAS: Jasso; PXT: PEMEX gas substation; RTPPC: refinery thermoelectrical power plant complex; SMA: Santa María Apaxco; TEP: Tepeji; TLX: Tlaxcoapan; TUL: Tula.

rate of 5 L/min, previously calibrated at standard conditions. In addition sequential filter samplers (SFS) equipped with $PM_{2.5}$ (Bendix 240 cyclones) and PM_{10} (Andersen SA254) samplers operated at a flow rate of 113 L/min were used to collect 12-hour samples (06:00 to 18:00 and from 18:00 to 06:00). Samples were collected on 47 mm Teflon-membrane (Pall Gelman Laboratory, Ann Arbor, MI, USA) and quartz-fiber filters (Pallflex Gelman Sciences CT, USA). Teflon filters were used for mass, trace element analyses, and for light transmission, whereas quartz filters were used for ion and elemental and organic carbon analyses [19].

2.4. Submicrometric Particles and Optical Properties. Light scattering coefficients were measured with an integrating nephelometer (Model 3563 TSI, Inc.) operating at 450, 550, and 700 nm. Submicrometric particle surface distribution was obtained with a scanning mobility particle sizer (SMPS) (Model 3936 TSI, Inc.). Black carbon mass concentrations were measured with an aethalometer (Model AE-16 Magee Scientific, Co) operating at 880 nm.

2.5. Stable Carbon Isotopes. Long-term atmospheric deposition patterns for selected trace metals, PAHs, and stable carbon isotopes covering an area of 4000 km^2 were determined with samples of ball-moss (*Tillandsia recurvata*) at 50 sites as atmospheric biomonitors. These patterns reflect the long-term air pollutant transport from the oil industry and other economic activities in Mezquital Valley according to the prevailing winds. This moss satisfies basic attributes of a biomonitoring organism, such as its widespread occurrence in the valley, and its dependence on atmospheric nutrients and humidity [20, 21]. Therefore metal, PAHs, and stable carbon isotope composition in this species serve as proxies of atmospheric emissions impact at different distances from the emission source. In this paper, stable carbon isotopes in *T. recurvata* were used as a tracer of long-term signature of the plume trajectory. Metals, stable isotopes, and PAHs in *T. recurvata* are described by Zambrano García et al. [22] to show the signature source of the principal emitters in Mezquital Valley.

Total flux emissions and tracking of the SO_2 plume were determined at major sources in the region to identify transport pathways towards Mexico City under different meteorological conditions using a mobile Differential Optical Absorption Spectroscopy (MiniDOAS) system. Details of the technique and results are described by Rivera et al. [5].

Figure 1 shows the sites where *T. recurvata* were sampled in the vicinity of the refinery and thermoelectric power plant complex (RTPPC), which is located nearby several small towns, at an altitude of around 2100 m above sea level. Note the mountain chain to the E-SE of the RTPPC which rises approximately 400 m above the valley. Winds measured in March to April, 2006 [22], and October to December, 2008 [23] in the region show highest speeds when coming from the NE and SW quadrants. Figure shows the SO_2 concentrations measured along the miniDOAS path.

3. Results and Discussion

3.1. Meteorology

3.1.1. Synoptic Overview. Field measurements and large-scale analysis showed that local meteorological conditions and air pollutants transport were affected by the synoptic systems development. Detailed descriptions on meteorological conditions during the MILAGRO campaign are reported by Fast et al. [24]. Three major synoptic-scale systems were observed during the field campaign. The more frequent events were high-pressure systems, remaining quasi-stationary at central Mexico, followed by troughs and rides

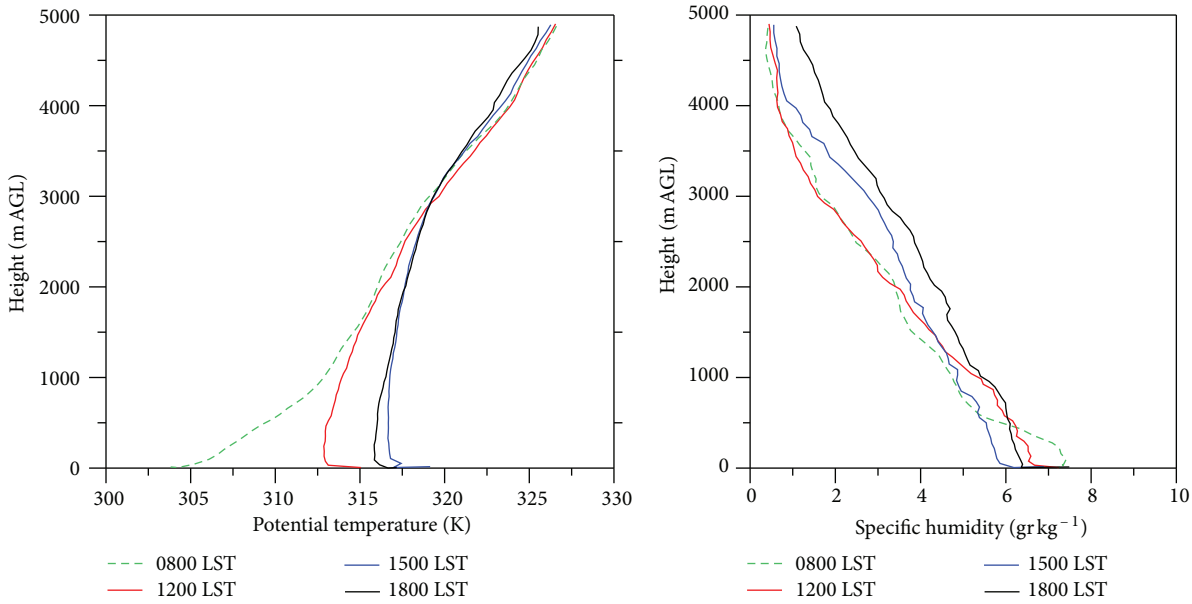

Figure 2: Mean potential temperature (a) and specific humidity profiles (b) at Tula.

passages at south-central U. S. Cold surges. The third and least frequent system was cold surges (northern) influencing mainly the coast line at Gulf of Mexico and was also present during the study period. Both during early March and on March 18-19, upper-level troughs propagated through south-central U. S. producing strong southwesterly winds in the central plateau. Two cold surges were observed on March 22 and 24–26 causing strong northerly near-surface flow over the Gulf of Mexico. High-pressure systems predominated during the remaining sampling days, and were typical characterized by clear skies, low humidity, and weak winds.

Winds below the mixing layer at 700 hPa (1000 m above ground level) were variable according to the dominant synoptic system in the region. Westerly and southwesterly winds were associated to a trough pass; northerly and easterly winds to high-pressure systems slowly moving from northwestern Mexico towards the east, and strong northerly near-surface flows over de Gulf of Mexico were associated to cold surges. The frequency of upper wind direction at 500 hPa measured at 06:00 h were 45.2% southwesterly, 35% westerly, 13% northeasterly, and 3.2% corresponding to south and northwesterly winds. Daily maximum surface temperature was over 22°C most of the days; however, during the period of March 24–26, during a cold surge passage, temperature dropped to 18°C. Surface wind speeds, varying from light to moderate, were observed throughout the study.

3.1.2. Height of the Boundary Layer. Figure 2 shows the mean potential temperature and specific humidity profiles for the field campaign. The profiles were obtained averaging all radiosonde data available at each launch time. During most of the sampling period (80% of the time), a stable layer was observed at 08:00 h, with the occasional presence of near-surface thermal inversions; by noon, when solar heating breaks the stable layer, a well-developed mixing layer reached up to 2000 m above ground level (AGL), with a shallow superadiabatic layer near the surface. Although potential temperature profiles were similar above 500 m at 15:00 and 18:00 h, the colder temperatures at 18:00 h, indicated the formation of a stable layer close to the surface (Figure 2(a)). Specific humidity profiles showed a reduction of water content with height, and a well-mixed atmosphere after the breakup of the stable layer. The difference on the water vapor content among vertical profiles was less than 4.0 g/Kg throughout the study (Figure 2(b)).

Data analysis of the radiosonde data showed that the mixing layer height (ML) varied significantly from 2500 to 4200 m AGL, reaching its average diurnal maximum at 15:00 h. When a strong cold surge entered Central Mexico during March 24-25, the ML decreased to less than 500 m AGL, due to a reduction in the solar radiation as a consequence of cloudy skies and scattered rain.

3.1.3. Mean Wind Profiles at the Boundary Layer. Figure 3 gives the mean wind profiles calculated from rawinsondes data during the field campaign at 08:00, 12:00, 15:00, and 18:00 hs. The horizontal lines represent variations with height of the wind persistence, defined as the ratio of the vectorial mean wind speed to scalar wind speed. Ratios close to one indicate almost no change in wind direction; on the contrary, values close to zero indicate a large variation in wind direction.

Figure 3(a) shows a highly variable and stratified atmosphere at 08:00 h. The change in wind persistence with height varied from less than 0.2 to greater than 0.6, being more stable at heights lower than 100 m AGL and above 5000 m

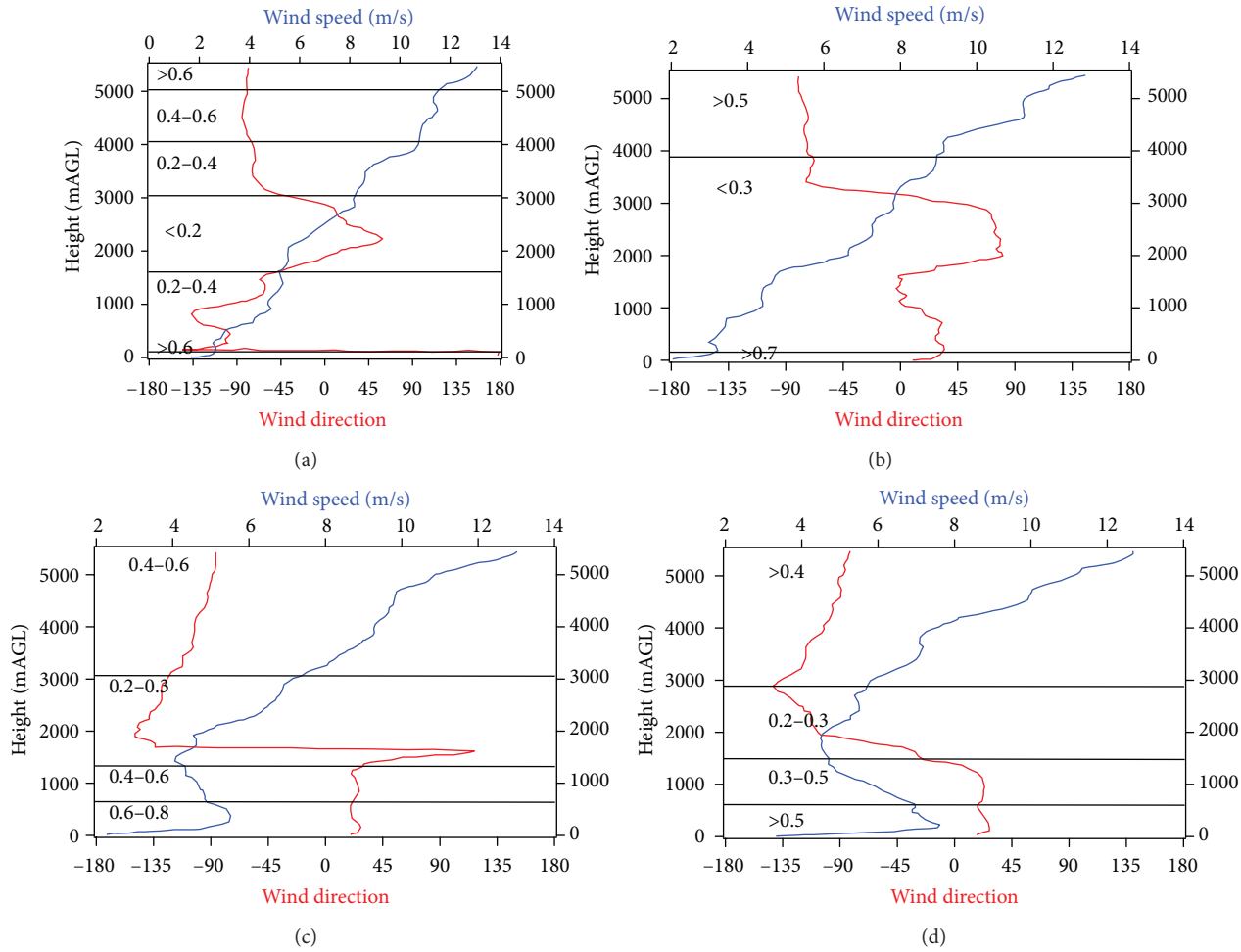

Figure 3: Mean wind profiles at Tula, during March-April, 2006. Horizontal lines represent the wind persistence value.

AGL. Near-surface southerly to southwesterly winds were observed regularly along the field campaign. At 12:00 h, a less stratified atmosphere was observed, although a varying wind speed layer, from 300 m to 4000 m AGL, still remained (Figure 3(b)). Below 1500 m AGL, northeasterly wind speed was more stable; however, wind speed increased constantly and therefore the wind persistence was low, reflecting the ML evolution into a well-mixed layer. At 15:00 h, the wind persistence ratio ranged from 0.2 to 0.86 under the lowest 5000 meters of the troposphere, although a clearly more homogeneous mixing layer was observed (Figure 3(c)). Below 1500 m, the mean northeasterly wind remained constant, and the wind speed profile shows a northeasterly jet near the surface, with a maximum value close to 6 m/s at 500 m AGL. Figure 3(d) shows the mean wind profile at 18:00 h, which is similar to the wind profile at 15:00 h, but with more variability in wind direction and with a stronger jet closer to the ground (at 250 m and maximum velocity of 7 m/s).

In summary, early in the morning (8:00 h), a shallow stable layer formed near the surface, with light south-southwesterly winds. These conditions favored the accumulation of air pollutants below 100 m with a limited dispersion towards the north Tula industrial complex. After midday, a well-developed mixing layer favored the mixing of pollutants at higher altitudes (up to 5000 m AGL). Simultaneously, a near-surface superadiabatic layer, with a clear northern wind component, brought back the previously-advected pollutants. In the afternoon and evening a thicker mixing layer reached on average 2500 to 3000 m height, featuring a weak low level jet (LLJ) near the surface. This LLJ was responsible of transporting air pollutants at regional scales. According to the authors' knowledge, this is the first time this feature is reported for the region.

LLJ can develop under favorable synoptic conditions anywhere in the world. This pattern is characterized by space scales between 20 and 200 km within the lowest 2000 m of the atmosphere, where strong diurnal oscillations and nocturnal accelerations occur [25]. The development of LLJ is associated with nocturnal temperature inversion, forming in the late afternoon or early evening and becoming strongest during the early morning hours of the next day, and then weakening or disappearing by late morning. From Figures 2(a), 3(c), and 3(d), it is clear that temperature and wind profiles fulfill these requirements. Although no early-morning sounding was available to corroborate that, maximum wind speed occurred at this time.

Table 2: Average, maximum, and minimum of 24 h and 12 h of PM_{10} and $PM_{2.5}$ during the sampling period of March 24–20 April, 2006.

	Jasso			Tepeji		
	Average	Maximum	Minimum	Average	Maximum	Minimum
$PM_{2.5}$ 24 h	31.0	52.0	14.3	25.7	53.1	14.5
$PM_{2.5}$ 06:00–18:00	45.5	70.3	18.2	35.5	75.1	16.8
$PM_{2.5}$ 18:00–06:00	31.0	59.2	10.3	24.9	37.6	12.0
PM_{10} 24 h	75.1	178.6	30.4	36.8	53.2	22.4

Implications of these meteorological conditions on human health are evident. First, the persistent stable atmospheric conditions in the morning favor the concentration of pollutants near ground, increasing the level of exposure of the inhabitants. This condition may worsen at winter time, when lowest temperatures drop below 0°C. On the other hand, the regional transport of pollutants increases the number of people exposed to these air pollutants. These results are in agreement with those recently reported by Almanza et al. [15]. By using dispersion models, the authors estimated the fraction of time at which the RTPPC plume hits the surface in the full domain. Regardless the concentration at which the plume reaches the ground, the impact on the Mexico MCMA may be 40% to 60% of the time [15].

3.2. Criteria Pollutants. Air quality standards (AQS) at JAS such as ozone (0.11 ppm, average of 1 h), carbon monoxide (11 ppm mobile average of 8 h), sulfur dioxide (0.13 ppm average of 24 h), and nitrogen dioxide (0.210 ppm, average of 1 h) were not exceeded [26]. Maximum hourly values were 0.034, 0.033, and 0.287 ppm for O_3, NO_2, and CO, respectively. The maximum average of 24 h for SO_2 was 0.0078 ppm, on April 5, even though this pollutant increased to 0.293 ppm at midday on April 14.

The results at TEP showed that CO and NO_2 concentrations were below their corresponding AQS values. However, the SO_2 exceeded the standard twice, on March 26 with 0.185 ppm, and April 14 with 0.190 ppm. O_3 also exceeded the standard during the April 27 with 0.122 ppm. In general, this site showed higher concentrations of SO_2 when compared to JAS, with maximum hourly values between 0.100 and 0.300 ppm.

Most of the SO_2 is released from the refinery and the RTPPC facilities at a height of 60 m above ground level, although the effective height of the emissions may rise above 1000 m, due to buoyancy provided by hot exhaust. Under these conditions, the emission plume travels long distances downwind before reaching the ground, which is in agreement with mini-DOAS measurements reported by Rivera et al. [5]. Sites located nearby the source are below the plume and thus report lower SO_2 concentrations when compared to those farther from the plume source (Figure 1(b)).

3.3. Particulate Matter (PM). Table 2 summarizes the PM10 24 h average concentrations during the sampling period for March 24-April 20, 2006. Also the 24 h average $PM_{2.5}$ concentrations during March 24-April 6, 2006 and 12 h average $PM_{2.5}$ concentrations during April 7–20, 2006 were given at standard conditions. In general, PM concentrations measured at the JAS urban-industrial site were higher than at TEP, which may indicate the magnitude of local limestone dust resuspension from quarrying. Particle contribution at this site is exacerbated by the cement industry which is also a heavy user of residual fuel oil, petroleum coke, and an assortment of industrial wastes.

PM mass concentrations oscillated substantially from day to day at both sites. The most extreme variations occurred at JAS in the PM_{10} fraction and PM_{10} levels at JAS showed considerably variations from 30.4 to 178.6 $\mu g/m^3$ with an average of 75.1 $\mu g/m^3$; the 24 h average of 120 $\mu g/m^3$ [27] was exceed twice during the study. While $PM_{2.5}$ ranged between 14.3 to 52.0 $\mu g/m^3$ with an average of 31.0 $\mu g/m^3$, the $PM_{2.5}$ standard of 65 $\mu m/m^3$ was not exceeded during the sampling campaign. High PM_{10} concentrations were observed on April 8 and 11 with values of 162.2 and 178.6 $\mu g/m^3$, respectively. Those two days had light wind speed in the morning (<1.56 m/s) with variable wind direction. After 10:00 h, southwest winds became more stable and increased their speeds to a maximum of 8.0 m/s at 18:00 h. On these days, the corresponding $PM_{2.5}$ mass concentrations (49.5 and 36.7 $\mu g/m^3$, resp.) were less than one-third of the PM_{10}, which is less than the $PM_{2.5}/PM_{10}$ average ratio of 0.41, and suggests that elevated PM_{10} concentrations can be attributed to local fugitive dust. Similar temporal variations of $PM_{2.5}$ mass concentrations were observed from March 26 to April 3 with a smooth increase from and with two peaks on the same dates as PM10. Similar PM10 levels were reported by Querol et al. [28] in the urban area of Mexico City with 24-hour averages ranging between 50 and 56 $\mu g/m^3$, and $PM_{2.5}$ between 24 and 40 $\mu g/m^3$; however, these values were measured during March as a part of the MILAGRO campaign and cannot be compared directly with our observations.

At TEP PM_{10} concentrations were higher during a longer period of time (April 5–13). In general, during April winds were light (2 m/s) and variable in average, although maximum daily speeds ranged from 7 to 9 m/s. During April 5–13, higher wind speeds were recorded compared to the period of April 14 to 19, where lower PM concentrations were observed, due to more stable wind conditions. Wind directions were variable before 8:00 h, were persistent from southeast until noon, and changed direction from northeast in the evening. PM_{10} concentrations at TEP ranged from 22.4 to 53.2 $\mu g/m^3$ with an average of 36.8 $\mu g/m^3$, while $PM_{2.5}$ varied between 14.5 to 53.1 $\mu g/m^3$ with an average of 25.7 $\mu g/m^3$. Although the fine fraction at both sites were

similar, the difference was driven by the PM_{10} fraction as the $PM_{2.5}/PM_{10}$ mass ratio ranged from 0.85 to 0.50 with an average of 0.68 indicating that this site is a receptor of the industrial emissions from the major sources of combustion processes.

The $PM_{2.5}/PM_{10}$ ratio at JAS is similar to those reported by Vega et al. [19] for Mexico City (0.46), and for the industrialized area of Salamanca (0.33) in Guanajuato [29], where the contribution of fugitive dust is considerable.

$PM_{2.5}$ was consistently higher during the morning periods (06:00–18:00h), with average values of 35.5 and 45.5 $\mu g/m^3$, and decreased during the night (18:00–06:00 h) to 24.9 and 31.0 $\mu g/m^3$ at TEP and JAS, respectively. This is consistent with a recurrent shallow stable layer formed near the surface before 8:00 h and light winds favoring particle accumulation. At TEP maximum concentrations of 75.1 and 37.6 $\mu g/m^3$ occurred in April 11 and 16 for morning and night, respectively. In contrast, JAS maximum concentrations were measured in the morning of April 8 (70.3 $\mu g/m^3$) and at night on April 7 (59.2 $\mu g/m^3$).

The aforementioned pattern is in agreement with the continuous black carbon measurements which were influenced by fresh emissions from major industrial combustion sources (Figures 4 and 7). Similar patterns were also reported for Mexico City during the same period of sampling [28]. It should be mentioned that carbonaceous aerosols, specifically black carbon, are the major absorbing aerosol species which may have an important warming impact at a regional scale. The aethalometer used to measure black carbon takes into account the flow rate, time, and a factor for the multiple scattering enhanced mass absorption efficiency [30].

There was a significant difference between both sites in the coarse fraction (PM_{10}-$PM_{2.5}$), JAS being the mostly impacted by particles resulting from local limestone dust from quarrying, as it ranged from 40 to 79% with an average of 56%. At TEP this fraction varied from 15 to 50% with an average of 32%,. These results are consistent with higher emission from fossil fuel combustion processes from the RTPPC), among other sources in the vicinity of TEP (21 km south from the sources). In turn, Querol et al. [28] reported 50% of coarse fraction at CENICA, similar to JAS, while the urban T0 site had a lower contribution of coarse fraction (30%), similar to TEP.

The incidence of respiratory diseases is higher in Tula than in any other area within Hidalgo State. Specifically, the central area of Tula the incidence of acute respiratory infections is the highest within Mexico [31]. In addition, Melgar-Paniagua et al. [13] reported that there is an association between PM concentration and the increase of respiratory morbidity and mortality in Tula. Furthermore, there is evidence that exposure to ambient PM chemical components, such as sulfate, metals, elemental, and organic carbon, is associated with adverse health outcomes [32, 33].

Results from chemical analysis, which will be presented in a future publication, showed that at JAS the higher concentrations of PM_{10} were driven by Ca, whilst in Mexico City the higher PM_{10} concentrations were correlated with Si [19]. High Ca concentrations are mainly due to limestone mining

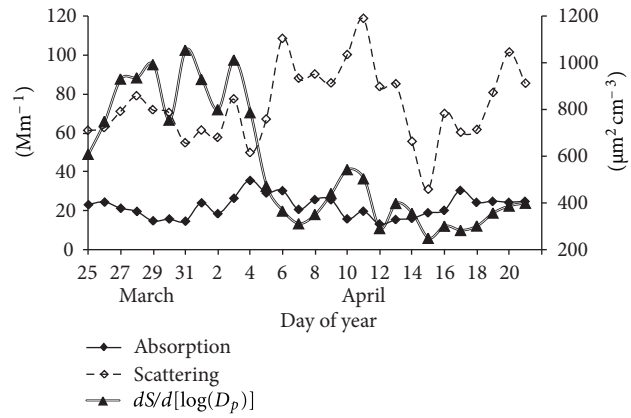

Figure 4: Daily aerosol light absorption and scattering obtained at 550 nm, and submicrometric particles surface distribution, at JAS from March 25 to April 21, 2006.

for cement materials and limestone quarries nearby JAS and in the surroundings of Tula [22]. This contrasts with Si-associated PM_{10}, which result from dust resuspension from the dry Texcoco Lake in Mexico City [19]. Higher Ca concentrations and in some cases also high $SO_4^=$ concentrations were also correlated with $PM_{2.5}$. Sulfates showed a gradually increase at TEP starting on April 9 and showed a peak on April 12. The results of the radiosonde data analysis, below 1000 m which is the maximum mixing layer height during the day, confirm that on April 12, there were persistent winds all day coming from north and northeast with an average velocity ranging from 4 to 9 m/s with direct influence from limestone quarries located upwind. On the other hand, Ca generally showed a similar pattern to PM_{10} mass with peaks driven by high Ca concentrations. On April 16, however, low Ca concentrations and high PM_{10} values were observed. A deeper mixing layer was developed on that day, reaching 3.5 km. Winds were lighter and its direction changed early in the morning from south to west at noon, and then in the afternoon from north to east in the evening. This suggests that different emission sources contributed to high particle concentration, including those from agricultural activities, where Si is abundant.

3.4. Optical Properties. Light scattering, absorption, and surface size distribution represent different physical properties of particles and no direct comparison among them is always possible; however, all these parameters are a function of particle size and an analysis of its behavior can give an insight from the origin of particles.

3.4.1. Light Scattering. Figure 4 shows the daily light scattering distribution determined with a nephelometer at 550 nm. In general, a large variability was observed along the sampling period with high light dispersion episodes observed on April 6–8 and April 11–13 when low mixing heights were observed. After April 15 the scattering values decreased to background values. Similar trends for 450 and 700 nm wavelengths were observed (not shown). This high dispersion associated with

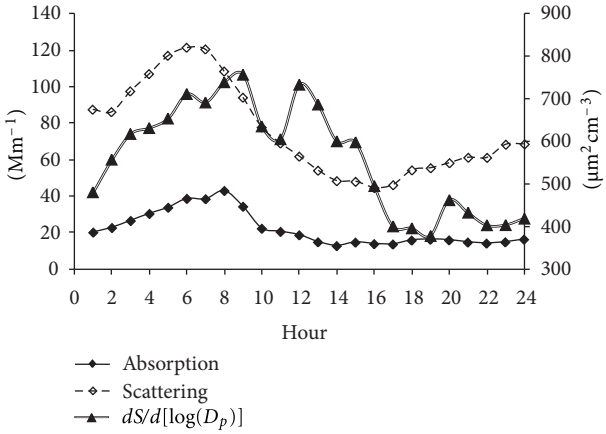

Figure 5: Hourly aerosol light absorption and scattering obtained at 550 nm; submicrometric particles surface distribution at JAS from March 25 to April 21, 2006.

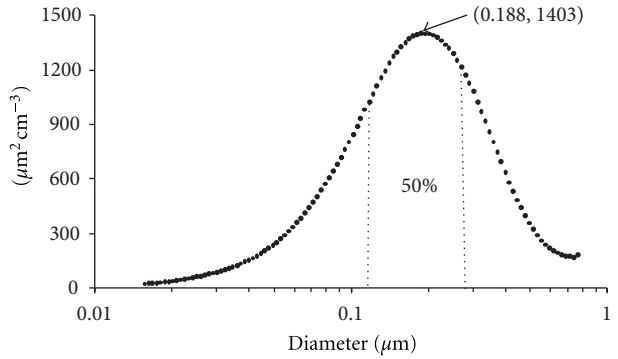

Figure 6: Submicrometric particles surface distribution by size, at JAS from March 25 to April 21, 2006.

low mixing heights is consistent with pollutant concentration near the surface. In contrast, a decrease in light scattering, and thus a greater visibility occurred when mixing heights were greater.

Since Tula is classified as a "critical area" due to the high SO_2 and PM emissions, it should also be expected to have high $SO_4^{=}$ concentration. Sulfate is an important light scattering aerosol species contributing to atmospheric cooling, formed from the atmospheric oxidation of SO_2 [30].

The hourly aerosol scattering at JAS, at 550 nm ranged from 44–121 Mm^{-1} with an average of 76 Mm^{-1}. When compared to the rural site of Tecamac (53 Mm^{-1}) located 29 Km northeast of Mexico City, this value was higher by a factor of 1.4, but much lower than the urban area of Mexico City (105 Mm^{-1}) reported by Marley et al. [34] during March 10–29, 2006. Light scattering is clearly an important factor during the night and before 10:00 h, with a substantial reduction afterwards (Figure 5).

Higher scattering values, due to a persistent shallow stable atmospheric layer which traps most primary pollutants emitted below 500 m (Figure 2), were observed at night and before 10:00 in the morning, reaching a maximum at 7:00 with values as high as 121 Mm^{-1}, 3.5 hours earlier than the maximum scattering values seen at Mexico City [34] suggesting a rapid secondary aerosol formation. After 10:00 h, a decrease of scattering values was observed due to the development of the mixing layer favoring the dilution of air pollutants.

3.4.2. Submicrometric Particles. Figures 4–6 show the submicrometric particle surface size distribution (dS/d[log(D_p)]), calculated by the SMPS system assuming spherical particles with diameters (D_p) from 15.7 to 764 nm, measured at JAS from March 24 to April 21, 2006. In general, highest values were observed during March 26 to April 5 (Figure 4). The hourly highest values were observed between 6:00 and 9:00 h and after noontime (12:00 to 15:00 h) (Figure 5). Particles with diameters between 0.118 and 0.269 μm contributed with 50% of the total particle surface size distribution. Particles smaller than 0.118 μm and higher than 0.269 μm contributed with 25% each (Figure 6). Implications of exposure to these particles on human health are presented by Buonanno et al. [35, 36], which studied average particle number size distribution data together with the people activity pattern to estimate the tracheobronchial and alveolar dose of submicrometer particles for different population age groups and under different exposure microenvironments in Italy.

3.4.3. Black Carbon. An absorption Angstrom exponent of 1 [34–38] was applied to the calculation of attenuation to determine its dependence with wavelength. Since almost all fresh emissions in this region come from the combustion of fossil fuel at the refinery and the power plant then the specific attenuation of 14625/λ [37] was used to convert black carbon concentrations measured at 880 nm and be able to compare to results of aerosol absorption at 550 nm measured at the same period reported by Marley et al. [34].

Figure 7 shows that the highest concentration of BC from 2:00 to 11:00 h is coincident with the reciprocal of wind speed (1/WS) peak. There is an increase of 10.3%/h of BC concentrations from 1:00 to 8:00 h, and a decrease of 4.2%/h of the 1/WS, suggesting that fresh emissions have a major effect than the light wind speed (1.36 to 1.85 ms^{-1}); furthermore, the boundary layer was stable favoring stagnation of pollutants. From 09:00 to 18:00 h, both BC and 1/WS decrease at a similar rate of 15 and 12%/h, respectively. During this period the mixing layer is more important than either the fresh emissions or the wind speed. From 19:00 to 24:00 h, the air parcel stagnation increased 22%/h meanwhile BC increased only 0.6%/h, so neither the fresh emissions nor the wind speed or the mixing layer were dominant for determining the levels of BC.

Figures 4 and 5 show the daily and hourly aerosol light absorption measured at 880 nm and corrected to 550 nm at JAS from March 24 to April 21, 2006. In general, there was a continuous increase during the first hours of the day, from 01:00 to 08:00 h, and then there was a decrease from 9:00 to 14:00 and from 15:00 to 24:00 h, there was an average absorption of 15 Mm^{-1}. On a daily basis, highest absorptions were observed during April 4–6 with up to 36 Mm^{-1} (Figure 4) which correlates with an excess of liquid products flaring in

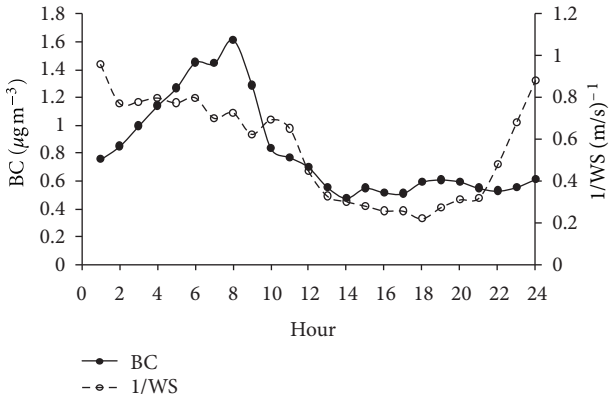

Figure 7: Hourly average black carbon (BC) concentration and reciprocal wind speed (1/WS).

the refinery due to a failure in a process that lasted two days. The highest absorption reached 43 Mm^{-1} between 2:00 and 9:00 h (Figure 5). The hourly aerosol light absorption varied between 13–43 Mm^{-1} with an average of 22 Mm^{-1} which is smaller compared to both values at Mexico City (37Mm^{-1}) and Tecamac (27 m^{-1}) reported by Marley et al., [34]. The lower light absorption at Tula compared to both sites results from the single point source behavior of the industrial complex; therefore the plume sweeps the region out according to local winds, and not always reaching the monitoring device. In addition, Marley et al. [39] observed large amounts of biomass burning contributing to carbonaceous aerosols at Tecamac and that Mexico City was significantly impacted by emissions from fossil fuels in addition to local and regional burning.

3.5. Tula-Vito-Apasco Industrial Corridor SO_2 Export. Nearly 20 plume transects were measured with a 3 to 8 h time-spam, for an equivalent distance of 120 to 320 km. The SO_2 plume direction was variable during the period of study, mostly affected by meteorology at synoptic scale. The plume's most frequent direction was from southeast after midday, when the wind at the surface was from NNE. Under this condition, the SO_2 plume did cross the Mexico-Queretaro highway, SW of the Tula-Vito-Apasco corridor. Other less frequent episodes showed the SO_2 dispersion towards the east of the industrial area, which after interacting with the mountain range diminishes the transport of the SO_2 plume outside the area.

Figure 1(b) shows the trajectory of the SO_2 dispersion plume observed on April 4, at 16:00 and 17:00 h. Two routes that were selected to follow the SO_2 plume. The red colored lines show the relative SO_2 column concentration measured using the MiniDOAS system. Route 1 was all around the refinery through the southeast. Route 2 includes a north-south transect from Tula City to Tepeji. The SO_2 plume is dispersed along routes 1 and 2 in the southwest direction. The aforementioned dispersion trajectory was the most common, although other less frequent trajectories were also observed. For instance on April 7, the SO_2 plume dispersed through the north and then at midday to the southeast (not shown).

On the other hand, wind roses (Figure 8) of the SO_2 concentrations (ppm) were drawn from March 18 and April 17 for the Villa de las Flores (VIF) and La Merced (MER) stations, which are located most north and downtown of Mexico City, respectively. The results showed that highest SO_2 concentrations (0.10 to 0.25 ppm) at VIF were associated to northerly wind flows (330°–30°). On the other hand, at MER the SO_2 concentrations were 25% lower than those observed at VIF, and the highest values (>0.02 ppm) occurred when winds flows were from the NE-E (45°–105°). These results suggest that SO_2 emissions from Mezquital Valley have an impact on the northern sector of MCMA. In turn, SO_2 concentrations were higher at VIF compared to those measured at JAS (0.13 ppm), implying that the height of the emitted plume from the RTPPC has a higher impact outside the emission point. This is in agreement with model simulations for Tula reported by de Foy et al. [40].

3.6. Long-Term Plume Trajectory. Figure 9 shows the emission plume that develops from the RTPPC as depicted by the higher vanadium and nickel concentrations and ^{13}C-depleted carbon values in *T. recurvata* in Mezquital Valley relative to background. These metal concentrations and carbon isotope composition represent the long-term pattern area of influence of the emissions from the complex and show that it impacts those towns located along a NE-SW axis between Tlaxcoapan and TEP, and further exits out the valley. The highest nickel and vanadium concentrations in *T. recurvata* were equally distributed at both sides of the axis. In contrast, δ^{13}C values show lighter values to the east of this axis. Metals are likely emitted with particles and would tend to disperse equally at both sides of the long-wind axis, settling within a relatively short distance from the emitter. In contrast, carbon would be mostly emitted as CO_2 and assimilated as such by the epiphyte. It thus appears that gas emissions are influenced by a mountain effect: when wind blows from the SE quadrant the plume disperses into the valley and dilutes the emitted CO_2. In contrast, when the wind direction is from the NW or NE quadrants, emissions tend to concentrate between the RTPPC and the mountain chain located to the S-SE of the complex. Therefore, the relatively longer residence time of the emissions under NW or NE quadrant winds lowers the ambient carbon isotope composition of CO_2.

The relative contribution of CO_2 emitted by the RTPPC can be estimated from the average δ^{13}C value of the epiphyte. The carbon isotope composition of *T. recurvata* decreased from an average of −14.6‰ outside the emitted plume to −15.4‰ inside the plume. This 1.8‰ decrease suggests that industrial emissions contribute with 5% of the total CO_2 incorporated by *T. recurvata* inside the plume. By stable isotope-mass balance, it follows that industrial CO_2 has a δ^{13}C value of −30.0‰, which is consistent with the range of −29.5 to −27.6‰ for CO_2 emitted for the combustion of diesel and fuel oil [41]. Considering a fractionation (Δ) of −1.3‰ between the fuel source and the emitted CO_2 [41],

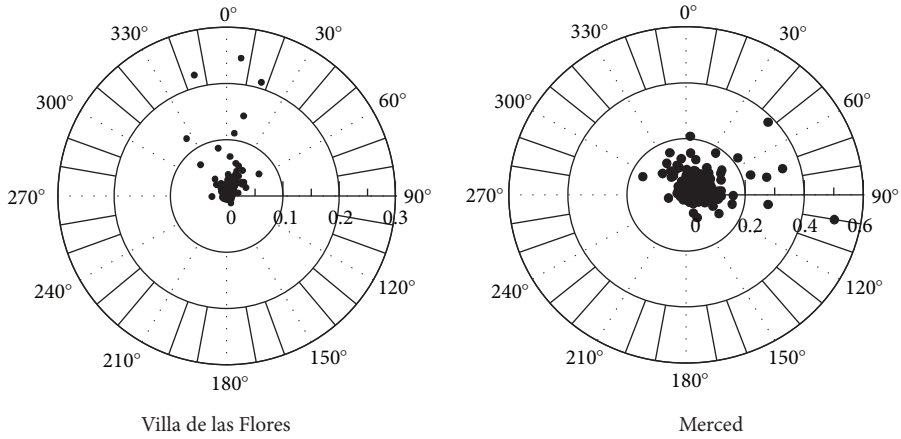

Figure 8: Wind roses of the SO_2 concentrations (ppm) for the Villa de las Flores (VIF) and La Merced (MER) stations from 18 of March and 17 of April.

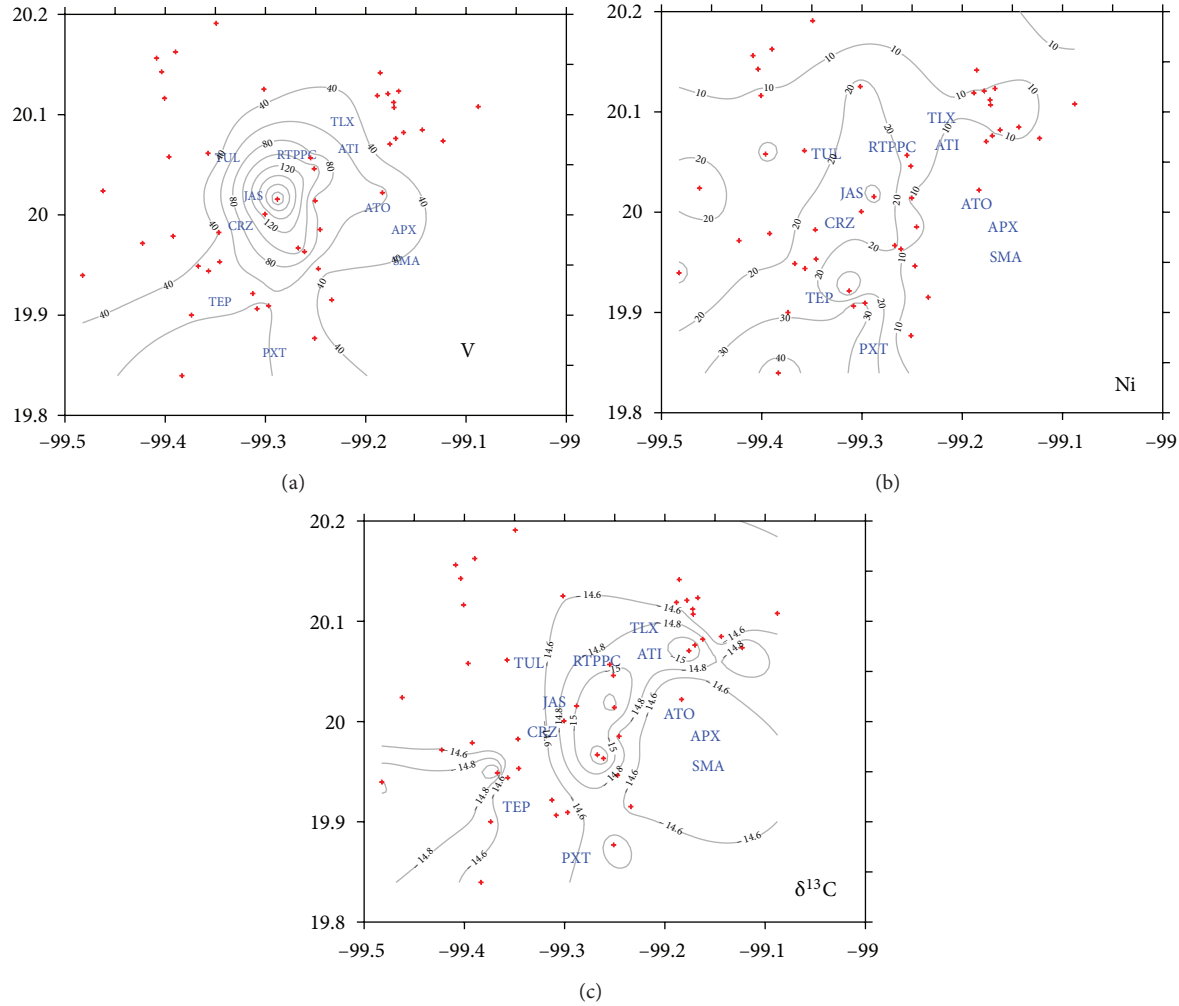

Figure 9: Nickel and vanadium concentrations (in mg/kg) and stable carbon isotope composition (in permile versus PDB) in *Tillandsia recurvata* samples collected in Mezquital Valley.

then the carbon isotope composition of the fuel used by the RTPPC is around −28.7‰.

4. Conclusions

The results of four-week monitoring campaign of particulate matter and gaseous pollutants, as well as meteorological parameters are presented. The present study was conducted in one of the most industrial energy-intense production corridors of Mexico, located 60 km north of Mexico City. The databases are also meant to be used as inputs for future modeling studies and to quantitatively determine the influence of emissions of this region on the air quality in the northern area of MCMA.

Early in the morning a shallow stable layer is formed, with light south-southwesterly winds. These conditions favor accumulation of air pollutants below 100 m and with a limited dispersion of pollutants towards the north of Tula. After midday, a well developed mixing layer is observed up to 1500 m, favoring the mixing of pollutants at higher altitudes. In addition, a superadiabatic layer near the surface, with a clear northern wind component, brings back the pollutants that were transported northward early in the morning. In the afternoon and evening, a similar vertical atmospheric profile is observed; a thicker mixing layer reaches in average 2500 to 3000 m, and a featuring weak low level jet responsible of transporting air pollutants at regional scales. According to the authors' knowledge, this is the first time this feature is reported for this region.

The results of the criteria pollutants concentration at TUL showed that during the study period, most of the pollutants were found to be below the standards, except for PM_{10} and SO_2 that were above the limits twice and O_3 once in each case. Nonetheless, the spatial distribution of these pollutants varies according to location and time of the day. The highest concentrations of O_3 and SO_2 were measured at the southeast of the refinery within a distance of more than 15 km.

Elevated PM_{10} concentrations (178.6 $\mu g/m^3$) exceeding the standard measured at the urban-industrial site of JAS were associated to the increase of wind speeds up to 8.0 m/s. Additionally, this site was highly impacted by local limestone dust since the coarse fraction ranged from 40 to 79% with an average of 56%. Preliminary results from chemical analysis showed that high PM_{10} concentrations were driven by calcium mainly due limestone mining for cement materials and limestone quarries nearby JAS and in the surroundings of Tula, whilst in Mexico City, it is driven by silicon. PM_{10} levels at TEP showed an average of 75.1 $\mu g/m^3$, while the $PM_{2.5}$ average was 25.7 $\mu g/m^3$, and an average $PM_{10}/PM_{2.5}$ mass ratio of 0.68 indicating that almost 70% of the PM_{10} are constituted by $PM_{2.5}$. The above suggests that this site was influenced by higher emission from fossil fuel combustion processes from the refinery and the power plant, among other sources in the vicinity.

$PM_{2.5}$ concentrations were influenced by a peak recorded during the morning, similar to the continuous black carbon measurements, which agrees with a recurrent stable layer formed near the surface before 8:00 h and light winds favoring particle accumulation.

Average hourly aerosol light absorption was 22 Mm^{-1} which is smaller compared to both urban and rural sites. Average hourly aerosol scattering (76 Mm^{-1}) was higher compared to a rural site but much lower than at Mexico City. Elevated values were related to uncommon flaring activities in the refinery in addition to changes in the boundary layer height. High scattering values were associated to a persistent shallow stable atmospheric layer which traps most primary pollutants emitted close to the surface. Low scattering values were related to the development of the mixing layer favoring the dilution of air pollutants.

Elevated BC concentrations were inversely coincident with the wind speed peak with light winds as the boundary layer is stable favoring stagnation of pollutants. In addition, the decrease of the 1/WS favored dilution of pollutants with the lowest levels of BC.

Stable carbon isotope measurements in the biomonitor species *Tillandsia recurvata* provide the long-term signature of pollutant dispersion in the region. Results show that the emission plume from the refinery and nearby thermoelectric power plant directly affects the SE sector of Mezquital Valley where the plume is directed by the prevalent winds and then constrained by a mountain range preventing its fast dispersion. Using stable isotope-mass balance, the carbon contribution as CO_2 near the emission source to this epiphyte is estimated at around 5% of the total assimilated by the plant.

The population in this region is exposed to a multi-pollutant environment, including high levels of sulfur dioxide, submicrometric particles, and black carbon. In addition, frequent adverse meteorological conditions in the morning may exacerbate acute and chronic exposition to these pollutants. The influence of emissions from the RTPPC also affects, to a less extent, the population of MCMA's northern sector. The above-mentioned results evidence the need to establish a contingency plan to avoid population exposure to high concentrations of pollutants in addition to the reduction in industrial emissions to improve wellbeing. Studies within the area that determine the impacts of specific particulate constituents and sources are needed for the effective design of air quality control policies. Finally, a continuous monitoring of both criteria pollutants and meteorological parameters along the Tula-Vito-Apasco corridor is needed to support actions considered in the contingency plan and to better understand impacts of industrial activities on human and ecosystems health.

Conflict of Interests

Authors do not have any conflict of interests to declare.

Acknowledgments

The authors gratefully acknowledge the support of PEMEX under Contract IMP-UAJ-DC-018-2006 and Dr. Judith Chow from the Dessert Research Institute for lending them the SFS equipments for the study.

References

[1] G. E. Streit and F. Guzman, "Mexico City air quality: progress of an international collaborative project to define air quality management options," *Atmospheric Environment*, vol. 30, no. 5, pp. 723–733, 1996.

[2] S. A. Edgerton, X. Bian, J. C. Doran et al., "Particulate air pollution in Mexico City: a collaborative research project," *Journal of the Air and Waste Management Association*, vol. 49, no. 10, pp. 1221–1229, 1999.

[3] L. T. Molina and M. J. Molina, *Air Quality in the Mexico Megacity. An Integrated Assessment*, Kluwer Academic, Dodrecht, The Netherlands, 2002.

[4] L. T. Molina, C. E. Kolb, B. De Foy et al., "Air quality in North America's most populous city—overview of the MCMA-2003 campaign," *Atmospheric Chemistry and Physics*, vol. 7, no. 10, pp. 2447–2473, 2007.

[5] C. Rivera, G. Sosa, H. Wöhrnschimmel, B. De Foy, M. Johansson, and B. Galle, "Tula industrial complex (Mexico) emissions of SO_2 and NO_2 during the MCMA 2006 field campaign using a mobile mini-DOAS system," *Atmospheric Chemistry and Physics*, vol. 9, no. 17, pp. 6351–6361, 2009.

[6] M. A. Martínez-Carrillo, C. Solís, K. Isaac-Olive, E. Andrade, R. I. Beltrán-Hernández, G. Martínez-Reséndiz et al., "Atmospheric elemental concentration determined by Particle-Induced X-ray emision at Tlaxcoapan in central Mexico, and its relation to Tula industrial-corridor emissions," *Microchemical Journal*, vol. 94, pp. 48–52, 2010.

[7] C. A. Pope and D. W. Dockery, "Health effects of fine particulate air pollution: lines that connect," *Journal of the Air and Waste Management Association*, vol. 56, no. 6, pp. 709–742, 2006.

[8] F. Dominici, R. D. Peng, M. L. Bell et al., "Fine particulate air pollution and hospital admission for cardiovascular and respiratory diseases," *Journal of the American Medical Association*, vol. 295, no. 10, pp. 1127–1134, 2006.

[9] M. L. Bell, F. Dominici, K. Ebisu, S. L. Zeger, and J. M. Samet, "Spatial and temporal variation in $PM_{2.5}$ chemical composition in the United States for health effects studies," *Environmental Health Perspectives*, vol. 115, no. 7, pp. 989–995, 2007.

[10] F. Dominici, R. D. Peng, K. Ebisu, S. L. Zeger, J. M. Samet, and M. L. Bell, "Does the effect of PM_{10} on mortality depend on PM nickel and vanadium content? A reanalysis of the NMMAPS data," *Environmental Health Perspectives*, vol. 115, no. 12, pp. 1701–1703, 2007.

[11] A. R. Osornio-Vargas, J. C. Bonner, E. Alfaro-Moreno et al., "Proinflammatory and cytotoxic effects of Mexico City air pollution particulate matter in vtro are dependent on particle size and composition," *Environmental Health Perspectives*, vol. 111, no. 10, pp. 1289–1293, 2003.

[12] I. Rosas Pérez, J. Serrano, E. Alfaro-Moreno et al., "Relations between PM_{10} composition and cell toxicity: a multivariate and graphical approach," *Chemosphere*, vol. 67, no. 6, pp. 1218–1228, 2007.

[13] E. M. Melgar-Paniagua, E. Vega-Rangel, L. M. Del Razo, C. A. Lucho-Constantino, S. J. Rothenberg, and A. De Vizcaya-Ruiz, "Distributed lag associations between respiratory illnesses and mortality with suspended particle concentration in Tula, a highly polluted industrial region in Central Mexico," *International Archives of Occupational and Environmental Health*, April 2012.

[14] B. de Foy, N. A. Krotkov, N. Bei et al., "Hit from both sides: tracking industrial and volcanic plumes in Mexico City with surface measurements and OMI SO_2 retrievals during the MILAGRO field campaign," *Atmospheric Chemistry and Physics*, vol. 9, no. 24, pp. 9599–9617, 2009.

[15] V. H. Almanza, L. T. Molina, and G. Sosa, "Soot and SO_2 contribution to the supersites in the MILAGRO campaign from elevated flares in the Tula Refinery," *Atmospheric Chemistry and Physics*, vol. 12, pp. 10583–10599, 2012.

[16] Secretaría del Medio Ambiente, "Inventario de emisiones 2006. SMA- GDF," 2006.

[17] Instituto Mexicano del Petróleo, "Estudio de las emisiones de la zona industrial de Tula y su impacto en la calidad del aire regional," PS-MA-IF-F21393-1, 2006.

[18] H. Tennekes, "The atmospheric boundary layer," *Physics Today*, vol. 27, no. 1, pp. 52–63, 1974.

[19] E. Vega, E. Reyes, H. Ruiz, J. García, G. Sánchez, G. Martínez-Villa et al., "Analysis of $PM_{2.5}$ and PM_{10} in Mexico City atmosphere during 2000–2002," *Journal of the Air & Waste Management Association*, vol. 54, pp. 786–798, 2004.

[20] M. E. Conti and G. Cecchetti, "Biological monitoring: lichens as bioindicators of air pollution assessment—a review," *Environmental Pollution*, vol. 114, no. 3, pp. 471–492, 2001.

[21] G. J. Husk, J. F. Weishampel, and W. H. Schlesinger, "Mineral dynamics in Spanish moss, *Tillandsia usneoides* L. (Bromeliaceae), from Central Florida, USA," *Science of the Total Environment*, vol. 321, no. 1–3, pp. 165–172, 2004.

[22] A. Zambrano García, C. Medina Coyotzin, A. Rojas Amaro, D. López Veneroni, L. Chang Martínez, and G. Sosa Iglesias, "Distribution and sources of bioaccumulative air pollutants at Mezquital Valley, Mexico, as reflected by the atmospheric plant *Tillandsia recurvata* L.," *Atmospheric Chemistry and Physics*, vol. 9, no. 17, pp. 6479–6494, 2009.

[23] Instituto Nacional de Ecología (INE), Campaña de monitoreo de calidad del aire de la Región Tula-Tepeji-Zumpango del 20 de Octubre al 5 de Diciembre del 2008, 2009.

[24] J. D. Fast, B. De Foy, F. A. Rosas et al., "A meteorological overview of the MILAGRO field campaigns," *Atmospheric Chemistry and Physics*, vol. 7, no. 9, pp. 2233–2257, 2007.

[25] Y. Wu and S. Raman, "Effect of land-use pattern on the development of low-level jets," *Journal of Applied Meteorology*, vol. 36, no. 5, pp. 573–590, 1997.

[26] Comisión Federal para la Protección contra Riesgos Sanitarios (Cofepris), "Mexican Oficial Standards for Criteria Pollutants," 2010, http://www.cofepris.gob.mx/MJ/Paginas/NormasPorTema/Calidad-de-aire.aspx.

[27] Diario Oficial de la Federación, "Modificación a la Norma Oficial Mexicana NOM-025-SSA1-1993, Salud ambiental," Criterios para evaluar la calidad del aire ambiente, con respecto a material particulado, 2005.

[28] X. Querol, J. Pey, M. C. Minguillón, N. Pérez, A. Alastuey, M. Viana et al., "PM speciation and sources in Mexico during the MILAGRO-2006 Campaign," *Atmospheric Chemistry and Physics*, vol. 8, pp. 111–128, 2008.

[29] E. Vega, H. Ruiz, G. Martínez-Villa et al., "Fine and coarse particulate matter chemical characterization in a heavily industrialized city in Central Mexico during Winter 2003," *Journal of the Air and Waste Management Association*, vol. 57, no. 5, pp. 620–633, 2007.

[30] G. Paredes-Miranda, W. P. Arnott, J. L. Jimenez, A. C. Aiken, J. S. Gaffney, and N. A. Marley, "Primary and secondary contributions to aerosol light scattering and absorption in Mexico City during the MILAGRO 2006 campaign," *Atmospheric Chemistry and Physics*, vol. 9, no. 11, pp. 3721–3730, 2009.

[31] Secretaría de Salud, Panorama Epidemiológico de la Región Tula-Tepeji, Hidalgo, Comisión para la Protección contra Riesgos Sanitarios del Estado de Hidalgo (COPRISEH), Subcomisión de Evidencia, Manejo de Riesgos y Trámites. Secretaría de Salud de Hidalgo, 2008.

[32] M. J. Strickland, L. A. Darrow, M. Klein et al., "Short-term associations between ambient air pollutants and pediatric asthma emergency department visits," *American Journal of Respiratory and Critical Care Medicine*, vol. 182, no. 3, pp. 307–316, 2010.

[33] R. D. Peng, M. L. Bell, A. S. Geyh et al., "Emergency admissions for cardiovascular and respiratory diseases and the chemical composition of fine particle air pollution," *Environmental Health Perspectives*, vol. 117, no. 6, pp. 957–963, 2009.

[34] N. A. Marley, J. S. Gaffney, T. Castro, A. Salcido, and J. Frederick, "Measurements of aerosol absorption and scattering in the Mexico City Metropolitan Area during the MILAGRO field campaign: a comparison of results from the T0 and T1 sites," *Atmospheric Chemistry and Physics*, vol. 9, no. 1, pp. 189–206, 2009.

[35] G. Buonanno, G. Giovinco, L. Morawska, and L. Stabile, "Corrigendum to 'Tracheobronchial and alveolar dose of submicrometer particles for different population age groups in Italy'," *Atmospheric Environment*, vol. 45, pp. 6216–6224, 2011.

[36] G. Buonanno, G. Giovinco, L. Morawska, and L. Stabile, "Corrigendum to 'Tracheobronchial and alveolar dose of submicrometer particles for different population age groups in Italy'," *Atmospheric Environment*, vol. 49, p. 423, 2012.

[37] A. D. A. Hansen, *The Aethalometer*, Magee Scientific Company, Berkeley, Calif, USA, 2003.

[38] R. W. Bergstrom, P. Pilewskie, P. B. Russell et al., "Spectral absorption properties of atmospheric aerosols," *Atmospheric Chemistry and Physics*, vol. 7, no. 23, pp. 5937–5943, 2007.

[39] N. A. Marley, J. S. Gaffney, M. Tackett, N. C. Sturchio et al., "The impact of biogenic carbon sources on aerosol absorption in Mexico City," *Atmospheric Chemistry and Physics*, vol. 9, pp. 1537–1549, 2009.

[40] B. de Foy, W. Lei, M. Zavala et al., "Modelling constraints on the emission inventory and on vertical dispersion for CO and SO_2 in the Mexico City Metropolitan Area using Solar FTIR and zenith sky UV spectroscopy," *Atmospheric Chemistry and Physics*, vol. 7, no. 3, pp. 781–801, 2007.

[41] D. Widory, "Combustibles, fuels and their combustion products: a view through carbon isotopes," *Combustion Theory and Modelling*, vol. 10, no. 5, pp. 831–841, 2006.

Hindawi Publishing Corporation
BioMed Research International
Volume 2013, Article ID 382058, 7 pages
http://dx.doi.org/10.1155/2013/382058

Research Article

Dehydroepiandrosterone Protects Endothelial Cells against Inflammatory Events Induced by Urban Particulate Matter and Titanium Dioxide Nanoparticles

Elizabeth Huerta-García,[1,2] Angélica Montiél-Dávalos,[3] Ernesto Alfaro-Moreno,[3] Gisela Gutiérrez-Iglesias,[2] and Rebeca López-Marure[1]

[1] *Departamento de Biología Celular, Instituto Nacional de Cardiología "Ignacio Chávez", Juan Badiano No. 1, Colonia Sección 16, Tlalpan, 14080 México, DF, Mexico*
[2] *Departamento de Posgrado. Escuela Superior de Medicina, Instituto Politécnico Nacional, Mexico*
[3] *Subdirección de Investigación Básica, Instituto Nacional de Cancerología, Mexico*

Correspondence should be addressed to Rebeca López-Marure; rlmarure@yahoo.com.mx

Received 5 September 2012; Revised 30 November 2012; Accepted 6 December 2012

Academic Editor: Per Schwarze

Particulate matter (PM) and nanoparticles (NPs) induce activation and dysfunction of endothelial cells characterized by inhibition of proliferation, increase of adhesion and adhesion molecules expression, increase of ROS production, and death. DHEA has shown anti-inflammatory and antioxidant properties in HUVEC activated with proinflammatory agents. We evaluated if DHEA could protect against some inflammatory events produced by PM_{10} and TiO_2 NPs in HUVEC. Adhesion was evaluated by a coculture with U937 cells, proliferation by crystal violet staining, and oxidative stress through DCFDA and Griess reagent. PM_{10} and TiO_2 NPs induced adhesion and oxidative stress and inhibited proliferation of HUVEC; however, when particles were added in combination with DHEA, the effects previously observed were abolished independently from the tested concentrations and the time of addition of DHEA to the cultures. These results indicate that DHEA exerts significant anti-inflammatory and antioxidative effects on the damage induced by particles in HUVEC, suggesting that DHEA could be useful to counteract the harmful effects and inflammatory diseases induced by PM and NPs.

1. Introduction

Particulate matter (PM) is an environmental factor that has been associated with increased cardiovascular morbidity and mortality, particularly mass concentrations of PM with aerodynamic sizes ≤2.5 or ≤10 μM ($PM_{2.5}$, PM_{10}). Numerous studies have shown associations between PM and risk of cardiac ischemia and arrhythmias, increased blood pressure, decreased heart rate variability, and increased circulating markers of inflammation and thrombosis [1]. Also, ultrafine particles (UFPs; PM < 0.1 μM) induce oxidative stress leading to inflammation and resulting in respiratory and cardiovascular disease, because they have high pulmonary deposition efficiency and their magnitudes in the particle number concentration are higher than larger particles; thus they have a much larger surface area. Such is the case of titanium dioxide nanoparticles (TiO_2 NPs) that cause several adverse effects on mammalian cells such as increase of reactive oxygen species (ROS) production and cytokines levels, reduction of cell viability and proliferation, and induction of apoptosis and genotoxicity [2].

We have previously shown that $PM_{2.5}$ and PM_{10} induce adhesion of U937 cells to human umbilical vein endothelial cells (HUVEC), which was associated with an increase in the expression of adhesion molecules such as E- and P-selectins, ICAM-1, PECAM-1, and VCAM-1 [3, 4]; besides, they induce production of ROS and NO and nuclear translocation of NF-κB [5]. Also, we have shown that TiO_2 NPs are internalized into HUVEC; they inhibit strongly cell proliferation; and induced cellular death (necrosis and apoptosis) [6]. Besides, TiO_2 NPs induce activation of HUVEC through an increase in adhesion and in the expression of adhesion molecules

and other molecules involved in the inflammatory process. These effects were associated with oxidative stress and NF-κB pathway activation [6]. Together, all these results indicate that all these particles induce HUVEC activation, suggesting that they may participate in the development of inflammatory diseases.

In previous works, we have shown that dehydroepiandrosterone (DHEA), an adrenal hormone, has shown anti-inflammatory and antioxidative roles in HUVEC treated with two proinflammatory molecules such as TNF-α and oxLDL [7, 8]. DHEA decreases the adhesion of monocytic cells to HUVEC, decreases the expression of early and late molecules of adhesion, and interferes with the translocation of NF-κB and IκB-α degradation. Also, DHEA inhibits ROS and NO production.

In this work, we hypothesized that DHEA could protect HUVEC against inflammatory events induced by PM_{10} and TiO_2 NPs. To test this, we exposed HUVEC to PM_{10} and TiO_2 NPs in combination with DHEA and evaluated the adhesion of monocytic cells, proliferation, and ROS and NO production.

2. Materials and Methods

2.1. Materials. RPMI 1640 and M199 media and trypsin were purchased from GIBCO/BRL (Grand Island, NY, USA), and fetal bovine serum (FBS) was HyClone (Logan, UT, USA). Sterile plastic material for tissue culture was from NUNC and COSTAR. Flow cytometry reagents were purchased from Becton Dickinson, Immunocytometry Systems (San José, CA, USA). TNF-α was purchased from R & D Systems (Minneapolis, MN, USA). Peroxidase-labeled monoclonal antibody against Von Willebrand factor was purchased from Santa Cruz Biotechnology (Santa Cruz, CA, USA). H_2DCFDA was purchased from Molecular Probes and TiO_2 NPs from Paris Drugstore (Mexico City, Mexico). All other chemicals were purchased from Sigma Aldrich (St. Louis, MO, USA).

2.2. Particles and Preparation. PM_{10} were collected from the north zone of Mexico City. Samples were taken three days per week throughout 2007 using a GMW high-volume particle collector (model 1200 VFC HV PM10, Sierra Andersen) to collect particles with mean aerodynamic diameters equal to or smaller than 10 μM. Particles were recovered from the filters as previously described [9].

At least 1 mg of particles was weighed and sterilized by autoclave the night before of each experiment. PM_{10} and TiO_2 NPs suspensions in M199 medium, at a concentration of 1 mg/mL, were prepared few minutes before cell exposure. Aliquots were taken from these suspensions and further diluted with culture medium until the required final concentration was obtained. TiO_2 NPs used were previously characterized by our work group [6]. Their characterization showed aggregates of spheres of less than 50 nm with a size distribution of aggregates between 105 and 1281 nm and a mean size of 421 nm, when TiO_2 NPs were suspended in M199 medium plus 10% FBS. In our assays, NPs were not sonicated because in our previous studies we did not observe difference in the biological effects induced by sonicated or nonsonicated TiO_2 NPs.

2.3. Endothelial Cell Cultures. Primary HUVEC cultures were obtained by proteolytic dissociation of the umbilical cord veins from normal deliveries, treated with collagenase type II (0.2 mg/mL), and cultured on gelatin-coated culture dishes in M199 supplemented with 10% FBS, glutamine (2 mM), heparin (1 mg/mL), and endothelial mitogen (20 μg/mL), as previously described [5]. Cells were used for all experiments on their second passage. The phenotype of HUVEC cultures was confirmed by Von Willebrand antigen staining. Cultures exposed to human recombinant TNF-α (10 ng/mL) or H_2O_2 (500 μM) were used as positive controls of endothelial activation.

2.4. Culture of U937 Cells. Human leukemia promonocytic U937 cells were cultured in RPMI-1640 medium supplemented with 10% FBS and L-glutamine (2 mM).

2.5. Adhesion of U937 Cells to Endothelial Cells. Adhesion was evaluated using U937 cells that were labeled with [^{3}H]-thymidine; 1×10^5 HUVEC were seeded in 24-well tissue-culture plates with 1 mL of supplemented M199 medium and treated with TNF-α (10 ng/mL), DHEA (1, 10, and 100 μM), TiO_2 NPs (10 μg/cm^2), and PM_{10} (20 μg/cm^2) for different times, whereas 6×10^6 U937 cells were incubated with 30 μCi of [^{3}H]-thymidine for 48 h. Pretreated HUVEC were co-cultivated for 3 h with 5×10^5 U937 cells/well. Each well was washed to eliminate U937 cells not attached to HUVEC. After this, cells were fixed with 95% methanol and lysed with NaOH (200 mM) for 12 h, and radioactivity was determined in a scintillation counter (Beckman Coulter model LS6500, Miami, FL, USA). Counts per minute (cpm) were considered directly proportional to the number of U937 cells adhered to HUVEC.

2.6. Crystal Violet Staining. Cell number was evaluated by crystal violet staining. HUVEC were cultured on 96-multiwell plates without and with DHEA (1, 10, and 100 μM), TiO_2 NPs (10 μg/cm^2), and PM_{10} (20 μg/cm^2) for 72 h. DHEA was added 1 h before exposure to particles. At the end of these treatments, cells were fixed with 100 μL of ice cold glutaraldehyde (1.1% in PBS) for 15 min at 4°C. Plates were washed three times by submersion in deionized water, air-dried, stained for 20 min with 100 μL of a 0.1% crystal violet solution (in 200 mM phosphoric acid buffer at pH 6). After careful aspiration of the crystal violet solution, the plates were extensively washed with deionized water, air-dried prior to the solubilization of the bound dye with 100 μL of a 10% acetic acid solution, and incubated during 30 min. Optical density of the plates was measured at 595 nm in a multiplate spectrophotometer.

2.7. Measurement of Reactive Oxygen Species. The oxidation of 2,7-dichlorodihydrofluorescein diacetate (H_2DCFDA)

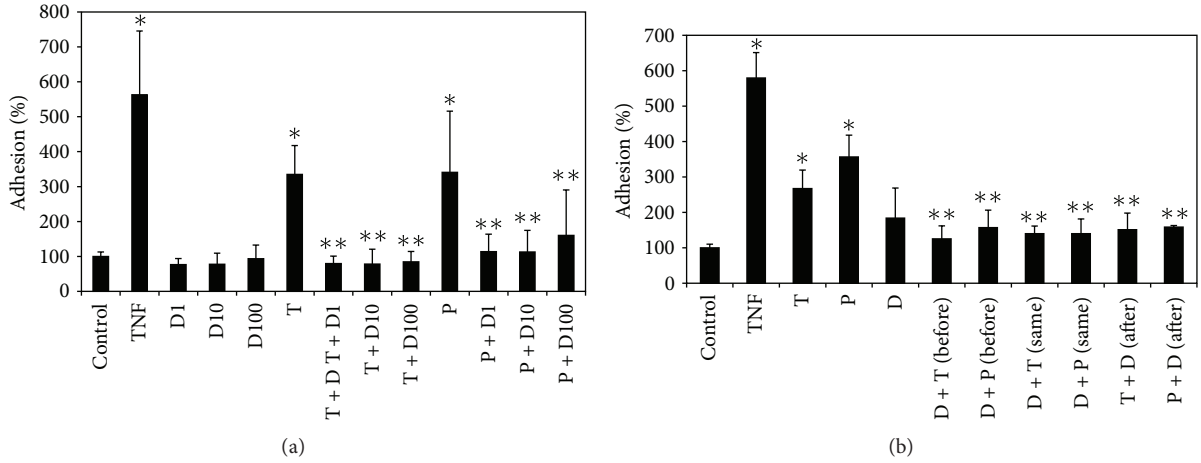

Figure 1: Effect of DHEA on the adhesion induced by particles. Cells were treated with 1 (D1), 10 (D10), and 100 μM (D100) of DHEA alone or in combination with 10 μg/cm^2 of TiO_2 NPs (T) or 20 μg/cm^2 of PM_{10} (P) for 24 h (a). After this, U937 cells labeled with [^{3}H]-thymidine were cultured with HUVEC for 3 h more, and adhesion was evaluated in a scintillation counter. TNF-α (10 ng/mL) was used as a positive control. In (b), DHEA was added 1 h before (before), at the same time (same), and 1 h after (after) the addition of TiO_2 NPs or PM_{10}. The results were expressed as percentage of adhesion with respect to untreated cells (100%) and shown as mean ± SD of three separate experiments. $^*P < 0.01$ compared with nontreated cells, and $^{**}P < 0.01$ compared with particles-treated cells.

into 2,7-dichlorodihydrofluorescein (DCF) was used to assess Ros generation. HUVEC were cultured without or with DHEA (1, 10, and 100 μM), TiO_2 NPs (10 μg/cm^2), and PM_{10} (20 μg/cm^2) or in combination for 3 h. DHEA was added 1 h before particles. H_2O_2 (500 μM) was used as positive control to induce oxidative stress. After treatment, cells were incubated with H_2DCFDA (10 μM) for 30 min at 37°C and washed twice with PBS. After an extensive wash, fluorescence was evaluated by flow cytometry (Facscalibur, Becton Dickinson). The mean fluorescence intensity was calculated by multiplying the number of events (fluorescent cells) by the mean of the intensity presented by the Cell Quest software used for the analysis.

2.8. Production of NO. Quantification of nitrite was used as an indirect method to determine the production of NO. Cells were seeded in 96 well plates (NUNC) at a density of 1×10^5 cells/well in M199 (phenol red free) and 10% FBS. Cells were cultured without or with DHEA (1, 10, and 100 μM), TiO_2 NPs (10 μg/cm^2), and PM_{10} (20 μg/cm^2) or in combination for 72 h. DHEA was added 1 h before particles. Unexposed cultures were used as negative controls. After treatment, 100 μL of the conditioned medium was diluted 1 : 2 with 100 μL of Griess solution and incubated for 15 min at room temperature. Previously, a standard curve was performed using known concentrations of $NaNO_2$. The optical density of the plates was measured at 540 nm (Microplate autoreader EL311, Bio-Tek Instruments, Winooski, VT, USA). The concentrations of $NaNO_2$ in control and exposed cultures were plotted against the standard.

2.9. Statistical Analysis. All the endpoints were measured at least three times. The results are expressed as mean ± standard deviation. Statistical significance was evaluated using one-way analysis of variance (ANOVA) test using GraphPad Prism, version 2.0 (GraphPad Software, CA, USA), followed by Duncan's multiple range test (MRT), to assess differences between group means. Differences were considered significant when $P < 0.01$. When a temporal curve was used to evaluate the nitrite production, the exposed cultures were compared with the controls at the respective time point.

3. Results

3.1. DHEA Inhibited the Adhesion Induced by TiO_2 NPs and PM_{10}. Adhesion of U937 cells to HUVEC was evaluated by a coculture assay. DHEA alone did not induce adhesion, whereas the treatment with TiO_2 NPs and PM_{10} induced a 2-fold increase in adhesion, compared to untreated cells; however, this was significantly inhibited until reaching basal levels when HUVEC were exposed to a pretreatment with DHEA (Figure 1(a)). All concentrations of DHEA inhibited the increase of adhesion induced by particles. In order to determine if the time of addition of DHEA was important to exert its protective effect, DHEA was added to HUVEC before, at the same time, and after treatment with TiO_2 NPs and PM_{10}. DHEA inhibited the adhesion induced by the particles independently from the time of addition (Figure 1(b)).

3.2. DHEA Abolished the Decrease of Proliferation Induced by TiO_2 NPs and PM_{10}. To examine the possible involvement of DHEA on the inhibition of proliferation induced by TiO_2 NPs and PM_{10}, HUVEC were exposed to DHEA alone or in combination with the particles, and proliferation was evaluated by crystal violet. Results showed that DHEA reverted almost completely the inhibition of proliferation induced by TiO_2 NPs at any concentration (Figure 2); however, DHEA

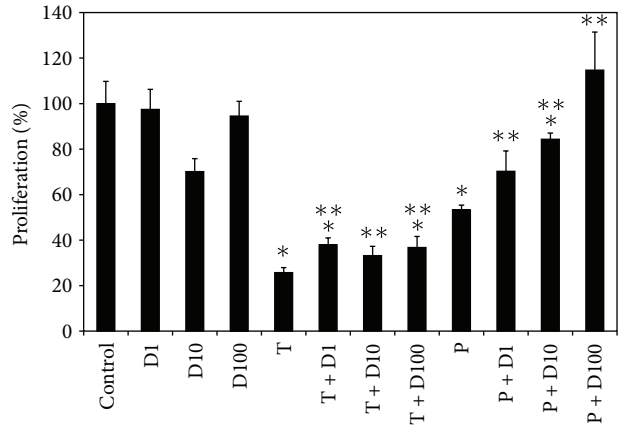

Figure 2: Effect of DHEA on the inhibition of proliferation induced by particles. Cells were treated with 1 (D1), 10 (D10), and 100 μM (D100) of DHEA alone or in combination with 10 μg/cm^2 of TiO_2 NPs (T) or 20 μg/cm^2 of PM_{10} (P) for 72 h. Cell proliferation was evaluated by crystal violet staining. Nontreated cells showed 100% of proliferation. The results are expressed as mean ± SD of three separate experiments. $^*P < 0.01$ compared with nontreated cells, and $^{**}P < 0.01$ compared with particles-treated cells.

at 100 μM in combination with PM_{10} (P + D100) abolished 100% the inhibition induced by PM_{10} alone.

3.3. DHEA Abolished the Increase of ROS and NO Induced by TiO_2 NPs and PM_{10}. Oxidative stress was determined indirectly by measuring the H_2O_2 and nitrite production by H_2DCFDA and Griess reagent, respectively. After exposure to TiO_2 NPs and PM_{10} for 24 h, fluorescence from most cells stained with H_2DCFDA indicated that intracellular H_2O_2 had accumulated strongly in HUVEC; however, this was significantly inhibited reaching almost basal levels by pretreatment with DHEA at all concentrations used (Figure 3). In relation to NO production, TiO_2 NPs and PM_{10} induced approximately an increase of 150% and 70% of nitrite concentration, respectively. When DHEA was added in combination with any of the particles, the induction was completely abolished to control levels (Figure 4).

4. Discussion

Our previous study showed that exposure of human endothelial cells to TiO_2 NPs and PM_{10} caused cytotoxic damage [7, 8]. We also have observed that DHEA has an anti-inflammatory and antioxidant effect, protecting HUVEC against the damage induced by TNF-α and oxLDL [1, 2]. In the present work, we determined that DHEA protects HUVEC against some inflammatory and oxidative effects induced by PM and NPs.

DHEA, at different concentrations, inhibited the adhesion of U937 cells to HUVEC induced by TiO_2 NPs and PM_{10}, independently from the time of administration of DHEA to the culture (Figure 1). Similar results have been found by Curatola and collaborators [10]. They observed that DHEA inhibited the adhesion of monocytes to cultured human coronary artery endothelial cells (HCAEC), in an estrogen- and androgen-receptor-dependent manner. Besides, DHEA is able to abolish the adhesion of U937 cells to HUVEC treated with proinflammatory molecules such as TNF-α and oxLDL and high concentrations of glucose [1, 2, 11].

In addition, we observed that the antiproliferative effect induced by TiO_2 NPs and PM_{10} on HUVEC was similarly reverted with DHEA (Figure 2). It has been described that the toxic potential of NPs is stronger than that induced by PM, because NPs have a much larger surface area, resulting in a high reactivity [12]; nevertheless, we showed that DHEA inhibited the antiproliferative effect of both particles, independently from their size.

DHEA, at all tested concentrations, abolished completely the oxidative stress induced by TiO_2 NPs and PM_{10}, decreasing the H_2O_2 and nitrite production (Figures 3 and 4). Some works have reported that the antioxidant effect of DHEA depends on its concentration [13, 14]. When DHEA was used at physiological concentrations in Chang liver cells, a protection against lipid peroxidation and cell death induced by cumene was observed; but in contrast, at pharmacological concentrations (10–50 μM), DHEA increased both lipid peroxidation and cell death after the prooxidant stimulus [15]. In the present study, we found that, at concentrations ranging from 1 to 100 μM, DHEA exerted an antioxidant effect. In contrast, other anti-inflammatory steroids such as dexamethasone induce oxidative stress [16]. Some works have shown that glucocorticoids therapy can elicit a variety of symptoms and signs, including growth retardation in children; immunosuppression; cardiovascular disorders like hypertension and atherosclerosis; osteoporosis; myopathy; and diabetes mellitus [17], while most importantly, no significant adverse or negative side effects of DHEA have been reported in clinical studies of men and women [18].

In other cells, it has been described that DHEA prevented the increased death evoked by glucose deprivation by inhibiting the production of superoxide anion in immunostimulated C6 glioma cells [19] and attenuated lipid peroxidation in high-glucose cultured mesangial cells [20]. In endothelial cells, we previously showed that DHEA inhibits ROS and NO production induced by high concentrations of glucose [11].

As well, in an *in vivo* model using ovariectomized rats, DHEA treatment restored the reduced Cu/Zn-SOD protein expression and eNOS phosphorylation and the increased NADPH oxidase protein expression in the aorta [21]. In rabbits fed with a high-fat diet supplemented with low-dose of DHEA, it showed a partial reduction of oxidative stress restoring the oxidative balance and the inflammatory state, showing a beneficial effect [22]. Besides, pretreatment with sulfated DHEA (DHEAS) reverses the stress-induced changes in behavioral and oxidative stress markers and also brain NOx levels in rats [23]. In healthy male Wistar rats, DHEA exerted a protective effect, particularly in the colon, by reducing the tissue susceptibility to oxidation of both lipids and proteins [24]. As a whole, these results suggest an important action of DHEA, improving endothelial function and having a beneficial action by acting as an antioxidant, when cells are exposed to several inflammatory molecules

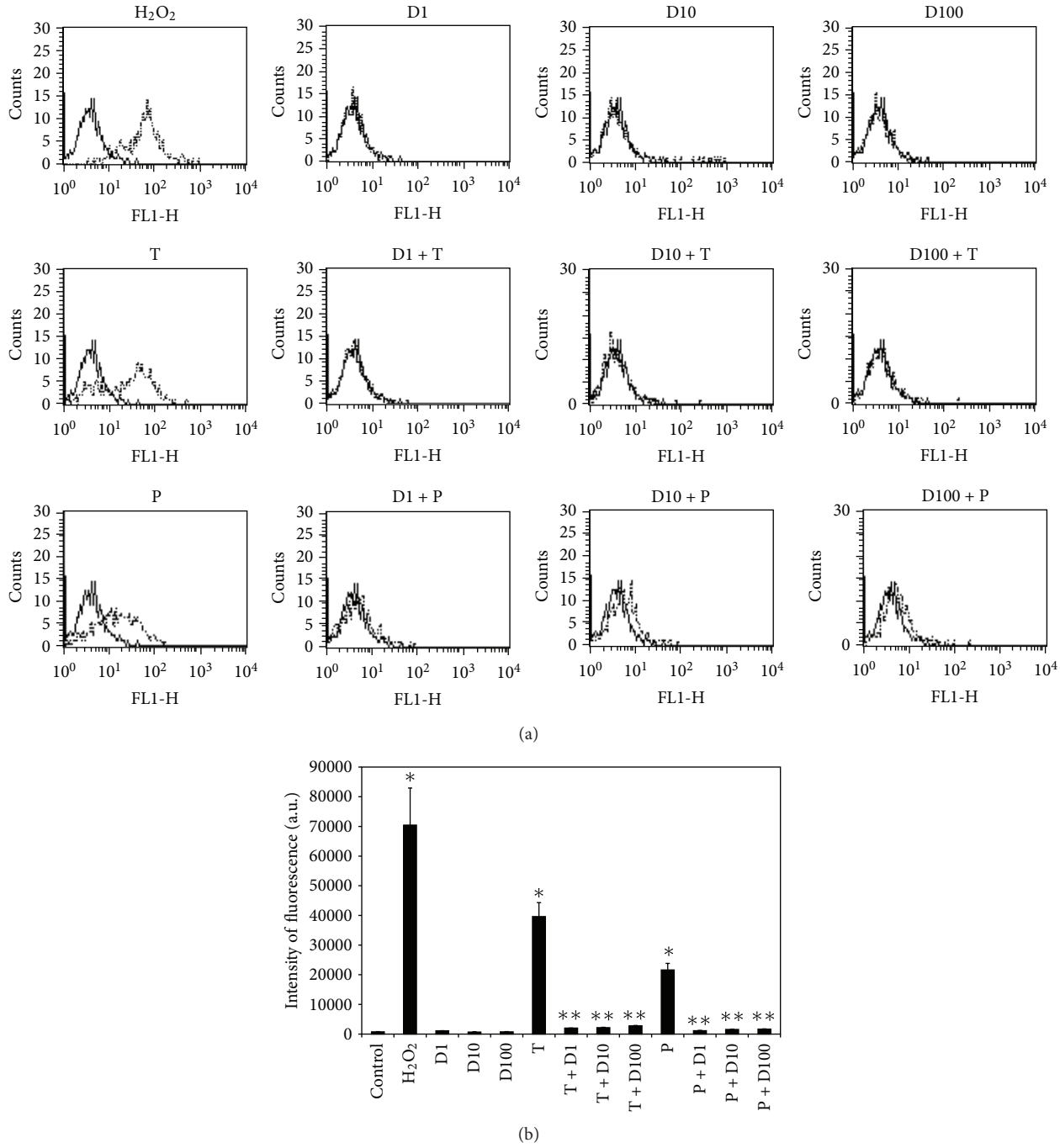

Figure 3: Effect of DHEA on ROS production induced by particles. Cells were treated with 1 (D1), 10 (D10), and 100 μM (D100) of DHEA alone or in combination with 10 μg/cm^2 of TiO_2 NPs (T) or PM_{10} (P) for 48 h. H_2O_2 (500 μM) was used as a positive control. ROS concentration was evaluated using H_2DCFDA by flow cytometry. In (a), continuous lines correspond to control cells without treatment, and dashed lines correspond to treated cells. Histograms match to one representative experiment of three performed in an independent way. In (b), fluorescence intensity was calculated through multiplying the number of events by the mean of the fluorescence intensity value. The results are expressed as mean ± SD of three separate experiments. $^*P < 0.01$ compared with nontreated cells, and $^{**}P < 0.01$ compared with particles-treated cells.

such as TNF-$\alpha$and oxLDL, high concentrations of glucose, and particles. All these results suggest that anti-inflammatory effects induced by DHEA share a similar signaling pathway.

In conclusion, our results show that DHEA could be useful as a protective agent in the prevention and treatment of inflammatory and cardiovascular effects induced by urban

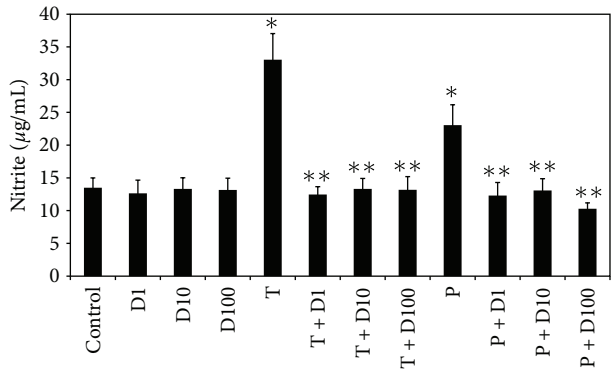

Figure 4: Effect of DHEA on NO production induced by particles. Cells were treated with 1 (D1), 10 (D10), and 100 μM (D100) of DHEA alone or in combination with 10 μg/cm^2 of TiO_2 NPs (T) or PM_{10} (P) for 72 h. NO concentration was evaluated using Griess reagent. Previously, a standard curve was performed using known concentrations of nitrite. Absorbance of the concentrations of control and problem samples was plotted against the standard curve. Data are represented as concentration of nitrite (μg/mL) and are expressed as mean ± SD of three separate experiments. * Indicates $P < 0.01$ compared with control cells, and $^{**}P < 0.01$ compared with particles-treated cells.

particulate matter and nanoparticles where endothelial dysfunction is involved.

Abbreviations

DHEA: Dehydroepiandrosterone
TNF-α: Tumor necrosis factor alpha
HUVEC: Human umbilical vein endothelial cells
ROS: Reactive oxygen species
H_2DCFDA: 2,7-Dichlorodihydrofluorescein diacetate.

Acknowledgments

The authors thank Dr. Gerardo Tinoco from the Hospital General de Zona de Troncoso 2 A, IMSS, Mexico, for the samples of umbilical cords. E. Huerta-Garcia (doctoral student from the Posgrado en Investigación en Medicina from the Escuela Superior de Medicina, Instituto Politécnico Nacional) was supported by CONACyT scholarship no. 227281. The present study was partially supported by the SEP-CONACyT Grant (106057).

References

[1] R. J. Delfino, C. Sioutas, and S. Malik, "Potential role of ultrafine particles in associations between airborne particle mass and cardiovascular health," *Environmental Health Perspectives*, vol. 113, no. 8, pp. 934–946, 2005.

[2] V. Stone, H. Johnston, and M. J. D. Clift, "Air pollution, ultrafine and nanoparticle toxicology: cellular and molecular interactions," *IEEE Transactions on Nanobioscience*, vol. 6, no. 4, pp. 331–340, 2007.

[3] A. Montiel-Dávalos, E. Alfaro-Moreno, and R. López-Marure, "PM2.5 and PM_{10} induce the expression of adhesion molecules and the adhesion of monocytic cells to human umbilical vein endothelial cells," *Inhalation Toxicology*, vol. 19, no. 1, pp. 91–98, 2007.

[4] E. Alfaro-Moreno, R. López-Marure, A. Montiel-Dávalos et al., "E-Selectin expression in human endothelial cells exposed to PM_{10}: the role of endotoxin and insoluble fraction," *Environmental Research*, vol. 103, no. 2, pp. 221–228, 2007.

[5] A. Montiel-Dávalos, M. J. Ibarra-Sánchez, J. L. Ventura-Gallegos et al., "Oxidative stress and apoptosis are induced in human endothelial cells exposed to urban particulate matter," *Toxicology in Vitro*, vol. 24, no. 1, pp. 135–141, 2010.

[6] A. Montiel-Dávalos, J. L. Ventura-Gallegos, E. Alfaro-Moreno et al., "TiO_2 nanoparticles induce dysfunction and activation of human endothelial cells," *Chemical Research Toxicology*, vol. 25, no. 4, pp. 920–930, 2012.

[7] G. Gutiérrez, C. Mendoza, E. Zapata et al., "Dehydroepiandrosterone inhibits the TNF-alpha-induced inflammatory response in human umbilical vein endothelial cells," *Atherosclerosis*, vol. 190, no. 1, pp. 90–99, 2007.

[8] R. López-Marure, C. Huesca-Gómez, M. D. J. Ibarra-Sánchez, A. Zentella, and O. Pérez-Méndez, "Dehydroepiandrosterone delays LDL oxidation in vitro and attenuates several oxLDL-induced inflammatory responses in endothelial cells," *Inflammation and Allergy—Drug Targets*, vol. 6, no. 3, pp. 174–182, 2007.

[9] E. Alfaro-Moreno, L. Martínez, C. García-Cuellar et al., "Biological effects induced in vitro by PM_{10} from three different zones of Mexico City," *Environment Health Perspectives*, vol. 110, no. 7, pp. 715–772, 2002.

[10] A. M. Curatola, K. Huang, and F. Naftolin, "Dehydroepiandrosterone (DHEA) inhibition of monocyte binding by vascular endothelium is associated with sialylation of neural cell adhesion molecule," *Reproductive Sciences*, vol. 19, no. 1, pp. 86–91, 2012.

[11] E. 1. Huerta-García, J. L. Ventura-Gallegos, M. E. Victoriano et al., "Dehydroepiandrosterone inhibits the activation and dysfunction of endothelial cells induced by high glucose concentration," *Steroids*, vol. 77, no. 3, pp. 233–240, 2012.

[12] P. J. A. Borm, D. Robbins, S. Haubold et al., "The potential risks of nanomaterials: a review carried out for ECETOC," *Particle and Fibre Toxicology*, vol. 3, article 11, 2006.

[13] J. Yamada, M. Sakuma, and T. Suga, "Induction of peroxisomal β-oxidation enzymes by dehydroepiandrosterone and its sulfate in primary cultures of rat hepatocytes," *Biochimica et Biophysica Acta*, vol. 1137, no. 2, pp. 231–236, 1992.

[14] J. Swierczynski, P. Bannasch, and D. Mayer, "Increase of lipid peroxidation in rat liver microsomes by dehydroepiandrosterone feeding," *Biochimica et Biophysica Acta*, vol. 1315, no. 3, pp. 193–198, 1996.

[15] M. Gallo, M. Aragno, V. Gatto et al., "Protective effect of dehydroepiandrosterone against lipid peroxidation in a human liver cell line," *European Journal of Endocrinology*, vol. 141, no. 1, pp. 35–39, 1999.

[16] M. D. Kraaij, S. W. van der Kooij, M. E. Reinders et al., "Dexamethasone increases ROS production and T cell suppressive capacity by anti-inflammatory macrophages," *Molecular Immunology*, vol. 49, no. 3, pp. 549–557, 2011.

[17] G. Bjelaković, S. Beninati, D. Pavlović et al., "Glucocorticoids and oxidative stress," *Journal of Basic and Clinical Physiology and Pharmacology*, vol. 18, no. 2, pp. 115–112, 2007.

[18] A. M. Traish, H. P. Kang, F. Saad et al., "Dehydroepiandrosterone (DHEA)-a precursor steroid or an active hormone in

human physiology," *Journal of Sexual Medicine*, vol. 8, no. 11, pp. 2960–2982, 2011.

[19] C. Young Shin, J. W. Choi, E. Sook Jang et al., "Dehydroepiandrosterone inhibits the death of immunostimulated rat C6 glioma cells deprived of glucose," *Brain Research*, vol. 922, no. 2, pp. 267–275, 2001.

[20] E. Brignardello, M. Gallo, M. Aragno et al., "Dehydroepiandrosterone prevents lipid peroxidation and cell growth inhibition induced by high glucose concentration in cultured rat mesangial cells," *Journal of Endocrinology*, vol. 166, no. 2, pp. 401–406, 2000.

[21] J. P. G. Camporez, E. H. Akamine, A. P. Davel, C. R. Franci, L. V. Rossoni, and C. R. De Oliveira Carvalho, "Dehydroepiandrosterone protects against oxidative stress-induced endothelial dysfunction in ovariectomized rats," *Journal of Physiology*, vol. 589, no. 10, pp. 2585–2596, 2011.

[22] M. Aragno, G. Meineri, I. Vercellinatto et al., "Cardiac impairment in rabbits fed a high-fat diet is counteracted by dehydroepiandrosterone supplementation," *Life Sciences*, vol. 85, no. 1-2, pp. 77–84, 2009.

[23] A. Chakraborti, K. Gulati, and A. Ray, "Involvement of nitric oxide in the protective effects of dehydroepiandrosterone sulphate on stress induced neurobehavioral suppression and brain oxidative injury in rats," *European Journal of Pharmacology*, vol. 652, no. 1–3, pp. 55–59, 2011.

[24] M. A. Pelissier, C. Trap, M. I. Malewiak, and R. Morfin, "Antioxidant effects of dehydroepiandrosterone and 7α-hydroxy- dehydroepiandrosterone in the rat colon, intestine and liver," *Steroids*, vol. 69, no. 2, pp. 137–144, 2004.

Hindawi Publishing Corporation
BioMed Research International
Volume 2013, Article ID 923475, 6 pages
http://dx.doi.org/10.1155/2013/923475

Research Article

Prior Lung Inflammation Impacts on Body Distribution of Gold Nanoparticles

Salik Hussain,[1,2,3] Jeroen A. J. Vanoirbeek,[2] Steven Haenen,[2] Vincent Haufroid,[4] Sonja Boland,[1] Francelyne Marano,[1] Benoit Nemery,[2] and Peter H. M. Hoet[2]

[1] *Laboratory of Molecular and Cellular Responses to Xenobiotics, CNRS EAC 7059, Unit of Functional and Adaptive Biology (BFA), Sorbonne Paris Cité, University of Paris Diderot, 75 013 Paris, France*
[2] *Lung Toxicology Research Unit, KU Leuven, 3000 Leuven, Belgium*
[3] *Clinical Research Unit, National Institute of Environmental Health Sciences (NIEHS), NIH, Research Triangle Park, North Carolina NC 27709, USA*
[4] *Louvain Centre for Toxicology and Applied Pharmacology, Catholic University of Louvain, 1200 Brussels, Belgium*

Correspondence should be addressed to Peter H. M. Hoet; peter.hoet@med.kuleuven.be

Received 5 September 2012; Revised 29 November 2012; Accepted 6 December 2012

Academic Editor: Ernesto Alfaro-Moreno

Introduction. Gold- (Au-) based nanomaterials have shown promising potential in nanomedicine. The individual health status is an important determinant of the response to injury/exposure. It is, therefore, critical to evaluate exposure to Au-nanomaterials with varied preexisting health status. *Objective*. The goal of this research was to determine the extent of extrapulmonary translocation from healthy and inflamed lungs after pulmonary exposure to AuNPs. Male BALB/c mice received a single dose of 0.8 mg · kg^{-1} AuNPs (40 nm) by oropharyngeal aspiration 24 hours after priming with LPS (0.4 mg·kg^{-1}) through the same route. Metal contents were analyzed in different organs by inductively coupled plasma-mass spectrometry (ICP-MS). *Results*. Oropharyngeal aspiration resulted in high metal concentrations in lungs ($P < 0.001$); however, these were much lower after pretreatment with LPS ($P < 0.05$). Significantly higher concentrations of Au were detected in heart and thymus of healthy animals, whereas higher concentrations of Au NPs were observed in spleen in LPS-primed animals. *Conclusions*. The distribution of AuNPs from lungs to secondary target organs depends upon the health status, indicating that targeting of distinct secondary organs in nanomedicine needs to be considered carefully under health and inflammatory conditions.

1. Introduction

Nanotechnologies have shown promising potentials in multiple sectors of everyday life. These advances span from material science to consumer products. More recently, various nanomaterials have proved themselves as excellent candidates for nanomedical applications. These range from diagnostics to drug and gene delivery applications. Gold (Au) is one of the major nanomaterials engineered for utilizations in medicine and electronics. The carrier properties of Au NPs make them promising candidates for delivering biological molecules into the cells thus making them an ideal platform for drug and gene delivery [1–4]. Au-based therapeutic strategies (hyperthermal therapy) mainly imply their role as heat-mediating objects (due to their strong light absorbing properties) to destroy particle-loaded cells/tissues [5, 6]. The absorbed light energy is dissipated into the particle surroundings leading to elevated temperatures in their vicinity. This hyperthermal property can further be used as therapeutic strategy to open drug carriers (polymer microcapsules) [7]. Moreover, Au NPs have shown promises as labelling/contrast agents (transmission electron microscopy/X-rays) and sensing agents. Another advantage of these materials is the possibility of utilizing previously mentioned properties at the same time (hyperthermal and photoacoustic imaging) to have combined schemes for the better evaluation of the biological phenomenon. Keeping in view the broad spectrum of *in vivo* applications of Au NPs, the potential deleterious effects of these NPs might become an issue which needs to be evaluated with care. Presently, there is a need to evaluate the potentials

deleterious effects of Au NPs in both *in vitro* and *in vivo* conditions as a discrepancy exists in the literature about the cytotoxic effects of Au NPs on different types of cells [8, 9].

It has been shown that some NPs can cross physiological barriers, reach to secondary target organs, and may lead to unexpected outcomes [10, 11]. There exists a discrepancy in the existing literature about the extrapulmonary translocation of NPs/ultrafine particles [10–12]; however, the NP size dependence of translocation is an accepted fact [13, 14]. Preexisting respiratory disorders (e.g., inflammation) may modify the effects of NPs on the respiratory tract and can influence the amount of translocated material. Under normal conditions, lungs are often primed with endotoxins from the inhaled air [15]. We hypothesized that preexisting inflammation may influence the ability of Au NPs to pass through the pulmonary barrier and other organs in the body. To verify this hypothesis, we tested Au (40 nm) NPs in LPS-treated mice as an airway inflammation model.

2. Materials and Methods

2.1. Reagents. Tetrachloroauric acid (99.999%, $3H_2O$) was purchased from Aldrich. Citrate Tribasic dihydrate (95%, $C_6H_5O_7Na_3$, $2H_2O$) and LPS (*Escherichia coli* O55: B5) were obtained from (Sigma-Aldrich, Steinheim, Germany). The glassware and magnetic beads were always cleaned prior to use with freshly prepared aqua regia (1 : 3 HNO_3 : HCl) followed by rinsing with ultrapure water (Millipore, conductivity: 0.8 mS·cm).

2.2. Animals. Male BALB/c mice (approximately 25 g, 6 weeks old) were obtained from Harlan (The Netherlands). The mice were housed in a conventional animal house with 12 h dark/light cycles. They received lightly acidified water and pelleted food (Trouw Nutrition, Gent, Belgium) ad libitum. All experimental procedures were approved by the Local Ethical Committee for Animal Experiments (Katholieke Universiteit Leuven, Leuvin, Belgium).

2.3. Au Nanoparticle Synthesis. Au NPs of 40 nm primary particle size were prepared in the laboratory (Institut d'Electronique Fondamentale UMR CNRS 8622, Université Paris-Sud, Orsay, France) by Turkevich method. Briefly, an aqueous solution of gold tetrachloroauric acid, with a weight content of 82.8 mg of gold, was heated until boiling point under vigorous stirring. Then, an aliquot of a 1% sodium citrate aqueous solution is added. Gold nanoparticles with average sizes of 39.8 nm were prepared by adjusting the ratio $[AuCl_{-4}]$/[Citrate] from 0.4 to 1.3. After the introduction of the citrate solution, a purple colour appeared which then turned to ruby red. The solution was then stirred and kept at boiling conditions for another 45 minutes to complete the reduction process. In these experiments, NP suspensions (0.4 mg/mL, i.e., 0.8 mg/kg) stabilized in 2.5 mM sodium citrate tribasic dihydrate (vehicle) were utilized to treat the mice.

2.4. Au NP Characterization. These particles were thoroughly characterized for their physicochemical characteristics including morphology, zeta potential (ζ), size distribution, and hydrodynamic diameters.

2.4.1. Transmission Electron Microscopy (TEM). Microscope measurements were performed using a Philips CM30 TEM (Philips FEI, Eindhoven, The Netherlands) operating at 300 kV. Small volumes of sample were deposited on copper mesh grids and covered with carbon coating films. The samples were then dried under an N_2 atmosphere in a glove box.

2.4.2. Dynamic Light Scattering. Dynamic light scattering (DLS) measurements were performed with a Brookhaven 90 Plus Nanoparticle Size Distribution Analyzer (scattering angle 90°, wavelength 659 nm, power 15 mW; Brookhaven Instruments Ltd, Redditch, UK). Correlation functions were analyzed using the Clementine package (maximum entropy method) for Igor Pro 6.02A (WaveMetrics, Portland, OR, USA). This resulted in intensity-weighted distribution functions versus decay times. By converting the decay times with instrument parameters and physical parameters to hydrodynamic diameters, an intensity-weighted size distribution is obtained. A log-normal fit was applied to each population, resulting in the intensity-weighted average hydrodynamic diameter of the population. Mass- and number-weighted distributions were estimated using the Rayleigh scattering approximation and a correction factor for the form factor of spherical particles.

2.4.3. ζ Potential Measurements. ζ potential measurements were performed on the same NP solutions as used for DLS. Au and ζ potential were measured with a Brookhaven 90Plus/ZetaPlus instrument applying electrophoretic light scattering. A primary and reference beam (659 nm, 35 mW) modulated optics and a dip-in electrode system were used. The frequency shift of scattered light (relative to the reference beam) from a charged particle moving in an electric field is related to the electrophoretic mobility of the particle. The Smoluchowski limit was used to calculate the ζ potential from the electrophoretic mobility.

2.5. LPS Treatment. LPS (*Escherichia coli* O55: B5, Sigma Aldrich) was suspended in HBSS and administered 10 μg/mouse (0.4 mg/kg). The dose of LPS was based on information available in the literature; the amount given induces only local (pulmonary) inflammation [16].

2.6. Experimental Design. On day, 1 animals were exposed to 10 μg (10 μL) of LPS or HBSS (vehicle for LPS) by oropharyngeal aspiration (Figure 1). On day 2, animals were administered 40 μL of 0.4 mg/mL (0.8 mg/kg) NP suspensions or vehicle through same route. On day 3 (24 hours later), the animals were sacrificed, blood was collected through retro-orbital plexus, and the organs were removed. Organs (brain, thymus, lung, heart, liver, spleen, kidney, and testis)

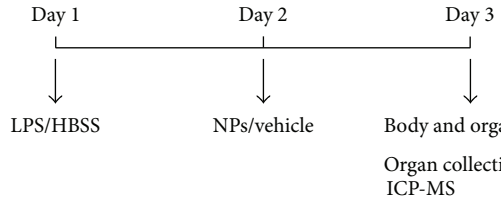

Figure 1: Experimental design. Animals ($n = 4$) were given 10 μL of LPS or its vehicle (HBSS) on day 1 by oropharyngeal route. On day 2, animals were administered 40 μL of NP suspension or vehicle for NPs (2.5 mM trisodium citrate) by the same route. Twenty four hours later, animals were weighed and sacrificed, organs were collected, wet organ weights were measured, and samples were processed for ICP-MS analysis.

were weighed to obtain wet weight. Each experimental group comprised of 4-5 animals.

2.7. Metal Content Analysis. After weighing, the organs were placed in glass tubes and digested using 2 mL pure 60% nitric acid (Sigma-Aldrich). The tubes were placed in a water bath at 80°C until all the tissues were solubilized. The samples were then analyzed for metal contents. The analytical determination of Au in samples was performed by inductively coupled plasma-mass spectrometry (ICP-MS) using Agilent 7500cx. Samples were diluted 100 times with a basic diluents (butanol 2%, EDTA 0.05%, NH_4OH 1%, and triton 0.05%) containing internal standards. The quantification of Au was performed using the unique 197Au isotope and 193Ir as an internal standard in the "nogas mode" (standard mode).

2.8. Statistical Analysis. Data are presented as mean ± SD where $n = 3$-4 animals per group. All groups were tested for normality using the Kolmogorov-Smirnov normality test. Since our data were normally distributed, we applied an analysis of variance (ANOVA) followed by Tukey's test for multiple comparisons using Graphpad (Graphpad Prism 4.01, Graphpad Software Inc., San Diego, USA). A level of $P < 0.05$ (two tailed) was considered significant.

3. Results

3.1. Au NP Characteristics. Au NP suspension optical spectroscopy analysis of Au NP revealed a single Plasmon peak around 520 nm. TEM analysis revealed spherical morphology of Au NPs (Figure 2(a)), and size distribution analysis indicated a single peak of Au NPs with 40 nm hydrodynamic diameter (Figure 2(b)). The ζ potential measurements in 2.5 mM sodium citrate solution (vehicle for animal exposure) indicated that Au NPs had −73 mV showing that electrostatic repulsions are important factor in stabilising the suspensions. This further confirmed the stabilising effect of citrate solution as these NPs showed lower negative ζ potentials in water (data were not shown).

3.2. Animal Study. Only lung relative weights differed significantly between saline and LPS-treated groups (data were not shown) due to inflammation and oedema caused by LPS in the lungs. Significant increases in metal concentration (relative to background values in an untreated group) in the lungs of the animals were detected by ICP-MS (Figure 3). After priming with LPS, lower amounts were detected in the lungs of primed animals as compared to those of nonprimed animals (Figure 3). In nonprimed animals, higher amounts of Au were detected in heart and thymus. However, a significant increase after LPS priming was observed in spleen (Figure 3 inset).

4. Discussion

This study was designed to assess the extrapulmonary translocation of Au NPs in a pulmonary inflammation model. Quantitative data indicated that 81% ± 10% of the aspirated dose remains in the lungs of the healthy animals, with 3% ± 3% and 6% ± 2% being found in heart and thymus, respectively. However, in LPS primed animals, only 25% ± 8% was detected in lungs, with 7% ± 5% detected in spleen and 3% ± 1% detected in thymus. Interestingly, we found that in LPS-primed animals, the amount of Au which reach spleen is 5-6 fold higher than found in healthy animals.

We demonstrate here that even in healthy animals, Au NPs reach secondary target organs after lung exposures. Moreover, striking differences in the target organs (spleen versus heart) between LPS exposed and unexposed animals is of particular interest. A graphical overview of the findings is presented in Figure 4. Recently, several reports have emphasized the potential applications of Au NPs in nanomedicine, but the possibilities of such secondary effects have not been illustrated. The mechanisms of translocation through the air-blood barrier remains unclear: epithelial uptake may occur and cause damage to epithelial cells; electron microscopic study demonstrated UFPs passage via the clefts between the alveolar epithelial cells in healthy conditions. As to the mechanisms of damages of the alveolar wall by LPS, it is suggested that macrophages and neutrophils activated by LPS release free radicals resulting in the degeneration of the air-blood barrier. Translocation of NPs from the air-blood barrier to the capillary lumen may take place through the degenerated structures with acute inflammatory condition [15, 17].

Is has also been observed that NPs potentiate an inflammatory response in subjects with lung inflammation. In view of the impact on (innate and adaptive) immunity, NPs influence cell populations, such as macrophages/monocytes, neutrophils, dendritic cells, natural killer cells, and lymphocyte [18–20]. The preexposure stimulation of the immune system with LPS, resulting in significant changes in the spleen, probably lays on the basis of the different distribution in inflammatory conditions [21].

An important fact is that these data are obtained using realistic NP doses (doses which do not induce inflammation in the lungs of healthy animals) contrary to the literature reports which used huge amounts of NPs to observe systemic translocation. Previously, it was demonstrated that the majority of the administered Au NPs are retained within the healthy lung and only small portion reaches systemic circulation after inhalation exposure [22].

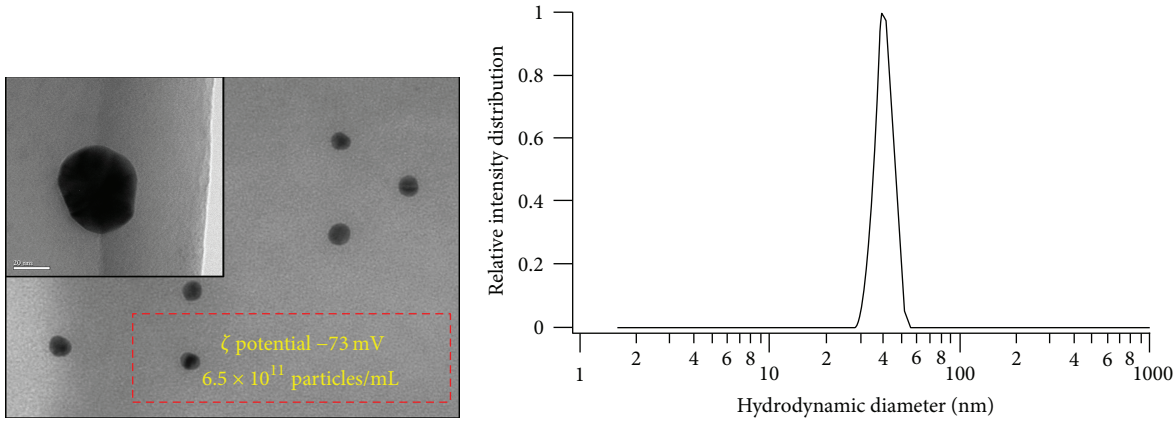

Figure 2: Characterization of Au NPs after suspension in 2.5 mm sodium citrate. (a) Transmission electron microscopic (TEM) image of 40 nm Au NPs. Inset shows a single particle at higher magnification (bar 20 nm). Box indicating ζ potential of these Au NP suspensions (in 2.5 mM sodium citrate) and particle number per mL. (b) Dynamic Light Scattering (DLS) analysis of Au nanoparticle suspension showing single population of Au nanoparticles, having 40 nm hydrodynamic diameter.

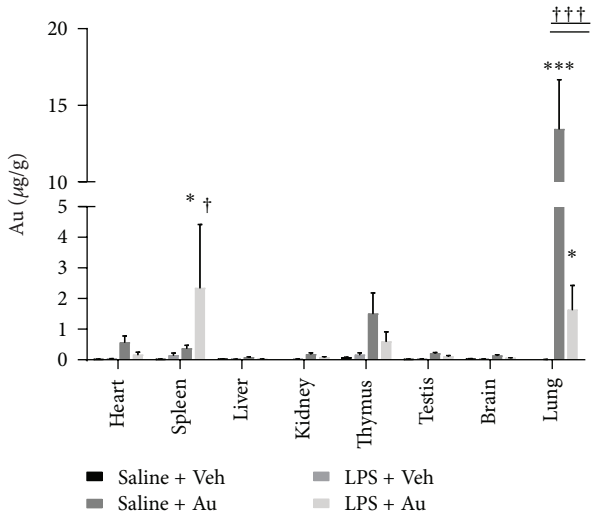

Figure 3: Body distribution of Au NPs with or without pretreatment with LPS. The concentration of Au NPs ($\mu g \cdot g^{-1}$ relative organ weight) in lungs (a) in different secondary organs (b) of animals with or without pretreatment with LPS. ∗ represents statistically different from respective (saline/LPS) control group without NPs and † represents statistically different from NP-treated group without LPS, $P < 0.05$ (two tailed). $^{***}P < 0.01$ and $^{\dagger\dagger\dagger}P < 0.01$.

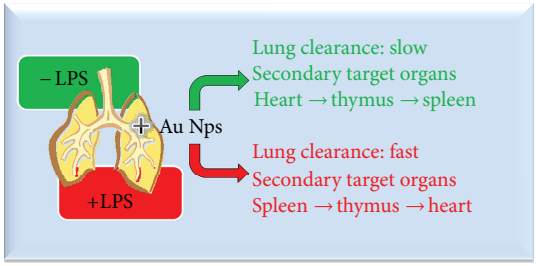

Figure 4: Schematic overview of the results presented in this study.

We have recently reported that in the experiments done in parallel with the same dose of Au NPs given through same route did not induced inflammation (neither an increase in bronchoalveolar lavage fluid cellularity nor cytokines) [23]. The reason for the increase in Au in the spleen after LPS exposure is not clear. LPS exposure provokes an inflammatory response, leading to influx of inflammatory cells in the lungs resulting in an increase in phagocytosis of deposited material by macrophages. These macrophages might play a central role in the transport and clearance of the Au NPs, thus explaining the lower amounts material after LPS exposure [24]. Moreover, we have recently showed increased numbers of Au laden macrophages in bronchoalveolar lavage fluids of "asthmatic" animals in a mouse model of diisocyanate-induced asthma [23]. It has been demonstrated that macrophages (in particular Kupffer cells) play the most important role in the clearance of intravenously injected Au NPs [25]. We are currently evaluating these mechanisms in detail, but we consider it timely and important to share our preliminary observations with the scientific community. However, in another study, it was shown that 15-day inhalation chamber exposure to Au NPs results in accumulation of significant amounts of Au in spleen along with many parts of digestive and cardiovascular system in rats [26]. Recent studies demonstrated the presence of gold nanoparticles and nanorods in spleen after intravenous exposures [27]. The differential interaction with lung lining fluid (in case of inhalation exposure) and blood proteins (in case of intravenous exposure) were postulated to be the reasons for differential body distributions of Au NPs in inhalation versus intravenous exposures [27]. We show here that Au NPs can reach spleen even in case of lung exposure. It could be speculated that there might exist the possibilities of immunomodulatory/immunotoxic effects of Au NPs. Moreover, it is noteworthy that it has been already shown that Au reduces the antigen presentation and autoimmune reactions in rheumatoid arthritis [28]. However, in depth, mechanistic

studies are needed to elucidate whether Au NPs exposure that can also result in similar outcome is unknown.

The shortcomings of the present study did not include directly measuring inflammatory response in the lungs (relying on the literature data/previous experience with the LPS dose to induce inflammation) and housing animals in metabolic cages to comprehensively estimate the clearance of NPs from the body and to account for the dose lost from the LPS-primed lungs. Moreover, the role of NP physicochemical characteristics, surface modification/functionalization, and protein corona need in-depth evaluations. Recently, It has been shown that protein corona can significantly modify the responses to biomedical nanoparticles and its complementary factor cell vision should also be considered [29].

5. Conclusion and Perspectives

In conclusion, our results confirm the hypothesis of particle translocation from the lungs to secondary organs like spleen, heart, and thymus. The observation that NPs target different organs depending on the health status of the animal warrants further studies to understand the mechanisms involved in this process and possible consequences. There is an urgent need of both *in vivo* and *in vitro* mechanistic studies to better understand the possible differences in interactions of Au NPs with different organ systems in the body. A particular focus must be made to understand the unexpected outcomes of Au NP exposures in animal models of different diseases. Moreover, mechanistic studies are warranted to understand the interaction of Au NPs with immune system.

6. Executive Summary

(i) Au NPs can cross the air-blood barrier in both healthy and inflamed lungs.

(ii) Preexisting inflammation alters the body distribution pattern of Au NP.

(iii) Distinct organ targeting in case of inflamed lungs indicates the need to evaluate the consequences of NP administration in diseases status.

Ethical Approval

The authors declare that appropriate institutional review board approval was obtained prior to animal experiments.

Conflict of Interests

The authors declare that they have no conflict of interests.

Acknowledgments

Jean-Pierre Abid is acknowledged for preparing the particles and Gladys Deumer for her technical assistance for Au determination. This work was supported by the Research Foundation Flanders (FWO G.0707.09).

References

[1] Y. Higuchi, S. Kawakami, and M. Hashida, "Strategies for in vivo delivery of siRNAs: recent progress," *BioDrugs*, vol. 24, no. 3, pp. 195–205, 2010.

[2] B. Duncan, C. Kim, and V. M. Rotello, "Gold nanoparticle platforms as drug and biomacromolecule delivery systems," *Journal of Controlled Release*, vol. 148, no. 1, pp. 122–127, 2010.

[3] J. Wang, M. Sui, and W. Fan, "Nanoparticles for tumor targeted therapies and their pharmacokinetics," *Current Drug Metabolism*, vol. 11, no. 2, pp. 129–141, 2010.

[4] B. Kim, G. Han, B. J. Toley, C. K. Kim, V. M. Rotello, and N. S. Forbes, "Tuning payload delivery in tumour cylindroids using gold nanoparticles," *Nature Nanotechnology*, vol. 5, no. 6, pp. 465–472, 2010.

[5] K. V. Chakravarthy, A. C. Bonoiu, W. G. Davis et al., "Gold nanorod delivery of an ssRNA immune activator inhibits pandemic H1N1 influenza viral replication," *Proceedings of the National Academy of Sciences of the United States of America*, vol. 107, no. 22, pp. 10172–10177, 2010.

[6] C. R. Patra, R. Bhattacharya, and P. Mukherjee, "Fabrication and functional characterization of goldnanoconjugates for potential application in ovarian cancer," *Journal of Materials Chemistry*, vol. 20, no. 3, pp. 547–554, 2010.

[7] R. A. Sperling, P. Rivera Gil, F. Zhang, M. Zanella, and W. J. Parak, "Biological applications of gold nanoparticles," *Chemical Society Reviews*, vol. 37, no. 9, pp. 1896–1908, 2008.

[8] E. E. Connor, J. Mwamuka, A. Gole, C. J. Murphy, and M. D. Wyatt, "Gold nanoparticles are taken up by human cells but do not cause acute cytotoxicity," *Small*, vol. 1, no. 3, pp. 325–327, 2005.

[9] Y. Pan, S. Neuss, A. Leifert et al., "Size-dependent cytotoxicity of gold nanoparticles," *Small*, vol. 3, no. 11, pp. 1941–1949, 2007.

[10] A. Nemmar, P. H. M. Hoet, B. Vanquickenborne et al., "Passage of inhaled particles into the blood circulation in humans," *Circulation*, vol. 105, no. 4, pp. 411–414, 2002.

[11] N. L. Mills, N. Amin, S. D. Robinson et al., "Do inhaled carbon nanoparticles translocate directly into the circulation in humans?" *American Journal of Respiratory and Critical Care Medicine*, vol. 173, no. 4, pp. 426–431, 2006.

[12] P. Wiebert, A. Sanchez-Crespo, J. Seitz et al., "Negligible clearance of ultrafine particles retained in healthy and affected human lungs," *European Respiratory Journal*, vol. 28, no. 2, pp. 286–290, 2006.

[13] E. Sadauskas, N. R. Jacobsen, G. Danscher et al., "Biodistribution of gold nanoparticles in mouse lung following intratracheal instillation," *Chemistry Central Journal*, vol. 3, no. 1, article 16, 2009.

[14] W. G. Kreyling, M. Semmler-Behnke, J. Seitz et al., "Size dependence of the translocation of inhaled iridium and carbon nanoparticle aggregates fürom the lung of rats to the blood and secondary target organs," *Inhalation Toxicology*, vol. 21, no. 1, pp. 55–60, 2009.

[15] H. Inoue, A. Shimada, T. Kaewamatawong et al., "Ultrastructural changes of the air-blood barrier in mice after intratracheal instillation of lipopolysaccharide and ultrafine carbon black particles," *Experimental and Toxicologic Pathology*, vol. 61, no. 1, pp. 51–58, 2009.

[16] P. R. M. Rocco, D. P. Momesso, R. C. Figueira et al., "Therapeutic potential of a new phosphodiesterase inhibitor in acute lung injury," *European Respiratory Journal*, vol. 22, no. 1, pp. 20–27, 2003.

[17] K. I. Inoue, H. Takano, R. Yanagisawa et al., "Effects of inhaled nanoparticles on acute lung injury induced by lipopolysaccharide in mice," *Toxicology*, vol. 238, no. 2-3, pp. 99–110, 2007.

[18] S. Hussain, J. A. Vanoirbeek, and P. H. Hoet, "Interactions of nanomaterials with the immune system," *Nanomedicine and Nanobiotechnology*, vol. 4, no. 2, pp. 169–183, 2012.

[19] D. L. R. Goncalves, R. de Liz, and D. Girard, "Activation of neutrophils by nanoparticles," *TheScientificWorldJOURNAL*, vol. 11, Article ID 768350, 9 pages, 2011.

[20] K. I. Inoue, H. Takano, R. Yanagisawa et al., "Effects of airway exposure to nanoparticles on lung inflammation induced by bacterial endotoxin in mice," *Environmental Health Perspectives*, vol. 114, no. 9, pp. 1325–1330, 2006.

[21] X. Xu, F. Deng, X. Guo et al., "Association of systemic inflammation with marked changes in particulate air pollution in Beijing in 2008," *Toxicology Letters*, vol. 212, no. 2, pp. 147–156.

[22] S. Takenaka, E. Karg, W. Kreyling et al., "Distribution pattern of inhaled ultrafine gold particles in the rat lung," *Inhalation Toxicology*, vol. 18, no. 10, pp. 733–740, 2006.

[23] S. Hussain, J. A. J. Vanoirbeek, K. Luyts et al., "Lung exposure to nanoparticles modulates an asthmatic response in a mouse model," *European Respiratory Journal*, vol. 37, no. 2, pp. 299–309, 2011.

[24] D. P. K. Lankveld, R. G. Rayavarapu, P. Krystek et al., "Blood clearance and tissue distribution of PEGylated and non-PEGylated gold nanorods after intravenous administration in rats," *Nanomedicine*, vol. 6, no. 2, pp. 339–349, 2011.

[25] E. Sadauskas, H. Wallin, M. Stoltenberg et al., "Kupffer cells are central in the removal of nanoparticles from the organism," *Particle and Fibre Toxicology*, vol. 4, article 10, 2007.

[26] L. E. Yu, L. Y. L. Yung, C. N. Ong et al., "Translocation and effects of gold nanoparticles after inhalation exposure in rats," *Nanotoxicology*, vol. 1, no. 3, pp. 235–242, 2007.

[27] S. K. Balasubramanian, J. Jittiwat, J. Manikandan, C. N. Ong, L. E. Yu, and W. Y. Ong, "Biodistribution of gold nanoparticles and gene expression changes in the liver and spleen after intravenous administration in rats," *Biomaterials*, vol. 31, no. 8, pp. 2034–2042, 2010.

[28] S. L. De Wall, C. Painter, J. D. Stone et al., "Noble metals strip peptides from class II MHC proteins," *Nature Chemical Biology*, vol. 2, no. 4, pp. 197–201, 2006.

[29] M. Mahmoudi, S. N. Saeedi-Eslami, M. A. Shokrgozar et al., "Cell "vision": complementary factor of protein corona in nanotoxicology," *Nanoscale*, vol. 4, no. 17, pp. 5461–5468, 2012.

Hindawi Publishing Corporation
BioMed Research International
Volume 2013, Article ID 652632, 12 pages
http://dx.doi.org/10.1155/2013/652632

Research Article

Inflammatory and Oxidative Stress Responses of an Alveolar Epithelial Cell Line to Airborne Zinc Oxide Nanoparticles at the Air-Liquid Interface: A Comparison with Conventional, Submerged Cell-Culture Conditions

Anke-Gabriele Lenz,[1] Erwin Karg,[2] Ellen Brendel,[1] Helga Hinze-Heyn,[1] Konrad L. Maier,[1] Oliver Eickelberg,[1] Tobias Stoeger,[1] and Otmar Schmid[1]

[1] *Comprehensive Pneumology Center, Institute of Lung Biology and Disease, Helmholtz Zentrum München, Ingolstaedter Landstrasse 1, 85758 Neuherberg, Germany*
[2] *Joint Mass Spectrometry Center, Helmholtz Zentrum München, Ingolstaedter LandstraBe 1, 85758 Neuherberg, Germany*

Correspondence should be addressed to Anke-Gabriele Lenz; alenz@helmholtz-muenchen.de

Received 27 August 2012; Accepted 23 November 2012

Academic Editor: Irma Rosas

The biological effects of inhalable nanoparticles have been widely studied *in vitro* with pulmonary cells cultured under submerged and air-liquid interface (ALI) conditions. Submerged exposures are experimentally simpler, but ALI exposures are physiologically more realistic and hence potentially biologically more meaningful. In this study, we investigated the cellular response of human alveolar epithelial-like cells (A549) to airborne agglomerates of zinc oxide (ZnO) nanoparticles at the ALI, compared it to the response under submerged culture conditions, and provided a quantitative comparison with the literature data on different types of particles and cells. For ZnO nanoparticle doses of 0.7 and 2.5 μg ZnO/cm^2 (or 0.09 and 0.33 cm^2 ZnO/cm^2), cell viability was not mitigated and no significant effects on the transcript levels of oxidative stress markers (HMOX1, SOD-2 and GCS) were observed. However, the transcript levels of proinflammatory markers (IL-8, IL-6, and GM-CSF) were induced to higher levels under ALI conditions. This is consistent with the literature data and it suggests that *in vitro* toxicity screening of nanoparticles with ALI cell culture systems may produce less false negative results than screening with submerged cell cultures. However, the database is currently too scarce to draw a definite conclusion on this issue.

1. Introduction

Exposure to airborne particles has been linked to adverse health effects including pulmonary inflammation, thrombosis, neurodegeneration, and cardiovascular disease [1–3]. A number of studies have indicated that particles with diameters below 100 nm have a more pronounced effect than larger particles, implying that nanoparticles (or ultrafine particles) are more toxic on a mass basis [3–6].

Zinc is an ubiquitous transition metal associated with industrial emissions (e.g., mining and smelting of zinc) that typically appears in the form of zinc oxide (ZnO) in ambient particulate matter (PM) [7–9]. ZnO is known as an occupational hazard, since inhalation of high concentrations of ZnO formed during welding activities can lead to metal fume fever [10, 11] associated with a marked upregulation of proinflammatory markers in the lung [11–13]. In addition to these inadvertently generated ZnO nanoparticles, there is a variety of ZnO nanostructures, which have shown great potential for nanotechnological products including manufacturing and pharmaceutical applications [14, 15]. However, there is increasing concern that the desirable technological

characteristics of nanosized ZnO may be countervailed by increased health and environmental risks due to toxic effects that do not occur for bulk ZnO. While the enhanced toxicity potential of nanoparticles is at least in part due to their inherently large surface-to-mass ratio [4, 6, 16, 17], there is also evidence that some metal particles trigger additional toxicological pathways making them more toxic (per surface area) than many other particle types (e.g., carbon, polystyrene) [18].

Cell-based *in vitro* toxicity assays are widely used to assess the toxicity of nanoparticles. These toxicological *in vitro* studies are typically performed using cell cultures grown under submerged conditions, where the toxin/stressor is dissolved or suspended (nonsoluble nanoparticles) directly in the cell culture medium covering the cells. While this approach is experimentally simple, submerged cell exposures have two main limitations. First, the particle dose interacting with the cells is typically unknown since the particle fraction reaching the cells can neither be readily measured nor always be calculated from the hydrodynamic properties of the particles (size, density, shape) [19]. This problem is especially pronounced for particles smaller than about 100 nm, when diffusion becomes the dominant transport mechanism [20], leading to loss of particles to lateral walls. The second limitation is that submerged cell-culture conditions represent an unrealistic and artificial environment for alveolar epithelial cells in the lungs. *In vivo* exposure through inhalation involves deposition of PM onto the lung epithelium, that is, the cells are exposed to inhaled air (airborne PM) from one side while being in contact with the blood circulation from the other side. Since submerged cell systems are completely covered with cell culture medium (see Figure 1(b)), *in vivo* exposure conditions can be mimicked more realistically by exposing epithelial cells at the air-liquid interface (ALI) (Figure 1(a)). Various ALI exposure systems have been introduced [21–28], but it is unclear whether the enhanced experimental complexity of the ALI exposures compared to submerged exposures is justified. For that reason, we compared the cellular response to nanoparticles after ALI and submerged exposure.

One of the most widely accepted paradigms of particle toxicity states that particles induce inflammation via oxidative stress and subsequent activation of redox-sensitive transcription factors [29]. Nel and colleagues refined and expanded this concept into the hierarchical oxidative stress paradigm [30, 31] suggesting the transition from an antioxidant defense response (tier1) to inflammation (tier2) and finally to cytotoxicity (tier3), if the induced stress is strong enough. Proinflammatory responses mediated by oxidative stress have been proposed to be not only crucial but also the most sensitive readout for particle toxicity [30]. We therefore measured three proinflammatory cytokines (interleukin-8 (IL-8), IL-6, and granulocyte macrophage colony-stimulating factor (GM-CSF)) and three oxidative stress markers (heme oxygenase 1 (HMOX1), superoxide dismutase (SOD-2), and glutamate-cysteine synthetase, catalytic subunit (GCS)) by qRT-PCR.

In this study the first ALI exposure of human epithelial-like cells (A549) to airborne agglomerates of ZnO nanoparticles is presented. The dose- and time-dependent cellular responses of the cells were compared after ZnO exposure under submerged and ALI conditions at two dose levels (0.7 and 2.5 $\mu g/cm^2$) and two time points (0 h or 2 h after incubation). From the exposure-specific *in vitro* toxicity data, we deduced corresponding lowest observed effect levels (LOELs) and compared them with similar studies available in the literature.

2. Materials and Methods

2.1. Materials. Common laboratory chemicals were purchased from Sigma-Aldrich (Taufkirchen, Germany). The particle exposure experiments were performed with commercially available powder of ZnO nanoparticles (NPs) (Alfa Aesar, Ward Hill, MA, USA ID 43141) with primary particle diameters between 24 and 71 nm (manufacturer information) and a measured BET surface area of $13 \pm 2\ m^2/g$, which agrees with the manufacturer specifications (15–45 m^2/g) within experimental uncertainties.

2.2. Cell Culture. In this study, the alveolar epithelial-like cell line (A549) from a human lung adenocarcinoma (obtained from ATTC, Manassas, VA, USA) representing the alveolar type II phenotype [32] was used.

For ALI exposure (Figure 1(a)), A549 cells were seeded on perforated Anodisc membranes (Whatman, Maidstone, UK; aluminum oxide, diameter: 47 mm, pore size: 0.2 μm) with about $1.6 \times 10^5/cm^2$ cells and cultivated in 25 mL Petri dishes under submerged conditions for 9 d at 37°C in DMEM/F12/L-Glut/15 mM HEPES buffer (Invitrogen, Germany) containing 100 U/mL penicillin, 100 μg/mL streptomycin, and 10% FCS. After 9 d a confluent layer with a cell density of approximately $5.1 \times 10^5/cm^2$ was obtained. 1 hour prior to particle exposure, the cells were transferred to the ALI, by taking the six cell-covered membranes from the Petri dishes and placing them in two cell exposure chambers (described below) using the same culture medium as above but without FCS. This arrangement allows nourishment of the cells with a cell culture medium through the perforated membrane from the bottom and exposure to airborne particles from the top. Immediately after ALI exposure, the cells were washed with PBS and gently scrapped off the membranes after adding trypsin/EDTA (for RT-PCR). For reasons discussed below, one of the cell-covered membranes in each ALI exposure chamber was incubated for a postincubation period of 2 h (submerged in 3 mL medium at 37°C) prior to determination of the biological endpoints.

For exposure under submerged conditions (Figure 1(b)), A549 cells were seeded at $2.5 \times 10^5/cm^2$ in 24-well plates and incubated for 16 h in DMEM/F12/L-Glut/15 mM HEPES buffer (Invitrogen, Germany) containing 100 U/mL penicillin, 100 μg/mL streptomycin, and 10% fetal calf serum (FCS) resulting in a cell density of approximately $3.5 \times 10^5/cm^2$.

2.3. Exposure at the ALI. The ZnO powder was aerosolized with a commercially available venturi-type dry powder disperser (Model SAG 410, TOPAS, Leipzig, Germany) optimized for output stability by taking the following measures: (i) the metal venturi nozzle was replaced by a ceramic nozzle to avoid chemical and mechanical erosion, (ii) the particle reservoir and the inlet of the venturi nozzle were permanently flushed with dry nitrogen instead of filtered ambient air to minimize clogging due to moisture effects, (iii) the scraper in the reservoir was modified to allow for permanent stirring of the powder especially at the bottom of the reservoir, (iv) the aerosol output was passed through a buffer volume to remove extremely large particles (sedimentation) and smoothen fluctuation in ZnO NP concentration, and (v) particle growth due to coagulation was minimized by diluting the aerosol (1 : 1) with compressed filtered air directly after generation.

A detailed description of the ALI exposure chamber used here was provided by Bitterle et al. [21]. Briefly, ZnO aerosol was generated at a flow rate of 1.5 L/min with the generator described above and evenly distributed to two cell exposure chambers (one for particle exposure or control) holding three cell-covered Anodisc membranes each. The two chambers were operated in parallel using symmetric flow splitters with the control atmosphere (clean air) being obtained by filtration with a PALL filter (BB50TE, PALL, Newquay, UK). Each chamber was supplied with 0.25 L/min aerosol-laden air (or filtered air for control), which was directed at a radially symmetric stagnation point flow profile over the cell-covered membrane. This design assures spatially uniform particle deposition onto the cells at a deposition fraction, which was experimentally determined to be almost constant (2% of the particles in the sample flow) over a broad particle size range of about 50 to 500 nm [33], due to the compensating effects of diffusional and gravitational deposition [34]. The air flow was conditioned to 37°C and 99.5 % relative humidity. A more detailed description of the ALI exposure chamber is provided by Bitterle et al. [21].

The particle number size distribution was measured immediately downstream of the exposure units with a scanning mobility particle sizer (SMPS, model 3080, TSI, St. Paul, MN, USA, combined with a TSI model 3025A condensation particle counter). By maintaining a constant particle concentration (within about ±20%) during the 3 h exposure time, the cell-delivered particle dose increased linearly with time. After 3 h the final dose was reached and the biological parameters were evaluated at this time point (referred to as 0 h) and after an additional 2-hour postincubation time at 37°C under submerged conditions (referred to as 2 h).

2.4. Exposures under Submerged Conditions. For ZnO exposures under submerged conditions, the culture medium in each well was replaced with serum-free medium into which NPs of 0.7 and 2.5 μg/cm^2 of well area were given by adding the appropriate volume of a freshly prepared 1 mg ZnO/mL H_2O stock suspension (vortexed and sonicated twice for 1 min intermittently immediately prior to application). The size distribution of the ZnO NPs in suspension was determined with a dynamic light scattering sizer (DLSS) (HPPS 5001 Malvern Instruments Ltd., Worcestershire, UK). As shown in the Results section, gravitational settling was sufficient for all particles to reach the cells within 1 h. Thus, the final particle dose was delivered to the cells after a 1 h exposure time. The biological parameters are reported relative to control conditions (incubated cell cultures without ZnO) either directly after the exposure time (referred to as 0 h) or after an additional 2 h postincubation time (referred to as 2 h).

2.5. qRT-PCR Measurements of Proinflammatory and Oxidative Stress Markers (mRNA Expression). Gene expression levels of interleukin-8 (IL-8), IL-6, granulocyte macrophage colony-stimulating factor (GM-CSF), the antioxidant enzyme heme oxygenase 1 (HMOX1), superoxide dismutase (SOD-2), and glutamate-cysteine synthetase, catalytic subunit (GCS), were measured by RT-PCR with SYBR green. After exposure, cells were lysed and homogenized in a buffer containing guanidine isothiocyanate and total RNA was isolated using a RNeasy kit according to the method recommended by the manufacturer (Quiagen, Germany). To detect cytokine mRNA expression, RNA was reverse-transcribed into cDNA using the First-Strand cDNA Kit (Pharmacia, Germany). For PCR amplification, the above-mentioned cDNA served as template and 3 μL was added together with the specific $5'$ and $3'$ primers to the Absolute QPCR SYBR Green Mixes from ABgene (Thermo Fisher Scientific, Germany). Quantitative PCR was performed in a *Taq*Man instrument (*Taq*Man ABI Prism 7700 Sequence Detector System; Perkin-Elmer, Germany) offering the advantage of fast and real-time measurement of fluorescent signals during amplification. The housekeeping gene glyceraldehyde-3-phosphate dehydrogenase (GAPDH) was used as internal reference to normalize the RNA levels of the genes being studied. The following primers were used (sense; antisense): IL-8 (ATGACTTCCAAGCTGGCCGTGGCT; TCTCAGCCCTCTTCAAAAACTTCTC), IL-6 (GACAGCCACTCACCTCTTC; CCAGGCAAGTCTCCTCAT), GM-CSF (CTTCCTGTGCAACCCAGATT; CTTGGTCCCTCCAAGATGAC), HMOX1 (AAGATTGCCCAGAAAGCCCTGGAC; AACTGTCGCCACCAGAAAGCTGAG), SOD-2 (CCTGGAACCTCACATCAACG; AACCTGAGCCTTGGACACC), GCS (GTTCTTGAAACTCTGCAAGAGAAG; ATGGAGATGGTGTATTCTTGTCC), GAPDH (CCATGAGAAGTATGACAACAGCC; TGGCAGGTTTTTCTAGACGG).

2.6. Viability Assay. Cell viability was measured with the cell proliferation reagent WST-1 (Roche Applied Sciences, Germany). The WST-1 reagent is a ready-to-use solution which was added to the cells at a concentration of 100 μL/mL. Light absorbance was measured after 30 min incubation at 37°C at 450 nm (iEMS Reader MF, Lab Systems).

2.7. Statistical Analysis. Results are presented as geometric mean and geometric standard error of the mean of at least four separate experiments (n = 4–7), since the data are not normally but close to log normally distributed. Data

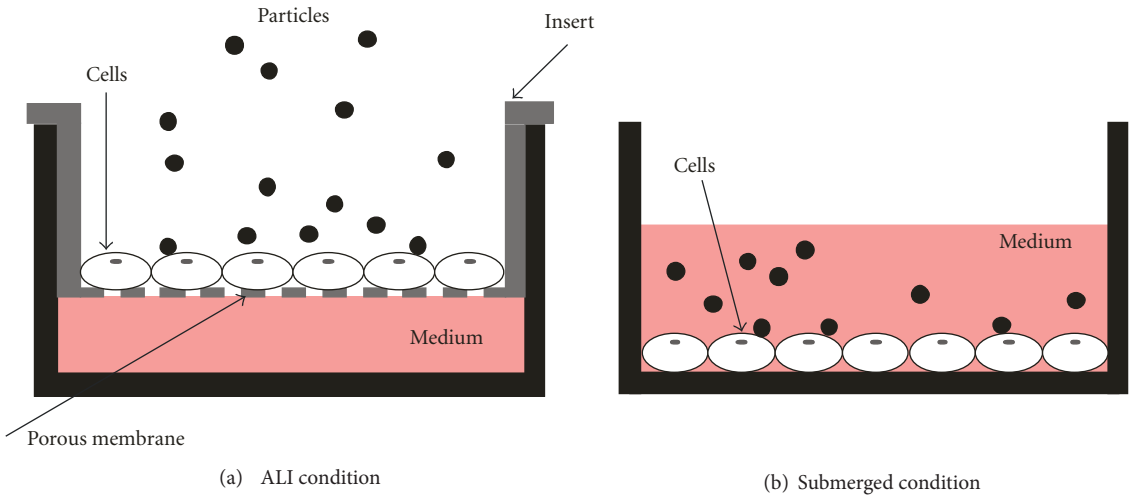

(a) ALI condition (b) Submerged condition

Figure 1: Schematic of the two cell exposure models used for studying particle-cell interaction. (a) Exposure at the air-liquid interface (ALI): airborne particles are directly deposited on cells grown at the air-liquid interface. (b) Exposure under submerged conditions: particles were suspended directly in the cell culture medium covering the cells.

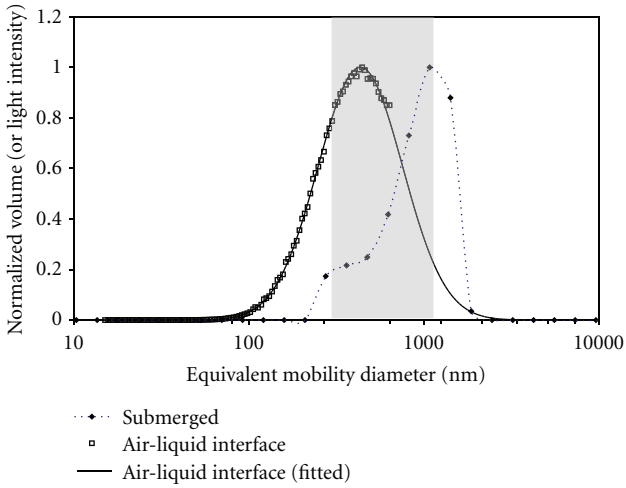

Figure 2: Typical ZnO particle size distribution during ALI submerged (SUB) exposure conditions, respectively. When comparing the particle size distributions during ALI and submerged exposures, one has to consider that different sizing instruments were used. As discussed in the text, both SMPS (ALI) and DLSS (submerged) measure the particle mobility diameter. Furthermore, the volume distribution (normalized to the maximum volume level) is approximately equal to the (normalized) light intensity distribution in the size range between about 315 to 1250 nm (highlighted by the grey shaded area), which encompasses most of the size regime of interest here. The ALI size distributions showed volume-weighted median diameters of about 335 ± 40 nm and a width of 1.77 ± 0.05 (geometric standard deviations). For the submerged conditions (SUB), dynamic light scattering measurements (DLSS) showed ZnO aggregates of about 900 nm (mobility diameter) with a less pronounced (~20%) secondary mode near 350 nm. Thus it is evident that the average ZnO agglomerates were considerably larger during submerged than during ALI exposure condition. For comparison with other studies, the number-weighted size distribution of the ZnO particles during ALI exposure had a count median diameter of about 140 nm (data not shown).

comparisons were carried out using the Kruskal Wallis test (Statgraphics plus 5.0), a nonparametric one-way analysis of variance (ANOVA). $P < 0.05$ was considered as statistically significant.

3. Results

3.1. Particle Size Distribution. The measurement of particle size distributions in different media, such as air and liquid during ALI and submerged exposure, respectively, requires the use of different measurement techniques, here scanning mobility sizing with an SMPS (ALI) and dynamic light scattering using a DLSS (submerged). The SMPS counts individual particles, which are size-selected based on their migration speed in an electric field [35]. The DLSS determines the mobility diameter from the time-dependent fluctuations of the scattered light intensity signal from an ensemble of suspended particles [36]. While both instruments measure the mobility diameter (x-axis of size distribution as depicted in Figure 2), the SMPS counts individual particles and the DLSS reports a signal proportional to the light intensity of a given particle [35]. Since the light intensity signal cannot be directly related to particle number concentration, the SMPS number distribution was converted into effective volume (or mass) distribution, which can be related to the scattered light intensity as described below. Accurate performance and comparability of both instruments was validated with NIST-traceable (National Institute of Standards and Technology, USA) reference particles.

For ALI exposures, the SMPS measurements of the ZnO aerosol revealed a count median (mobility) diameter (CMD) and geometric standard deviation of 141 ± 12 nm and 1.77 ± 0.05, respectively. Since the CMD is larger than the diameter of the primary ZnO NPs (24–71 nm), it is evident that the ZnO aerosol mainly consists of agglomerated (nonspherical) structures. For the two dose levels studied here, the mean

and standard deviation of the number concentration was $(3.5 \pm 0.45) \times 10^5$ and $(9.5 \pm 0.9) \times 10^5$ particles/cm^3. This corresponds to average mass concentrations of 10.1 mg/m^3 and 30.4 mg/m^3, respectively, with an almost constant mass (or volume) median diameter (±standard deviation) of 335 ± 40 nm. As mentioned above, for comparison of SMPS and DLSS, data the SMPS data were converted from number- into mass-based (volume-based) size distribution taking into account the nonspherical shape of the ZnO particles as follows. First, the number size distribution was converted into volume distribution (assuming spherical particle shape for now) and fitted as lognormal distribution using the Hatch-Choate equations for consistent conversion of the count median into mass median diameter. Integration of the volume distribution yields the total volume. For correct conversion into particle mass accounting for the nonspherical particle shape, the volume is multiplied by the effective density of 4.6 g/cm^3 [37], which was experimentally determined by dividing the gravimetrically determined particle mass by the (spherical) particle volume determined from the SMPS data (see Figure 2). The fact that the effective density of the ZnO aerosol is smaller than the bulk density of ZnO (5.6 g/cm^3) is consistent with the agglomerated structure of the ZnO particles [37]. The relatively small difference between effective and bulk density indicates that the particles have a relatively compact (sphere-like) structure.

Although exposures under submerged conditions were performed with the same ZnO particles as used for ALI exposures, ZnO particles suspended in the cell culture medium were more agglomerated and hence larger than those dispersed in air (ALI exposure). As seen from the DLSS size distribution depicted in Figure 2, the ZnO particles, suspended in cell medium for 30 min, displayed a minor mode near 350 nm (about 20% of total mass) and a more pronounced mode near 900 nm (~80% of total particle mass). For accurate comparison of the DLSS sizing data, one has to relate the volume-based size distribution derived from the SMPS data with the light intensity values of the DLSS. For particle sizes near the wavelength λ of the light source (between about $\lambda/2$ and 2λ), it has been shown that the light-intensity-to-volume ratio is almost constant [38]. Thus for the Malvern DLSS ($\lambda = 633$ nm), we can assume that the normalized light intensity distribution (normalized to the maximum of the intensity spectrum) as shown in Figure 2 is approximately equal to the normalized volume (or mass) distribution obtained from the SMPS in the size range between 315 and 1250 nm (shaded area in Figure 2), which covers most of the size range of interest for the present study. Outside this range, the light intensity level is systematically lower than the corresponding volume level [38].

In summary, it is evident that the ALI size distribution was dominated by ZnO agglomerates with a volume median diameter near 350 nm. While this mode is also seen during submerged exposures, most of the particle mass (~80%) resides in a mode near 900 nm indicating that suspending the ZnO particles in cell culture medium for 30 min leads to enhanced particle size due to agglomeration effects.

3.2. Particle Dosimetry. For reliable comparison of the cellular dose-response relationship under ALI and submerged culture conditions, the biological response should be correlated to the cell-delivered particle dose (D_M) normalized to the cell-covered surface area. Here D_M is given by

$$D_M = \frac{M\,\mathrm{Dep}}{A_{\mathrm{cell}}}, \tag{1}$$

where M is the particle mass passing or floating over the cell layer during the exposure, Dep is the deposition efficiency (fraction of particles depositing onto the cell layer), and A_{cell} is the area covered by the exposed cells.

For the ALI exposure, M is calculated from $M = mQt$, where m is the average mass concentration (ZnO mass per volume air; 10.1 and 30.4 mg/m^3 for the low and high dose level, resp.), $Q = 0.25$ L/min is the volumetric flow rate passing over the cell layer, and $t = 3$ h is the exposure time. With $A_{\mathrm{cell}} = 12.6$ cm^2 (per culture membrane) and Dep = 0.02 [21, 33], we find from (1) that $D_{M,\mathrm{ALI}} = 0.7$ and 2.2 μg ZnO/cm^2 for the low and high doses, respectively. With the specific BET surface area of 13 m^2/g, this corresponds to BET surface area doses of 0.09 and 0.29 cm^2 ZnO/cm^2, respectively.

For submerged exposures, we substitute M by $M = mV$ in (1), where m is the ZnO particle mass concentration in the stock suspension (here 1 mg/mL) and V is the volume of the ZnO stock suspension (here 1.4 or 5 μL) added to the culture medium (1 mL). Under the assumption that all particles contained in the medium will deposit on the cells within 3 h (i.e., Dep = 1; will be justified below) we find from (1) that $D_{M,\mathrm{sub}} = 0.7$ and 2.5 μg ZnO/cm^2 (with $A_{\mathrm{cell}} = 2.0$ cm^2) or 0.09 and 0.33 cm^2 ZnO/cm^2, respectively.

As a justification for Dep = 1 under submerged conditions, the following aspects were considered [39]: (I) Is the particle deposition dominated by sedimentation or diffusion (the latter would result in loss of particles to the lateral walls and hence Dep < 1) and (II) if sedimentation dominates particle deposition, is the exposure time long enough for all particles (even the ones near the top of the cell culture well) to reach the cells at the bottom of the well? To address these issues, we calculated the gravitational settling velocity and the mean diffusional displacement speed of the particles in water to be 56 mm/h and 0.033 mm/h, respectively [20], where we assumed an average particle diameter of 900 nm (see Figure 2). Since the ratio of gravitational to diffusional displacement speed is about 1700 for 900 nm particles with a density of 4.6 g/cm^3 (ZnO), sedimentation is the dominant deposition mechanism; that is, negligible particle loss to lateral walls is expected. Secondly, for a sedimentation speed of 56 mm/h and a 50 mm depth of the cell culture medium (1 mL of medium; 2 cm^2 cross-sectional area of well), all ZnO particles are expected to deposit onto the cells within about 1 h.

As a caveat we note that due to differences in deposition kinetics during ALI and submerged exposures (as described above), the final dose was delivered to the cells after 3 h and 1 h, respectively.

3.3. Biological Endpoints. Several biological endpoints were investigated after ZnO exposures of the A549 cells representing human alveolar epithelium type II cells [32, 40]. First, cell viability was determined to exclude the possibility that the observed effects of ZnO NPs on gene expression levels are negatively biased due to cytotoxic effects. No effects on cell viability were seen for the ZnO concentrations investigated here for both ALI (viability in % of (submerged) unchallenged control: 93.5% ± 2.1, at ≤2.2 $\mu g/cm^2$) and submerged conditions (94% ± 7.99, at ≤2.5 $\mu g/cm^2$). Hence, the cellular response to ZnO exposure was not significantly hampered by reduced cell viability and there was no significant reduction in cell viability due to exposure of the cells to the air-liquid interface.

ALI exposure of A549 cells to ZnO NPs caused elevated levels of mRNA coding for IL-8, GM-CSF, and IL-6 as shown in Figure 3(a) (left panel). IL-8 showed a significant increase with increasing dose and time. The time response of GM-CSF was similar to that of IL-8, but no significant dose effect was observed. IL-6 was increased for all ALI exposure scenarios, but no significant dependence on dose or time was observed. On the other hand, the oxidative stress markers HMOX1 and SOD-2 showed no significant increases in mRNA expression except for GCS mRNA which was slightly, but statistically significantly increased for both time points of the high dose level (1.8-fold and 3-fold increased at 0 h and 2 h, resp., see Figure 3(b), left panel).

Under submerged conditions, the expression levels of all proinflammatory markers were lower than those under ALI conditions (Figure 3(a), right panel). For IL-8 only the high dose showed a significant induction of 1.9-fold and 3.7-fold at the two time points, and IL-6 was increased (4-fold) for the high dose at 2 h. Out of the three oxidative stress markers, a significant expression was observed only for HMOX1 (2.7-fold) after 2 h (Figure 3(b), right panel).

In summary, compared to the submerged conditions, ALI exposure showed slight, but statistically significant enhancements in mRNA expression of IL-8, GM-CSF, and IL-6 for all dose levels and time points as well as for the high dose level of GCS (both time points). The only case where the submerged exceeded the ALI response was HMOX1 (high dose, 2 h). Thus the ALI exposure system was generally more sensitive to mRNA induction than the submerged exposure assay especially for the proinflammatory markers.

4. Discussion

To the best of our knowledge, the data presented here represents the first *in vitro* measurements of the cellular response to an exposure of airborne agglomerates of ZnO particles at the ALI. We model inhalation exposure to ZnO NPs with the widely used A549 cell line. A549 cells represent human alveolar epithelial type II cells [32, 40], which are considered the defenders of the alveoli because they are important producers of cytokines [41] and metabolically more active than type I pneumocytes [42, 43]. Consequently, A549 cells are widely regarded as a valid model cell system for pulmonary particle toxicity studies [44, 45].

The data presented here are consistent with positive dose-response correlations. Focusing on ALI conditions first, we find that the IL-8 response (2 h postincubation time) is enhanced for the higher concentration with a 94.5% confidence level ($P = 0.055$). A positive dose-response is also found for GCS (2 h postincubation time; 95% confidence level). On the other hand, no significant response is found for HMOX1 and SOD2 for any of the concentrations used here, since none of these parameters is upregulated. Furthermore, the lack of a dose-response correlation for GM-CSF and IL-6 might be due to reaching the saturation levels already for the lower concentration. Similar considerations can be conducted for the submerged cell culture data. A positive dose-response is seen for IL-8 (both time points), IL-6, and HMOX-1 after 2 h postincubation time. All other parameters are not changed.

While historically *in vitro* particle toxicity studies have been performed with submerged cell systems, various ALI exposure systems have recently been introduced in an attempt to mimic more realistically the exposure conditions during particle inhalation [21–28]. Further advantages of ALI exposures include the preservation of the physicochemical characteristics of the airborne particles (e.g., particle agglomeration and/or particle-medium interactions such as partial dissolution of ZnO in cell culture medium are avoided [46]), the synergistic effects between particulate and gaseous compounds can be investigated (e.g., relevant for combustion emissions) and the biological complexity can be more adequately represented (e.g., surfactant coating can be added to of alveolar epithelial cells). Last but not least, it is typically technically simpler to determine the cell-delivered particle dose under ALI than submerged conditions [47, 48]. Some of the recently introduced ALI exposure systems utilize aerosolized nanoparticle suspensions instead of dry airborne nanoparticles [28]. While these systems allow for cell exposure at the ALI, partial dissolution and possibly agglomeration of the nanoparticles cannot be ruled out with these systems.

Although ALI exposures have become more widely used, there is very little quantitative information on whether and how the exposure type (ALI and submerged) affects the cellular response. A summary of the currently available studies is listed in Table 1 and will be discussed below. In Table 1 all but one investigator utilizes gene expression analysis instead of protein determination as toxicological readout. Gene expression is commonly preceding protein expression; however, the latter can additionally be regulated at the posttranscriptional level. In some cases, protein expression without associated gene expression can occur. However, this is not the case for any of the markers listed in Table 1. Hence, both protein and gene expressions are suitable for toxicity studies. The advantages of gene expression analysis by qPCR include higher sensitivity than the measurement of protein levels, simultaneous quantification of several markers and higher cost efficiency. For these reasons, gene expression analysis was used in the present study to screen for representative markers of different acute response pathways related to inflammation and oxidative stress.

As mentioned above, the cellular response to nanoparticles depends on numerous aspects including cell type, pre- and postprocessing of the cells, state of cell differentiation, particle dose, deposition kinetics, and physicochemical particle characteristics. Matching all of these aspects is very difficult, if not impossible, since, for instance, the state of cell differentiation is inherently different under submerged and ALI culture conditions [49–51] and particle deposition rates onto the cell system may vary significantly for submerged and ALI conditions, since they depend on agglomeration state and carrier medium of the particles (air or liquid). Hence, any study on cellular response under ALI versus submerged cell conditions should provide as much details on these aspects as possible as is done in the following section.

Exposures were performed at two dose levels with no statistically significant difference for the two exposure types (low: 0.7 μg/cm^2; high: 2.2 μg/cm^2 (ALI) and 2.5 μg/cm^2 (submerged)). In addition, the cell type (A549) was identical for both exposure types and the cell densities (cells per cm^2) were similar at the time of exposure. Preprocessing of the cells was different because it had to be adapted to the two different exposure conditions, whereas postprocessing of the cells was identical. There have been several studies indicating differences in cell differentiation due to transfer of the cells from submerged to ALI culture conditions even at the first investigated time points between a few hours and 1 d [49–51]. However, we assume that in the present study the state of cell differentiation was similar, since cells were kept under submerged conditions except for a brief period of time during ALI exposure (1 h prior to exposure; 3 h during exposure). This is supported by the fact that we found no statistically significant differences in cell viability as well as IL-8 mRNA and HMOX-1 mRNA after transfer of the cells to ALI conditions. This is an important aspect, since with an already strained antioxidant defense, as, for instance, reported by [49], cells may be more susceptible to the effects of the particle exposure. Other important aspects for ALI-submerged comparisons are related to the particle characteristics. For ALI conditions, the count median and mass median particle diameters were 141 nm and 335 nm, respectively, and the rate of particle deposition onto the cells was constant (within 20%) during the 3 h exposure time by keeping the sample flow and the ZnO aerosol concentration constant. Under submerged conditions, the size of the ZnO particles increased from a mass median diameter of about 350 nm to about 900 nm within about 30 min due to agglomeration, which results in an approximately 3-fold deposition rate; that is, the entire ZnO dose is delivered to the cells with about 1 h. Hence, differences in deposition kinetics may affect the comparison of the two exposure scenarios. Since the total number of primary particles in the medium is not changing with the agglomeration state, agglomeration does not affect the number of primary particles or the surface area dose delivered to the cells. However, agglomerate size may influence the biological response of the A549. Furthermore, ZnO is partially soluble in aqueous media [30]. Hence, the Zn^{2+}/ZnO ratio may be different under ALI and submerged conditions with higher Zn^{2+}/ZnO ratios to be expected under submerged conditions due to the relatively high dissolution of ZnO in the cell culture medium.

In spite of some experimental differences between submerged and ALI exposures, as described above, it is instructive to compare the ZnO dose-response curves observed under ALI and submerged conditions and relate these findings to similar data sets for other particle and pulmonary cell types from the literature. This can be done by determining the dose range in which the lowest observed effect levels (LOELs) occurred. If none of the two dose levels investigated here showed a statistically significant response, the LOEL lies above the highest dose level (>2.5 μg/cm^2). If the low dose showed no response, but the high dose did, then the LOEL falls in the range of 0.7–2.5 μg/cm^2. If both dose levels showed a response, then the LOEL is below <0.7 μg/cm^2.

As seen from Table 1, our data indicate that four biological parameters (mRNA levels of IL-8, GM-CSF, IL-6, and GCS) showed lower LOELs and hence elevated response levels under ALI conditions. The results for two of the six investigated parameters (HMOX1, SOD-2) were inconclusive, since the investigated dose regime was not broad enough to discern differences in LOEL. Similar results were reported by other studies with pulmonary cell lines and primary cells reported in the literature (Table 1). Volckens and colleagues [26] exposed primary human bronchial epithelial cells to concentrated coarse ambient particulate matter. Applying our LOEL scheme to their data indicates that the mRNA levels of IL-8 and HMOX1 were more pronounced under ALI conditions, while no conclusive result was found for COX-2 mRNA expression. Holder and colleagues [24] investigated Diesel exhaust particles with a human bronchial epithelial cell line (16HGE14o). As seen from Table 1, they found no conclusive result for IL-8 protein levels but state that a much smaller dose was required to induce similar IL-8 expression levels. We contend that this claim is not substantiated by their data, since in contrast to submerged exposures their IL-8 response under ALI conditions was not statistically significantly different from unity (according to their own statistical analysis). It is important to note that the currently available data on submerged versus air-liquid exposure comparisons is limited, but diverse. As seen from Table 1 the data were generated with both immortalized and primary cell cultures as well as with different particle types, various biological endpoints, and different pre-/postprocessing protocols. These differences are likely to result in exposure-dependent differences in the state of cell differentiation, particle-cell interaction, and deposition kinetics. In spite of this heterogeneity, none of the currently available studies has identified a biological parameter, which responded to be more sensitive to particle challenge under submerged exposure conditions than under ALI conditions. While it cannot be inferred that this is true for all possible biological endpoints, the currently available data suggest that air-liquid interface exposures are a more "conservative" toxicity test than submerged systems, that is, ALI cell systems are likely to lead to less false negatives.

To put the particle dose levels typically used for *in vitro* toxicity testing into perspective, it is instructive to consider

Table 1: Comparison of the lowest observed effect levels (LOELs) for nanoparticles exposure of cells exposed at ALI and submerged conditions.

Reference	Particle type	Human epithelial cell type	Time at ALI prior to exposure	Exposure time ALI	Postincubation time ALI	Exposure time Submerged	Postincubation time Submerged	Biological parameter	Dose for the lowest observed effect level (LOEL)[1] Submerged (μg/cm^2)	ALI (μg/cm^2)	ALI more sensitive than submerged
[26]	Coarse urban PM	Bronchial (primary)	3 d	3 h	0 h	0 h	1 h	IL-8 (mRNA)	12.5–25	≤2.0	yes
								HOX-1 (mRNA)	25–65	≤2.0	yes
								COX-2 (mRNA)	≤7.0	≤2.0	unclear
[24]	Diesel soot	Bronchial (16HBE14o)	?[2]	6 h	20 h	6 h	20 h	IL-8 (protein)	0.25–1.88	>0.1	unclear
This study	Agglomerated ZnO nanoparticles	Alveolar type II (A549)	1 h	3 h	0 h	1 h	0 h	IL-8 (mRNA)	0.7–2.5	<0.7	yes
								GM-CSF (mRNA)	>2.5	0.7[3]	yes
								IL-6 (mRNA)	>2.5	<0.7	yes
								HMOX1 (mRNA)	>2.5	>2.2	unclear
								SOD-2 (mRNA)	>2.5	>2.2	unclear
								GCS (mRNA)	>2.5	0.7–2.5	yes

[1] LOEL: lowest dose in μg/cm^2 at which a statistically significant effect ($P < 0.05$) was observed relative to the control.
[2] Not stated in publication.
[3] Here: 0.7 μg/cm^2 showed a significant effect, while 2.2 μg/cm^2 was not statistically significant due to larger variability in the data. Hence, we assume that 0.7 μg/cm^2 is a good estimate for LOEL.

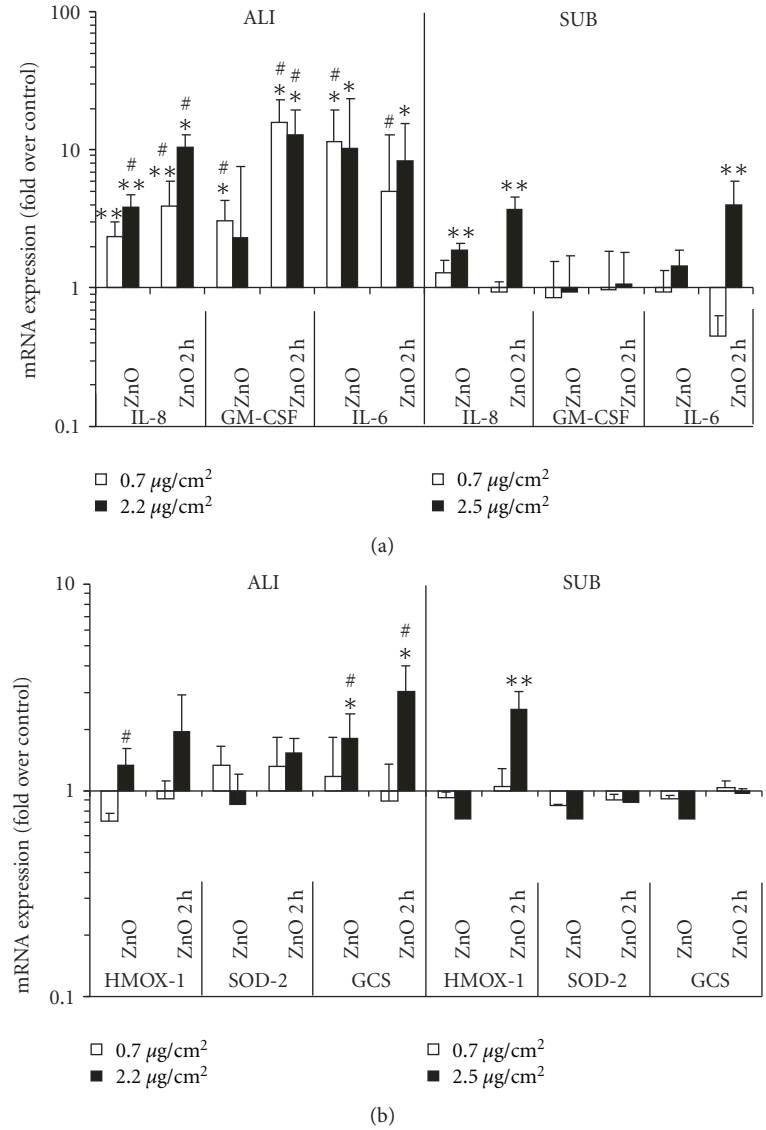

Figure 3: Comparison of the effect of ZnO on proinflammatory and oxidative stress markers in A549 cells following exposure at the ALI and under submerged (SUB) conditions. (a) mRNA expression of proinflammatory cytokines (IL-8, GM-CSF, and IL-6) was measured with RT-PCR either directly after (0 h after incubation) or two hours after the exposure (2 h). (b) Same as (a), but for oxidative stress markers (HMOX1, SOD-2, and GCS). The postincubation of the cells after ALI exposure was also performed under submerged conditions. The mRNA values were normalized to glyceraldehyde-3-phosphate dehydrogenase (GAPDH) levels and expressed as the fold increase over control (the control level was set to unity) which was filtered air and pure medium for ALI and SUB, respectively. The data show the geometric means and geometric standard error of the mean based on 4 to 7 independent experiments. Due to differences in the deposition kinetics described in the experimental section, the final dose was delivered to the cells after 3 h (ALI, open bars 0.7 μg/cm^2 and solid bars 2.2 μg/cm^2) or 1 h (submerged, open bars 0.7 μg/cm^2 and solid bars 2.5 μg/cm^2). The symbol (∗) indicates significant differences from control levels at $P < 0.05$, and (∗∗) at $P < 0.01$. The symbol (#) indicates mRNA values which are statistically different from the corresponding submerged mRNA levels (differences are 2.8 to 12-fold ($P > 0.05$)).

that the currently recommended Occupational Safety and Health Administration (OSHA) standard for ZnO fume (and many other occupational dusts) is 5 mg of ZnO fume per cubic meter of air (mg/m^3) averaged over an eight-hour-per-day work shift. Assuming an accumulated breathing volume of 3 m^3 in 8 h, a lung surface area of 140 m^2, an alveolar deposition efficiency of 10–50% depending on particle size, and negligible clearance from the alveolar regime within 24 h [52], the OSHA standard corresponds to a daily alveolar surface dose of 1.1–5.4 ng/cm^2, which is about 3 orders of magnitudes smaller than what was deposited during the ZnO ALI exposures performed here (0.7–2.2 μg/cm^2). Furthermore, it can be seen from Table 1 that the LOEL during submerged exposures is typically between 1 and 65 μg/cm^2, which is in the range of the expected lifetime dose (4–18 μg/cm^2) under worst case conditions represented by

a worker exposed to the OSHA (ZnO) dust limit (5 mg/m^3) for 5 days per week, 50 weeks per year for 45 years (where we assumed that only about 30% of the lung-deposited particles remain in the alveoli due to alveolar clearance mechanisms). As the *in vitro* dose is deposited onto the cells within a few hours instead of 45 years, this does not represent a realistic *in vivo* exposure scenario. In spite of these unrealistically high dose levels, *in vitro* cell tests are useful for pharmacological and toxicological prescreening of substances and studies of cellular response mechanisms, but lower cellular doses may be desirable. Table 1 suggests that an incremental progress may be possible with ALI cell systems. In combination with other measures such as the use of multicell cocultures instead of single-cell cultures, this may lead to significantly more realistic *in vitro* dose rates in the future.

5. Conclusion

In this study the *in vitro* response of pulmonary epithelial cells to different types of (nano-)particles was compared for air-liquid interface (ALI) and submerged exposure conditions. The scarce data pool on this issue was expanded by presenting the first ALI data on airborne agglomerates of ZnO nanoparticles using alveolar epithelial-like type II cells (A549). For ZnO, the lowest observed effect levels (LOELs) of the proinflammatory markers (mRNA gene expression of IL-8, IL-6, and GM-CSF) were lower under ALI than under submerged conditions, while no significant response was observed for most of the oxidative stress markers (HMOX1, SOD-2, and GCS). These findings are consistent with the few previous comparative studies on this issue indicating that toxicity testing with the conventional submerged systems may yield more false negatives than the more recently developed ALI systems.

The dose levels used here and in similar studies reported in the literature are in the range of an entire lifetime dose of occupational dust received by a heavily exposed worker. The ability to induce cellular responses at somewhat lower and hence more realistic dose levels under ALI conditions may provide biologically more meaningful data than those obtainable with the conventional submerged exposures. Further advantages of ALI cell systems include the biologically more realistic exposure scenario (cells in the lungs are exposed under ALI-like not submerged conditions), the absence of inadvertent modifications of the particle properties in the cell culture medium (e.g., agglomeration, partial dissolution), and the possibility of direct dose measurement (e.g., quartz crystal microbalance). Depending on the application, these aspects may outweigh the larger experimental complexity of ALI exposures. However, quantitative comparisons of the cellular response under ALI and submerged culture conditions are still very limited. Thus, further studies are needed to address these issues.

References

[1] H. Schulz, V. Harder, A. Ibald-Mulli et al., "Cardiovascular effects of fine and ultrafine particles," *Journal of Aerosol Medicine*, vol. 18, no. 1, pp. 1–22, 2005.

[2] R. Rückerl, A. Ibald-Mulli, W. Koenig et al., "Air pollution and markers of inflammation and coagulation in patients with coronary heart disease," *American Journal of Respiratory and Critical Care Medicine*, vol. 173, no. 4, pp. 432–441, 2006.

[3] A. Peters, H. E. Wichmann, T. Tuch, J. Heinrich, and J. Heyder, "Respiratory effects are associated with the number of ultrafine particles," *American Journal of Respiratory and Critical Care Medicine*, vol. 155, no. 4, pp. 1376–1383, 1997.

[4] T. Stoeger, C. Reinhard, S. Takenaka et al., "Instillation of six different ultrafine carbon particles indicates a surface area threshold dose for acute lung inflammation in mice," *Environmental Health Perspectives*, vol. 114, no. 3, pp. 328–333, 2006.

[5] R. Duffin, L. Tran, D. Brown, V. Stone, and K. Donaldson, "Proinflammogenic effects of low-toxicity and metal nanoparticles *in vivo* and *in vitro*: highlighting the role of particle surface area and surface reactivity," *Inhalation Toxicology*, vol. 19, no. 10, pp. 849–856, 2007.

[6] T. Stoeger, S. Takenaka, B. Frankenberger et al., "Deducing *in vivo* toxicity of combustion-derived nanoparticles from a cell-Free oxidative potency assay and metabolic activation of organic compounds," *Environmental Health Perspectives*, vol. 117, no. 1, pp. 54–60, 2009.

[7] I. Y. R. Adamson, H. Prieditis, C. Hedgecock, and R. Vincent, "Zinc is the toxic factor in the lung response to an atmospheric particulate sample," *Toxicology and Applied Pharmacology*, vol. 166, no. 2, pp. 111–119, 2000.

[8] T. B. Councell, K. U. Duckenfield, E. R. Landa, and E. Callender, "Tire-wear particles as a source of zinc to the environment," *Environmental Science and Technology*, vol. 38, no. 15, pp. 4206–4214, 2004.

[9] M. L. Sammut, J. Rose, A. Masion et al., "Determination of zinc speciation in basic oxygen furnace flying dust by chemical extractions and X-ray spectroscopy," *Chemosphere*, vol. 70, no. 11, pp. 1945–1951, 2008.

[10] J. M. Fine, T. Gordon, L. C. Chen et al., "Characterization of clinical tolerance to inhaled zinc oxide in naive subjects and sheet metal workers," *Journal of Occupational and Environmental Medicine*, vol. 42, no. 11, pp. 1085–1091, 2000.

[11] W. G. Kuschner, A. D'Alessandro, H. Wong, and P. D. Blanc, "Early pulmonary cytokine responses to zinc oxide fume inhalation," *Environmental Research*, vol. 75, no. 1, pp. 7–11, 1997.

[12] M. Lindahl, P. Leanderson, and C. Tagesson, "Novel aspect on metal fume fever: Zinc stimulates oxygen radical formation in human neutrophils," *Human and Experimental Toxicology*, vol. 17, no. 2, pp. 105–110, 1998.

[13] R. J. Vandebriel and W. H. De Jong, "A review of mammalian toxicity of ZnO nanoparticles," vol. Nanotechnology, Science and Application, no. 5, pp. 61–71, 2012.

[14] G. J. Nohynek, J. Lademann, C. Ribaud, and M. S. Roberts, "Grey goo on the skin? Nanotechnology, cosmetic and sunscreen safety," *Critical Reviews in Toxicology*, vol. 37, no. 3, pp. 251–277, 2007.

[15] A. Nel, T. Xia, L. Mädler, and N. Li, "Toxic potential of materials at the nanolevel," *Science*, vol. 311, no. 5761, pp. 622–627, 2006.

[16] G. Oberdörster, E. Oberdörster, and J. Oberdörster, "Nanotoxicology: an emerging discipline evolving from studies of ultrafine particles," *Environmental Health Perspectives*, vol. 113, no. 7, pp. 823–839, 2005.

[17] T. Stoeger, O. Schmid, S. Takenaka, and H. Schulz, "Inflammatory response to TiO_2 and carbonaceous particles scales best

with BET surface area," *Environmental Health Perspectives*, vol. 115, no. 6, pp. A290–A291, 2007.

[18] T. Stoeger and O. Schmid, *Dose-Response Relationships*, Informa Healthcare, London, UK, 2009.

[19] K. M. Waters, L. M. Masiello, R. C. Zangar et al., "Macrophage responses to silica nanoparticles are highly conserved across particle sizes," *Toxicological Sciences*, vol. 107, no. 2, pp. 553–569, 2009.

[20] D. Shaw, *Introduction to Colloid and Surface Chemistry*, Butterworth Heinemann, Oxford, UK, 4th edition, 1992.

[21] E. Bitterle, E. Karg, A. Schroeppel et al., "Dose-controlled exposure of A549 epithelial cells at the air-liquid interface to airborne ultrafine carbonaceous particles," *Chemosphere*, vol. 65, no. 10, pp. 1784–1790, 2006.

[22] S. Diabaté, S. Mülhopt, H. R. Paur, and H. F. Krug, "The response of a co-culture lung model to fine and ultrafine particles of incinerator fly ash at the air-liquid interface," *ATLA Alternatives to Laboratory Animals*, vol. 36, no. 3, pp. 285–298, 2008.

[23] M. Savi, M. Kalberer, D. Lang et al., "A novel exposure system for the efficient and controlled deposition of aerosol particles onto cell cultures," *Environmental Science and Technology*, vol. 42, no. 15, pp. 5667–5674, 2008.

[24] A. L. Holder, D. Lucas, R. Goth-goldstein, and C. P. Koshland, "Cellular response to diesel exhaust particles strongly depends on the exposure method," *Toxicological Sciences*, vol. 103, no. 1, pp. 108–115, 2008.

[25] M. Aufderheide and U. Mohr, "A modified CULTEX system for the direct exposure of bacteria to inhalable substances," *Experimental and Toxicologic Pathology*, vol. 55, no. 6, pp. 451–454, 2004.

[26] J. Volckens, L. Dailey, G. Walters, and R. B. Devlin, "Direct particle-to-cell deposition of coarse ambient particulate matter increases the production of inflammatory mediators from cultured human airway epithelial cells," *Environmental Science and Technology*, vol. 43, no. 12, pp. 4595–4599, 2009.

[27] B. M. Rothen-Rutishauser, S. C. Kiama, and P. Gehr, "A three-dimensional cellular model of the human respiratory tract to study the interaction with particles," *American Journal of Respiratory Cell and Molecular Biology*, vol. 32, no. 4, pp. 281–289, 2005.

[28] A. G. Lenz, E. Karg, B. Lentner et al., "A dose-controlled system for air-liquid interface cell exposure and application to zinc oxide nanoparticles," *Particle and Fibre Toxicology*, vol. 6, article 32, 2009.

[29] K. Donaldson and C. L. Tran, "Inflammation caused by particles and fibers," *Inhalation Toxicology*, vol. 14, no. 1, pp. 5–27, 2002.

[30] T. Xia, M. Kovochich, M. Liong et al., "Comparison of the mechanism of toxicity of zinc oxide and cerium oxide nanoparticles based on dissolution and oxidative stress properties," *ACS Nano*, vol. 2, no. 10, pp. 2121–2134, 2008.

[31] N. Li, T. Xia, and A. E. Nel, "The role of oxidative stress in ambient particulate matter-induced lung diseases and its implications in the toxicity of engineered nanoparticles," *Free Radical Biology and Medicine*, vol. 44, no. 9, pp. 1689–1699, 2008.

[32] K. A. Foster, C. G. Oster, M. M. Mayer, M. L. Avery, and K. L. Audus, "Characterization of the A549 cell line as a type II pulmonary epithelial cell model for drug metabolism," *Experimental Cell Research*, vol. 243, no. 2, pp. 359–366, 1998.

[33] A. Tippe, U. Heinzmann, and C. Roth, "Deposition of fine and ultrafine aerosol particles during exposure at the air/cell interface," *Journal of Aerosol Science*, vol. 33, no. 2, pp. 207–218, 2002.

[34] J. M. Desantes, X. Margot, A. Gil, and E. Fuentes, "Computational study on the deposition of ultrafine particles from Diesel exhaust aerosol," *Journal of Aerosol Science*, vol. 37, no. 12, pp. 1750–1769, 2006.

[35] P. A. Baron and K. Willeke, *Aerosol Measurement*, Wiley-Interscience, New York, NY, USA, 2001.

[36] M. Kaszuba, M. T. Connah, F. K. McNeil-Watson, and U. Nobbmann, "Resolving concentrated particle size mixtures using dynamic light scattering," *Particle and Particle Systems Characterization*, vol. 24, no. 3, pp. 159–162, 2007.

[37] O. Schmid, E. Karg, D. E. Hagen, P. D. Whitefield, and G. A. Ferron, "On the effective density of non-spherical particles as derived from combined measurements of aerodynamic and mobility equivalent size," *Journal of Aerosol Science*, vol. 38, no. 4, pp. 431–443, 2007.

[38] J. Gebhart, *Optical Direct-Reading Techniques: Light Intensity Systems*, Wiley Interscience, New York, NY, USA, 2001.

[39] J. G. Teeguarden, P. M. Hinderliter, G. Orr, B. D. Thrall, and J. G. Pounds, "Particokinetics *in vitro*: Dosimetry considerations for *in vitro* nanoparticle toxicity assessments," *Toxicological Sciences*, vol. 95, no. 2, pp. 300–312, 2007.

[40] B. T. Smith, "Cell line A549: a model system for the study of alveolar type II cell function," *American Review of Respiratory Disease*, vol. 115, no. 2, pp. 285–293, 1977.

[41] A. W. Stadnyk, "Cytokine production by epithelial cells," *FASEB Journal*, vol. 8, no. 13, pp. 1041–1047, 1994.

[42] H. Fehrenbach, "Alveolar epithelial type II cell: defender of the alveolus revisited," *Respiratory Research*, vol. 2, no. 1, pp. 33–46, 2001.

[43] E. L. Herzog, A. R. Brody, T. V. Colby, R. Mason, and M. C. Williams, "Knowns and unknowns of the alveolus," *Proceedings of the American Thoracic Society*, vol. 5, no. 7, pp. 778–782, 2008.

[44] A. D. P. Carero, P. H. M. Hoet, L. Verschaeve, G. Schoeters, and B. Nemery, "Genotoxic effects of carbon black particles, diesel exhaust particles, and urban air particulates and their extracts on a human alveolar epithelial cell line (A549) and a human monocytic cell line (THP-1)," *Environmental and Molecular Mutagenesis*, vol. 37, no. 2, pp. 155–163, 2001.

[45] E. Herzog, H. J. Byrne, A. Casey et al., "SWCNT suppress inflammatory mediator responses in human lung epithelium *in vitro*," *Toxicology and Applied Pharmacology*, vol. 234, no. 3, pp. 378–390, 2009.

[46] R. B. Reed, D. A. Ladner, C. P. Higgins, P. Westerhoff, and J. F. Ranville, "Solubility of nano-zinc oxide in environmentally and biologically important matrices," *Environmental Toxicology and Chemistry*, vol. 31, no. 1, pp. 93–99, 2012.

[47] H. R. Paur, F. R. Cassee, J. Teeguarden et al., "*In-vitro* cell exposure studies for the assessment of nanoparticle toxicity in the lung-a dialog between aerosol science and biology," *Journal of Aerosol Science*, vol. 42, no. 10, pp. 668–692, 2011.

[48] P. M. Hinderliter, K. R. Minard, G. Orr et al., "ISDD: a computational model of particle sedimentation, diffusion and target cell dosimetry for *in vitro* toxicity studies," *Particle and Fibre Toxicology*, vol. 7, no. 1, article 36, 2010.

[49] S. Kameyama, M. Kondo, K. Takeyama, and A. Nagai, "Air exposure causes oxidative stress in cultured bovine tracheal epithelial cells and produces a change in cellular glutathione

systems," *Experimental Lung Research*, vol. 29, no. 8, pp. 567–583, 2003.

[50] F. Blank, B. M. Rothen-Rutishauser, S. Schurch, and P. Gehr, "An optimized *in vitro* model of the respiratory tract wall to study particle cell interactions," *Journal of Aerosol Medicine*, vol. 19, no. 3, pp. 392–405, 2006.

[51] A. J. Ross, L. A. Dailey, L. E. Brighton, and R. B. Devlin, "Transcriptional profiling of mucociliary differentiation in human airway epithelial cells," *American Journal of Respiratory Cell and Molecular Biology*, vol. 37, no. 2, pp. 169–185, 2007.

[52] W. G. Kreyling, J. J. Godleski, S. T. Kariya, R. M. Rose, and J. D. Brain, "*In vitro* dissolution of uniform cobalt oxide particles by human and canine alveolar macrophages," *American Journal of Respiratory Cell and Molecular Biology*, vol. 2, no. 5, pp. 413–422, 1990.

Hindawi Publishing Corporation
BioMed Research International
Volume 2013, Article ID 583513, 10 pages
http://dx.doi.org/10.1155/2013/583513

Research Article

Milan PM1 Induces Adverse Effects on Mice Lungs and Cardiovascular System

Francesca Farina,[1] Giulio Sancini,[1] Eleonora Longhin,[2] Paride Mantecca,[2] Marina Camatini,[2] and Paola Palestini[1]

[1] *Department of Health Science, POLARIS Research Center, University of Milan-Bicocca, 48 Via Cadore, 20900 Monza, Italy*
[2] *Department of Environmental Science, POLARIS Research Center, University of Milan-Bicocca, 1 piazza della Scienza, Milan 20126, Italy*

Correspondence should be addressed to Giulio Sancini; giulio.sancini@unimib.it

Received 23 July 2012; Revised 12 October 2012; Accepted 18 October 2012

Academic Editor: Abderrahim Nemmar

Recent studies have suggested a link between inhaled particulate matter (PM) exposure and increased mortality and morbidity associated with cardiorespiratory diseases. Since the response to PM1 has not yet been deeply investigated, its impact on mice lungs and cardiovascular system is here examined. A repeated exposure to Milan PM1 was performed on BALB/c mice. The bronchoalveolar lavage fluid (BALf) and the lung parenchyma were screened for markers of inflammation (cell counts, tumor necrosis factor-α (TNF-α); macrophage inflammatory protein-2 (MIP-2); heme oxygenase-1 (HO-1); nuclear factor kappa-light-chain-enhancer of activated B cells p50 subunit (NFκB-p50); inducible nitric oxide synthetase (iNOS); endothelial-selectin (E-selectin)), cytotoxicity (lactate dehydrogenase (LDH); alkaline phosphatase (ALP); heat shock protein 70 (Hsp70); caspase-8-p18), and a putative pro-carcinogenic marker (cytochrome 1B1 (Cyp1B1)). Heart tissue was tested for HO-1, caspase-8-p18, NFκB-p50, iNOS, E-selectin, and myeloperoxidase (MPO); plasma was screened for markers of platelet activation and clot formation (soluble platelet-selectin (sP-selectin); fibrinogen; plasminogen activator inhibitor 1 (PAI-1)). PM1 triggers inflammation and cytotoxicity in lungs. A similar cytotoxic effect was observed on heart tissues, while plasma analyses suggest blood-endothelium interface activation. These data highlight the importance of lung inflammation in mediating adverse cardiovascular events following increase in ambient PM1 levels, providing evidences of a positive correlation between PM1 exposure and cardiovascular morbidity.

1. Introduction

Epidemiology studies have shown that increased levels of particulate matter (PM) in ambient air are associated with aggravation of respiratory diseases and cardiovascular function impairment. These adverse events have been correlated with exposure to fine PM (particles with aerodynamic diameter $\leq 2.5\ \mu$m) [1], even if the pathophysiological mechanisms remain still unclear.

Lung PM penetration and clearance are size dependent: larger particles (greater than 10 μm), deposited in the upper airways, are removed by the mucociliary clearance mechanism, while smaller particles (below 10 μm) reach deeper the lungs and are only partially removed by alveolar macrophages (AMs) [2].

Following PM deposition in the lungs, AMs rapidly phagocytose particles and migrate towards the bronchoalveolar junction [3]. A large number of ultrafine particles ($\leq 0.1\ \mu$m in aerodynamic diameter), however, poses a substantial burden for the macrophage phagocytic system and results in increased number of particles coming in contact with the respiratory epithelium. Damage to the capillary endothelium and type I alveolar cells has been observed as one of the earliest events in lung toxicity mediated by particles, leading to neutrophils recruitment and triggering the onset of an acute inflammatory status [2, 4]. Moreover,

PM contains transition metals able to generate reactive oxygen molecules which in turn exert a cytotoxic effect on lung cells [2].

Translocation of inhaled nanoparticles across the alveolar-blood barrier has been demonstrated in animal studies for a range of nanoparticles delivered by inhalation or instillation [5–7]. Convincing demonstration of translocation has been difficult to achieve in humans [8, 9]; however, given the deep penetration of nanoparticles into the alveoli and the close apposition of the alveolar wall and capillary network, such particle translocation seems plausible either as a naked particle or after ingestion by AMs.

Many authors proposed the hypothesis that fine particles inhalation provokes a low grade inflammatory response in the lung, causing an exacerbation of preexisting lung diseases. We previously reported [10] that a single intratracheal instillation of fine particles in mice stimulates mild lung inflammation. The present study extends these findings by showing that the repeated deposition of particulate matter in the lungs triggers the onset of systemic adverse events.

Milan's particles concentration and its chemical composition have been widely examined [11, 12]. Despite the number and quality of chemical data, the biological effects produced on *in vivo* and *in vitro* systems have been only recently and partly investigated [4, 10, 13, 14]. In this paper we present and discuss pulmonary and cardiovascular adverse events induced in mice by intratracheal instillation of Milan PM1. This fraction represents PM with aerodynamic diameter $\leq 1\ \mu$m [15], constituted by almost 40% of particles ≤ 400 nm in diameter. Lonati and Giugliano [16] monitored particles size distribution in four different sites in Milan and concluded that, at open air sites, 99.5% of the total number of particles are characterised by a diameter smaller than 1 μm.

2. Materials and Methods

2.1. Animals. Male BALB/c mice (7-8 weeks old) were purchased from Harlan Laboratories (Italy); food and water were administered *ad libitum*. Mice were housed in plastic cages under controlled environmental conditions (temperature 19–21°C, humidity 40–70%, lights on 7 am–7 pm). The established rules of animal care approved by Italian Ministry of Health (DL 116/92) were followed. Intratracheal instillations have been performed in mice under controlled general anaesthesia to avoid pain and discomfort. During the whole experiments we found no changes in mice weights or behaviour.

2.2. PM Sources and Chemical Characterization. Atmospheric PM1 was collected during 2007-2008 in a Milan urban area as described in previous papers [13]. The sampling site was located at Torre Sarca, an urban site with high vehicle traffic. Samplers were located in a fenced area at about 2.5 m from the ground, 10 m from the road, and 30 m from the nearest traffic light.

PM1 was sampled and chemical analyses were performed as described in Perrone et al. [17]; Milan PM1 chemical composition (inorganic ions, elements, and PAHs) is summarized in Table 1.

Particles' suspensions were prepared as follow: just before the intratracheal instillation, PM1 aliquots were properly diluted in sterile pyrogen-free saline, sonicated and vortexed, and then immediately instilled in mice.

2.3. Dose. Our study was designed to measure the systemic response to repeated PM1 exposure and test in an animal model the hypothesis that sustained PM1 exposure could exert cardiovascular dysfunctions. Similar investigations have been previously based on very high PM exposure rate in single or repeated intratracheal instillation [20–23].

Lung inflammation play a key role in enhancing the extrapulmonary translocation of particles [21]. So, we tested the threshold valid to lengthen the PM1 proinflammatory effects within lungs of our BALB/c mice, and it resulted higher than the estimated daily dose possibly deposited at the hot spot of lungs in worst pollution conditions. Ideally, *in vivo* studies should be performed with realistic dose levels, but, as already indicated for *in vitro* systems [24], short-term *in vivo* applications have some limitations, first of all the necessity to obtain measurable responses within few days.

We started from the dose used by Happo et al. [22], who instilled in mice a cumulative dose of 0.82 mg/animal of fine PM in a week, and we reduced the cumulative dose to 0.3 mg/animal of PM1 within the same time frame, in order to avoid particles lungs overload. The PM dose here used is not directly correlated to human urban PM exposures, but it has been determined as the lowest which induces a mild but still sustained lung inflammatory response in PM1 exposed mice.

2.4. Intratracheal PM1 Instillation and Broncho Alveolar Lavage. Animal testing was carried out by instilling 4 mice for each experimental group and the experiment was replicated twice, for a total of 8 sham and 8 PM1-treated mice.

Male BALB/c mice were briefly exposed to a mixture of 2.5% isoflurane (flurane) anesthetic gas and kept under anaesthesia during the whole instillation procedure. Once a deep stage of anaesthesia was reached, mice were intratracheally instilled by means of MicroSprayer Aerosolizer system (MicroSprayer Aerosolizer- Model IA-1C and FMJ-250 High Pressure Syringe, Penn Century, USA) with 100 μg of PM1 in 100 μL of isotonic saline solution, or 100 μL of isotonic saline solution (sham) as previously reported [4, 10, 14]. Each mouse was placed in a supine position, the mouth was opened and the tongue was gently moved aside using a pince to better incannulate the trachea. The particles were suspended in the appropriate solution just before the intratracheal instillation. PM1-treated and sham mice were allowed to recover under visual control before placing them back in plastic cages, under controlled environmental conditions. The intratracheal instillation was performed on days 0, 3, and 6, for a total of three instillations. 24 h after the last instillation, mice from each experimental group were euthanized

Table 1: Table summarizing mean chemical composition (μg/μg PM) of 8 PM1 pooled samples (modified by "Seasonal variations in chemical composition and *in vitro* biological effects of fine PM from Milan" [17]). Inorganic ions explained about the 43% of the PM mass, the sum of all elements explained about the 0.8% while the contribution of PAHs was 0.016%. BaP: benzo[a]anthracene; BeP: benzo[e]pyrene; Bb+jF: benzo[b+j]fluoranthene; BkF: benzo(k)fluoranthene; BaP: benzo[a]pyrene; dBahA: dibenzo[a,h]anthracene; BghiP: benzo[g,h,i]perylene; IcdP: indeno[1,2-Cd]pyrene. Particles size distribution over the Milano metropolitan area has been studied by Ferrero and colleagues [18]. Concerning sources, traffic and heating during cold season constitute the 49–53% of the primary combustion sources of fine PM; during warm season they constitute about the 25%, while secondary sources are predominant (50–66%) [19]. Elemental carbon (primarily from traffic) contributes for about 10–15% to the fine fraction; organic matter, calculated applying a specific organic matter-to-organic carbon conversion factor to each source, contributes for 31–38% to the fine fraction [19].

Inorganic ions		Elements		PAHs	
	Mean		Mean		Mean
F^-	0.0001125	Al	0.000334	BaA	0.000011
Cl^-	0.0061875	As	0.000025	Cr	0.000016
NO_3^-	0.1905875	Ba	0.000046	BeP	0.000025
PO_4^{3-}	0.001	Cd	0.00001	Bb+jF	0.000041
SO_4^{2-}	0.091325	Cr	0.00005	BkF	0.00001
Na^+	0.0022375	Cu	0.000369	BaP	0.000017
NH_4^+	0.1348875	Fe	0.005804	dBahA	0.000001
K^+	0.0062875	Mn	0.000081	BghiP	0.000022
Mg^{2+}	0.0001125	Mo	0.000053	IcdP	0.000015
Ca^{2+}	0.0012125	Ni	0.00005		
		Pb	0.000251		
		V	0.000025		
		Zn	0.00099		

with an anesthetic mixture overdose (Tiletamine/Zolazepam-Xylazine and isoflurane). The effects were assessed 24 h after the last treatment since the greatest inflammatory response occurs by this time [22]. The broncho alveolar lavage (BAL) procedure, pellets, and supernatant recovery have been performed as described in Mantecca et al. [4, 14].

2.5. BALf Biochemical Assays

2.5.1. Cell Counts. After centrifugation, the BALf pellets were resuspended in 500 μL of DMEM (10% FBS, 1% penicillin-streptomycin, 1% glutamine), and total and differential cells counts performed as described in Mantecca et al. [4, 14].

2.5.2. LDH and ALP. LDH and ALP assays were performed on cell-free BALf supernatants. The commercially available kits for alkaline phosphatase (DALP-250 QuantiChrom Alkaline Phosphatase Assay Kit, Gentaur Molecular) and lactate dehydrogenase (DLDH-100 QuantiChrom Lactate Dehydrogenase Kit, Gentaur Molecular) were employed according to the manufacturers' instructions.

2.5.3. Cytokines. The analyses of proinflammatory cytokines released in the BALf was performed by DuoSet ELISA kits for tumour necrosis factor-α and macrophage inflammatory protein-2 (TNF-α and MIP-2; R&D Systems) according to the manufacturer's protocols.

2.6. Lung and Heart Biochemical Analyses. The lungs of sham and PM1-treated mice, at the end of BAL procedure, were quickly excised from the chest and washed in ice cold isotonic saline solution. The left lobes were dissected and submitted to histology, the right lobes were preserved for the biochemical analyses. For protein assays, lungs were minced at 4°C, suspended in NaCl 0.9%, briefly homogenized for 30 seconds at 11000 rpm with Ultra-Turrax T25 basic (IKA WERKE) and sonicated for other 30 seconds.

Then samples were submitted to trichloroacetic acid (TCA) precipitation according to the procedure described in Farina et al. [10]. The pellets were suspended in water and protein quantity determined by BCA method (Sigma Aldrich, USA).

Thereafter, lung homogenates of sham and PM1-treated mice were loaded on SDS-PAGE and submitted to electrophoresis, followed by Western blot. The membranes were stained with Ponceau and the protein loading was assessed by densitometry (BIORAD Densitometry 710, program Quantity one) as described [25]. After blocking, blots were incubated for 2 h with the primary antibody diluted in PBS-Tween20/milk. Lung parenchyma was tested for Cyp1B1, HO-1, Caspase8-p18, NFκB-p50, Hsp70, E-selectin, and iNOS (anti-Cyp1B1 1 : 200, anti-HO-1 1 : 200, anti-Casp8-p18 1 : 200, anti-NFκB-p50 1 : 200, anti-Hsp70 1 : 200, anti-E-selectin 1 : 200, anti-iNOS 1 : 200, all by Santa Cruz). Then, blots were incubated for 1.5 h with horseradish peroxidase-conjugated anti-rabbit IgG (1 : 5000) or anti-goat IgG (1 : 2000) diluted in PBS-T/milk.

Proteins were detected by ECL using the SuperSignal detection kit (Pierce, Rockford, IL). Immunoblot bands were analyzed and the optical density (OD) quantified by KODAK (Kodak Image Station 2000R); all the data have been

normalized to β-actin (anti-β-actin 1 : 1500 by Sigma) and each protein in PM1-treated group was normalized to the corresponding sham group.

Heart tissue from sham and PM1-treated mice was submitted to all the procedures above described for lungs, and homogenates tested for HO-1, Caspase8-p18, NFκB-p50, E-selectin, iNOS, and MPO (anti-HO-1 1 : 200, anti-Casp8-p18 1 : 200, anti-NFκB-p50 1 : 200, anti-E-selectin 1 : 200, anti-iNOS 1 : 200, anti-MPO, all by Santa Cruz).

2.7. Lung Histopathological Analyses. Once excised, the left lungs from sham and PM1 treated mice were fixed in Bouin's solution, embedded in paraffin, cross-sectioned at 7 μm thickness by a rotary microtome, mounted on slides, and stained by hematoxilin and eosin (HE). Some sections were mounted onto Superfrost slides and processed for the immunohistochemical detection of HO-1, as previously reported [4], using a rabbit anti-HO-1 polyclonal antibody (Santa Cruz), and the peroxidase-based Vectastain Elite ABC Kit (Vectastain Laboratories) to visualize the immunochemical reaction. Slides were observed under a Zeiss Axioplan light microscope and images taken with a ZeissAxioCam MRc5 digital camera interfaced with the Axiovision Real 4.6 software.

2.8. Blood Analyses. Blood of sham and PM1-treated mice was collected by intracardiac puncture. Plasma has been recovered after two centrifugation, the first at 2000 g for 20 minutes and the second at 10000 g for 10 minutes at 4°C to completely remove platelets, and then submitted to sP-Selectin (Quantikine Mouse sP-selectin, R&D Systems), fibrinogen (Mouse Fibrinogen Antigen assay, Molecular Innovations), PAI-1 (murine PAI-1 activity assay, Molecular Innovations), and cytokines analyses (TNF-α and MIP-2; R&D Systems).

2.9. Statistical Analyses. Results are expressed as mean ± standard error of the mean (SE). Data distribution was tested by Shapiro-Wilk test; statistical differences were tested accordingly by t-test or non parametric U Mann-Whitney test. Statistical differences were considered to be significant at the 95% or 99% level ($P < 0.05$ or $P < 0.01$).

3. Results

3.1. BALf Analyses

3.1.1. Cell Counts. Significant increases of total cells number and lymphocytes (Ls) percentage (Table 2) have been found in PM1-treated mice. Polymorphonuclear cells (PMNs) percentage (sham 9.41 ± 2.75%, PM1-treated 14.27 ± 5.51%) as well as alveolar macrophages (AMs) percentage (sham 90.35 ± 2.79%; PM1-treated 84.72 ± 5.86%) were basically unaffected by PM1 treatment. However, AMs full of particles are clearly visible in the BALf of PM1-treated mice (Figures 1(a)–1(c)).

3.1.2. LDH, ALP, and Cytokines. Lactate dehydrogenase (LDH) and alkaline phosphatase (ALP) activities significantly increased in the BALf of PM1-treated mice (Table 2).

MIP-2 concentration increased in the BALf of PM1-treated mice (Table 2), while TNF-α was unchanged (sham 22.30 ± 6.89 pg/mL, PM1-treated 20.84 ± 6.57 pg/mL).

3.2. Lung Analyses. PM1 treatment induced a significant reduction of Hsp70 (heat shock protein 70, a functionally related protein involved in proteins folding) and a significant increase in HO-1 levels (heme oxigenase-1, a stress related protein which catalyzes heme degradation) in the lung parenchyma (Table 2 and Figure 2(a)), while iNOS (inducible nitric oxide synthase) was unchanged (sham 1 ± 0.35; PM1-treated 5.02 ± 0.52). The immunohistochemical analyses to evidence the HO-1 expression confirmed the activation of this antioxidant protective protein in the deep lung. HO-1 was mainly localized in AMs and in the alveolar epithelium (Figures 3(a) and 3(b)).

NFκB rules the transcription of different genes, including pro- and antiapoptotic, and pro- and anti-inflammatory ones. A significant increase of its active fragment p50, as well as of the active fragment of the proapoptotic marker Caspase8-p18, was detected in the lungs of PM1-treated mice (Table 2 and Figure 2(a)).

Cyp1B1, a cytochrome of the P450 superfamily involved in the activation of many xenobiotics and in polycyclic aromatic hydrocarbons (PAHs) metabolism, did not increase in PM1-treated mice (sham 1 ± 0.12; PM1-treated 1.32 ± 0.07) as well as the E-selectin (sham 1 ± 0.21; PM1-treated 1.33 ± 0.18), a cell adhesion molecule related to inflammation.

Following PM1 exposure, 24 h after the last instillation, the histological evaluation of PM1-exposed lungs fail to disclose massive inflammation (Figures 4(a) and 4(b)). The most significant evidence in PM1 treated lungs was the ubiquitous presence in the alveolar airspace of AMs full of PM1 associated to lyses of the alveolar epithelium (Figures 4(b) and 4(c)). These data evidenced the active involvement of AMs in PM1 clearance and the direct cytotoxic effects elicited by PM1 on the lung alveolar epithelium, as confirmed by LDH, ALP, and Caspase-8 analyses.

3.3. Heart Analyses. MPO (myeloperoxidase, a marker of acute inflammation), iNOS, and E-selectin did not increase in heart of PM1-treated mice (MPO: sham 1 ± 0.16, PM1-treated 1.07 ± 0.15; iNOS: sham 1 ± 0.07, PM1-treated 0.95 ± 0.1; E-selectin: sham 1 ± 0.18, PM1-treated 0.94 ± 0.09). Consistent with these observations, 24 h after the last intratracheal instillation of PM1, HO-1 was basically unchanged (sham 1 ± 0.13; PM1-treated 1.05 ± 0.06), while NFκB-p50 and Caspase8-p18 levels increased (Table 2 and Figure 2(b)).

3.4. Blood Analyses. Prothrombogenic and proinflammatory markers were analysed within the plasma of sham and PM1-treated mice: sP-selectin, a well-known marker of the activated platelet/endothelium interface, was significantly increased 24 h after the last intratracheal instillation in PM1-treated mice (Table 2). Fibrinogen (sham 2.89 ± 0.10 ng/mL,

Table 2: Table summarizing significant results in BALf, lung, heart, and blood in sham and PM1-treated mice, 24 h after the last intratracheal instillation. Concerning protein markers in lung and heart tissues, the data were normalized for the corresponding β-actin signal in each lane and expressed in relative to sham value. Data distribution was tested by Shapiro-Wilk test; statistical differences were tested by t-test or by non parametric U Mann-Whitney test. The data are expressed as mean ± SE. Sham versus PM1-treated: $^{*}P < 0.05$; $^{**}P < 0.01$.

		Sham		PM1		P
		Mean	±s.e.	Mean	±s.e.	
BALf	Total cells ($E + 05$)	7.28	1.41	10.48	1.43	*
	% Ls	0.24	0.14	0.78	0.26	**
	LDH (IU/L)	19.49	1.59	27.5	0.4	**
	ALP (IU/L)	0.07	0.02	0.15	0.01	**
	MIP-2 (pg/mL)	58.99	9.52	102.12	12.12	*
Lung	Hsp70	1	0.04	0.75	0.03	*
	HO-1	1	0.04	5.28	0.97	*
	NFκB-p50	1	0.18	3.12	0.13	*
	Casp8-p18	1	0.04	1.42	0.11	*
Heart	NFκB-p50	1	0.02	1.37	0.08	*
	Casp8-p18	1	0.19	1.84	0.18	*
Blood	sP-selectin (ng/mL)	97.8	6.82	132.03	4.87	**

PM1-treated 2.91 ± 0.07 ng/mL) and PAI-1 plasma concentration (sham 0.15 ± 0.05 ng/mL, PM1-treated 0.23 ± 0.03 ng/mL), as well the cytokines MIP-2 and TNF-α (under kit detection limits, data not shown), were unaffected by PM1 intratracheal instillation.

4. Discussion

Our previous investigations [10] disclosed that a single instillation of fine particles in mice stimulates mild lung inflammation. The current study extends these findings, showing that repeated instillations of fine particulate matter trigger systemic adverse effect. The systemic response following repeated particle exposure could be due to a different pattern of the inflammatory mediators released from the lung, as compared with acute exposure.

4.1. Inflammation and Injury in Mice Lungs. Increased BALf total cells counts in PM1-treated mice suggested a recruitment of proinflammatory cells in the alveolar spaces indeed, 24 h after the third instillation an increase in Ls percentage was clearly visible as well as AMs burdened by particles (Figures 1(a)–1(c)).

In the BALf of healthy mice, AMs are abundant (>90%) while neutrophils are rare [26]. The PM1-intratracheal instillation could facilitate the deposition of particles in the alveolar spaces, where they come in contact with AMs, the first cells actively engaged in the clearance of inhaled particles [27]. Many studies have demonstrated that inhaled fine particles and aggregates of ultrafine particles are able to burden AMs thus impairing their phagocytosis [2, 28]. Such AMs in the BALf of treated mice could trigger lymphocellular inflammatory reaction within the bronchoalveolar districts. Following particles phagocytosis, AMs usually migrate to bronchoalveolar junctions, where they tend to accumulate and aggregate [29], releasing inflammatory mediators thus inducing a slight influx of neutrophils.

An increase in the number of T lymphocytes has already been demonstrated in bronchial biopsies of healthy human volunteers exposed to PM [30]; moreover, PM has been shown to drive T-cell mediated cytokine production in the BALf of treated mice [31]. Many potentially biologically active components such as endotoxin, metals, polycyclic aromatic hydrocarbons (PAHs), and ozone might activate lymphocytes in the lung of PM-treated mice [23, 31]. PM1 induced changes in total and differential cells counts may be due both to a mild PMNs and Ls recruitment associated to reduced AMs migration toward the bloodstream.

In our *in vivo* study no significant change in TNF-α concentration was evident in the BALf of PM1-treated mice, while MIP-2 concentration was significantly increased comparing to sham, suggesting that inflammation is still present 24 h after the third intratracheal instillation of PM1.

However within the lungs, PM1 failed to induce the expression of proinflammatory adhesion molecules associated with endothelial activation, as confirmed by the E-selectin levels basically unchanged in sham and PM1-treated mice.

Fine and ultrafine particles have large surface area and therefore the adsorbed chemicals are largely bioavailable for redox or electrophilic chemistry [32]. It has been proposed that the proinflammatory process induced by particles could be related to the presence of PAHs [33]. Becker et al. [34] found that also Cr, Mn, Fe, Al, Si, Ti, and Cu may be related with cytokines production. Organic chemical components and transition metals associated with PM1 may thus contribute to adverse health effects based on their ability to induce oxidative stress responsible for the lung alveolar inflammation.

Oxidative stress and proinflammatory cytokines are known to induce HO-1 expression in various cell types,

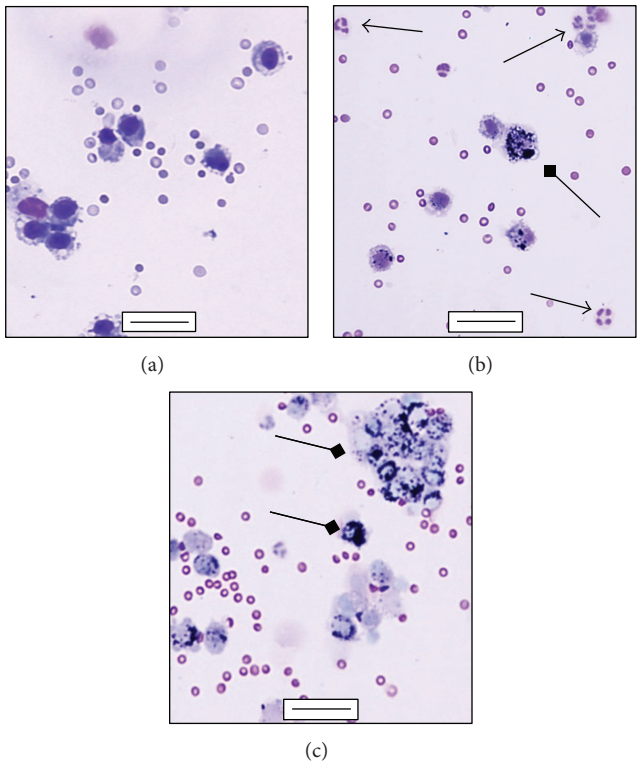

Figure 1: Differential staining of BALf cells. (a) Alveolar macrophages in the BALf collected 24 h postinstillation from sham; (b) and (c) alveolar macrophages engulfing particles (square arrows) and infiltration of PMNs (arrows) in the BALf collected 24 h after the last intratracheal instillation from PM1-treated mice. (a), (b), (c) bars = 50 μm.

including type II pneumocytes and AMs [35]. HO-1 acts as defence protein and its deficiency leads to enhanced endothelial cells injury [36]: the role of HO-1 is to catabolize the heme group from the cytosol, thus generating CO, biliverdin (converted to bilirubin) and Fe^{2+}; all these products are thought to play a putative protective role against the inflammation onset and progression [37]. HO-1 increased in PM1-treated mice in agreement with previous data related to airborne pollutant toxicity both *in vivo* [4, 10, 38] and *in vitro* systems [39, 40], and could account for the mild ongoing lung inflammation we found in PM1-treated mice. Due to the role of HO-1 in regulating cellular heme availability for structural and functional heme-dependent proteins [41], within lungs no change in Cyp1B1 and iNOS levels were induced by PM1.

AMs infiltrated in the lung parenchyma are positively stained for HO-1, thus suggesting that AMs in PM1-treated mice were suffering for oxidative stress due to the large burden of particles. Within the lungs, the pool of inflammatory phagocytes is the most significant and important cellular ROS generating system [42]; metals and organic substances adsorbed on PM surface have been related to their phagocytic oxidative burst [42].

Several transition metals adsorbed onto fine particles have been proved to trigger the generation of reactive oxygen species, in turn able to activate NFκB, one of the most important mechanisms involved in PM induced pulmonary toxicity [43]. In our investigations, p50, one of the active subunits of the NFκB transcription factor, increased in PM1-treated mice, in agreement with previous findings [10].

It has been reported [2, 44] that ultrafine particles, which are not efficiently cleared via mucociliary or macrophage-mediated mechanisms, very likely may enter the epithelial cells, cause injury to the integrity of the alveolar and endothelial cells thus spreading within the circulatory system. Increased LDH and ALP activity in the BALf of PM1-treated mice could be strictly related to the alveolar epithelium damage. Supporting this hypothesis and in agreement with previous investigations [4, 10, 14, 22, 41], histological analyses showed signs of alveolar cells damage within lungs of PM1-treated mice. Gerlofs-Nijland et al. [33] suggested that metals may contribute to the alveolar cell lyses and consequently to the LDH leakage in the BALf. In addition, the significant increase in Caspase-8 activation found in lung parenchyma of PM1-treated mice strengthens the hypothesis of a direct cell damage and apoptosis on AMs and lung epithelial cells mediated by fine particles [45].

It is generally known that HSPs are increased during cell stress. Surprisingly, Hsp70 levels in lung parenchyma of PM1-treated mice were significantly lower than in sham. Also, Stoeger et al. [46] reported reduced Hsp70 mRNA expression after particles instillation in BALB/c mice. Indeed, Hsp70 in the lungs is expressed by bronchial epithelium, alveolar cells and AMs [47]. HSPs may have a rapid turnover, especially during cell stress [48], and both the synthesis and chaperoning action of HSPs are energy requiring. Therefore, we might speculate that an energy imbalance and the increased turnover of lung epithelial cells, as demonstrated by high ALP activity in the BALf, did not permit the synthesis of sufficient quantities of Hsp70.

Taking together, these results prove that PM1 promotes in instilled mice a mild ongoing lung inflammation in agreement with previous findings [32], thus triggering pro-oxidative and cytotoxic effects, both on AMs and lung cells.

4.2. Effects on Mice Cardiovascular System. Epidemiological studies provided evidences of serious health hazards linked to human exposure within highly polluted urban centres PM [49].

Growing experimental evidences suggest that inhaled smallest particles can indeed translocate into the blood systemic circulation reaching extrapulmonary organs, such as heart and brain [50]. These adverse systemic effects might occur after fine or ultrafine particles inhalation basically in the absence of symptomatic and clinically detectable lung inflammation [32]. In our study, no variations in several inflammation and oxidative stress markers on heart tissues of PM1-treated mice were observed. However, an increase in NFκB-p50 expression has been found in heart tissue, as already described after nanoparticles intratracheal instillation in rats [51].

Once again we observed increased activation of Caspase-8 in the hearts of PM1-treated mice, thus indicating the activation of the Caspase cascade. Cardiomyocytes apoptosis

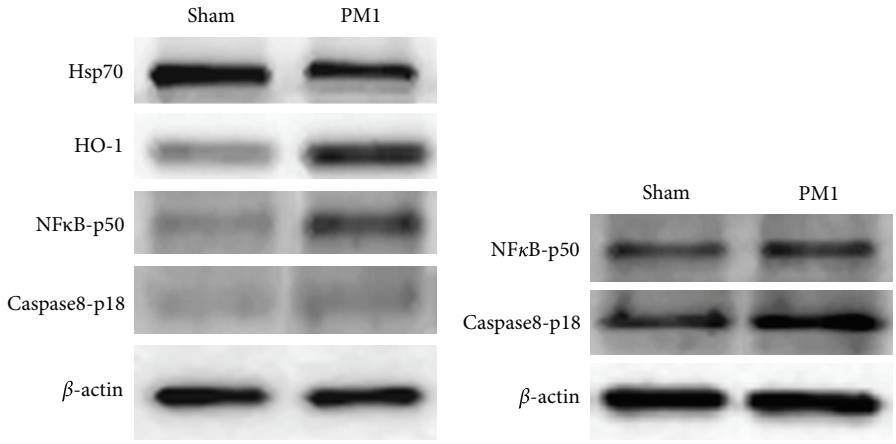

Figure 2: Protein analyses. (a) Representative western blottings showing Hsp70, HO-1, NFκB-p50, Caspase8-p18 and β-actin in lung parenchyma in sham and PM1-treated mice. (b) Representative western blottings showing NFκB-p50, Caspase8-p18 and β-actin in hearts of sham and PM1-treated mice.

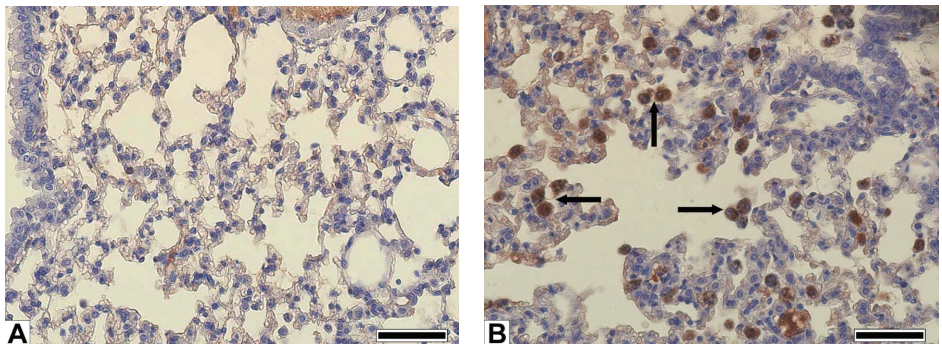

Figure 3: Lung parenchyma HO-1. Immunohistochemistry of HO-1 in lung tissues. Immunochemical reaction was developed by peroxidase and is visible as brown precipitate of DAB. (a) Sham lung showing no appreciable HO-1 signal; (b) PM1-treated lung showing intense HO-1 signal in particles' engulfed in alveolar macrophages (arrows). (a) and (b) bars = 50 μm.

may be involved in the cardiac function impairment triggered by fine PM [52]. These findings are in agreement with the assumption that PM1 mainly exerts a direct cytotoxic effect on heart.

A direct correlation has been found between fine particles inhalation and increased fibrinogen level, plasma viscosity and red blood cell count [53]. Many data indicates the adhesion of platelets to the endothelium before the development of manifest atherosclerotic lesions [54]. Furthermore, is generally accepted that platelets contribute to the final stages of cardiovascular diseases, thus in thrombosis and myocardial infarction [55]. Soluble P-selectin (sP-selectin) is considered a marker of an activated platelet/vasculature/blood interface, as it can be released by activated platelets as well as by activated endothelial cells [53]. Indeed, we found a significant increase in sP-selectin concentration within plasma of PM1-treated mice, though both fibrinogen and PAI-1 concentration did not change and TNF-α and MIP-2 concentration were under the kit detection limits.

Among several hemostasis and inflammation mediators, only sP-selectin blood concentration was associated with preclinical cardiovascular risk, thus conferring to sP-selectin assay a clinical usefulness for detecting and managing high cardiovascular risk in primary prevention [56].

5. Conclusions

Short term exposure to PM1 induced in the lungs of BALB/c mice a mild inflammation, still ongoing 24 h after the last instillation. Particles escaping phagocytosis by impaired and overloaded macrophages could then elicit their cytotoxic effect directly on alveolar cells.

The inhaled PM1 could exert a progression of preexisting peripheral arterial occlusive disease sustaining the adhesion of platelets to the endothelium and considerably increasing thrombosis and myocardial infarction risks.

A better understanding of mediators and mechanisms of these processes is mandatory if strategies have to be

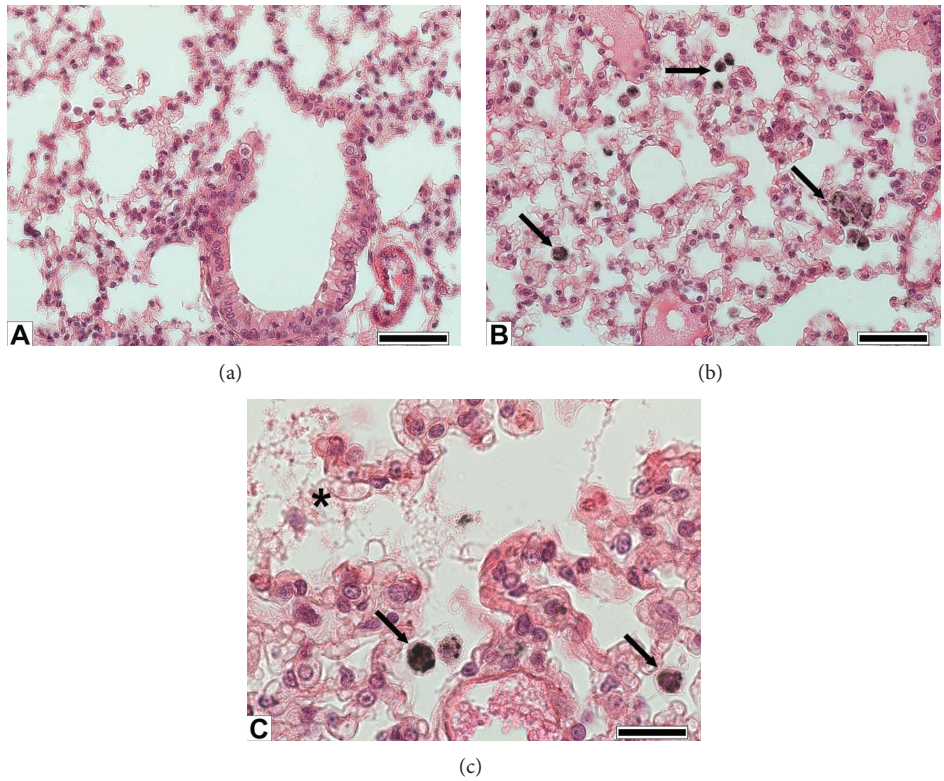

(a) (b)

(c)

Figure 4: Lung histology. (a) Sham lung parenchyma showing bronchiolar and alveolar epithelia; (b) PM1-treated lung showing abundant alveolar macrophages engulfing particles (arrows); (c) detail of alveoli of a lung instilled with PM1 showing particles phagocytosis by alveolar macrophages and damage of the alveolar epithelium (asterisk). (a), (b) bars = 50 μm; and (c) bar = 20 μm.

developed for individual protection to the PM-induced cardiovascular risk.

Authors' Contribution

F. Farina and G. Sancini contributed equally to this work.

Conflict of Interests

The authors do not have any conflict of interests.

Acknowledgments

The authors thank the researchers of the Atmospheric Chemistry group supervised by Professor E. Bolzacchini, especially M. G. Perrone, operating in the POLARIS Research Center, Department of Environmental Science, University of Milan Bicocca, for their precious contribution in PM1 sampling and chemical characterization. This research has received a financial support by the Cariplo Foundation to the Project TOSCA "Toxicity of particulate matter and marker of risk". Farina obtained a grant for this project.

References

[1] G. Polichetti, S. Cocco, A. Spinali, V. Trimarco, and A. Nunziata, "Effects of particulate matter (PM10, PM2.5 and PM1) on the cardiovascular system," *Toxicology*, vol. 261, no. 1-2, pp. 1–8, 2009.

[2] S. Salvi and S. T. Holgate, "Mechanisms of particulate matter toxicity," *Clinical and Experimental Allergy*, vol. 29, no. 9, pp. 1187–1194, 1999.

[3] U. Heinrich, U. Mohr, R. Fuchst, and C. Brockmeyer, "Investigation of a potential co-tumorigenic effect of the dioxides of nitrogen and sulphur and of diesel engine exhaust on the respiratory tract of Syrian golden hamsters," Research Report 29, Health Effects Institute, Cambridge, Mass, USA, 1989.

[4] P. Mantecca, F. Farina, E. Moschini et al., "Comparative acute lung inflammation induced by atmospheric PM and size-fractionated tire particles," *Toxicology Letters*, vol. 198, no. 2, pp. 244–254, 2010.

[5] A. Nemmar, H. Vanbilloen, M. F. Hoylaerts, P. H. M. Hoet, A. Verbruggen, and B. Nemery, "Passage of intratracheally instilled ultrafine particles from the lung into the systemic circulation in hamster," *American Journal of Respiratory and Critical Care Medicine*, vol. 164, no. 9, pp. 1665–1668, 2001.

[6] W. G. Kreyling, M. Semmler, F. Erbe et al., "Translocation of ultrafine insoluble iridium particles from lung epithelium to extrapulmonary organs is size dependent but very low," *Journal of Toxicology and Environmental Health Part A*, vol. 65, no. 20, pp. 1513–1530, 2002.

[7] G. Oberdörster, Z. Sharp, V. Atudorei et al., "Extrapulmonary translocation of ultrafine carbon particles following whole-body inhalation exposure of rats," *Journal of Toxicology and*

Environmental Health Part A, vol. 65, no. 20, pp. 1531–1543, 2002.

[8] A. Nemmar, P. H. M. Hoet, B. Vanquickenborne et al., "Passage of inhaled particles into the blood circulation in humans," *Circulation*, vol. 105, no. 4, pp. 411–414, 2002.

[9] N. L. Mills, N. Amin, S. D. Robinson et al., "Do inhaled carbon nanoparticles translocate directly into the circulation in humans?" *American Journal of Respiratory and Critical Care Medicine*, vol. 173, no. 4, pp. 426–431, 2006.

[10] F. Farina, G. Sancini, P. Mantecca, D. Gallinotti, M. Camatini, and P. Palestini, "The acute toxic effects of particulate matter in mouse lung are related to size and season of collection," *Toxicology Letters*, vol. 202, no. 3, pp. 209–217, 2011.

[11] R. Vecchi, G. Marcazzan, G. Valli, M. Ceriani, and C. Antoniazzi, "The role of atmospheric dispersion in the seasonal variation of PM1 and PM2.5 concentration and composition in the urban area of Milan (Italy)," *Atmospheric Environment*, vol. 38, no. 27, pp. 4437–4446, 2004.

[12] M. Giugliano, G. Lonati, P. Butelli, L. Romele, R. Tardivo, and M. Grosso, "Fine particulate (PM2.5-PM1) at urban sites with different traffic exposure," *Atmospheric Environment*, vol. 39, no. 13, pp. 2421–2431, 2005.

[13] M. Gualtieri, P. Mantecca, V. Corvaja et al., "Winter fine particulate matter from Milan induces morphological and functional alterations in human pulmonary epithelial cells (A549)," *Toxicology Letters*, vol. 188, no. 1, pp. 52–62, 2009.

[14] P. Mantecca, G. Sancini, E. Moschini et al., "Lung toxicity induced by intratracheal instillation of size-fractionated tire particles," *Toxicology Letters*, vol. 189, no. 3, pp. 206–214, 2009.

[15] N. Sabbagh-Kupelwieser, H. Horvath, and W. W. Szymanski, "Urban aerosol studies of PM1 size fraction with reference to ambient conditions and visibility," *Aerosol and Air Quality Research*, vol. 10, no. 5, pp. 425–432, 2010.

[16] G. Lonati and M. Giugliano, "Size distribution of atmospheric particulate matter at traffic exposed sites in the urban area of Milan (Italy)," *Atmospheric Environment*, vol. 40, supplement 2, pp. 264–274, 2006.

[17] M. G. Perrone, M. Gualtieri, L. Ferrero et al., "Seasonal variations in chemical composition and in vitro biological effects of fine PM from Milan," *Chemosphere*, vol. 78, no. 11, pp. 1368–1377, 2010.

[18] L. Ferrero, M. G. Perrone, S. Petraccone et al., "Vertically-resolved particle size distribution within and above the mixing layer over the Milan metropolitan area," *Atmospheric Chemistry and Physics*, vol. 10, no. 8, pp. 3915–3932, 2010.

[19] M. G. Perrone, B. R. Larse, L. Ferrero et al., "Sources of high PM2.5 concentrations in Milan, Northern italy: molecular marker data and CMB modelling," *Science of the Total Environment*, vol. 414, pp. 343–355, 2012.

[20] M. Naota, A. Shimada, T. Morita, K. Inoue, and H. Takano, "Translocation pathway of the intratracheally instilled C60 fullerene from the lung into the blood circulation in the mouse: possible association of diffusion and caveolae-mediated pinocytosis," *Toxicologic Pathology*, vol. 37, no. 4, pp. 456–462, 2009.

[21] J. Chen, M. Tan, A. Nemmar et al., "Quantification of extrapulmonary translocation of intratracheal-instilled particles in vivo in rats: effect of lipopolysaccharide," *Toxicology*, vol. 222, no. 3, pp. 195–201, 2006.

[22] M. S. Happo, R. O. Salonen, A. I. Hlinen et al., "Inflammation and tissue damage in mouse lung by single and repeated dosing of urban air coarse and fine particles collected from six European cities," *Inhalation Toxicology*, vol. 22, no. 5, pp. 402–416, 2010.

[23] V. Saunders, P. Breysse, J. Clark, A. Sproles, M. Davila, and M. Wills-Karp, "Particulate matter-induced airway hyperresponsiveness is lymphocyte dependent," *Environmental Health Perspectives*, vol. 118, no. 5, pp. 640–646, 2010.

[24] H. R. Paur, F. R. Cassee, J. Teeguarden et al., "In-vitro cell exposure studies for the assessment of nanoparticle toxicity in the lung-A dialog between aerosol science and biology," *Journal of Aerosol Science*, vol. 42, no. 10, pp. 668–692, 2011.

[25] R. Daffara, L. Botto, E. Beretta et al., "Endothelial cells as early sensors of pulmonary interstitial edema," *Journal of Applied Physiology*, vol. 97, no. 4, pp. 1575–1583, 2004.

[26] R. F. Henderson, "Use of bronchoalveolar lavage to detect respiratory tract toxicity of inhaled material," *Experimental and Toxicologic Pathology*, vol. 57, no. 1, pp. 155–159, 2005.

[27] M. T. Kleinman, C. Sioutas, M. C. Chang, A. J. F. Boere, and F. R. Cassee, "Ambient fine and coarse particle suppression of alveolar macrophage functions," *Toxicology Letters*, vol. 137, no. 3, pp. 151–158, 2003.

[28] M. Lundborg, S. E. Dahlén, U. Johard et al., "Aggregates of ultrafine particles impair phagocytosis of microorganisms by human alveolar macrophages," *Environmental Research*, vol. 100, no. 2, pp. 197–204, 2006.

[29] J. L. Mauderly, M. B. Snipes, and E. B. Barr, "Pulmonary toxicity of inhaled diesel exhaust and carbon black in chronically exposed rats," Report 68, Health Effects Institute, Cambridge, Mass, USA, 1994.

[30] S. Salvi, A. Blomberg, B. Rudell et al., "Acute inflammatory responses in the airways and peripheral blood after short-term exposure to diesel exhaust in healthy human volunteers," *American Journal of Respiratory and Critical Care Medicine*, vol. 159, no. 3, pp. 702–709, 1999.

[31] D. M. Walters, P. N. Breysse, and M. Wills-Karp, "Ambient urban Baltimore particulate-induced airway hyperresponsiveness and inflammation in mice," *American Journal of Respiratory and Critical Care Medicine*, vol. 164, no. 8, pp. 1438–1443, 2001.

[32] A. K. Cho, C. Sioutas, A. H. Miguel et al., "Redox activity of airborne particulate matter at different sites in the Los Angeles Basin," *Environmental Research*, vol. 99, no. 1, pp. 40–47, 2005.

[33] M. E. Gerlofs-Nijland, A. Campbell, M. R. Miller, D. E. Newby, and F. R. Cassee, "Toxicity of inhaled traffic related particulate matter," *Journal of Physics: Conference Series*, vol. 151, Article ID 012049, 2009.

[34] S. Becker, L. A. Dailey, J. M. Soukup, S. C. Grambow, R. B. Devlin, and Y. C. T. Huang, "Seasonal variations in air pollution particle-induced inflammatory mediator release and oxidative stress," *Environmental Health Perspectives*, vol. 113, no. 8, pp. 1032–1038, 2005.

[35] L. E. Fredenburgh, M. A. Perrella, and S. A. Mitsialis, "The role of heme oxygenase-1 in pulmonary disease," *American Journal of Respiratory Cell and Molecular Biology*, vol. 36, no. 2, pp. 158–165, 2007.

[36] S. W. Ryter and R. M. Tyrrell, "The heme synthesis and degradation pathways: role in oxidant sensitivityHeme oxygenase has both pro- and antioxidant properties," *Free Radical Biology and Medicine*, vol. 28, no. 2, pp. 289–309, 2000.

[37] T. A. Reiter and B. Demple, "Carbon monoxide mediates protection against nitric oxide toxicity in HeLa cells," *Free Radical Biology and Medicine*, vol. 39, no. 8, pp. 1075–1088, 2005.

[38] L. Risom, M. Dybdahl, J. Bornholdt et al., "Oxidative DNA damage and defense gene expression in the mouse lung after short-term exposure to diesel exhaust particles by inhalation," *Carcinogenesis*, vol. 24, no. 11, pp. 1847–1852, 2003.

[39] B. Y. Chin, M. A. Trush, A. M. K. Choi, and T. H. Risby, "Transcriptional regulation of the HO-1 gene in cultured macrophages exposed to model airborne particulate matter," *American Journal of Physiology*, vol. 284, no. 3, pp. L473–L480, 2003.

[40] P. H. Danielsen, P. Møller, K. A. Jensen et al., "Oxidative stress, DNA damage, and inflammation induced by ambient air and wood smoke particulate matter in human A549 and THP-1 cell lines," *Chemical Research in Toxicology*, vol. 24, no. 2, pp. 168–184, 2011.

[41] G. Li Volti, V. Sorrenti, P. Murabito et al., "Pharmacological induction of heme oxygenase-1 inhibits iNOS and oxidative stress in renal ischemia-reperfusion injury," *Transplantation Proceedings*, vol. 39, no. 10, pp. 2986–2991, 2007.

[42] H. Greim and R. Snyder, *Toxicology and Risk Assessment: A Comprehensive Introduction*, John Wiley & Sons, 2008.

[43] Q. Cao, S. Zhang, C. Dong, and W. Song, "Pulmonary responses to fine particles: differences between the spontaneously hypertensive rats and wistar kyoto rats," *Toxicology Letters*, vol. 171, no. 3, pp. 126–137, 2007.

[44] A. Elder and G. Oberdörster, "Translocation and effects of ultrafine particles outside of the lung," *Clinics in Occupational and Environmental Medicine*, vol. 5, no. 4, pp. 785–796, 2005.

[45] C. J. Obot, M. T. Morandi, T. P. Beebe, R. F. Hamilton, and A. Holian, "Surface components of airborne particulate matter induce macrophage apoptosis through scavenger receptors," *Toxicology and Applied Pharmacology*, vol. 184, no. 2, pp. 98–106, 2002.

[46] T. Stoeger, S. Takenaka, B. Frankenberger et al., "Deducing in vivo toxicity of combustion-derived nanoparticles from a cell-Free oxidative potency assay and Metabolic activation of organic compounds," *Environmental Health Perspectives*, vol. 117, no. 1, pp. 54–60, 2009.

[47] S. Marschall, M. A. Rothschild, and M. Bohnert, "Expression of heat-shock protein 70 (Hsp70) in the respiratory tract and lungs of fire victims," *International Journal of Legal Medicine*, vol. 120, no. 6, pp. 355–359, 2006.

[48] D. Kültz, "Evolution of the cellular stress proteome: from monophyletic origin to ubiquitous function," *Journal of Experimental Biology*, vol. 206, no. 18, pp. 3119–3124, 2003.

[49] S. Hertel, A. Viehmann, S. Moebus et al., "Influence of short-term exposure to ultrafine and fine particles on systemic inflammation," *European Journal of Epidemiology*, vol. 25, no. 8, pp. 581–592, 2010.

[50] G. Oberdörster and M. J. Utell, "Ultrafine particles in the urban air: to the respiratory tract—and beyond?" *Environmental Health Perspectives*, vol. 110, no. 8, pp. A440–A441, 2002.

[51] R. Para, *Evaluation of toxicological effects of intra tracheal instilled CeO2 nanoparticles on the heart of male sprague-dawley rats [Ph.D. thesis]*, 2011.

[52] J. Zhao, Y. Xie, X. Qian, R. Jiang, and W. Song, "Acute effects of fine particles on cardiovascular system: differences between the spontaneously hypertensive rats and wistar kyoto rats," *Toxicology Letters*, vol. 193, no. 1, pp. 50–60, 2010.

[53] E. Cozzi, C. J. Wingard, W. E. Cascio et al., "Effect of ambient particulate matter exposure on hemostasis," *Translational Research*, vol. 149, no. 6, pp. 324–332, 2007.

[54] S. Massberg, K. Brand, S. Grüner et al., "A critical role of platelet adhesion in the initiation of atherosclerotic lesion formation," *Journal of Experimental Medicine*, vol. 196, no. 7, pp. 887–896, 2002.

[55] I. Weinberger, J. Fuchs, E. Davidson, and Z. Rotenberg, "Circulating aggregated platelets, number of platelets per aggregate, and platelet size during acute myocardial infarction," *American Journal of Cardiology*, vol. 70, no. 11, pp. 981–983, 1992.

[56] G. Chironi, C. Dosquet, M. Del-Pino et al., "Relationship of circulating biomarkers of inflammation and hemostasis with preclinical atherosclerotic burden in nonsmoking hypercholesterolemic men," *American Journal of Hypertension*, vol. 19, no. 10, pp. 1025–1031, 2006.

Hindawi Publishing Corporation
BioMed Research International
Volume 2013, Article ID 685074, 9 pages
http://dx.doi.org/10.1155/2013/685074

Research Article

Quantification of Cigarette Smoke Particle Deposition *In Vitro* Using a Triplicate Quartz Crystal Microbalance Exposure Chamber

Jason Adamson, David Thorne, John McAughey, Deborah Dillon, and Clive Meredith

British American Tobacco, Group R&D, Regents Park Road, Southampton SO15 8TL, UK

Correspondence should be addressed to Jason Adamson; jason_adamson@bat.com

Received 3 October 2012; Accepted 22 November 2012

Academic Editor: Ernesto Alfaro-Moreno

There are a variety of smoke exposure systems available to the tobacco industry and respiratory toxicology research groups, each with their own way of diluting/delivering smoke to cell cultures. Thus a simple technique to measure dose *in vitro* needs to be utilised. Dosimetry—assessment of dose—is a key element in linking the biological effects of smoke generated by various exposure systems. Microbalance technology is presented as a dosimetry tool and a way of measuring whole smoke dose. Described here is a new tool to quantify diluted smoke particulate deposition *in vitro*. The triplicate quartz crystal microbalance (QCM) chamber measured real-time deposition of smoke at a range of dilutions 1 : 5–1 : 400 (smoke : air). Mass was read in triplicate by 3 identical QCMs installed into one *in vitro* exposure chamber, each in the location in which a cell culture would be exposed to smoke at the air-liquid interface. This resulted in quantification of deposited particulate matter in the range 0.21–28.00 μg/cm^2. Results demonstrated that the QCM could discriminate mass between dilutions and was able to give information of regional deposition where cell cultures would usually be exposed within the chamber. Our aim is to use the QCM to support the preclinical (*in vitro*) evaluation of tobacco products.

1. Introduction

Modelling human disease processes *in vitro* is important for our understanding of the risks associated with human exposure to known and unknown inhaled chemicals or toxicants. These *in vitro* models can be used for mechanistic-based research and/or to assess potential harm of consumer goods, such as household products, cosmetics, or tobacco products. Although it can be argued that *in vitro* models have limitations in human physiological relevance, it is believed that these models have potential to reduce the financial and ethical burden on *in vivo* animal testing.

Looking specifically at the toxicological assessment of tobacco smoke, there are a number of *in vitro* models of toxicity using whole smoke exposure systems already in use [1–9]. Exposure system setups may differ greatly but their function and purpose is shared. A smoking machine/robot is used to generate and/or dilute mainstream whole smoke; this is delivered to an exposure chamber/module containing a simple or complex *in vitro* model of the lung at the air-liquid interface (ALI) so that a biological endpoint (usually related to one of the major smoking related diseases) can be assessed. As with the diversity of exposure systems and setups available, the same can be said of the *in vitro* model and endpoint testing. These may range from something as simple as a cytotoxicity assessment using a continuous cell line [1, 2, 8] through to complex endpoints assessing intracellular markers [9], or utilise more sophisticated cell cultures such as primary cell lines [10, 11], coculture systems, 3D-tissue models, or whole lung slices [3]. Currently, there are no defined *regulatory* protocols for whole smoke exposure systems, but these are being developed to support human *in vitro* models of disease. Aforementioned, there are a vast number of whole smoke exposure systems described in the literature, either commercially available [1–9] or one-off in-house setups [10, 12, 13]. Additionally, tobacco smoke is a concentrated and complex mix of at least 5,600 chemicals and toxicants found across two phases, the particulate (tar) and

vapour phase [14]. Thus, assessing smoke dose is challenging. Consequently, when presenting whole smoke dose-response data, authors variously describe "dose" in many different ways: as a percentage of smoke; a fraction of smoke; ratios of smoke to air; puff number; total number of cigarettes smoked; total exposure of micrograms per culture insert; a flow rate of mixing air and vacuum applied to a smoke dilutor, all depending on the machine being used to generate and dilute the smoke [15]. Hence there is a need to accurately quantify particle and/or chemical deposition in our *in vitro* systems, such that comparisons of biological endpoints between different systems can be achieved with improved precision and accuracy both within and ultimately between laboratories. This is of increasing importance to scientists and regulators as it will allow consistent interpretation of results and quick cross-comparison of biological endpoints for defined smoke doses [16, 17]. Dosimetry (the assessment/measurement/quantification of smoke dose) is therefore a key element that can unite the biological effects of whole smoke generated by various and diverse exposure systems [3].

There are small numbers of chemicals or markers which can be quantified to assess tobacco smoke dosimetry; most of these dosimetry measurements assess the particulate phase due to the challenges of measuring individual components in the vapour phase, especially at higher smoke dilutions (lower concentrations) [15]. Chemicals/markers have been selected historically due to their facile quantification and include, but are not limited to: carbon monoxide [5] and oxides of nitrogen (NO_x) which are in the gas phase; solanesol [18] and nicotine which are particulate markers; carbonyls which are split between phases; particulate matter as a whole either via gravimetric or chemical methods [7, 15].

Adamson et al. [15] reported a gravimetric method of particulate deposition quantification using a single quartz crystal microbalance (QCM) which robustly measured whole smoke particulate dose. The QCM is a sensitive gravimetric balance capable of measuring and detecting changes in mass of thin oscillating adherent films, within the nanogram range [19–22]. Previously, Adamson et al. [15] presented a new application (of an existing microbalance technology) of a single QCM unit in a chamber to assess the real-time deposition of tobacco smoke *in vitro* with verification by a chemical fluorescence method for smoke particle deposition. We now present a new, unique, and characterised dosimetry tool where the exposure chamber base accommodates 3 identical QCM units (Figure 1), termed the triplicate QCM chamber or *3-in-1* QCM chamber. Primarily, the study objectives were to assess/give an indication of regional deposition within the chamber (uniformity of particle deposition to cell cultures) where the previous single unit QCM could not show us this, and to increase robustness through the use of higher replicate numbers per run (from 1 to 3). For users of this exposure chamber, both sets of additional information are new and useful and could not have been provided by the single unit QCM. In this study we investigated the ability of the triplicate QCM to detect mass differences of whole smoke dilutions from 1 : 5 to 1 : 400 (smoke : air, volume : volume), for 30 minutes/run. The range 1 : 5–1 : 400 was selected as this represents the RM20S dilutions used in the laboratory to generate a biological dose response using robust *in vitro* primary and continuous cell cultures [1, 7, 9].

Figure 1: British American Tobacco's standard exposure chamber used for *in vitro* exposures to whole smoke at the air-liquid interface was modified to accommodate the 3 QCM units. The picture shows a top view of the 3-in-1 QCM exposure chamber base (crystal ø = 2.54 cm; cell support insert ø = 2.4 cm). QCM position 1 is proximal to the passive exhaust port ∗. QCM positions 2 and 3 are distal to the exhaust port and behind position 1 on the right and left, respectively.

Our results demonstrated that the QCM was able to discriminate mass between each dilution and was able to give information of regional deposition where ALI cell culture inserts would usually be at positions 1, 2, and 3 in the chamber (Figure 2). Furthermore, these results showed absolute agreement with the single unit QCM data previously reported [15]. Overall, the integrated triplicate QCM tool delivered robust, real-time, quantitative whole smoke mass measurements at nanogram levels and demonstrated an achievable dose response.

2. Materials and Methods

2.1. Whole Cigarette Smoke Generation. Reference cigarettes (3R4F, 9.4 mg pack tar) (University of Kentucky, Lexington, KY, USA) were used for all experiments. Whole cigarette smoke was generated and diluted using two identical Borgwaldt RM20S smoking machines (Borgwaldt-kc, Hamburg, Germany) within the same laboratory, as previously described [1, 15]. The smoking machines and individual syringes from each machine were used interchangeably and at random and statistical analysis of the data thereafter showed that this had no effect on mass values obtained at the same dilution (data not shown). Five smoke dilutions

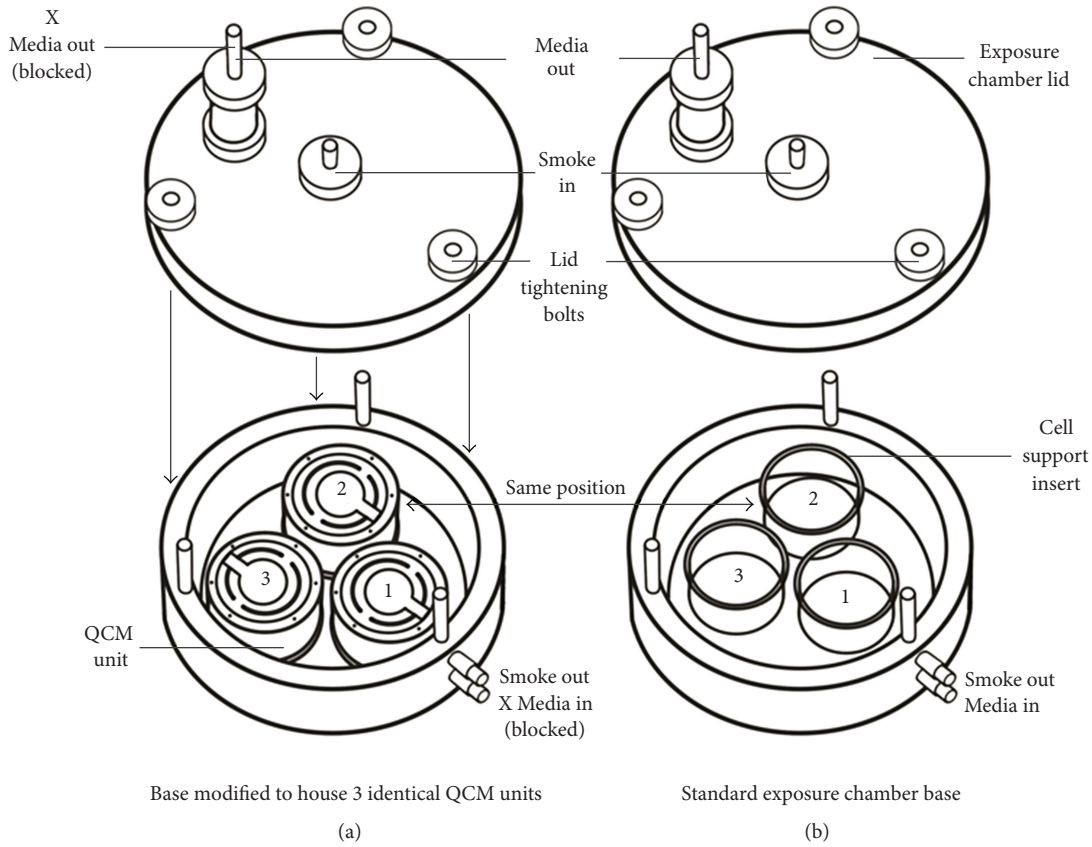

Figure 2: A schematic diagram of the triplicate QCM exposure chamber. (a) Crystals are installed directly into and replace the 3 positions where (b) cells would usually be exposed to whole smoke at the air-liquid interface. Illustration by J. Adamson.

were programmed as a ratio of smoke to air—1 : 5, 1 : 10, 1 : 25, 1 : 100, and 1 : 400 (smoke : air, volume : volume)—and 5 replicate experiments were conducted per dilution (n = 5). For all experiments, the machine smoked for 30 minute duration at ISO 4387 : 2000 smoking regime (35 mL puff over 2 seconds, once a minute, to a defined number of 6 puffs/cigarette). After the last cigarette was extinguished, the QCMs were left to record real-time data until all residual smoke in the chamber had deposited and mass values were observed to plateau and stabilise, usually taking an additional 10 minutes.

To prove deposition was due to smoke particulate alone, a Cambridge filter pad (CFP) (Borgwaldt-kc, Hamburg, Germany) was installed inline of smoke generation just prior to entry to the chamber for an additional single run of 1 hour (twice the duration of a standard run). As CFPs effectively trap 99.9% particulate matter [14, 23], anything detected by the QCM would therefore give an indication of nonparticulate mass activity within the exposure chamber during a smoke run.

2.2. The QCM Exposure Chamber Module. The previously described *in vitro* whole smoke exposure chamber manufactured for BAT by Curbridge Engineering (Southampton, UK) [7] had its base adapted to symmetrically house 3 identical commercially available QCM microbalance units (Vitrocell Systems GmbH, Waldkirch, Germany). The QCM housing units were installed with 5 MHz AT cut quartz crystals held between two Au/Cr polished electrodes, 1 inch (2.5 cm) diameter as described by Mülhopt et al. [19] (Figure 1). The QCM read at a resolution of 10 nanogram/cm^2/second [15].

Before smoke exposure, the 3-in-1 QCM chamber was sealed and acclimatised in an incubator at 37°C to ensure quartz crystal stability. Quartz crystal stability was reached by zeroing the software before exposure until the baseline showed negligible drift (zero point stability) of less than 20 ng/cm^2 over a duration of a few minutes. This took 5–10 minutes of zeroing prior to and between exposures in a stable environment. During longer periods of stability where the crystal was zeroed over a period of a few hours at constant environmental conditions, we were able to observe absolute zero point stability (0.00±0.01 μg/cm^2) for 5 minutes prior to smoke exposure. During the deposition phase, the QCM recorded mass every 2 seconds for the 30 minute smoke exposure and 10 minute plateau phase, reporting as mass per unit area. Cell culture media was not included in the chamber for these mass measurements therefore media-in and media-out ports were blocked airtight to stop smoke leaking. After whole smoke exposure and between consecutive runs, quartz crystals were cleaned *in situ* (within the chamber, still screwed into their housing units). The crystal's surface was wiped with a soft lint-free tissue and

70% ethanol, and then polished to a shine. Crystals were not removed/replaced between readings; however, these should be replaced if broken or if their surface is severely scratched. Crystal stabilisation time was greatly reduced from up to 60 minutes to around 10 minutes when the crystals were cleaned *in situ*.

2.3. Statistics. Data were reported as a mean ± standard deviation. The individual value plot of QCM-detected mass (Figure 3(a)), the multi-vari chart (Figure 3(b)), and the interaction plot comparing both QCM devices (Figure 4) were created using MINITAB v.16 statistical software. Main effects plots to check experimental variables (not shown) and a one-way ANOVA test using Tukey method to assess differences between QCM positions and QCM devices were also determined using MINITAB. All residual plots for all graphs generated by MINITAB were checked to ensure the quality of the data obtained. Real-time traces of deposited mass (Figure 5) were made using Microsoft Excel.

3. Results

The 3-in-1 QCM exposure chamber was able to record particulate mass in a dose-dependent manor in the dilution range 1 : 5–1 : 400 (smoke : air, v/v) (Figure 3(a)). Mean deposited mass ranged from 0.21 μg/cm^2 (210 ng/cm^2) ±0.06 μg/cm^2 at the most dilute dose of 1 : 400, up to 28.00 μg/cm^2 (27,998 ng/cm^2) ±2.25 μg/cm^2 at the most concentrated dose of 1 : 5. This mass range was obtained from the means of all three QCM positions per dose (n = 5/position). A one-way analysis of variance (ANOVA) test showed that, as expected, there were significant differences between dilutions ($P \leq 0.05$); however, 1 : 100 and 1 : 400 dilutions had grouped confidence intervals indicating that overall mass values were in the same range at these high dilutions.

The data were presented by individual QCM position so that the regional deposition around the chamber could be assessed (Figure 3(a)). QCM position 1 is most proximal to the passive exhaust port where smoke exits the chamber, whereas positions 2 and 3 are paired distal to the port, right and left, respectively (Figures 1 and 2). To assess the distribution of particulate deposition around the chamber positions *at all the dilutions tested*, a multi-vari chart was produced (Figure 3(b)). This chart demonstrates the uniformity of particle deposition in the biological exposure range, showing the mean deposited mass of the three QCM positions at all five dilutions tested. There were no significant differences between QCM positions 1, 2, and 3 for all dilutions tested—1 : 5 (P = 0.205), 1 : 10 (P = 0.186), 1 : 25 (P = 0.923), 1 : 100 (P = 0.794), and 1 : 400 (P = 0.435).

The dose-response data generated from this triplicate QCM tool was compared with the aforementioned single unit QCM [15], and good parity was observed between them with no statistically significant difference between the different tools at all dilutions tested (Figure 4). For dilutions 1 : 10–1 : 400 deposition was highly comparable between the two tools (≤5%) (Table 1). At the most concentrated dilution of 1 : 5, the difference in detected deposited mass between the tools was 8.4% (Table 1). Considering the entire range tested, the difference between both tools at all dilutions was <10% which we would consider to be an acceptable difference (fit for purpose).

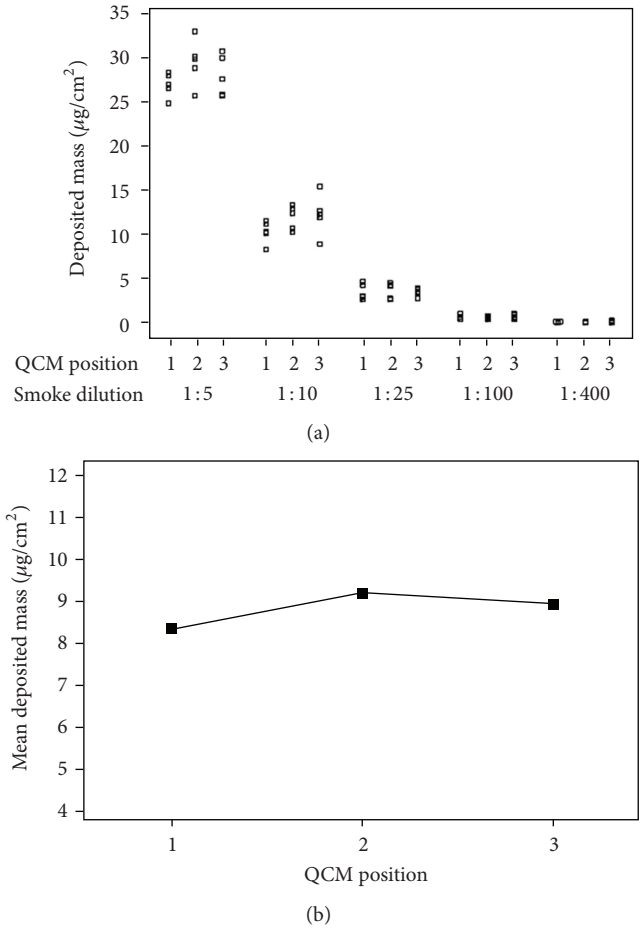

Figure 3: Triplicate QCM deposition data. (a) An individual value plot showing deposited particle mass quantification of ISO whole smoke (9.4 mg) diluted in the range 1 : 5–1 : 400 (smoke : air, v/v), n = 5/position. (b) A multi-vari chart of mean deposited mass at all five dilutions 1 : 5–1 : 400. The chart shows the average distribution of particulate deposition around the chamber within the range tested, from 25 values (5 dilutions at n = 5/dilution). There was no statistically significant difference in deposition between the three QCM positions.

Finally, a Cambridge filter pad (CFP) was placed inline of smoke generation to occlude particulate entering the chamber—the purpose was to assess semivolatile deposition or potentially the behavior of other gases. Figure 5 shows a real-time trace of particulate detection during an extended smoke exposure of 1 hour at the highest smoke concentration of 1 : 5 (smoke : air, v/v) with a CFP inline. The trace showed that mass increased over time, but this increase was nominal considering the high tar level of 3R4F cigarettes (9.4 mg) and the high concentration of whole smoke chosen (1 : 5). There was an increase of 78 ng/cm^2 with the CFP inline compared with particulate matter deposition of 27,998 ng/cm^2 for

Table 1: Mean deposited mass values obtained from the single unit QCM [15] ($n = 5$) compared to the 3-in-1 QCM unit ($n = 15$); the percentage difference between mean mass detected by the two tools; the P values indicating no significant difference between tools at all dilutions tested. For the single unit, the values were the mean of 5 repeat experiments with the QCM (in position 2 of the chamber) [15]; for the triplicate QCM the values were the mean of 5 repeat experiments and 3 QCM positions per repeat ($n = 15$).

	Mean deposited mass (μg/cm^2) ± SD				
Dilution (1 : X)	5	10	25	100	400
Single unit	25.75 ± 2.30	10.51 ± 0.42	3.29 ± 0.24	0.69 ± 0.09	0.22 ± 0.03
Triplicate unit	28.00 ± 2.25	11.51 ± 1.81	3.64 ± 0.72	0.75 ± 0.20	0.21 ± 0.06
Difference (%)	8.4	4.5	5.2	4.9	2.3
P value	0.071	0.245	0.304	0.503	0.573

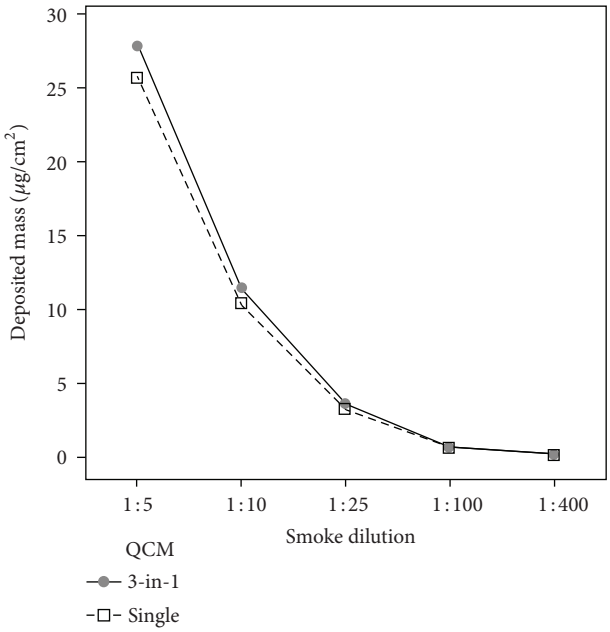

Figure 4: An interaction plot of the data means for the single unit QCM [15] and the 3-in-1 QCM, at the five airflows tested. There was no statistically significant difference between the two different devices.

diluted whole smoke at the same dilution of 1 : 5. Furthermore, after 1 hour of smoking the overall mass reached was <200 ng/cm^2 (mean of the 3 positions was 156 ng/cm^2). Whilst the initial chart would suggest that negligible mass was detected and that the traces were flat lined, however, when the scale was adjusted (Figure 5 pullout) a repeated and conserved saw-tooth pattern was observed, indicative (at least in time) of some transient mass deposition, probably constituents of diluted vapour phase or water vapour entering the chamber. In addition, a further inline CFP measurement at the higher smoke dilution of 1 : 400 showed a similar saw-tooth mass deposition pattern of negligible cumulative mass (not reported). The single "n-shaped" unit observed here would suggest a small increase, plateau, and decrease in mass as diluted vapour phase smoke was delivered to the chamber. This could be an indication of semivolatile deposition on the QCM surface followed by evaporation as airflow through the chamber changed per puff.

As noted, cumulative mass over 60 minutes with the CFP inline was 156 ng/cm^2/hr. If the sum of the transient peaks is calculated with subsequent reevaporation ignored (Figure 5), the cumulative mass was approximately 620 ng/cm^2/hr. This amount of detected mass is too low to be water vapour or vapour phase in its totality. The repeat pattern does suggest some components of the vapour phase but it would be difficult to identify semivapour phase revolatilising here without additional chemistry analysis. Rodgman and Perfetti [24] cite an example cigarette of generating 7.5 mg vapour phase and 17.4 mg NFDPM (nicotine free dry particulate matter). If this proportionality is maintained for the 3R4F cigarette, ISO yields of 9.4 mg NFDPM, 0.87 mg water (measured), and 4.1 mg vapour phase (estimated) and calculating orders of magnitude and the contribution of particulate, vapour, and water from a 3R4F cigarette, we would expect to see about 14,000 ng for total vapour phase and about 2,800 ng for water. Thus what we have identified on the QCM with the particulate phase occluded is too low to be either water or total vapour.

4. Discussion

In this study we present a new and unique tool (Figure 1) to quantify diluted whole smoke particulate matter deposition *in vitro*. This tool measured real-time deposition at a range of dilutions 1 : 5–1 : 400 (smoke : air, v/v) resulting in quantification of deposited particulate matter in the range 0.21–28.00 μg/cm^2, most dilute to most concentrated smoke dilution (Figure 3(a)). The technology was able to detect deposited mass with such resolution that it could identify puff-by-puff profiles, probably of some vapour phase constituents alone (when particles were occluded with a filter pad) (Figure 5). For the first time, mass values were read in triplicate by 3 identical QCM units installed into the exposure chamber, each in exactly the same location as the cell culture inserts would be exposed to whole smoke at the ALI (Figure 2). This information is particularly useful to users of the chamber as it demonstrates uniformity, with no difference in particle deposition to the 3 positions where culture inserts would be exposed to smoke.

To further assess the sensitivity of the QCM technology, a Cambridge filter pad (CFP) was placed inline of smoke generation to effectively occlude the particulate fraction of whole smoke. The hypothesis here was that no particulate

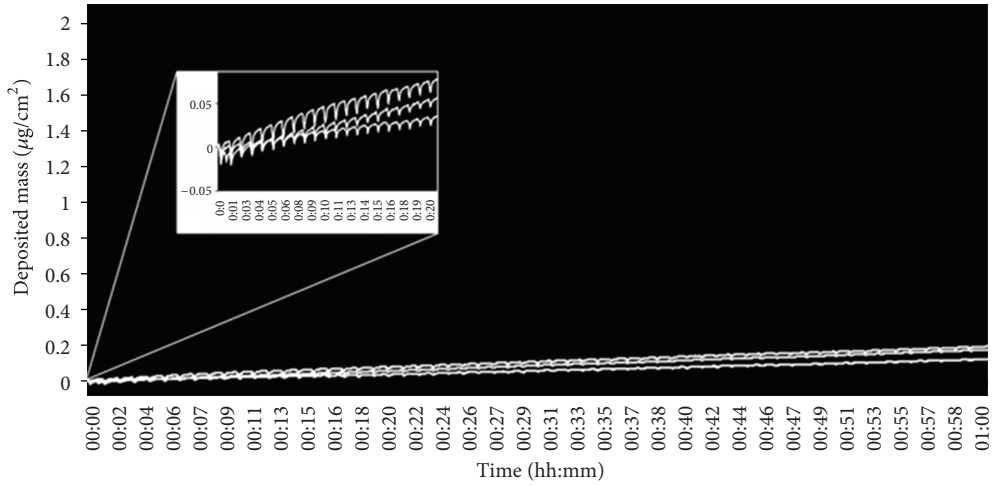

Figure 5: Deposition when a Cambridge filter pad (CFP) was placed prior to the QCM chamber to trap particulate matter. Cigarettes (3R4F) were smoked at the ISO regime at a dilution of 1 : 5 (smoke : air, v/v) for 1 hour. When the scale is adjusted to see the trace more clearly, note the distinct and repeated "n-shaped" pattern of mass increase and decrease per puff over time. The 3 traces represent the 3 QCMs within the chamber: QCM position 1, bottom; QCM position 2, top; QCM position 3, middle.

mass would be detected and anything being detected would be derived from the diluted gas/vapour phase delivered to the chamber. As predicted, nominal mass was detected in the range <200 ng/cm^2 in 1 hour; however, a distinct and repeated saw-tooth pattern was observed in the real-time trace (Figure 5). Although we are yet to identify what is being deposited on the QCM surface when the CFP is inline, we predict this could be an indication of some vapour phase components condensing and evaporating as airflow through the chamber changes per puff. Elution, chemical analysis, and quantification will help us potentially identify what part of the vapour phase is deposited on the exposed QCM surface, and we plan to do this in subsequent studies.

There are unique challenges not only in the identification of smoke components but also their quantitation [14]. Of the particulate matter which is being quantified by the QCM, grossly it approximates 16% water, 6% nicotine, and 78% "tar" (NFDPM), of which the major components of NFDPM are alcohols (20%), acids (17%), and aldehydes and ketones (14%) [14]. Sophisticated analytical tools, such as gas-chromatography mass spectrometry (GC/MS), are required to further identify these compounds. The challenge persists when it is estimated that components representing less than 1 mg of the particulate phase remain unidentified, averaging in the low nanogram and picogram levels [14]. At the ALI cell exposure surface, the particles depositing will have a soluble and an insoluble fraction. Therefore there will be species available to the thin surface liquid which lines the cell monolayer. There is little direct information published on soluble particle components and cellular interactions at the ALI, but recent in-house data suggests that a soluble fraction is 40%–90% of the particle droplet. Lastly and as previously discussed, vapour phase components are largely overlooked by this sampling method; Figure 5 demonstrates the minor quantities of material being deposited when the diluted smoke passes through a CFP.

We previously published a study demonstrating the use of a single unit QCM in the same exposure chamber [15]. Based on that data obtained, and usefulness of the tool, we further developed the triplicate chamber to support *in vitro* testing and confirm uniformity of particle deposition around the chamber, where the single unit QCM device could not show us this. As well as allowing us to assess potential positional deposition around the exposure chamber, this expanded tool allowed us to increase dosimetry replicate number per exposure. Within each dilution tested, there were no statistically significant differences in deposition around the 3 positions in the chamber (Figure 3(b)) with P values for all dilutions greater than 0.1.

Data obtained from the triplicate QCM exposure chamber compared to that obtained from the previously published single unit device [15] confirmed they were performing equally (Figure 4). At dilutions greater than 1 : 10, the results obtained from the two tools differed by 5% or less in terms of quantified mean deposited mass; this is to be expected as interrun variability. At 1 : 5 dilution, the difference was slightly higher at 8.4% (Table 1). But overall, these differences were all <10% (a range of 6.1% across the dilution range tested) which we would deem to be acceptable.

We have presented a new study demonstrating an additional/expanded, novel, and simple tool used to quantify tobacco smoke deposition *in vitro* in real time. The QCM technology itself is not new and in the past it has been used for such activities as environmental monitoring [21, 25], biological applications [26, 27], and inhalation toxicity assessment of (nontobacco) aerosols and engineered nanoparticles *in vitro* [19, 28, 29]. However, the utilisation and combination of these technologies for assessment of whole smoke exposure *in vitro* is novel. Certainly, QCM technology has many potential applications in the field of inhalation toxicology, not just tobacco smoke.

As discussed previously, there are many different setups available to industry and other respiratory toxicology research groups; in this study we used the Borgwaldt RM20S to dilute and deliver mainstream smoke to the triplicate QCM. Because so many different smoking machine and exposure systems are used, it is clear there needs to be a simple and aligned method of measuring dose *in vitro*; this is especially the case with the current switch from liquid to ALI exposures of aerosols *in vitro* [16]. Dosimetry is therefore a key element that can link the biological effects of tobacco smoke generated by various exposure systems [3]. As dose measurements with a QCM allow real-time, fast, and accurate determination of the cell deposited dose [28], we believe microbalance technology offers a way forward, not only for the assessment of whole smoke but also for other inhalable toxicants [30]. In terms of human smokers, this tool can be used to generate deposition values *in vitro* consistent with values measured in human smokers. For example, in this study QCMs detected deposition of diluted particulate matter *in vitro* in the range 0.21–28.00 $\mu g/cm^2$. For context, McAughey et al. [31] estimated daily deposited lung doses in the order of 40–100 $\mu g/cm^2$ in the extrathoracic region, 1.0–2.0 $\mu g/cm^2$ in the bronchial/bronchiolar region, and 0.1–0.2 $\mu g/cm^2$ in the alveolar-interstitial region, based on human smoking data for lung retention and regional deposition. These human values in the lower range 0.1–2.0 $\mu g/cm^2$ (bronchial-alveolar) further align with our *in vitro* exposure system: primarily it is cells of the bronchial epithelium or alveolar (A549) cells which would be used in these biological models of disease and exposed at the ALI in this chamber.

The 3-in-1 tool described here was compared to the previously published single QCM chamber (Figure 4). Currently, neither of the these QCM chambers can accommodate cell cultures at the same time as deposition quantification (the 3-in-1 cannot house cells as there is no space, and yet the single QCM has not been tested concurrently with media and/or cell cultures). However, this is something we will look at in future studies. Thus the operational advantage of the triplicate QCM versus the single QCM chamber is to increase replicate number from one to three during a single smoke exposure. This would be useful for deposition dose-range studies of different cigarettes types, for example. To obtain directly comparable chemistry deposition data alongside QCM deposition, the single QCM chamber should be used as positions 1 and 3 are available to house nude cell support inserts. Furthermore, if cell cultures could be supported on inserts for a whole smoke exposure without basal media, then this single unit tool could be used to obtain deposition data at the same time as a biological response. As the data have shown here, there is no statistically significant difference between the tools, thus both QCM chambers have applicability depending on the design of the experiment and the desired outcome.

5. Conclusion

In this study, the QCM successfully determined deposited smoke mass generated from the Borgwaldt RM20S Smoking Machine, but it can easily be adapted to assess smoke mass produced from other commercially available smoking machines. Consequently, we predict that this tool may help align smoke exposure technologies. Additionally, the 3-in-1 QCM exposure chamber, although designed to quantify deposited smoke mass *in vitro*, could potentially be used to assess other types of aerosol delivery to *in vitro* cultures, such as manufactured particles and fibres, some aerosolised cosmetics, household products, or pesticides. Certainly aerosols similar to tobacco whole smoke which are submicron liquid spherical droplets would be easy to detect. Hence the scope of this tool is vast. The 3-in-1 QCM also offers a robust and efficient alternative to traditional chemistry methods or supports such methods and delivers additional benefits of particulate quantification: (1) it is single person operated; (2) no other resource or reagents are required; (3) data is generated fast, in real time and because of this; (4) it can be used as a QC device to rapidly assess the status of a smoke exposure or identify issues with machine smoking and dilution.

Until now, there have been few (if any) reliable and accurate methods of determining particulate dose delivered to the exposure chamber in real time. Thus biological dose-response data has been presented as the machine's programmed ratio of smoke to air, with the expectation that smoke dilutions delivered from the smoking robot are robust and repeatable. In the case of the Borgwaldt RM20S, precision of smoke dilution and delivery has been previously investigated and proven to be reliable by a number of physicochemical and analytical methods, and this has been published [1, 5]. The addition of this QCM work further supports our confidence in the machine's ability to dilute and deliver smoke reliably.

Finally, we propose to continue to use these QCM tools to support the preclinical *in vitro* evaluation of tobacco products and accurately quantify particle dose delivery to cell cultures. In addition, this tool has been shown to align generated deposition values *in vitro* consistent with values measured in human smokers.

Conflict of Interests

The authors report no conflict of interests and acknowledge they are all permanent employees of British American Tobacco.

Authors' Contributions

J. Adamson and D. Thorne conceived and designed the study. J. Adamson performed the experimental work and data analysis and prepared the paper. D. Thorne, J. McAughey, D. Dillon, and C. Meredith provided scientific support, reviewed, and approved the final paper.

Acknowledgments

The authors would like to thank Sophie Hughes and Marianna Gaça for their scientific and technical expertise in

support of the initial development of this technology, and Annette Dalrymple at BAT for editing the paper.

References

[1] J. Adamson, D. Azzopardi, G. Errington, C. Dickens, J. McAughey, and M. D. Gaca, "Assessment of an *in vitro* whole cigarette smoke exposure system: the Borgwaldt RM20S 8-syringe smoking machine," *Chemistry Central Journal*, vol. 5, article 50, 2011.

[2] M. Aufderheide, J. W. Knebel, and D. Ritter, "An improved *in vitro* model for testing the pulmonary toxicity of complex mixtures such as cigarette smoke," *Experimental and Toxicologic Pathology*, vol. 55, no. 1, pp. 51–57, 2003.

[3] J. Chi-Jen Lin, R. Jean-Phillippe, J. Verreault et al., "An *ex vivo* approach to the differential parenchymal responses induced by cigarette whole smoke and its vapor phase," *Toxicology*, vol. 293, no. 1–3, pp. 125–131, 2012.

[4] Y. Fukano, M. Ogura, K. Eguchi, M. Shibagaki, and M. Suzuki, "Modified procedure of a direct *in vitro* exposure system for mammalian cells to whole cigarette smoke," *Experimental and Toxicologic Pathology*, vol. 55, no. 5, pp. 317–323, 2004.

[5] N. Kaur, M. Lacasse, J. P. Roy et al., "Evaluation of precision and accuracy of the Borgwaldt RM20S® smoking machine designed for *in vitro* exposure," *Inhalation Toxicology*, vol. 22, no. 14, pp. 1174–1183, 2010.

[6] H. Maunders, S. Patwardhan, J. Phillips, A. Clack, and A. Richter, "Human bronchial epithelial cell transcriptome: gene expression changes following acute exposure to whole cigarette smoke *in vitro*," *American Journal of Physiology*, vol. 292, no. 5, pp. L1248–L1256, 2007.

[7] J. Phillips, B. Kluss, A. Richter, and E. D. Massey, "Exposure of bronchial epithelial cells to whole cigarette smoke: assessment of cellular responses," *ATLA Alternatives to Laboratory Animals*, vol. 33, no. 3, pp. 239–248, 2005.

[8] M. J. Scian, M. J. Oldham, D. B. Kane, J. S. Edmiston, and W. J. McKinney, "Characterization of a whole smoke *in vitro* exposure system (Burghart Mimic Smoker-01)," *Inhalation Toxicology*, vol. 21, no. 3, pp. 234–243, 2009.

[9] D. Thorne, J. Wilson, T. S. Kumaravel, E. D. Massey, and M. McEwan, "Measurement of oxidative DNA damage induced by mainstream cigarette smoke in cultured NCI-H292 human pulmonary carcinoma cells," *Mutation Research*, vol. 673, no. 1, pp. 3–8, 2009.

[10] W. Zhang, S. Case, R. P. Bowler, R. J. Martin, D. I. Jiang, and H. W. Chu, "Cigarette smoke modulates PGE2 and host defence against Moraxella catarrhalis infection in human airway epithelial cells," *Respirology*, vol. 16, no. 3, pp. 508–516, 2011.

[11] C. Beisswenger, J. Platz, C. Seifart, C. Vogelmeier, and R. Bals, "Exposure of differentiated airway epithelial cells to volatile smoke *in vitro*," *Respiration*, vol. 71, no. 4, pp. 402–409, 2004.

[12] J. St-Laurent, L. I. Proulx, L. P. Boulet, and E. Bissonnette, "Comparison of two *in vitro* models of cigarette smoke exposure," *Inhalation Toxicology*, vol. 21, no. 13, pp. 1148–1153, 2009.

[13] A. Gualerzi, M. Sciarabba, G. Tartaglia, C. Sforza, and E. Donetti, "Acute effects of cigarette smoke on three-dimensional cultures of normal human oral mucosa," *Inhalation Toxicology*, vol. 24, pp. 382–389, 2012.

[14] T. A. Perfetti and A. Rodgman, "The complexity of tobacco and tobacco smoke," *Beitrage zur Tabakforschung International*, vol. 24, no. 5, pp. 215–232, 2011.

[15] J. Adamson, S. Hughes, D. Azzopardi, J. McAughey, and M. Gaca, "Real-time assessment of cigarette smoke particle deposition *in vitro*," *Chemistry Central Journal*, vol. 6, article 98, 2012.

[16] H. R. Paur, F. R. Cassee, J. Teeguarden et al., "*In-vitro* cell exposure studies for the assessment of nanoparticle toxicity in the lung-A dialog between aerosol science and biology," *Journal of Aerosol Science*, vol. 42, no. 10, pp. 668–692, 2011.

[17] J. G. Teeguarden, P. M. Hinderliter, G. Orr, B. D. Thrall, and J. G. Pounds, "Particokinetics *in vitro*: dosimetry considerations for *in vitro* nanoparticle toxicity assessments," *Toxicological Sciences*, vol. 95, no. 2, pp. 300–312, 2007.

[18] A. K. Armitage, M. Dixon, B. E. Frost, D. C. Mariner, and N. M. Sinclair, "The effect of inhalation volume and breath-hold duration on the retention of nicotine and solanesol in the human respiratory tract and on subsequent plasma nicotine concentrations during cigarette smoking," *Beiträge zur Tabakforschung International*, vol. 21, pp. 240–249, 2004.

[19] S. Mülhopt, S. Diabaté, T. Krebs, C. Weiss, and H. R. Paur, "Lung toxicity determination by *in vitro* exposure at the air liquid interface with an integrated online dose measurement," *Journal of Physics: Conference Series*, vol. 170, Article ID 012008, 2009.

[20] A. L. Smith and H. M. Shirazi, "Principles of quartz crystal microbalance/heat conduction calorimetry: measurement of the sorption enthalpy of hydrogen in palladium," *Thermochimica Acta*, vol. 432, no. 2, pp. 202–211, 2005.

[21] A. Yuwono and P. Schulze Lammers, "Odour pollution in the environment and the detection instrumentation," *Agricultural Engineering International*, vol. 6, 2004.

[22] G. Saubrey, "Verwendung von Schwingquarzen zur Wagung dunner Schichten und zur Mikrowagung," *Zeitschrift für Physik*, vol. 155, pp. 206–222, 1959.

[23] M. D. Johnson, J. Schilz, M. V. Djordjevic, J. R. Rice, and P. G. Shields, "Evaluation of *in vitro* assays for assessing the toxicity of cigarette smoke and smokeless tobacco," *Cancer Epidemiology Biomarkers and Prevention*, vol. 18, no. 12, pp. 3263–3304, 2009.

[24] A. Rodgman and T. A. Perfetti, *The Chemical Components of Tobacco and Tobacco Smoke*, CRC Press, Taylor & Francis Group, 2009.

[25] N. E. Klepeis, W. R. Ott, and P. Switzer, "Real-time measurement of outdoor tobacco smoke particles," *Journal of the Air and Waste Management Association*, vol. 57, no. 5, pp. 522–534, 2007.

[26] E. Uttenthaler, M. Schräml, J. Mandel, and S. Drost, "Ultrasensitive quartz crystal microbalance sensors for detection of M13-Phages in liquids," *Biosensors and Bioelectronics*, vol. 16, no. 9–12, pp. 735–743, 2001.

[27] H. C. Yeh, R. S. Turner, R. K. Jones, B. A. Muggenburg, D. L. Lundgren, and J. P. Smith, "Characterization of aerosols produced during surgical procedures in hospitals," *Aerosol Science and Technology*, vol. 22, no. 2, pp. 151–161, 1995.

[28] G. A. Lenz, E. Karg, B. Lentner et al., "A dose-controlled system for air-liquid interface cell exposure and application to zinc oxide nanoparticles," *Particle and Fibre Toxicology*, vol. 6, article 32, 2009.

[29] L. Müller, M. Gasser, D. O'Raemy et al., "Realistic exposure methods for investigating the interaction of nanoparticles with the lung at the air-liquid interface *in vitro*," *Insciences Journal*, vol. 1, no. 1, pp. 30–64, 2011.

[30] S. Bakand and A. Hayes, "Troubleshooting methods for toxicity testing of airborne chemicals *in vitro*," *Journal of Pharmacological and Toxicological Methods*, vol. 61, no. 2, pp. 76–85, 2010.

[31] J. J. McAughey, C. J. McGrath, and C. J. Dickens, "Particle metrics for mainstream tobacco smoke: implications for dose," *Journal of Aerosol Medicine & Pulmonary Drug Delivery*, vol. 22, no. 2, pp. 179–180, 2009.

Hindawi Publishing Corporation
BioMed Research International
Volume 2013, Article ID 328934, 11 pages
http://dx.doi.org/10.1155/2013/328934

Research Article

Toxicity of Silver Nanoparticles at the Air-Liquid Interface

Amara L. Holder and Linsey C. Marr

Department of Civil and Environmental Engineering, Virginia Tech, 411 Durham Hall (0246), Blacksburg, VA 24061, USA

Correspondence should be addressed to Linsey C. Marr; lmarr@vt.edu

Received 8 August 2012; Revised 10 October 2012; Accepted 14 November 2012

Academic Editor: Ernesto Alfaro-Moreno

Silver nanoparticles are one of the most prevalent nanomaterials in consumer products. Some of these products are likely to be aerosolized, making silver nanoparticles a high priority for inhalation toxicity assessment. To study the inhalation toxicity of silver nanoparticles, we have exposed cultured lung cells to them at the air-liquid interface. Cells were exposed to suspensions of silver or nickel oxide (positive control) nanoparticles at concentrations of 2.6, 6.6, and 13.2 μg cm^{-2} (volume concentrations of 10, 25, and 50 μg ml^{-1}) and to 0.7 μg cm^{-2} silver or 2.1 μg cm^{-2} nickel oxide aerosol at the air-liquid interface. Unlike a number of *in vitro* studies employing suspensions of silver nanoparticles, which have shown strong toxic effects, both suspensions and aerosolized nanoparticles caused negligible cytotoxicity and only a mild inflammatory response, in agreement with animal exposures. Additionally, we have developed a novel method using a differential mobility analyzer to select aerosolized nanoparticles of a single diameter to assess the size-dependent toxicity of silver nanoparticles.

1. Introduction

As the number of nanotechnology-based consumer products in the marketplace grows, so too does the potential for inhalation exposures to nanomaterials. Aerosolized nanoparticles have been shown to be released during many phases of production: particle synthesis [1–4], handling of dry powders [5] and liquid suspensions of nanoparticles [6], and machining composite materials containing nanoparticles [7]. Experimental studies have shown that engineered nanoparticles released by sprays and powders can potentially deposit in the respiratory system [8–11].

Due to their antibacterial qualities, silver nanoparticles are widely used in consumer products. Nanosilver is present in ~30% of the available products containing nanomaterials [12], and of these, ~14% have a high potential for inhalation exposure [13]. Inhalation exposures are likely to occur with personal hygiene and cleaning products that are intended to be sprayed. Because these consumer products release silver nanoparticles into the breathing zone of consumers, it is imperative to determine the potential hazards associated with inhaling silver nanoparticles.

A safe level for airborne silver nanoparticles has yet to be determined. Inhaled silver has been detected in the blood, liver, brain, and kidneys of exposed rats [14, 15]. Despite the wide distribution of silver throughout the body, no adverse effects were observed in hematology and histopathology assessments at low doses (~0.06 mg m^{-3}) [15]. Animals exposed to silver subacutely at a high dose, 3.3 mg m^{-3}, showed minimal pulmonary inflammation or cytotoxicity [16]. In contrast, animals exposed to a moderate dose, 0.5 mg m^{-3}, showed signs of chronic inflammation in the lungs and abnormalities in the liver [17, 18]. *In vitro* studies with silver nanoparticles have shown stronger effects, with many different cell lines showing reduced viability or oxidative stress response at doses ranging from the order of 1 μg mL^{-1} to 100 μg mL^{-1} [19–21]. Cell studies have also shown a size-dependent effect; the smallest particles (~5–15 nm) required a lower mass dose to cause decreased viability and greater oxidative stress [22–24].

There are several possible explanations for the variation among *in vitro* studies and the differences between the *in vitro* and inhalation studies. Firstly, the properties of the silver nanoparticles used in each study likely differed. The inhalation studies were all performed with metallic silver nanoparticles (10–20 nm) condensed from silver vapor generated from either a spark discharge apparatus [14] or

a furnace [25]. Alternatively, all of the *in vitro* studies were performed with silver nanoparticles either synthesized in solution or purchased in powder form, some of which had coatings, and resuspended in aqueous media. Secondly, the exposure route may have affected toxicity. Silver nanoparticles in cell culture media may aggregate into larger particles, obscuring the effects of the nanoparticles, or over time may release silver ions which can also cause a toxic effect apart from that of the nanoparticles [26, 27].

One way to bridge the gap between animal inhalation studies and *in vitro* studies is to expose cells at the air-liquid interface (ALI) [28]. In this method, cells are exposed to air, and aerosolized particles are then deposited directly onto the cell surface. For *in vitro* studies intended to probe particle toxicity associated with inhalation exposure, this approach is thought to be more physiologically realistic compared to exposure in a liquid suspension. This technique has been used to investigate tobacco smoke [29], diesel exhaust [30, 31], smoke from building material combustion [32], flame-generated cerium oxide nanoparticles [33], metal salt nanoparticles [34], and magnetic nanoparticles [35].

Inhalation exposures of engineered nanoparticles have been identified as posing a relatively high risk across the spectrum of potential health and environmental impacts of nanotechnology [36, 37]. An improved understanding of the toxicity of silver nanoparticles is needed because of their widespread use in commercial products, potential for release into the air [12, 13], and evidence of adverse effects in animal inhalation studies [17, 18]. The objective of this work is to evaluate the toxicity of commercially available aerosolized silver nanoparticles on human alveolar epithelial cells exposed at the ALI. Additionally, a novel approach is used to expose cells to particles within a narrow range of diameters, allowing for the first ever measurement of size-dependent toxicity free of the effects of aggregation.

2. Methods

2.1. Exposure Chamber Design and Characterization. The exposure chamber consisted of an electrostatic precipitator (ESP) and collagen-coated Transwells (Corning, 12 mm inserts, 0.4 μm pore size, 1.12 cm^2 growth surface), which contained the cells. The objectives of the chamber design were to (1) direct particles to the cell surface using an electrostatic field, (2) direct air flow across the top of the Transwells rather than directly at the cell surface, and (3) allow for multiple wells to be exposed at once. A schematic of the chamber is shown in Figure 1.

The chamber is constructed of two aluminum plates (15.2 cm in diameter, 6.4 cm thick) forming the top and bottom surfaces and an acrylic pipe (14.6 cm in diameter, 3.5 cm in height) forming the cylindrical wall. Four equally spaced inlets around the acrylic cylinder allow four wells to be exposed simultaneously. The inlet air flows over the Transwells and exits through an outlet in the center of the top plate. An electric field is generated in the chamber by connecting the lower plate to a negative high-voltage DC supply (EMCO, model 4120N) and the upper plate to ground. The clear acrylic wall insulates the ground electrode from the high-voltage electrode and also allows visualization of the wells during an exposure. The Transwells are placed upside down, and cells are grown on what is now the top side of the Teflon membrane (typically the bottom side), in order to minimize the vertical distance that particles must travel before depositing on the cell surface. This orientation maximizes deposition efficiency.

Particle deposition on the Teflon membrane (i.e., the Transwell cell culture surface) was measured with a fluorescein aerosol of a single diameter. The aerosol generation and single-diameter exposure are described below. A foil substrate was placed on the membrane to collect deposited fluorescein particles. Fluorescein was extracted with 0.5 mL of nanopure water, and fluorescence was measured on a plate reader (Molecular Devices, SpectraMax M2). Approximately 100% of the deposited fluorescein can be recovered with this method. The deposition efficiency was calculated as the percentage of mass depositing on the Transwell relative to the total mass entering the inlet, which was derived from measurements of particle number concentration by a condensation particle counter (CPC, TSI model 3025A). The deposition efficiency for each particle diameter (50, 75, and 100 nm) was measured in three wells in three separate experiments, except for 50 nm, which was measured in four separate experiments. In exposure experiments, the dose of nanoparticles depositing on the cells was calculated by applying the deposition efficiency to the inlet aerosol concentration. Although the nanoparticles tested have higher densities than the fluorescein particles, the deposition efficiencies are not affected. Particle motion in the vertical direction is dominated by the balance between the electrostatic force and the drag force; the inertia of the particle is negligible compared to these two forces.

2.2. Aerosol Generation and Characterization. Silver (30–50 nm coated with polyvinyl pyrrolidone, PVP 0.2% wt) and nickel oxide (10–20 nm), as a positive control, nanoparticles were purchased from a commercial supplier (NanoAmor, Houston, TX, USA). Nanoparticle stock suspensions were prepared by dispersing the particles in sterile nanopure water with a probe sonicator (Misonix, 3000) at a concentration of 0.5 mg mL^{-1}. Suspensions were sonicated on ice at approximately 50 W for 5 min alternating with a 5 min rest on ice. The process was repeated three times to optimize between maximizing breakup of the aggregates and minimizing volume loss to evaporation. The resulting size distribution in suspension was measured by dynamic light scattering (DLS, Malvern Zetasizer Nano). A drop of the suspension was dried on a transmission electron microscope (TEM) grid, and samples were then analyzed with a TEM (Philips EM420). Elemental analysis was performed with a scanning electron microscope (FEI Quanta 600 FEG) equipped with an energy dispersive X-ray spectrometer (EDX, Bruker Quantax 400).

Aerosols were generated with a constant output atomizer (TSI, model 3076), which was cleaned with aqua regia between runs. The nanoparticle aerosols were dried with a

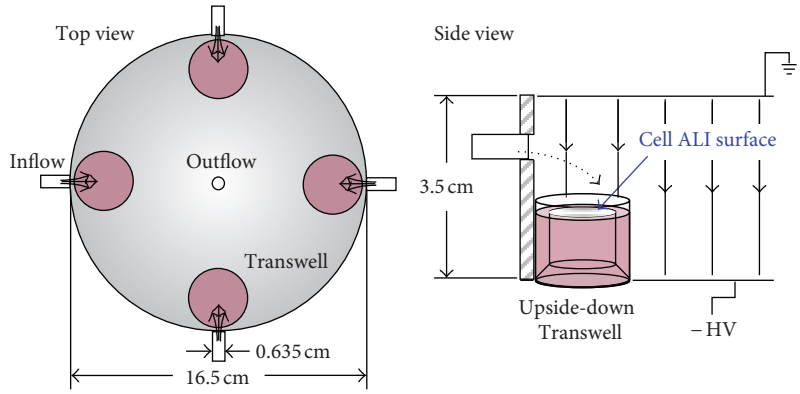

FIGURE 1: Schematic of the electrostatic precipitator exposure chamber. Aerosol flow entered through four inlets spaced at 90 degrees around the chamber wall and exited through an outlet on the upper plate. Cells were grown on upside-down Transwells that were placed immediately in front of an aerosol inlet.

diffusion dryer, charge neutralized with a Kr85 source (TSI, model 3012), and mixed with CO_2 to a concentration of 5%. The size distribution was measured with a scanning mobility particle sizer consisting of a differential mobility analyzer (TSI, model 3081) and the CPC. Aerosol samples for electron microscopy were collected by placing a TEM grid on a Transwell inside the ESP.

2.3. Cell Culture and Assays. All experiments were performed with a human alveolar cell line (A549, Sigma ECACC). This cell line has frequently been used to assess the toxicity of nanoparticle suspensions because it is representative of Type II pneumocytes and is a model for the alveolar epithelium [38, 39]. This region of the lung is particularly susceptible to the effects of nanoparticles because it has the largest deposition fraction for particles in the 10–100 nm size range and does not have the protective mucus lining found in the nasal and bronchial regions [40]. Cells were grown in F12 medium using Kaighn's modification (F12K, Invitrogen) with 10% fetal bovine serum (FBS, Invitrogen) and 1% antibiotic/antimycotic (Invitrogen). Nickel oxide nanoparticles were used as a positive control as they have previously been shown to generate more reactive oxygen species compared to other nanoparticles and cause a cytotoxic response in the A549 cell line [38].

Measurements of cellular response were made with several assays commonly used to assess response from nanoparticles [24, 38, 41]. Cytotoxicity was assessed with a lactate dehydrogenase (LDH) assay (kit from Sigma) and methylthiazol tetrazolium (MTT) assay (Sigma). Leakage of the LDH protein is measured as an indicator of a loss of membrane integrity. The exposure medium was collected after nanoparticle exposure and centrifuged for 10 min at 10,000 rpm to remove the nanoparticles from the medium. The extracellular LDH concentration in the supernatant was measured following the manufacturer's protocol. The metabolic activity of the cells was measured with an MTT assay. After the postexposure incubation period, cells were incubated another 1.5 hr with MTT (1 mM) in F12K medium. After incubation, the medium was aspirated, the formazan was solubilized with dimethyl sulfoxide, and the absorbance at 540 nm was measured on a plate reader (SpectraMax M2). A proinflammatory response was assessed by measuring the secretion of the pro-inflammatory cytokine interleukin 8 (IL-8) with an ELISA assay (kit from Invitrogen). IL-8 secretion is routinely measured to assess inflammatory response to aerosols [41]. The exposure medium was collected and centrifuged for 10 min at 10,000 rpm to remove the nanoparticles. The supernatant was kept frozen at −8°C until the assay was performed according to manufacturer's instructions.

2.4. ALI Exposure. Cells were plated on collagen-coated Transwell inserts at a density of $10^5\,\#\,cm^{-2}$ following a protocol modified from Gohla et al. [42]. Briefly, inserts were turned upside down, and 0.15 mL of cell suspension was placed on the bottom of the insert. The insert was placed inside an incubator at 37°C with 5% CO_2 for 3 hr while the cells attached to the Teflon membrane. The excess medium was removed, and the inserts were placed with the right side up in a 12-well plate and grown submerged (1.0 mL medium in the bottom chamber, 0.5 mL medium in the upper chamber) for two days before the exposure.

In preparation for an ALI exposure, the Transwell inserts were placed upside down inside sterile glass wells (2.6 cm in diameter, 2.2 cm deep), 8 mL of medium was added to the well, and 0.1 mL of medium was placed on top of the insert to prevent the insert from drying out. The glass wells and inserts were then placed inside the chamber for the duration of the aerosol exposure (i.e., dosing period). A second group of wells was placed in an identical chamber to serve as the control group. Each chamber was wiped down with ethanol before the exposure to maintain sterility.

Two ALI exposure scenarios were used in this study: whole aerosol (polydisperse) exposure and single-diameter (monodisperse) exposure. The whole aerosol was drawn into the ESP chamber with the voltage set at −2.4 kV. In this arrangement, a neutral charge distribution with both positive and negative charges was established by passing the aerosol through the Kr85 source; only the positively charged particles

deposited on the exposed wells. For the single-diameter exposure, the nanoparticle aerosol was first routed through the differential mobility analyzer to select positively charged particles of a single diameter. This monodisperse aerosol was then drawn into the exposure chamber (kept at −2.4 kV), where the particles deposited on the wells. For both exposure scenarios, a control experiment with no particles, attained by placing a filter (Pall, Fiberfilm T60A20) upstream of the chamber, was conducted simultaneously.

The cells were dosed at the ALI for 2 hr with the whole aerosol or 3 hr with a single-diameter aerosol; the extra hour was intended to increase the mass deposited. After being dosed, the inserts were returned to a 12-well plate, where they were incubated submerged in 1.0 mL of F12K media with 10% FBS at 37°C with 5% CO_2 for 24 hr. The media was then collected to measure LDH and IL-8 concentrations, and the MTT assay was begun. Each ALI exposure condition was done once on triplicate wells.

2.5. Suspension Exposure. For comparison with the ALI technique, cells were also exposed to nanoparticles in liquid suspensions. Cells were plated in 12-well plates at a density of 10^5 # cm^{-2} and grown for two days before an exposure. Nanoparticle stock suspensions were generated the previous day in sterile nanopure water and diluted with F12K medium with 10% FBS to 10, 25, and 50 $\mu g\,mL^{-1}$ immediately before the exposure. We estimate that all particles in suspension deposited in approximately 5 hrs, which results in a deposited dose of 2.6, 6.6, and 13.2 $\mu g\,cm^{-2}$ on the cell layer. This dose range was selected to cover the expected ALI concentration and to be comparable to concentration ranges used in similar *in vitro* studies with silver nanoparticles [24, 43]. Cells were dosed with the nanoparticle suspension (1 mL per well) and kept in an incubator at 37°C with 5% CO_2 for 24 hr. As was done with the ALI exposures, a single dose (rather than repeated dosing) and the 24 hr incubation period were selected to be comparable to previous studies with silver nanoparticles [24, 43]. After the exposure, the medium was collected for the LDH assay and for IL-8 measurement, and the MTT assay was begun. Each suspension exposure condition was done once on triplicate wells.

2.6. Statistical Analysis. Results are presented as the median and the 25th and 75th percentiles. Errors were propagated through the calculated parameters using a bootstrap analysis. Significance was assessed between exposed and control wells using a Kruskal-Wallis test. Differences between conditions were deemed significant for P values less than 0.05.

3. Results

3.1. Particle Deposition. Fluorescein particle deposition on the Teflon membrane was measured for three diameters of particles (50, 75, and 100 nm), as shown in Table 1. The deposition efficiency was highest for the larger 100 and 75 nm diameter particles and dropped off for the 50 nm particles. Over time, charge buildup on the chamber wall tended to reduce the deposition efficiency for the smaller-diameter particles. To prevent this, we wiped down the chamber with nanopure water to remove charged particles that accumulated on the chamber surface. Deposition efficiencies varied by <30% between runs and 15–25% between wells at different locations in the chamber in a single run.

Table 1: Deposition efficiency (median and 25th and 75th percentiles) of fluorescein particles on the cell culture surface. Efficiencies are averaged over three replicate measurements and the three chamber inlets used for the cell exposures, except for 50 nm diameter particles, which were measured in four replicate experiments.

Diameter (nm)	Deposition efficiency (%) Median (25th, 75th)
50	38.2 (32.5, 63.1)
75	63.3 (53.1, 74.9)
100	63.5 (52.7, 75.5)

3.2. Nanoparticle Aerosol. Atomizing the suspension of silver nanoparticles resulted in an aerosol that consisted of particles with a geometric mean diameter of 37 nm and a volume-weighted geometric mean diameter of 169 nm (Figure 2). Electron microscopy confirmed that the aerosol particles had the same physical characteristics as the silver nanoparticles in suspension. The particles were approximately spherical with diameters of ~50 nm and were composed of silver with a crystalline diffraction pattern.

A comparison between the volume-weighted size distribution of a silver nanoparticle suspension and aerosol is shown in Figure 2. The volume distribution in suspension was dominated by small particles and peaked at approximately 20 nm with a second mode at 68 nm. The larger mode from the suspension approximately corresponds to the aerosol distribution; an exact match is not expected due to different sizing methods. The smaller size mode was not apparent in the aerosol distribution. This mode was likely composed of PVP released from the particle surface during sonication, as no silver particles in this size range were observed under TEM. Similarly, Foldbjerg et al. [20] attributed a peak at 11 nm after sonication of the same NanoAmor PVP-coated silver nanoparticles to free particles composed of PVP.

3.3. Cellular Response to Nanoparticles in Suspension. Exposure to suspensions of nanoparticles was used to gauge the range of responses of this cell line to the silver and nickel oxide nanoparticles. Results of three different assays are presented in Table 2 as a percent of the control group for comparison of different types of exposure. Silver nanoparticle suspensions caused a mild cytotoxic and proinflammatory response. Cell metabolism as measured by the MTT assay decreased with increasing dose of silver nanoparticles. The LDH release in cells exposed to silver nanoparticle suspensions was slightly less than the control value, suggesting that the silver nanoparticles may have interfered with the assay. The nickel oxide suspensions, used as a positive control, also showed a mild dose-dependent cytotoxic response.

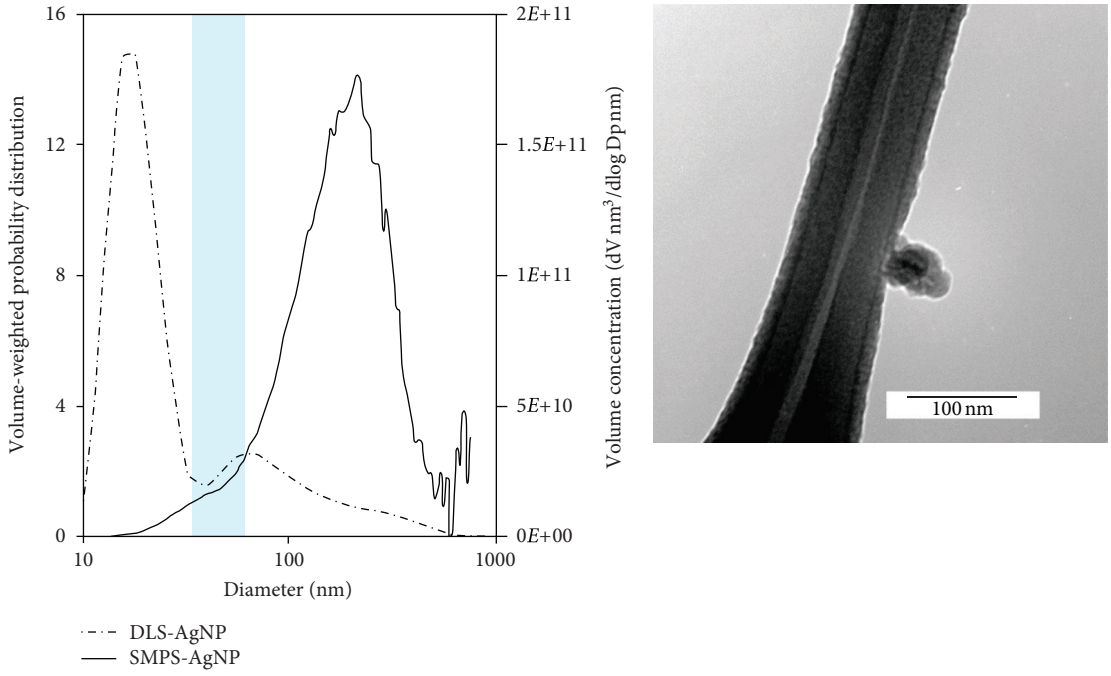

Figure 2: (a) Volume-weighted size distributions of silver nanoparticles in suspension (DLS) and as aerosols (SMPS) (left). The DLS measurement corresponds to the left axis, and the SMPS measurement corresponds to the right axis. The shaded area is the manufacturer's specified range of particle diameters. (b) Transmission electron microscope image of a ~50 nm silver nanoparticle on a lacey carbon grid (right).

However, the nickel oxide nanoparticles did not cause a pro-inflammatory response and were actually shown to decrease the release of IL-8 or cause an anti-inflammatory response.

Particles may interfere with cellular assays and cause false toxic or false nontoxic responses to be measured [44]. To check for possible interference of nanoparticles with assay results, we also performed each assay with a known quantity of nanoparticles but without cells. After the incubation period, the nanoparticles were removed by centrifugation (10 min at 10,000 rpm). Neither nanoparticle type affected the MTT assay. However, the silver nanoparticles were found to inactivate or bind LDH protein and thus prevent its measurement; similarly, Han et al. [45] observed that silver nanoparticles in a carbon matrix inactivated LDH protein in a dose-dependent manner. Silver nanoparticles at a concentration of 10 μg mL^{-1} reduced the measurable LDH to 42% of the original concentration, and higher silver nanoparticle concentrations resulted in a greater percentage of the original LDH being bound. Because of this dose-dependent removal, the LDH assay for cells exposed to silver nanoparticles was considered suspect, although at the low doses applied at the ALI the LDH assay may not be strongly affected by the silver nanoparticles. The nickel oxide nanoparticles did not bind the LDH protein at any concentration tested. Similar measurements with IL-8 were performed, and neither the silver nor the nickel oxide nanoparticles bound sizable amounts of the IL-8 molecule. Only about 8% of the IL-8 concentration was adsorbed at the highest nanoparticle concentration of 100 μg mL^{-1}.

The dose at the ALI was slightly lower than the lowest dose in suspension when normalized by the cell growth area. The silver aerosol caused a mild cytotoxic effect observed by increased LDH release. Conversely the metabolic rate (MTT) for cells exposed to silver nanoparticles was increased. The silver aerosol also resulted in increased IL-8 secretion. In all cases, the interquartile range was relatively high and none of the observed effects were statistically significant compared to the control. In contrast, the nickel oxide aerosol caused a strong cytotoxic effect with reduction of cellular metabolism (MTT) and membrane integrity (LDH). Similar to the suspension exposure, the aerosolized nickel oxide nanoparticles caused a decrease in IL-8 secretion compared to the control group.

3.4. Cellular Response by Size. Cells were exposed to particles of a single-diameter aerosol for 3 hr to achieve doses in the range of 5 to 26 ng cm^{-2} (Table 3). The number dose was calculated from the deposition efficiency measured for each particle diameter, and the surface area and volume dose were calculated from the number dose assuming spherical particle geometry. The dose for each size nanoparticle was different due to the nonuniform size distribution (Figure 2) and the particle charging efficiency varied with size before selection by the DMA. In terms of particle number, the dose was greatest for the 50 nm particles, followed by the 75 nm particles, and then the 100 nm particles. In terms of mass and surface area, doses were greatest for the 100 nm particles and decreased with decreasing diameter. Despite the

Table 2: Cellular response to nanoparticles dosed in suspension and at the ALI (median and 25th and 75th percentiles of three replicate wells for each condition, except where noted). Doses are presented per unit cell growth area, and responses are presented as percent control (ALI control is filtered air) to compare across several different experiments.

Material	Exposure	Dose ($\mu g\,cm^{-2}$)	MTT (% control) Median (25th, 75th)	LDH leakage (% control) Median (25th, 75th)	IL-8 (% control) Median (25th, 75th)
Silver	Suspension	2.6	94 (86, 97)	97 (95, 99)[a]	96 (94, 100)
		6.6	88 (83, 94)	95 (94, 98)[a]	98 (96, 102)
		13.2	80 (77, 85)*	92 (91, 96)[a]	112 (105, 122)
	ALI	0.7 (0.6, 0.7)	110 (66, 185)	96 (91, 265)[a]	136 (19, 389)
Nickel oxide	Suspension	2.6	93 (80, 97)	101 (99, 103)	—
		6.6	88 (76, 91)*	105 (102, 106)	105 (77, 117)
		13.2	83 (79, 86)*	107 (106, 109)*	87 (58, 89)
	ALI	2.1 (1.8, 2.2)	32 (14,76)	180 (160,324)*	15 (14, 44)*

*Statistically significant at a P value of 0.05. [a]Values may be artificially low as silver nanoparticles were found to prevent the measurement of LDH protein.

Table 3: Number, surface area, and mass dose (median and 25th and 75th percentiles) of silver nanoparticles applied to cells as a function of diameter.

Diameter (nm)	Number ($\# \times 10^6\,cm^{-2}$) Median (25th, 75th)	Surface Area ($mm^2\,cm^{-2}$) Median (25th, 75th)	Mass ($ng\,cm^{-2}$) Median (25th, 75th)
50	7.6 (4.0, 8.7)	0.06 (0.03, 0.07)	5 (3, 6)
75	5.5 (4.7, 6.5)	0.10 (0.08, 0.12)	13 (11, 15)
100	4.7 (3.9, 5.5)	0.15 (0.12, 0.17)	26 (22, 30)

large variation in the number of 50 nm particles deposited, the mass was not greatly affected, as these particles have very little mass. The decreasing number dose and increasing mass and surface area dose with particle diameter provide an opportunity to investigate the most appropriate dose metric.

To facilitate visualization of the results in Figure 3, the response for single-diameter exposures is compared to the control, and then the difference from 100% is calculated such that an adverse response is positive (i.e., 100%-percent control for MTT and percent control-100% for IL-8). The response is then normalized by number, surface area, and mass dose to facilitate comparison between exposures to particles of different diameters with different dose metrics. Silver nanoparticles of all diameters tested caused a cytotoxic response, as measured by the MTT assay. The response normalized by number dose was greatest for the 75 nm particles and least for the 50 nm and 100 nm diameter particles. In other words, the same number of 75 nm diameter particles caused greater response than either the 50 nm or 100 nm diameter particles. The 100 nm diameter particles caused the lowest response for the mass and surface area dose metric, suggesting that there may be a size threshold for the response to silver nanoparticles. None of the particles caused an inflammatory response that was statistically different from that of the control group.

4. Discussion

4.1. Toxicity of Silver Nanoparticles. Characterizing the hazard associated with inhaling silver nanoparticles is urgently needed because of their widespread prevalence in consumer products and the high likelihood of their aerosolization during product use. The American Conference of Governmental Industrial Hygienists (ACGIH) has set a threshold limit value of $0.01\,mg\,m^{-3}$ for soluble silver and $0.1\,mg\,m^{-3}$ for insoluble silver. These values were determined from epidemiology studies on workers exposed to silver dust, where few adverse health effects were observed apart from the development of argyria [46]. Likewise, rat inhalation exposure studies found no significant effects below $0.1\,mg\,m^{-3}$ [15]. In the current study, silver nanoparticles in suspensions showed minimal cytotoxicity and only at a high dose of $50\,\mu g\,mL^{-1}$ ($13.2\,\mu g\,cm^{-2}$). Additionally, when exposed at the ALI, cells exhibited no significant toxicity to any dose (from 0.005 to $0.7\,\mu g\,cm^{-2}$) of silver nanoparticles of any size. These doses are well above the maximum estimated alveolar dose of $0.001\,\mu g\,cm^{-2}$ for a worker breathing at a rate of $1\,m^3\,hr^{-1}$ at the ACGIH recommended threshold limit value for silver of $0.1\,mg\,m^{-3}$, assuming a fraction depositing in the alveolar region of 0.3 and an alveolar surface area of $75\,m^2$. The ALI dose is also well above the estimated dose from exposure to consumer products containing silver nanoparticles. Quadros and Marr [8] estimated a dose of 75 ng of silver from the worst case exposure to consumer products containing nanomaterials, resulting in an alveolar dose of $0.015\,pg\,cm^{-2}$, seven orders of magnitude higher than the dose at the ALI. Our results suggest, in agreement with the ACGIH threshold limit value, that a onetime exposure to silver nanoparticles from consumer products or in the workplace will not cause adverse effects. We recommend future studies with the ALI

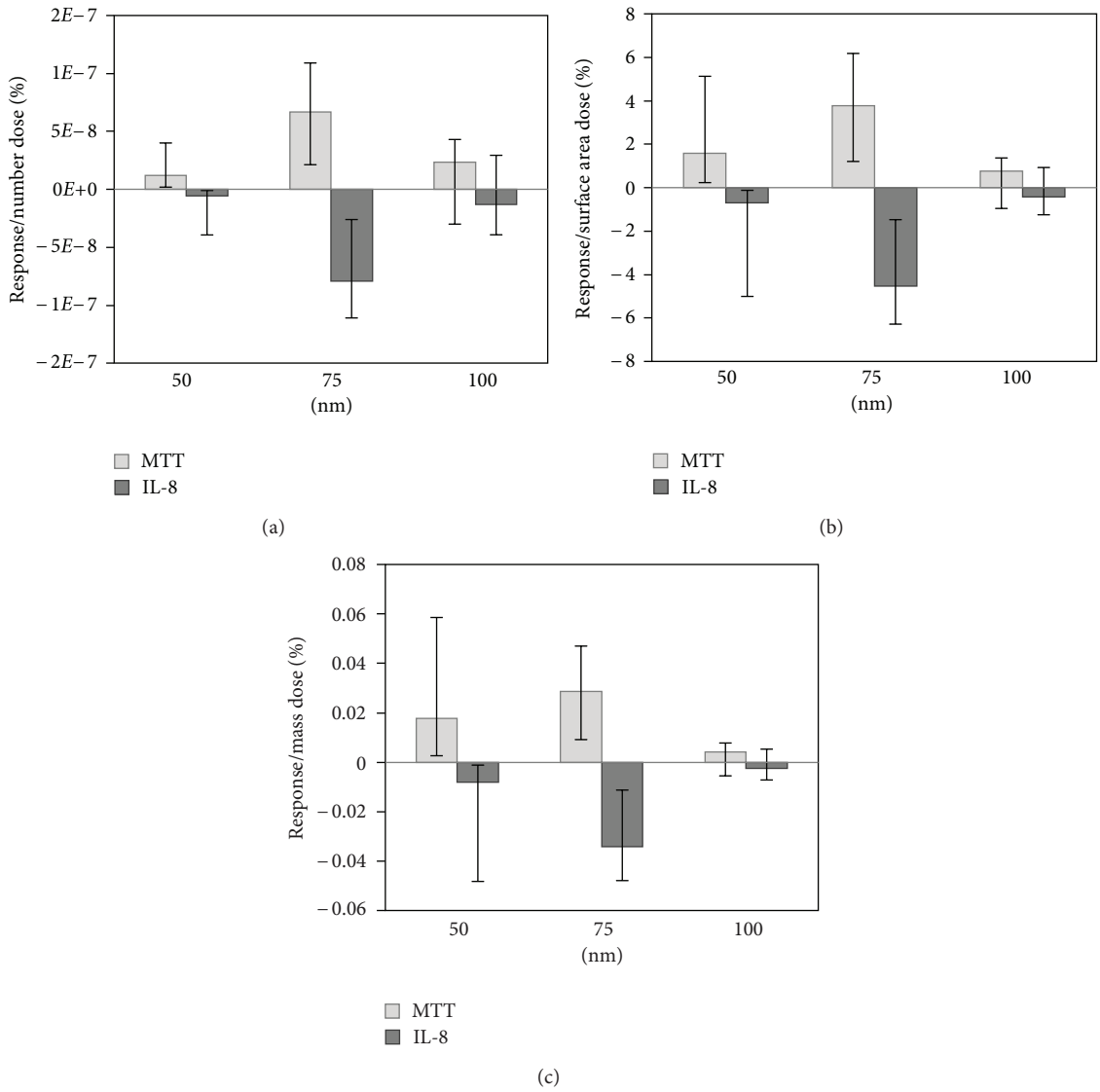

Figure 3: Percent response normalized by (a) number, (b) surface area, and (c) mass dose. Percent response for MTT is calculated as 100%-percent control and for IL-8 as percent control-100% so that an adverse response from each assay is plotted as a positive value and a beneficial response is plotted as a negative value, with zero being no change from the control value. Median values are presented with error bars representing the 25th and 75th percentiles of three replicates for the control and each diameter exposure, except for the 50 nm exposure, for which only two valid replicates were obtained.

system incorporating repeated exposures, which are more likely to occur than the single acute dosing that we have used here and which are common in conventional toxicity testing.

These results fall within the range of values reported in the literature for *in vitro* assessments. Measurements of cytotoxicity of silver nanoparticles in mammalian cells have shown large variability, with concentrations causing 50% viability reductions (lethal dose 50, LD_{50}) ranging from 0.8 $\mu g\,mL^{-1}$ in media [47] to 1 $mg\,mL^{-1}$ [48]. Some of the variabilities in these results may be due to the different susceptibility of different cell types to silver nanoparticles. Schrand et al. [19] observed varying degrees of cytotoxicity from the same hydrocarbon-coated silver nanoparticles in different cell lines. Additionally, the different types of particles may explain some of the variabilities. For example, a suspension of water-soluble 10 nm silver nanoparticles [49] exhibited toxicity in the HepG2 cell line at a concentration of about 3.6 $\mu g\,mL^{-1}$ as opposed to 10 nm polyethylenimine-coated silver nanoparticles which caused toxicity in HepG2 cells at a concentration of 1 $mg\,mL^{-1}$ [48]. One conclusion is that the particular particle type used in this study, 30–50 nm PVP-coated silver nanoparticles manufactured by NanoAmor (Houston, TX, USA), is relatively nontoxic to A549 cells at the ALI and only mildly toxic at higher doses in suspension. The size-dependent effects were not conclusive, as no toxic or inflammatory response was statistically significant compared to the control group. However, the data suggested that the 50 nm and 75 nm particles may be more toxic than the

100 nm particles despite having much lower mass doses than the larger particles. A recent study also found size-dependent results; suspensions of 5 nm PVP-coated silver nanoparticles were toxic at a concentration of 6.25 $\mu g\,mL^{-1}$ while 100 nm particles showed no toxicity even at the highest dose of 25 $\mu g\,mL^{-1}$ [50]. Further study is needed to confirm whether a size-dependent effect exists for silver nanoparticles.

4.2. ALI Exposure for Nanotoxicity Studies. Although the ALI exposure method is still in the early developmental stages, it is much less expensive and easier to perform than animal testing, while allowing for a controlled exposure with relatively well-characterized nanoparticle doses. While the ALI exposure is more difficult to carry out than conventional *in vitro* suspension exposures because of the added complexity of generating an aerosol and measuring particle deposition, it allows for an *in vitro* exposure to aerosolized particles in their native state and a more accurate determination of true cell dose. True cell dose for suspension exposures is impacted by particle aggregation in the culture medium and dependent upon particle transport through the medium to the cell surface. Following the analysis of Teeguarden et al. [51], assuming spherical monodisperse particles (~100 nm, from DLS measurement), we estimate that the majority of the particles have deposited on the cell surface in ~5 hr. This deposition time is comparable to the ALI dosing period of 2-3 hr. Considering the similar dosing periods, the greater response at the ALI compared to suspension is likely due to different particle physical/chemical characteristics rather than to differences in the dosing period. Another potential artifact of suspension exposures is that the particles may interfere with cellular response assays. We found that the silver nanoparticles prevented measurement of the LDH leakage in a dose-dependent fashion. Because of this interference, we suggest that future studies with silver nanoparticles investigate different measures of cellular response, such as the tightness of the monolayer, which will not be susceptible to such particle interferences.

A major limitation to the ALI approach is achieving adequate mass or number of particles depositing on the cells. The approach used in this study, like several others reported in the literature [52–55], relies on an electric field to enhance the deposition efficiency of charged particles onto the cell layer. It is possible that the charge on the particles may affect toxicity as gold nanoparticles with differently charged ligands have been shown to exhibit charge-dependent effects [56]. However, it is unlikely that the one or two extra positive charges on the silver nanoparticles will have a measurable impact on the particle toxicity. Another drawback to our ALI exposure method is the large degree of variation in the measures from replicate wells. A part of this variation is due to variation in dose, that is, the well-to-well deposition efficiencies. Our system achieved greater deposition efficiencies than systems relying on gravitational and diffusional deposition (7% [57]) as well as other systems employing electrostatic deposition (2% [52], 15–30% [53–55]). Well-to-well differences in deposition were larger than desired but similar to those of other systems, which had standard deviations as high as 30% [52]. We expect that much of the variation is due to uncertainties in the dose measurement rather than actual variations of the amount deposited. The fluorescein aerosol was assumed to be constant in time, so fluctuations of up to 10% in the aerosol concentration stemming from instabilities in the aerosol generator and uncertainty in the CPC measurement added to the uncertainty of the calculated deposition efficiency. An additional factor contributing to the large variation among cellular responses was the difficulty of culturing and exposing cells on the upside-down Transwell. Cells were not always plated uniformly because the cell suspension did not always spread evenly across the Transwell bottom. Evidence of this could be seen in well-to-well variations of the filtered air control that were in some cases larger than the variation seen in the deposition efficiencies. However, using the Transwells in the upside-down orientation was necessary to avoid losses of nanoparticles to the Transwell walls and achieve a measurable deposition of nanoparticles. We expect that a considerable amount of the variation could be reduced if a modified Transwell or alternative culturing methods could be developed.

A novel aspect of this work was the ability to restrict exposure to nanoparticles of a single diameter. Additionally, with the ALI we were able to determine the particle number dose for each condition and to compare the results using different dose metrics. Although surface area has frequently been used as a metric to explain particle effects [36], number dose has not been adequately investigated as a dose metric perhaps because of the difficulty of determining the number dose with conventional suspension exposures. We were only able to achieve low mass doses with our system and were unable to detect a significant cellular response with the rather innocuous silver nanoparticles. We expect that larger doses could be achieved with our exposure system by using a unipolar charger to improve the charging efficiencies of nanoparticles [58] and using a coarser size selection method as opposed to a DMA, which selects a very narrow size range of the aerosol. Additionally, a different aerosolization method capable of generating higher concentrations of monodisperse nanoparticles, such as electrospray, might be considered [59].

5. Conclusions

This research has shown the ALI dosing method to be effective at delivering microgram quantities of nanoparticles to the cell surface within a few hours. Additionally, the ALI approach can be used to expose cells to nanoparticles of a single diameter, albeit at low doses. The silver nanoparticles used in this study caused minimal cytotoxicity and only a mild inflammatory response. These results are consistent with the minimal response observed in rat inhalation exposures at lower concentrations [15]. Indications of a size-dependent response were observed but were not conclusive. The ALI method shows great promise for investigating the size dependence of nanoparticle toxicity and should be developed further because of its physiologically relevant exposure technique. Future methodological development should focus on increasing the concentrations of particles of a single

diameter that can be delivered to the cell surface and reducing variability in the deposition efficiency.

Acknowledgments

The authors thank Joseph Freeman, Lee Wright, and Tea Andric for the use of their cell culturing facilities. They thank Steve Cox, Brett Farmer, Tom Wertalik, Julie Petruska, and Jody Smiley for their contribution to designing and building the electrostatic precipitator. They thank Bojeong Kim, John McIntosh, Stephen McCartney, Andrea Tiwari, Marina Eller Quadros, and Jennifer Benning for their assistance with the aerosolization and characterization of nanoparticles. This work was funded by the NSF Center for the Environmental Implications of Nanotechnology (EF-0830093) and the Virginia Tech Institute for Critical Technology and Applied Science.

References

[1] B. Yeganeh, C. M. Kull, M. S. Hull, and L. C. Marr, "Characterization of airborne particles during production of carbonaceous nanomaterials," *Environmental Science and Technology*, vol. 42, no. 12, pp. 4600–4606, 2008.

[2] M. Sahu and P. Biswas, "Size distributions of aerosols in an indoor environment with engineered nanoparticle synthesis reactors operating under different scenarios," *Journal of Nanoparticle Research*, vol. 12, no. 3, pp. 1055–1064, 2010.

[3] J. Park, B. K. Kwak, E. Bae et al., "Characterization of exposure to silver nanoparticles in a manufacturing facility," *Journal of Nanoparticle Research*, vol. 11, no. 7, pp. 1705–1712, 2009.

[4] J. Wang, C. Asbach, H. Fissan et al., "How can nanobiotechnology oversight advance science and industry: examples from environmental, health, and safety studies of nanoparticles (nano-EHS)," *Journal of Nanoparticle Research*, vol. 13, no. 4, pp. 1373–1387, 2011.

[5] S. J. Tsai, E. Ada, J. A. Isaacs, and M. J. Ellenbecker, "Airborne nanoparticle exposures associated with the manual handling of nanoalumina and nanosilver in fume hoods," *Journal of Nanoparticle Research*, vol. 11, no. 1, pp. 147–161, 2009.

[6] D. R. Johnson, M. M. Methner, A. J. Kennedy, and J. A. Steevens, "Potential for occupational exposure to engineered carbon-based nanomaterials in environmental laboratory studies," *Environmental Health Perspectives*, vol. 118, no. 1, pp. 49–54, 2010.

[7] S. J. Tsai, A. Ashter, E. Ada, J. L. Mead, C. F. Barry, and M. J. Ellenbecker, "Airborne nanoparticle release associated with the compounding of nanocomposites using nanoalumina as fillers," *Aerosol and Air Quality Research*, vol. 8, no. 2, pp. 160–177, 2008.

[8] M. E. Quadros and L. C. Marr, "Silver nanoparticles and total aerosols emitted by nanotechnology-related consumer spray products," *Environmental Science and Technology*, vol. 45, pp. 10713–10719, 2011.

[9] A. W. Nørgaard, K. A. Jensen, C. Janfelt, F. R. Lauritsen, P. A. Clausen, and P. Wolkoff, "Release of VOCs and particles during use of nanofilm spray products," *Environmental Science and Technology*, vol. 43, no. 20, pp. 7824–7830, 2009.

[10] Y. Nazarenko, H. Zhen, T. Han, P. U. Lioy, and G. Mainelis, "Potential for inhalation exposure to engineered nanoparticles from nanotechnology-based cosmetic powders," *Environmental Health Perspectives*, vol. 120, no. 6, pp. 885–892, 2012.

[11] H. Hagendorfer, C. Lorenz, R. Kaegi et al., "Size-fractionated characterization and quantification of nanoparticle release rates from a consumer spray product containing engineered nanoparticles," *Journal of Nanoparticle Research*, vol. 12, no. 7, pp. 2481–2494, 2010.

[12] S. W. P. Wijnhoven, W. J. G. M. Peijnenburg, C. A. Herberts et al., "Nano-silver - A review of available data and knowledge gaps in human and environmental risk assessment," *Nanotoxicology*, vol. 3, no. 2, pp. 109–138, 2009.

[13] M. E. Quadros and L. C. Marr, "Environmental and human health risks of aerosolized silver nanoparticles," *Journal of the Air and Waste Management Association*, vol. 60, no. 7, pp. 770–781, 2010.

[14] S. Takenaka, E. Karg, C. Roth et al., "Pulmonary and systemic distribution of inhaled ultrafine silver particles in rats," *Environmental Health Perspectives*, vol. 109, no. 4, pp. 547–551, 2001.

[15] J. H. Ji, J. H. Jung, S. S. Kim et al., "Twenty-eight-day inhalation toxicity study of silver nanoparticles in Sprague-Dawley rats," *Inhalation Toxicology*, vol. 19, no. 10, pp. 857–871, 2007.

[16] L. V. Stebounova, A. Adamcakova-Dodd, J. S. Kim et al., "Nanosilver induces minimal lung toxicity or inflammation in a subacute murine inhalation model," *Particle and Fibre Toxicology*, vol. 8, no. 1, article 5, 2011.

[17] J. H. Sung, J. H. Ji, J. D. Park et al., "Subchronic inhalation toxicity of silver nanoparticles," *Toxicological Sciences*, vol. 108, no. 2, pp. 452–461, 2009.

[18] J. H. Sung, J. H. Ji, J. U. Yoon et al., "Lung function changes in Sprague-Dawley rats after prolonged inhalation exposure to silver nanoparticles," *Inhalation Toxicology*, vol. 20, no. 6, pp. 567–574, 2008.

[19] A. M. Schrand, M. F. Rahman, S. M. Hussain, J. J. Schlager, D. A. Smith, and A. F. Syed, "Metal-based nanoparticles and their toxicity assessment," *Wiley Interdisciplinary Reviews*, vol. 2, no. 5, pp. 544–568, 2010.

[20] R. Foldbjerg, P. Olesen, M. Hougaard, D. A. Dang, H. J. Hoffmann, and H. Autrup, "PVP-coated silver nanoparticles and silver ions induce reactive oxygen species, apoptosis and necrosis in THP-1 monocytes," *Toxicology Letters*, vol. 190, no. 2, pp. 156–162, 2009.

[21] S. Arora, J. Jain, J. M. Rajwade, and K. M. Paknikar, "Cellular responses induced by silver nanoparticles: in vitro studies," *Toxicology Letters*, vol. 179, no. 2, pp. 93–100, 2008.

[22] J. Park, D. H. Lim, H. J. Lim et al., "Size dependent macrophage responses and toxicological effects of Ag nanoparticles," *Chemical Communications*, vol. 47, no. 15, pp. 4382–4384, 2011.

[23] W. Liu, Y. Wu, C. Wang et al., "Impact of silver nanoparticles on human cells: effect of particle size," *Nanotoxicology*, vol. 4, no. 3, pp. 319–330, 2010.

[24] C. Carlson, S. M. Hussein, A. M. Schrand et al., "Unique cellular interaction of silver nanoparticles: size-dependent generation of reactive oxygen species," *Journal of Physical Chemistry B*, vol. 112, no. 43, pp. 13608–13619, 2008.

[25] J. H. Ji, J. H. Jung, I. J. Yu, and S. S. Kim, "Long-term stability characteristics of metal nanoparticle generator using small ceramic heater for inhalation toxicity studies," *Inhalation Toxicology*, vol. 19, no. 9, pp. 745–751, 2007.

[26] C. N. Lok, C. M. Ho, R. Chen et al., "Silver nanoparticles: partial oxidation and antibacterial activities," *Journal of Biological Inorganic Chemistry*, vol. 12, no. 4, pp. 527–534, 2007.

[27] S. Kittler, C. Greulich, J. Diendorf, M. Köller, and M. Epple, "Toxicity of silver nanoparticles increases during storage because of slow dissolution under release of silver ions," *Chemistry of Materials*, vol. 22, no. 16, pp. 4548–4554, 2010.

[28] S. Bakand, A. Hayes, and F. Dechsakulthorn, "Nanoparticles: a review of particle toxicology following inhalation exposure," *Inhalation Toxicology*, vol. 24, no. 2, pp. 125–135, 2012.

[29] M. Aufderheide, J. W. Knebel, and D. Ritter, "An improved in vitro model for testing the pulmonary toxicity of complex mixtures such as cigarette smoke," *Experimental and Toxicologic Pathology*, vol. 55, no. 1, pp. 51–57, 2003.

[30] A. L. Holder, D. Lucas, R. Goth-Goldstein, and C. P. Koshland, "Inflammatory response of lung cells exposed to whole, filtered, and hydrocarbon denuded diesel exhaust," *Chemosphere*, vol. 70, no. 1, pp. 13–19, 2007.

[31] D. J. Cooney and A. J. Hickey, "Cellular response to the deposition of diesel exhaust particle aerosols onto human lung cells grown at the air-liquid interface by inertial impaction," *Toxicology in Vitro*, vol. 25, no. 8, pp. 1953–1965, 2011.

[32] F. Lestari, A. R. Green, G. Chattopadhyay, and A. J. Hayes, "An alternative method for fire smoke toxicity assessment using human lung cells," *Fire Safety Journal*, vol. 35, no. 6, pp. 411–429, 2011.

[33] B. Rothen-Rutishauser, R. N. Grass, F. Blank et al., "Direct combination of nanoparticle fabrication and exposure to lung cell cultures in a closed setup as a method to simulate accidental nanoparticle exposure of humans," *Environmental Science and Technology*, vol. 43, no. 7, pp. 2634–2640, 2009.

[34] M. D. Cheng, "Effects of nanophase materials (≤20 nm) on biological responses," *Journal of Environmental Science and Health A*, vol. 39, no. 10, pp. 2691–2705, 2004.

[35] O. Baber, M. Jang, D. Barber, and K. Powers, "Amorphous silica coatings on magnetic nanoparticles enhance stability and reduce toxicity to in vitro BEAS-2b cells," *Inhalation Toxicology*, vol. 23, no. 9, pp. 532–543, 2011.

[36] A. D. Maynard and E. D. Kuempel, "Airborne nanostructured particles and occupational health," *Journal of Nanoparticle Research*, vol. 7, no. 6, pp. 587–614, 2005.

[37] E. Bergamaschi, "Occupational exposure to nanomaterials: present knowledge and future development," *Nanotoxicology*, vol. 3, no. 3, pp. 194–201, 2009.

[38] S. Lu, R. Duffin, C. Poland et al., "Efficacy of simple short-term in vitro assays for predicting the potential of metal oxide nanoparticles to cause pulmonary inflammation," *Environmental Health Perspectives*, vol. 117, no. 2, pp. 241–247, 2009.

[39] A. Kroll, C. Dierker, C. Rommel et al., "Cytotoxicity screening of 23 engineered nanomaterials using a test matrix of ten cell lines and three different assays," *Particle and Fibre Toxicology*, vol. 8, no. 1, article 9, 2011.

[40] G. Oberdörster, E. Oberdörster, and J. Oberdörster, "Nanotoxicology: an emerging discipline evolving from studies of ultrafine particles," *Environmental Health Perspectives*, vol. 113, no. 7, pp. 823–839, 2005.

[41] J. G. Ayres, P. Borm, F. R. Cassee et al., "Evaluating the toxicity of airborne particulate matter and nanoparticles by measuring oxidative stress potential—a workshop report and consensus statement," *Inhalation Toxicology*, vol. 20, no. 1, pp. 75–99, 2008.

[42] A. Gohla, K. Eckert, and H. R. Maurer, "A rapid and sensitive fluorometric screening assay using YO-PRO-1 to quantify tumour cell invasion through Matrigel," *Clinical and Experimental Metastasis*, vol. 14, no. 5, pp. 451–458, 1996.

[43] S. G. Mukherjee, N. O'claonadh, A. Casey, and G. Chambers, "Comparative in vitro cytotoxicity study of silver nanoparticle on two mammalian cell lines," *Toxicology in Vitro*, vol. 26, no. 2, pp. 238–251, 2012.

[44] A. L. Holder, R. Goth-Goldstein, D. Lucas, and C. P. Koshland, "Particle-induced artifacts in the MTT and LDH viability assays," *Chemical Research in Toxicology*, vol. 25, no. 9, pp. 1885–1892, 2012.

[45] X. Han, R. Gelein, N. Corson et al., "Validation of an LDH assay for assessing nanoparticle toxicity," *Toxicology*, vol. 287, no. 1–3, pp. 99–104, 2011.

[46] P. L. Drake and K. J. Hazelwood, "Exposure-related health effects of silver and silver compounds: a review," *Annals of Occupational Hygiene*, vol. 49, no. 7, pp. 575–585, 2005.

[47] E. J. Park, J. Yi, Y. Kim, K. Choi, and K. Park, "Silver nanoparticles induce cytotoxicity by a Trojan-horse type mechanism," *Toxicology in Vitro*, vol. 24, no. 3, pp. 872–878, 2010.

[48] K. Kawata, M. Osawa, and S. Okabe, "In vitro toxicity of silver nanoparticles at noncytotoxic doses to HepG2 human hepatoma cells," *Environmental Science and Technology*, vol. 43, no. 15, pp. 6046–6051, 2009.

[49] S. Kim, J. E. Choi, J. Choi et al., "Oxidative stress-dependent toxicity of silver nanoparticles in human hepatoma cells," *Toxicology in Vitro*, vol. 23, no. 6, pp. 1076–1084, 2009.

[50] D. H. Lim, J. Jang, S. Kim, T. Kang, K. Lee, and I. H. Choi, "The effects of sub-lethal concentrations of silver nanoparticles on inflammatory and stress genes in human macrophages using cDNA microarray analysis," *Biomaterials*, vol. 33, no. 18, pp. 4690–4699, 2012.

[51] J. G. Teeguarden, P. M. Hinderliter, G. Orr, B. D. Thrall, and J. G. Pounds, "Particokinetics in vitro: dosimetry considerations for in vitro nanoparticle toxicity assessments," *Toxicological Sciences*, vol. 95, no. 2, pp. 300–312, 2007.

[52] J. Volckens, L. Dailey, G. Walters, and R. B. Devlin, "Direct particle-to-cell deposition of coarse ambient particulate matter increases the production of inflammatory mediators from cultured human airway epithelial cells," *Environmental Science and Technology*, vol. 43, no. 12, pp. 4595–4599, 2009.

[53] J. P. Stevens, J. Zahardis, M. MacPherson, B. T. Mossman, and G. A. Petrucci, "A new method for quantifiable and controlled dosage of particulate matter for in vitro studies: the electrostatic particulate dosage and exposure system (EPDExS)," *Toxicology in Vitro*, vol. 22, no. 7, pp. 1768–1774, 2008.

[54] M. Sillanpää, M. D. Geller, H. C. Phuleria, and C. Sioutas, "High collection efficiency electrostatic precipitator for in vitro cell exposure to concentrated ambient particulate matter (PM)," *Journal of Aerosol Science*, vol. 39, no. 4, pp. 335–347, 2008.

[55] M. Savi, M. Kalberer, D. Lang et al., "A novel exposure system for the efficient and controlled deposition of aerosol particles onto cell cultures," *Environmental Science and Technology*, vol. 42, no. 15, pp. 5667–5674, 2008.

[56] N. M. Schaeublin, L. K. Braydich-Stolle, A. M. Schrand et al., "Surface charge of gold nanoparticles mediates mechanism of toxicity," *Nanoscale*, vol. 3, no. 2, pp. 410–420, 2011.

[57] E. Bitterle, E. Karg, A. Schroeppel et al., "Dose-controlled exposure of A549 epithelial cells at the air-liquid interface to airborne ultrafine carbonaceous particles," *Chemosphere*, vol. 65, no. 10, pp. 1784–1790, 2006.

[58] P. Intra and N. Tippayawong, "An overview of unipolar charger developments for nanoparticle charging," *Aerosol and Air Quality Research*, vol. 11, no. 2, pp. 187–209, 2011.

[59] S. C. Kim, D. R. Chen, C. Qi et al., "A nanoparticle dispersion method for in vitro and in vivo nanotoxicity study," *Nanotoxicology*, vol. 4, no. 1, pp. 42–51, 2010.